Magnetic Stress Analysis of Structural Steel

by

Richard Anthony Langman, Dip. Tech., MSc.

Submitted in fulfilment of the requirements for the degree of

Doctor of Philosophy

UNIVERSITY OF TASMANIA

HOBART

1986

I declare that this thesis does not contain anything that has been accepted for the award of a degree or diploma in any other university, and also that, to the best of my knowledge and belief, the thesis does not contain a copy or a paraphrase of material written or published by anyone else except where due reference to it is made in the text of the thesis.

SUMMARY

The original aim of this project (on which the thesis is based) was to design an instrument that would measure stress in steel nondestructively by means of magnetic measurements, using the known fact that the magnetic properties of most steels are significantly affected by stress. It soon became apparent that there was a paucity of relevant magnetic theory, and so the project was widened to include a (mostly experimental) study of the effect of stress on the magnetisation curves of mild steel. These were measured for magnetisation parallel and perpendicular to the stress and for tensile and compressive stresses. The highest sensitivity to stress occurs on the steepest part of the magnetisation curve, which is where the stress-instrument is used, and is also where the theory is least satisfactory. Thus another aim is to relate magnetisation measurements and theory at moderate field strengths.

The thesis is in three parts:

I A review of experimental magnetic stress analysis, for the period 1950-1980; work by about 12 individuals or groups is included.

II An account of the author's experimental results, both for the development of the instrument to measure stress (called the Rotation Rig) and also for the more basic measurements of magnetic properties of steel under stress. Some work is also included on the effect of plastic strain and on the relation between Barkhausen noise and the rotation rig results.

III A review of magnetomechanical theory, including a contribution from the author; theories or concepts that have some relevance are by Brown, Goodenough, Ginsburg, Watson, and Jiles and Atherton.

The first aim, that of designing an instrument to measure stress, has been achieved. Strictly, only the differences in principal stresses, and their directions, can be measured. The results are analagous to photoelastic modeling but working on the actual steel instead of a plastic model. The

rotation rig is cheap, quick, and convenient to use, and has an error of about 10MPa in optimum conditions.

The second aim, that of producing a theory to explain quantitatively the effect of stress on magnetisation at moderate magnetic fields, has not been achieved. In fact the complexity of the magnetic behaviour of steel makes any theory likely to be rather complicated. However, the symmetry of the experimental results on mild steel are explained theoretically by the author.

Many of the measurements, especially those with biaxial stresses, have not been made before, and are a framework on which to base further theory.

CONTENTS

PART I

PREFACE

This thesis is an account of my research in magnetic stress analysis (M.S.A.) for the 9 years from 1976 to 1984. It is an unusual topic and has been studied by very few people during the last decade. My interest in it started when I worked for British Rail research department during 1968-71. A problem that concerned them was that on warm days there was too much residual compression in some continuously welded rails and this could make them buckle. I attempted at that time to measure the stress in a rail by means of the change in impedance of a coil around a piece of rail as it was compressed. The change was no more than 2% at 100MPa. I decided that when the differing compositions, temperature of measurement, and general difficulties of working outside were taken into account, a 2% change was not enough on which to base a reliable method of measuring stress. And yet I knew that for some steels the change of magnetic properties with stress was large: a factor of five or so. I felt that it should be possible to make use of such a large change as a basis of a magnetic method of measuring stress in steels in general.

There was no relevant information available on rail steel and very little on mild steel; also the (magnetomechanical) theory seemed fragmented and poorly connected with experimental results. It was from this unsatisfactory state of affairs that my interest in M.S.A. stemmed.

The words "magnetic stress analysis" were first used by Hoselitz in 1952. My use of them here is meant to convey an engineering attitude. An alternative such as "magnetomechanical effects" has rather more theoretical connotations.

My aim at the start (1976) was to develop an instrument that would make use of the stress-dependence of the magnetic properties of steels. It would be used on a steel surface and, hopefully, give an indication of (1) the pattern of stress, (2) whether there was plastic strain, (3) whether

fatigue failure might occur in future. I concentrated on low carbon steels, since these make up the bulk of steel usage and would be easily available when samples were needed for experiments. As work progressed the first aim, measurement of the stress pattern, became more important to me than the other two; I did very little work on plastic strain and none on fatigue failure.

In parallel with the development of an instrument went some measurement of magnetic properties (mostly hysteresis or B vs. H loops) in order to provide data for some tentative theory that tried to explain why the instrument behaved as it did.

The contents of this thesis are in 3 parts:

I A review of existing methods of M.S.A. with the emphasis on those with engineering applications rather than scientific investigation.

II An account of my experimental work.

III A review of magnetomechanical theory. Included in this is my addition to it, and also an assessment of what still needs to be explained.

As already mentioned, very little has been published on M.S.A., and that which has tends to be spread over a wide range of journals. There is no book on the subject. So, I have attempted to make this thesis a balanced account of M.S.A., instead of the more specialised account that is usual for a PhD. Thus, in addition to my own work that occupies part II, chapter 13, and the appendix, I have included in part I accounts of other people's work on M.S.A. (with a few of my own comments). In part III I have included several other theories or analytical models. Not all aspects of all these models are relevant, or probably even correct, but I feel that it will be necessary to select some features from them in order to get a model that more nearly describes what actually happens inside stressed steel.

I should point out here that my theory, in chapter 13, that deals with the effect of stress on magnetisation at moderate magnetic fields, is based on a particular set of magnetic conditions in the steel that may or may not

exist in practice to any significant extent. The justification for the theory is that it does explain an important feature of my experimental results, especially at lower stresses. However, it does not explain another feature that occurs at higher stresses. The inference is not so much that the theory is wrong but that other magnetic conditions have been ignored which come into play significantly at the higher stresses.

During the period of research I had five papers published. One of the rules of a higher degree thesis is that it be complete in itself (i.e. not use undue reference to other papers). This has meant that some material in parts II and III is already in these published papers. However, I have tried to minimise such duplication. (These papers are not included here but are listed at the start of the references).

Acknowledgements

I would like to express my thanks to the following people for their help:

The workshop staff of the Electrical Engineering Department, for the equipment they have made for me.

The workshop staff of the Civil and Mechanical Engineering Department for their guidance when I was using testing machines, and also Dr.R.F.Rish (of the same Department) for his interest - and therefore encouragement - in the early days of this work.

My supervisors, Professor C.H.Miller and Dr.C.G.Foster; the latter especially for his advice on the mechanical side of my experimental work.

The late professor B.D.Cullity, of the University of Notre Dame, Indiana, whose excellent book "Introduction to Magnetic Materials" has helped me many times. Professor Cullity was particularly interested in the effect of stress on magnetisation and, although I never met him, his contributions to the non-destructive testing aspect of M.S.A. were an example for me to try to emulate.

Mr.G.Thé and Dr.P.E.Doe for allowing me the use of their computer and printer (respectively) on which to prepare the thesis, and Mr.A.P.Taskunas for advice on its layout.

Finally, my thanks to Ruth, my wife, who helped with the rather boring job of getting the draft thesis on to a word processor so that it could be edited and printed.

CHAPTER 1

A REVIEW OF MAGNETIC TECHNIQUES IN EXPERIMENTAL STRESS ANALYSIS

1.1 Introduction

Chapter 1 of the thesis is a review of the techniques and results of magnetic stress analysis (M.S.A.). It covers the period 1960-1984, although some work that is mentioned dates back to the 1940s. The order in which the topics are listed is not particularly significant, and in fact they cover such a diverse range that no one way of classifying or ordering them is better than any other.

The techniques of M.S.A. use in general one of only three phenomena:

(1) A change of magnitude of secondary magnetic properties (mainly permeability and coercivity) with stress.

(2) A change from isotropic to anisotropic magnetic properties with stress.

(3) Barkhausen noise is affected by stress and by plastic deformation.

However, almost without exception there is no theory given that backs up the experimental results, nor even any measurements of a more basic kind such as B vs. H (hysteresis) loops. This makes comparison of the various techniques and results difficult, and, incidentally, emphasizes the importance of basic measurements as a starting point for the development of an instrument for M.S.A.

In order to complete the picture historically it is worth going back to before the 1940s, and so section 1.2 is a very brief summary, with an emphasis on books or review papers, of the early work on the magnetic properties of iron and steel.

1.2 Early work on the magnetic properties of iron and steel

Ewing (E1,1892) showed B vs. H curves for steel with varying amounts of carbon and pointed out that these differed when the steel was heat treated. His book was the first to deal in some detail with the magnetisation of iron, nickel, and cobalt, including their magnetostriction and the effects of stress.

At that time the magnetic analysis of steels (i.e. relating the magnetic properties to the composition of the steel) had hardly begun. In the years that followed measurements were made of B vs. H curves and loops for many types of steels, particularly in Japan and in the U.S.A. For example, figure 1.1 shows results of some measurements by Smith and Sherman (S4,1914) on four different steels: rail steel, wrought iron, mild steel and silicon steel. Each sample was 600mm long and 10mm in diameter (400mm long for compression tests), and was held at constant stress while the B. vs. H curve was measured with a Burrows permeameter. No theoretical work was attempted that could explain even qualitatively the results that were obtained.

Spooner (S1,1927) summarised the results to date in his book "Properties and Testing of Magnetic Materials"; by about that time the investigations had centered on two types of steels:-

(1) The high (0.8-1.2%) carbon steels which, when quenched, made "good" permanent magnets, and

(2) The electrical steels, that contained 1-4% of silicon, and that had high permeabilities at high flux densities, and low hysteresis losses.

(The last chapter of Spooner's book is entitled "magnetic analysis", and this is probably the first time that these words were used to denote the use of magnetic properties to identify different mechanical or chemical states of steel). After the 1920s the high carbon steels were abandoned for permanent magnet use and there was very little interest in them as far as their magnetic properties were concerned.

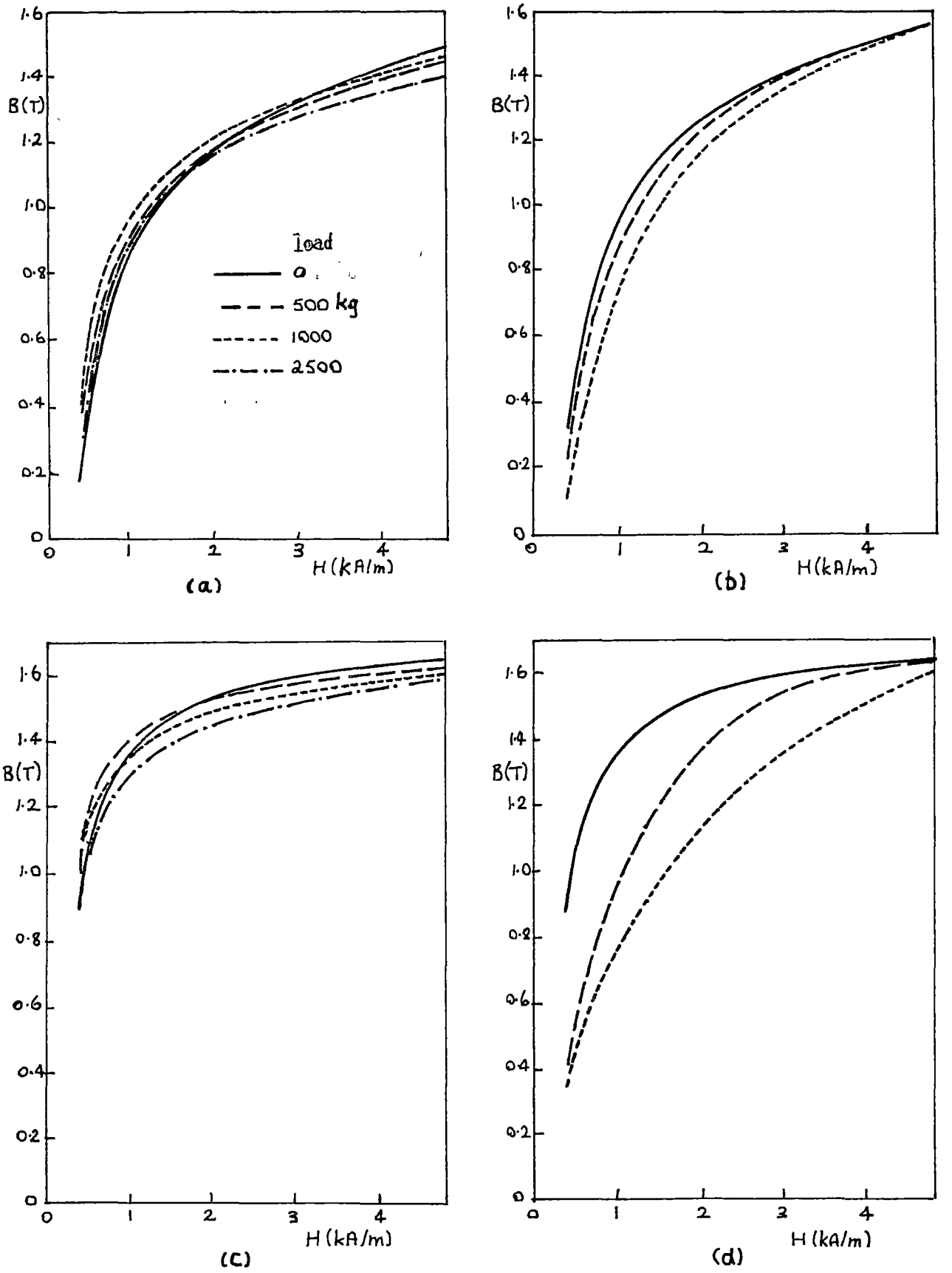

Figure 1.1 Smith and Sherman [S4]:
B vs. H curves at constant stress.
Rail steel: (a) in tension, (b) in compression.
Wrought Iron: (c) in tension, (d) in compression.

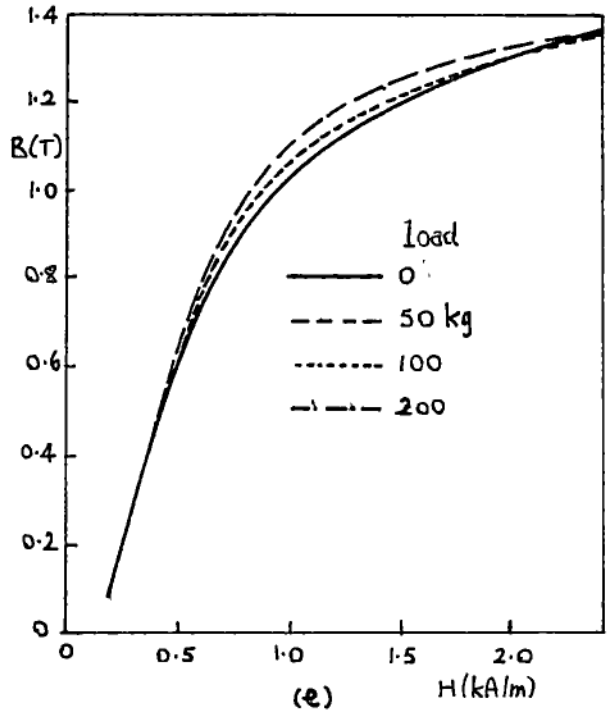

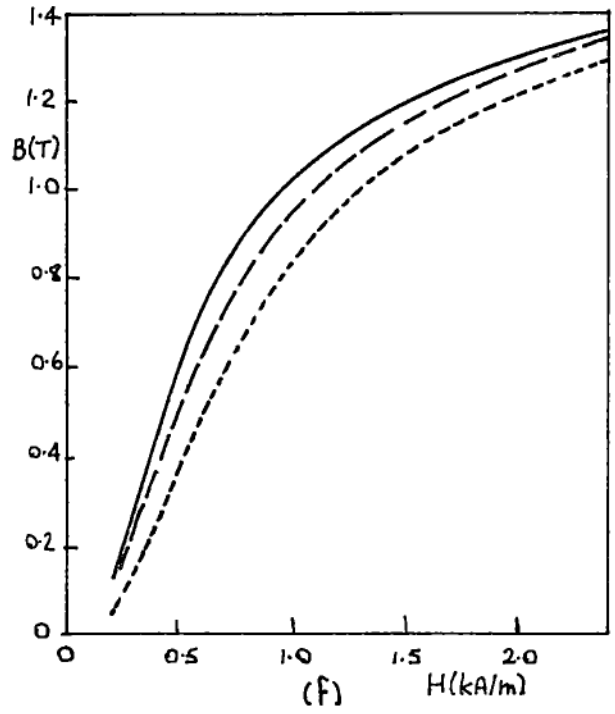

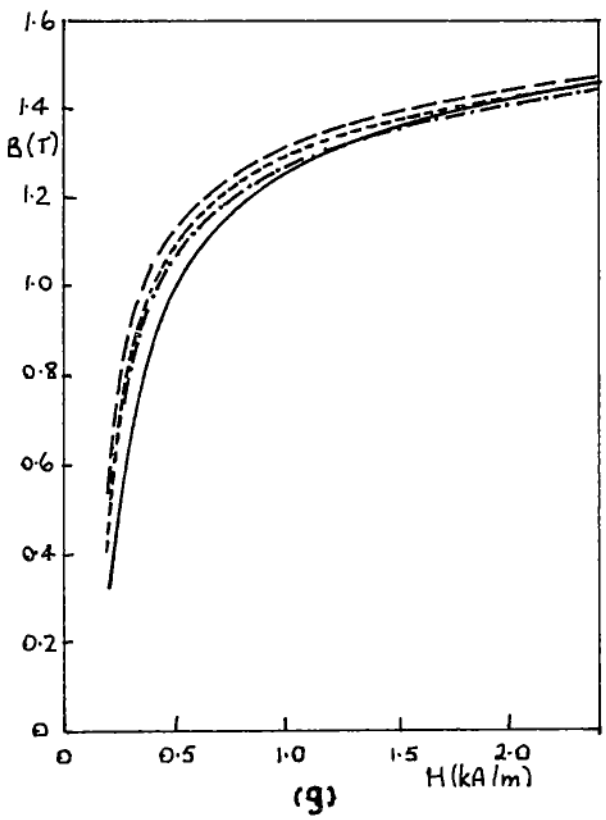

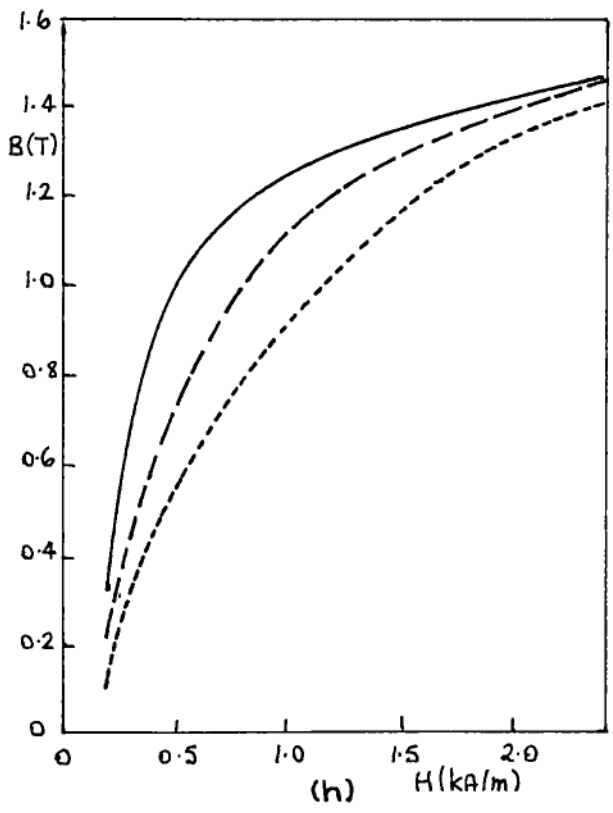

Figure 1.1 (continued)
Mild Steel: (e) in tension, (f) in compression.
Silicon Steel: (g) in tension, (h) in compression.

In the early 1930s Becker (and others) proposed a theory of crystal anisotropy and magnetostriction that made possible the qualitative explanation of some phenomena. Interest in research then turned to the detailed study of single crystals of the ferromagnetic elements in order to build up the new theory. Much effort went into preparing extremely pure samples so that distortion of the crystal lattice by impurities was as low as possible. Nothing was done on the impure, magnetically uninteresting carbon steels. This is borne out by Hoselitz (H1,1952), whose book is a more up to date version of Spooner's. He also mentions some of the early work on the carbon steels but the references he gives on this topic are more or less the same as Spooner's, which confirms that investigation of the carbon steels ceased round about 1930.

In the 1950's magnetic analysis of structural steels came to be included, along with ultrasonic and X-ray testing, in what was called Non-Destructive Testing (N.D.T.). The idea of N.D.T. is that tests (usually in situ) can be done to locate cracks in metal structures, or to tell whether the metal has undergone changes in its internal structure due to fatigue, or to check that the composition of metals (at steel works) is correct. These tests do not involve the destruction or permanent alteration of the metal. The people involved in N.D.T. were mainly metallurgists and mechanical engineers who were interested in the applications, rather than the theory, of magnetic testing, and so no significant progress was made in magnetic theory.

1.3 A method for predicting the failure of metals

P.E.Cavanagh [C1,1946]) measured the losses in cylindrical samples of metal when they were magnetised by A.C. in a surrounding coil. These losses (due to eddy currents only in non-ferrous metals, and due to eddy currents and hysteresis in steels) varied with the applied stress. He used an instrument called the DuMont Cyclograph to obtain a chart of loss vs.

stress. The Cyclograph was an electronic oscillator that compared the test specimen with a standard specimen. The amplitude of its output varied with the losses in the core of the test specimen. It is described in more detail than in the original paper in a book by Lewis [L1,1951]. Figure 1.2 shows results for different metals (no units are given for the loss). The corresponding stress vs. strain graphs are also shown.

The basis of the method is that the loss increases suddenly when the metal yields. Cavanagh then used this with some success to test wire ropes. Figure 1.3 shows a scan, with the Cyclograph, of good and bad wire ropes as they were tensioned. The bad rope eventually broke at a nominal stress of 140MPa compared with 320MPa for the good one.

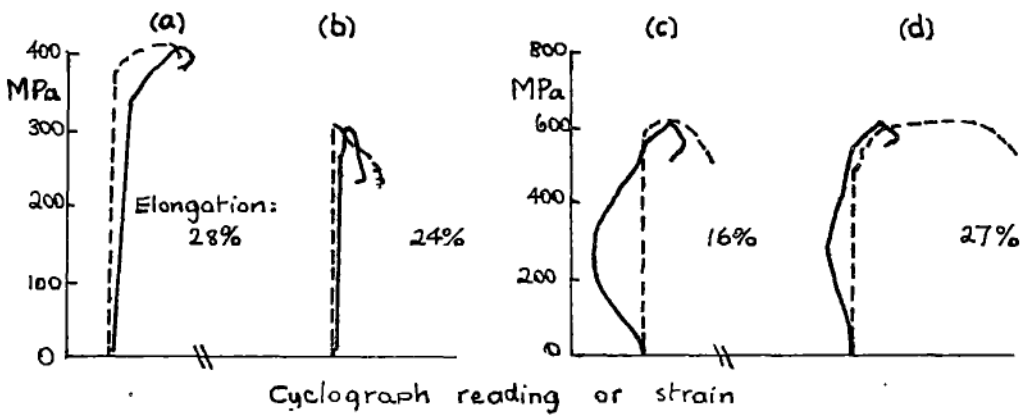

Figure 1.2 Cavanagh [C1]: Comparison of stress vs. core loss (Cyclograph, full line), and stress vs. strain (dashed line) for standard 1/2" dia. samples: (a) 70-30 brass, (b) copper, (c) 0.2% carbon steel, (d) 0·95% carbon steel.

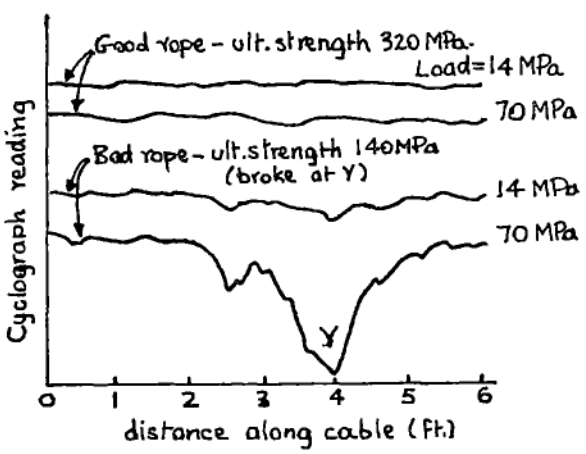

Figure 1.3 Variations in Cyclograph output using 5/8" wire ropes under various loads, [C1].

Later, in 1948, Cavanagh and Wlodeck [C8] describe an instrument they called the Dyna-magnetic Analyser that could measure microstresses in steel and hence study the behaviour during fatigue testing. This was based on an earlier paper by Wlodeck [W1,1944] in which he measured the voltage induced in a search coil around 8mm diameter steel samples. The sample was tensioned sinusoidally (between zero and maximum tension) at 50Hz and the amplitude and waveform of the search coil voltage was recorded. Figure 1.4 shows some waveforms, for different peak stresses, for SAE 1026 steel. At about 320MPa the voltage suddenly increases; this is brought out clearly in figure 1.4b which shows the (rectified) voltage vs. peak stress. Enough detail is given in the paper to enable an estimate to be made of the change in flux density in the steel: 0.0008T for the 0-9MPa stress, and 0.013T for the 0-385 MPa. These are fairly small changes, and in fact the experimental conditions appear to be similar to those measured by W.F.Brown in his theory of the irreversible effects of stress at constant, low, applied field.

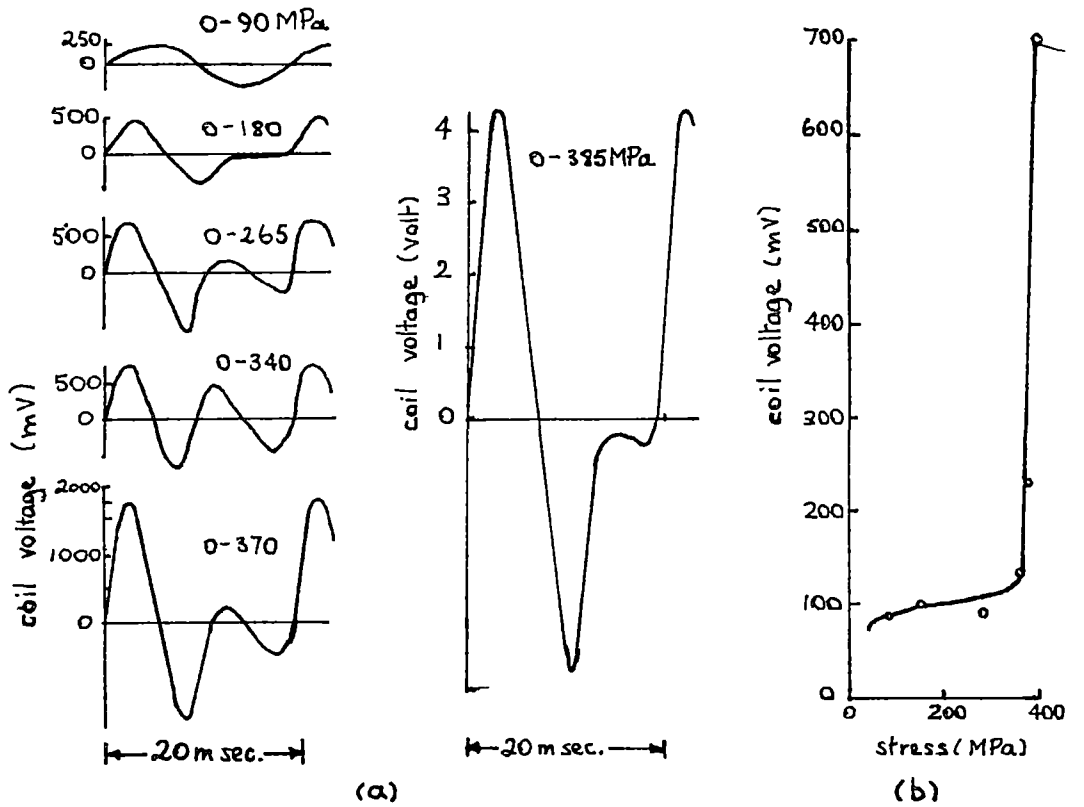

Figure 1.4 (a) Waveform of coil voltage for various amplitudes of stress cycles, for SAE1026 steel, (b) corresponding coil voltage (rectified) vs. peak stress, [W1].

(This investigation by Cavanagh and its particular application to wire ropes is the only one of its kind that is mentioned in several books on N.D.T.; for example, in those by Lewis [L1] and McGonnagle [M1,1961], as well as by Hoselitz. However, a review of electromagnetic methods of testing wire ropes, by Wait [W6,1979], does not include Cavanagh's work, but cites instead nine other studies on this topic, the first of which was in 1929. All used either D.C. or A.C. magnetisatiom of the wire rope and all were wholly experimental investigations with no attempt at theory. The point to be made is that work on M.S.A. has been published in many and varied types of journals, and while I hope in this review to cover a varied range of techniques and applications - and different countries - there is no guarantee that I have not overlooked some distinctive work).

1.4 Torquemeters

In 1954 Beth and Meeks [B1] proposed a means of measuring torque in a rotating steel shaft by measuring its reluctance in the directions of principal mechanical stress. Figure 1.5a shows the idea. A torque on the shaft makes the permeability of the steel decrease in the direction of principal compression relative to that of principal tension. Hence the reluctance of the flux path between 2 and 4 is less than that between 1 and 3. The magnetic circuit is completed by the rather complicated five pole yoke shown in figures 1.5b and 1.5c. Coil 5 provides the excitation, and search coils 1-4 are connected in a Wheatstone Bridge fashion.

The change of reluctance, expressed as a galvanometer deflection, was found to vary linearly with torque up to a shear stress at the surface of the shaft of about 8000lb/in^2 (50MPa). Excitation frequency was 1800Hz. Shafts of both low and high carbon steel were tested. Hysteresis was noticed, i.e. the galvanometer deflection for a torque increasing from zero was different to that for the same torque but reached by decreasing from a higher value.

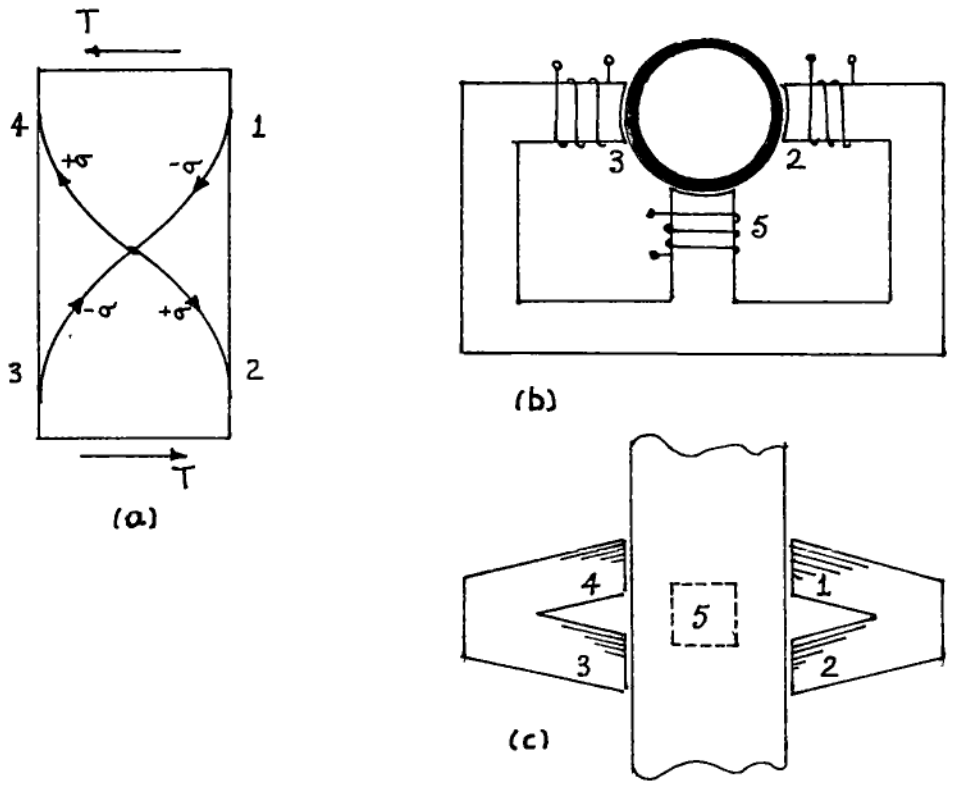

Figure 1.5 The torquemeter of Beth and Meeks [B1]:
(a) Shaft under tension, showing directions of principal stresses, (b) yoke to complete the magnetic circuit, (c) axial view of yoke.

Their technique was refined by Dahle [D1,1960] who worked for the Swedish company A.S.E.A. The torquemeter was marketed under the name of the "Ring Torductor". Not much numerical detail is available on it but the magnetising frequency was 50Hz, and a high current was needed to ensure linearity and to prevent torque hysteresis. The torque shaft could be an extension of, or a sleeve over, the original motor shaft, and so could be made of a steel that would give good results magnetically and yet still transmit the torque satisfactorally. (In contrast, the wire rope tester described by Cavanagh tested a sample that was designed purely for its job as a wire rope and not out of any consideration for its magnetic properties).

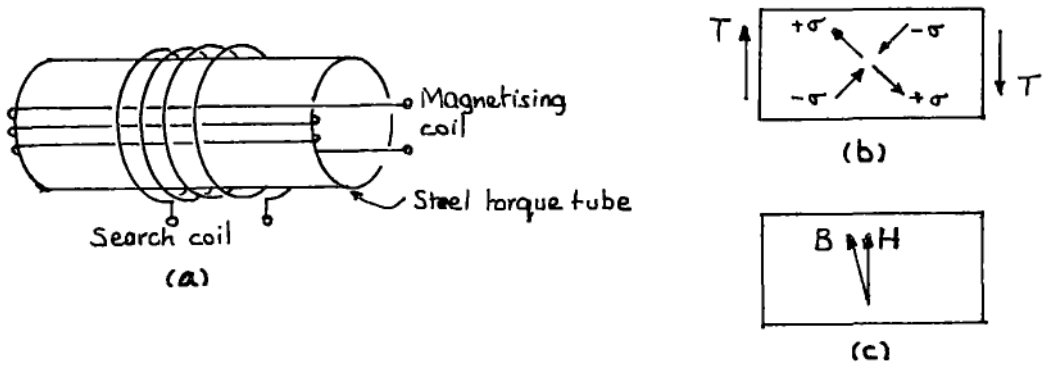

Figure 1.6 The torque transducer of Barton and Ionides [B2]: (a) position of coils, (b) principal stresses due to an applied torque T, (c) shift of flux density B towards the direction of tension. H is the field of the magnetising coil.

Barton and Ionides [B2,1966] used a slightly different geometry for a torquemeter, which is shown in figure 1.6.

The magnetising coil rotates with the torque-tube and is fed (via slip rings) with alternating current to produce a circumferential magnetic field H. A search coil surrounds the tube. The tube is annealed so as to be as near as possible magnetically isotropic so that when not in tension all the magnetisation is circumferential and the voltage induced in the search coil is zero. When the tube is torsioned there is a slight shift of flux into the axial direction and a voltage is induced in the search coil.

The main reason for this choice of geometry was to obtain a simple magnetic circuit that was amenable to quantitative analysis. Previous arrangements had complicated magnetic circuits. Other aims were to develop a torquemeter whose output was independent of the speed of rotation of the shaft and, above all, that was to be linear to better than 1%. In order to achieve such linearity the tube was magnetised to well above the knee of the initial magnetisation curve. Heating of the tube due to eddy currents set the upper limit to the magnetisation, but at 2400 A/m the linearity was better than 0.2% up to a shear stress of 80Mpa. 1% was easily achieved on a prototype in industry.

In a companion paper [B3,1965] the authors predict the shift in direction of the flux. On the assumption that only domain rotation occurs as a result of the stress, they sum the three components of energy (magnetostatic, magnetoelastic, and crystal anisotropy) and then minimise the total for all domain directions. (The general form of these energy components and details of Barton and Ionides' analysis are given in chapter 12). Figure 1.7 shows the predicted and the measured results. The torque-tube was 1.427 inches mean diameter and 0.05 inch wall thickness. The RMS magnetising force was 2400 A/m and a 300 turn search coil was used. Tube temperature was 80°C. The angle through which the flux rotated was quite small, of the order of one degree.

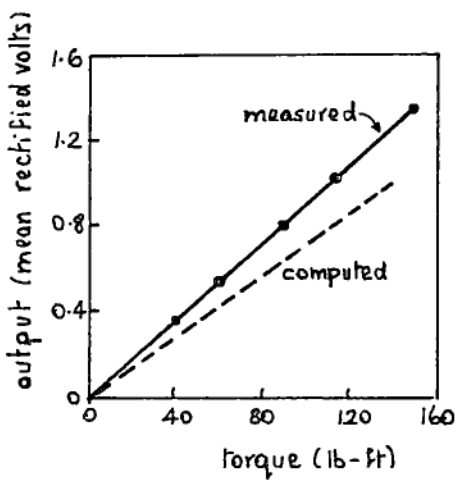

Figure 1.7 Barton and Ionides: output signal vs. applied torque. The computed result is for iron and the measured one is for mild steel. 140lb-ft is equivalent to a principal stress of 72MPa,[B3].

Of all the M.S.A. techniques that are described here this is the only case where theory is related to experiment and where the agreement between them is within 10%, which is good for this sort of situation. This fact encouraged me to use this method (that of measuring the shift of direction of the flux with stress) as a basis for an instrument that would measure stress on a flat surface.

1.5 On-line measurement of the shape of rolled steel sheet

Syke and Murray [S2,1967] describe the development of equipment to measure the stress in thin (less than 1mm) sheets of steel as they are being cold-rolled to reduce their thickness. If the pattern of stress is not correct then when the tension (needed to pull the steel through the rolling mills) is released and the sheet is cut up, it can become wavy. Such sheet is then said to have bad "shape".

The principle involved is that plane stress causes different permeabilities for magnetisation parallel and perpendicular to the axis of principal stress. Figure 1.8a shows the positions of magnetising cores, placed so as to magnetise in directions longitudinal (parallel) and transverse to the motion of the sheet. Detector cores and coils are placed on the other side of the sheet. Figure 1.8b shows how the voltages induced in the two detecting coils vary with stress. These are combined to give V_Δ which also varies linearly with stress but is unaffected by moderate changes in air-gap, sheet thickness, and metallurgical properties of the steel. A signal (summed for an array of sensors spread across the sheet) is then used to control the force on the rollers down stream of the sensors in an attempt to correct the stress pattern and hence to improve the shape of the final product.

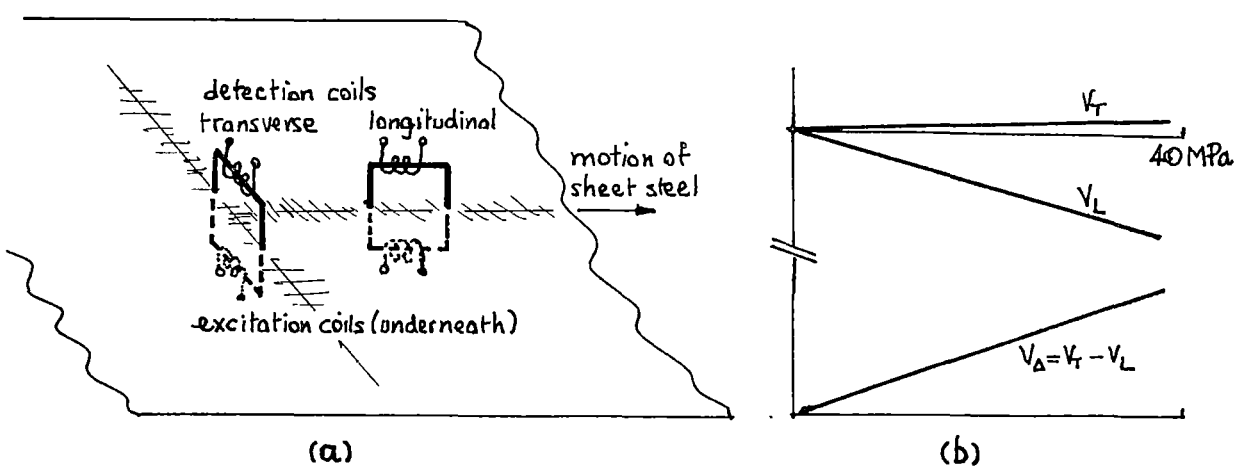

Figure 1.8 Syke and Murray [S2]: shape measurement on steel sheet: (a) location of excitation and detection coils, (b) detection coil output vs. stress (V_t = transverse coil, V_l = longitudinal coil).

(The authors report that experiments in the laboratory and on a production rolling mill gave promising results and that the development of a production prototype instrument was in progress. However, I could not find any later account of this project and so do not know whether it was ever used routinely on-line).

1.6 Indication of stress by internal induction

A paper by M. Lambeck (L2,1977) of Germany describes a technique of stress measurement that is quite different to previous ones. Figure 1.9 shows what is meant by internal induction. If the magnetisation of the sample is reversed a voltage u_t is induced between the transverse pair of contacts, and a voltage u_l is induced between the longitudinal contacts.

Figures 1.10a and 1.10b are sketches (from a C.R.O.) of u_l for the two faces of a thin strip of Mumetal bent as shown in figure 1.10c. The contacts are about 5mm apart, positioned where the strain is 4×10^{-4}. The peak field strength is 1550A/m at a frequency of 80Hz, and the amplifier has a band width of 10kHz to 100kHz. The sketches show that pulses of voltage appear around H = 0 and about 500A/m. The author states that the reproducability permits a surface stress of 1MPa to be resolved.

Other C.R.O. traces show the u_t waveform for a plastically strained sample of Mumetal. Lambeck claims that the signals are "unambiguously related to bending, thus yielding information on the magnitude and sign of the stress", and also that this technique seems to be more simple and direct than Barkhausen methods.

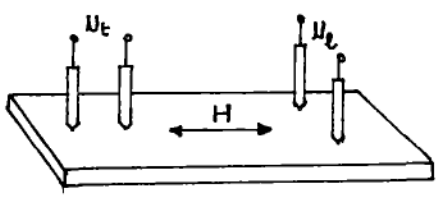

Figure 1.9 M.Lambeck [L2]: position of contacts for the measurement of transverse (u_t) and longitudinal (u_l) internal voltages.

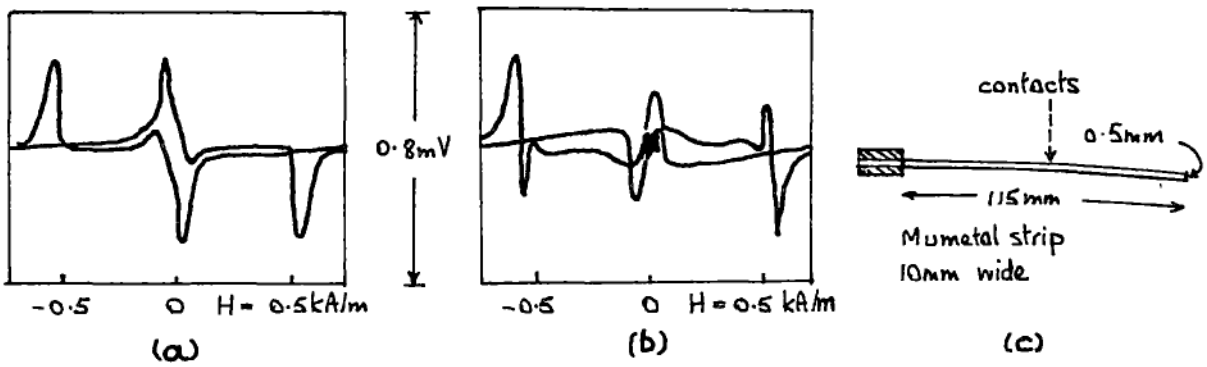

Figure 1.10 Longitudinal internal voltages for a bent strip of Mumetal: (a) C.R.O. trace for the contacts on the upper face, (b) C.R.O. trace for the lower face, (c) dimensions of Mumetal strip and position of contacts, [L2].

(A puzzling aspect is the relatively high field that was applied: of the order of 1000A/m. For unstrained Mumetal the coercivity lies between 1 and 3A/m, and so 100A/m would cause complete saturation. The C.R.O. traces of figure 1.10 show changes of flux occurring at about 500A/m as well as around zero field. No reason for the flux change at 500A/m is given; in fact there is very little discussion of what might be going on inside the Mumetal that could give rise to the voltage picked up by the contacts).

1.7 Soviet work on Magnetic Stress Analysis

There are two special problems associated with the papers published in the Soviet Union:

(1) Almost all that are in English are translations from the Russian. Often merely the finer shades of meaning are lost in the translation, but in some cases it is just not clear what has been done.

(2) Incomplete information about equipment in the original (Russian) paper. There seem to be standard pieces of equipment, which I do not know anything about, that presumably enable those who use them to relate, for example, flux density or field to voltage. When graphs use voltage instead of change of flux density they are sometimes not much use. Also, the types of steel are classified by a method that is not listed in the usual reference books.

Together, (1) and (2) make much of the Soviet literature less use than it could be. This is a pity because there is no doubt that a lot of work has been done on M.S.A. in the Soviet Union. What follows are summaries of relevant papers that appeared mainly in Defektoskopiya, (a cover to cover English translation of which is done by Consultants Bureau of New York).

Rodigin and Syrochkin [R1,R2,1973] describe a method for inspecting the (mechanical) hardness and tensile strength of steel tubes. The tube is placed inside a much longer solenoid that produces an alternating magnetic field of about 5000A/m. The voltage of the solenoid, which is related to the flux density in the tube, is noted. The tube is then compressed axially, the same field as before is applied, and the new voltage noted. The difference ΔU between the two voltages (i.e., with and without stress) is then a guide to whether the tube has been correctly heat treated.

In order to use the value of ΔU to reject or accept a tube, the data of figure 1.11 is needed. For an unquenched tube ΔU is greater for compression than for tension: thus compression produces the higher sensitivity. Also for compression, ΔU for an unquenched tube is more than for a quenched one. Thus, in the inspection, a large ΔU signifies an unquenched, and hence a reject, tube.

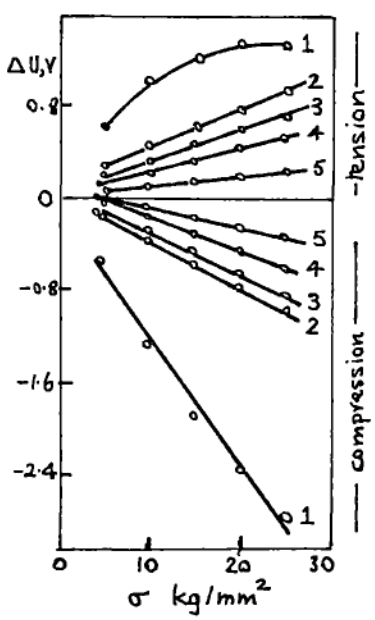

Figure 1.11 Rodigin and Syrochkin [R1,R2]: relation between voltage difference ΔU and stress σ for tubes of 40Kh steel (1) unquenched (2)-(5) quenched at 370, 340, 300, and 260°C respectively. Field = 3000A/m.

Figure 1.12 shows how the values of |ΔU| are grouped for tube samples of slightly differing composition (different melts) and heat treatment. Figure 1.12a relates the ΔU to the tensile strength, and 1.12b relates it to the hardness. In figure 1.12a regions I and III correspond to reject tubes, and region II (0.81<|ΔU|<1.17 volt), to sound ones.

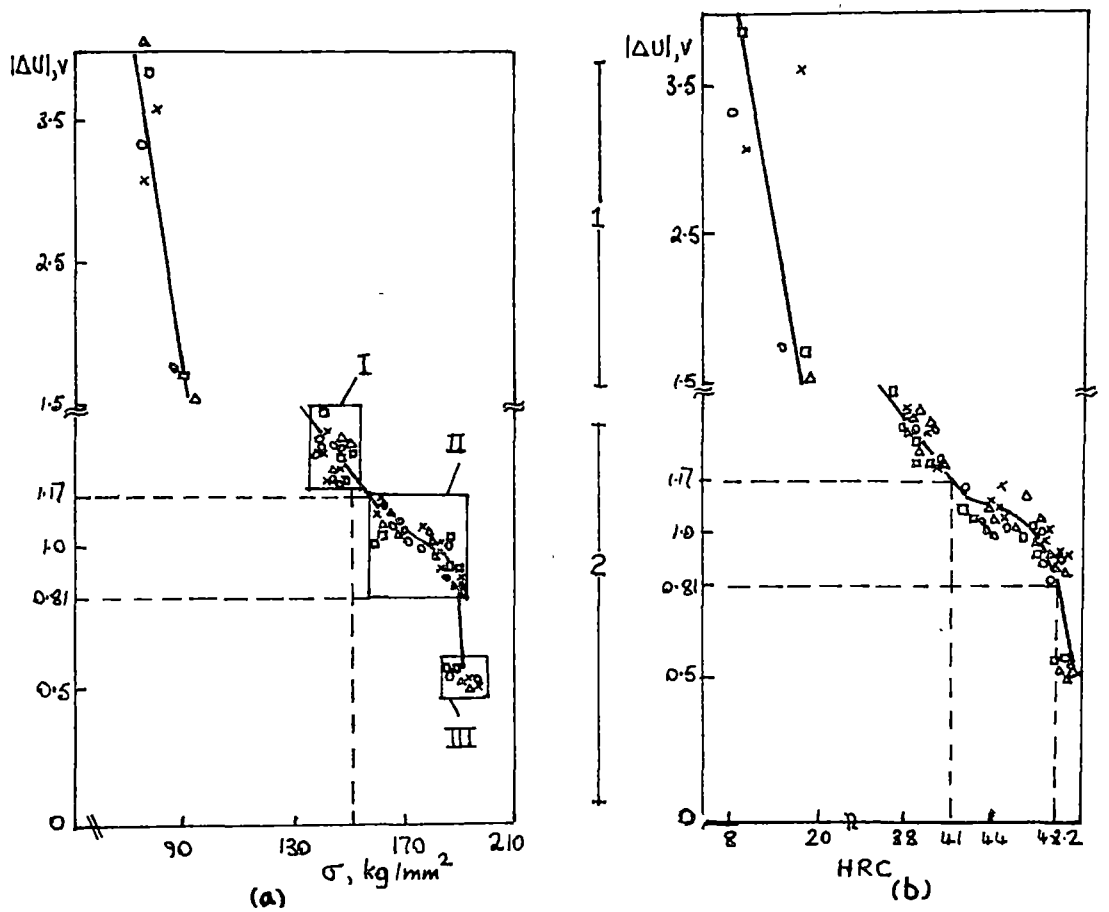

Figure 1.12 Dependence of the absolute value of ΔU on (a) strength, (b) hardness for compression σ=19kg/mm² and H_m=72 Oe; (1) differently normalised original objects (2) isothermally quenched objects; (I-II) objects with low and normal tensile strengths (III) objects with a hardness above the norm. The vertical broken line indicates the value of σ_B=150kg/mm². o,Δ,□,x, indicate first, second, third, and fourth melts respectively, [R1,R2].

Zheleznov et al [Z1,1972] describe a way of measuring the stress in steel plates. Unfortunately, the geometry of the probe is not given in the paper and other references to it were unobtainable. It is probable that the probe is similar to the three pole tripod one used by the same team to measure the loss in transformer laminations, and this is shown in figure

1.13 (taken from reference Z2). In use the probe is placed with its poles against the steel under test. A difference in permeability between poles 1-2 and 1-3 produces a voltage V_2 in coils C2-C3 in series. C1 is the excitation coil, supplied at 400Hz.

An example of some results, from reference [Z1], are for a steel plate that was slightly bent, with one side (A) in residual compression and the other side (B) in residual tension. Figure 1.14a shows how the voltage V_2 from the probe varied as the plate was tensioned. V_2 decreased as the stress in side A (initially compressive) decreased through zero and then

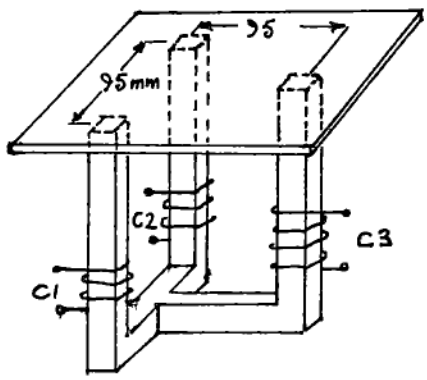

Figure 1.13 Zheleznov et al [Z2]: magnetising core and coils for testing stresses in steel sheet.

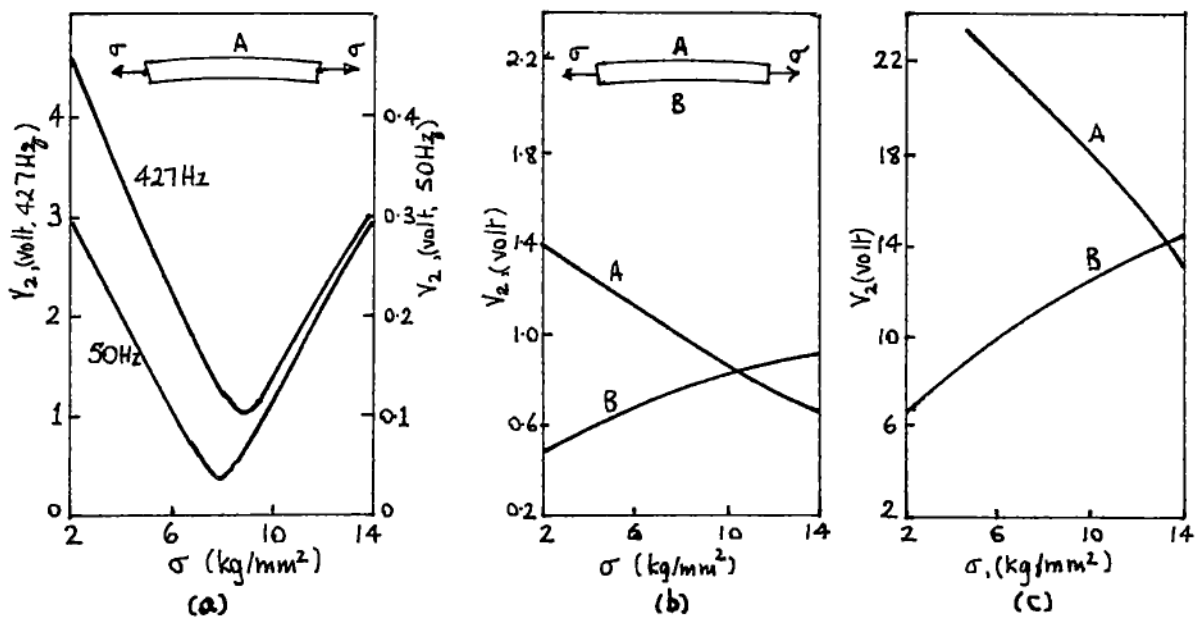

Figure 1.14 Output voltage V_2 of tripod core vs. applied tensile stress for a permanently bent steel strip (type of steel not known): (a) V_2 for side A of strip, at 50Hz and 427Hz: strip slightly bent to start with, (b) strip bent more to start with, (c) as (b) but for 427Hz, [Z1].

increased as the stress went positive (tension). Results are given for two excitation frequencies, 50Hz and 427Hz, for side A. If the plate was bent more to start with, the voltage for both faces varied as in figures 1.14b and 1.14c. The authors claim that by alternating the frequency and scanning over the plates they could build up a picture of the stress pattern in it. A calibration specimen was necessary. (This paper refers to the one by Syke and Murray on shape measurement. It is unusual for a Soviet paper to contain a reference of a non-Soviet origin).

Astashenko and Zatsepin [A1,1979] describe a magnetic method of measuring the hardness of items made of tool steel (U8A steel, 0.8%C). Many steels show a monotonic relation between coercivity and hardness. This is not so for this particular steel; figure 1.15 shows how coercivity H_c and hardness HRC are related to a third parameter, quenching temperature. For a range of quenching temperature between 300°C and 550°C H_c is not uniquely related to HRC.

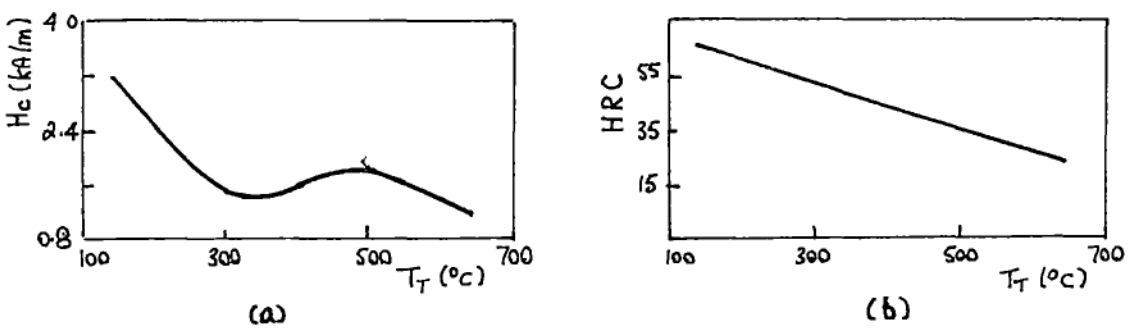

Figure 1.15 Ashtashenko et al [A1]: (a) Coercivity H_c, (b) hardness HRC vs. tempering temperature T_T for 0.8% carbon steel. Quenching temperature is 850°C.

The new method, that overcomes this difficulty, uses an instrument called the FITA-1. This has a probe of two U- shaped cores that are placed on the sample to be tested, as shown in figure 1.16a. It is used as follows. Core I is energised with D.C. to give a field H_1, then switched off. Core II is then energised to give a field H_2 ($<H_1$) perpendicular to H_1. A field

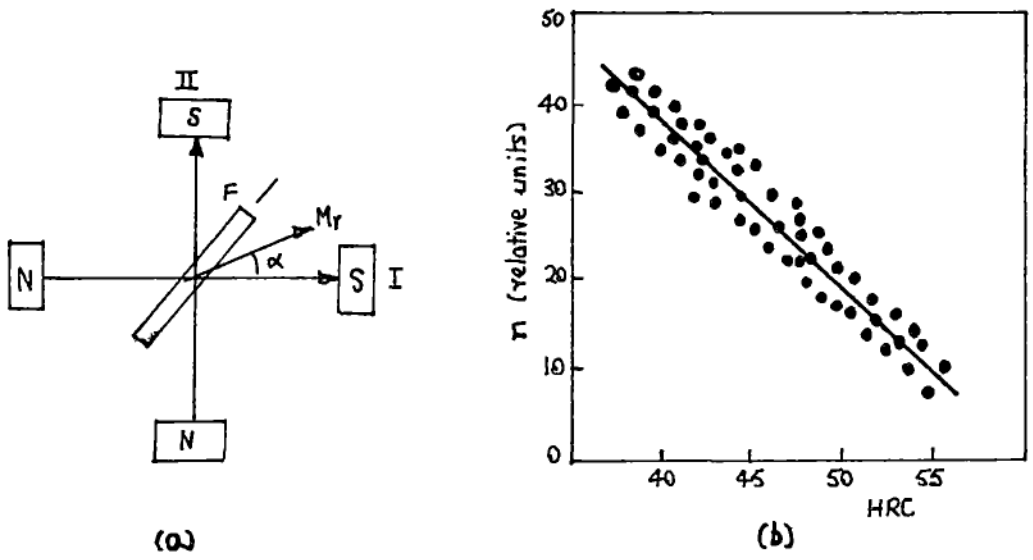

Figure 1.16 (a) Locations I and II of the pairs of poles of the FITA-1 instrument, (b) FITA-1 output n (n is related to angle α) vs. hardness, [Ai].

probe F is then turned until it records the maximum value of the residual magnetisation M_r at some angle α. (core II is still energised). The FITA-1 reading n is somehow related to α. Figure 1.16b shows n vs. hardness for many samples of steel. The correlation between n and HRC is -0.94, with a standard deviation of 0.06.

The instrument has been used in the 50th Anniversary of the U.S.S.R. Izhevsk Metallurgical Plant, and considerably decreased the inspection time (of 1 minute using a standard TSh-2A tester) to 5 seconds per item. The authors say that the FITA-1 can also be used to measure tensile and yield strengths, grain size, and first order (?) mechanical stress, but do not give any details. (It would also be useful to know the values of H_1, and H_2, the relation between α and n, and details of the position of the sensor on the items being inspected).

Kaptsov and Ivanov [K1,1983] describe the use of a microprocessor to process the readings from a transducer. The interesting aspect in this context is the form of the transducer and the fact that it measures stresses. Figure 1.17 shows the geometry of the transducer. Coil 1 carries a sawtooth waveform magnetising current whose frequency can be varied

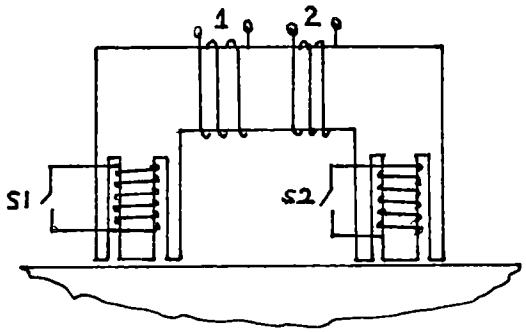

Figure 1.17 The stress transducer of Kaptsov and Ivanov [K2].

between 400 and 1000Hz. The coils S1 and S2 can be open-circuit or short-circuit. When open-circuit, the voltage induced in coil 2 is $U_3 = K/(2R_1+R_2)$, where R_1 is the reluctance of each air gap and R_2 that of the flux path in the steel under test. The cross sectional area of the middle part of each pole (on which is wound the shorting coil) is equal to that of the two outer parts together.

When S1 and S2 are shorted, no flux goes through them and the air gap reluctance is increased to $2R_1$. Thus if the current in coil 1 is kept as before, with S1 and S2 now shorted, $U_3' = K/(4R_1+R_2)$. Hence $K/R_2 = U_3U_3'/(U_3-U_3')$, and the effect of the air gap is eliminated. The authors say that in practice the incomplete elimination of the air gap term creates an error of 1.8 to 2.5%. (Presumably R_2 is affected by the stress in the steel, but no details are given of how the transducer is positioned on the steel or of how K/R_2 varies with stress. There is a reference to an inventor's certificate for a transducer for mechanical stress but this is in Russian and also is not in a journal that is in an accessible library)

Another instrument for measuring stress is described by Zhuravskii et al [Z3,1984]. Results are given for transformer steel and not for structural steels but the transducer is of interest, as also is the theory that is given. Figure 1.18 shows the design of the "sensor". This is cylindrical, shaped like a ferrite pot core, of 80mm outside diameter. Magnetisation is A.C., but the frequency is not stated, nor is the flux density in the transformer lamination under test. The output of the sensor is the voltage induced in the small search coil.

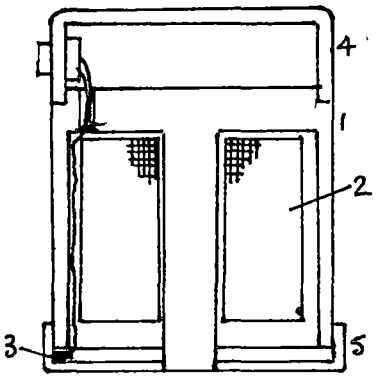

Figure 1.18 The stress transducer of Zhuravskii et al [Z3]. 1- cylindrical magnetic core, 2- magnetising coil, 3-search coil with axis parallel to magnetising coil, 4- and 5-nonmagnetic covers.

The susceptibility X depends on:

(1) the internal [residual?] stress σ_i according to

$$X = I_s^2/(\alpha\lambda_s\sigma_i) \qquad (2)$$

where I_s is the saturation magnetisation, λ_s is the saturation magnetostriction, and α is a numerical factor of the order of unity.

(2) The applied stress σ, according to

$$X_{\parallel} = X_{o\parallel} + a\sigma/\sigma_i - b(\sigma/\sigma_i)^2 \qquad (3)$$

$$X_{\perp} = X_{o\perp} - a\sigma/\sigma_i - b(\sigma/\sigma_i)^2 \qquad (4)$$

$X_{\parallel}$ and $X_{\perp}$ are the longitudinal and transverse susceptibilities of the steel at a tensile stress σ ; the extra "o" subscript refers to the zero-applied-stress value, and a and b are coefficients. Equation (2) follows from Kersten's theory of the interaction of domain walls and an assumed periodic variation of internal stress; its derivation is given by Hoselitz [H1]. Equations (3) and (4) are from Soviet text books. No other information is given about the constants a and b - whether, for instance, they depend on the excitation currents.

Figure 1.19 shows some results with the transducer. 1.19a is search coil voltage vs. direction, for different values of tension. Polar coordinates are used. There is only slight anisotropy with no applied tension, which suggests that the steel is not grain-orientated. Figure 1.19b shows voltage vs. applied stress for four values of magnetising force (M.M.F.). At high M.M.F.s an increase of tension decreases the voltage (and hence the

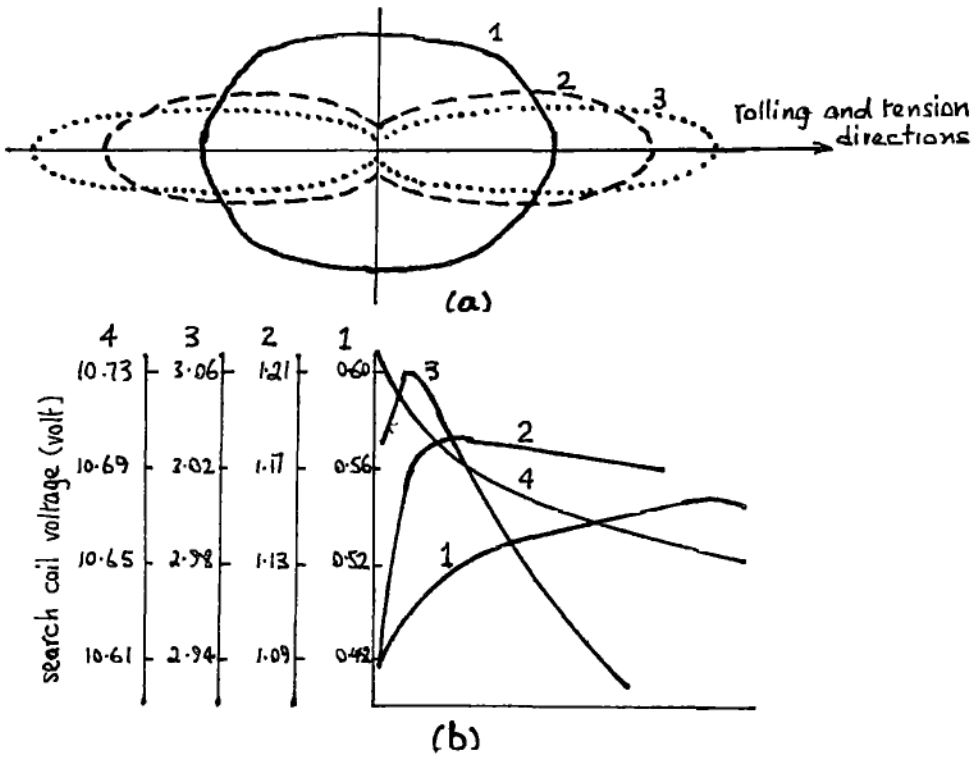

Figure 1.19 (a) The influence of tensile stresses on the instrument readings as it is rotated. Tension is applied parallel to the rolling direction of the lamination. (1) σ=0 (2) σ=2kg/mm² (3) σ=5kg/mm², (b) instrument reading vs. stress for various values of the excitation M.M.F. The tension and the search coil are parallel to the rolling direction. (1) 10, (2) 20, (3) 80, (4) 2000Amp-turns, [Z3].

permeability) whereas at low M.M.F.s the voltage always increases with tension. This behaviour is catered for by equations (3) and (4), and is related to the change in the sign of the magnetostriction as the field strength increases.

To conclude this section on Soviet magnetic stress analysis, mention should be made of a recent review paper by Mikheev and Gorkunov [M3,1981] entitled "The physical basis of magnetic structure analysis". It is a long paper and no attempt is made here to summarise it. However, it is noteworthy because the list of references contains 14 non-Soviet ones, including authors such as W.F.Brown, Dijkstra, Becker and Döring, Träuble, Kondorski, Néel, and Goodenough.

1.8 Magnetic Stress Analysis in Japan

The Japanese research into M.S.A. that is described here came to my notice via a request from professor H.Yamada (of the Faculty of Engineering, Shinshu University, Nagano) for copies of some papers I had written. Following on from this request, I also received papers on similar M.S.A. work that was carried out at the Ship Research Institute, Tokyo. Some were written in Japanese, and some were English translations. This summary is based on two of the papers.

(1) S. Abuku and C.Takizawa [A7,1974]: "Magnetic measurement of residual stress induced in carbon steel by uniaxial plastic deformation".

Figure 1.20a shows the shape of the probe. Poles 1 and 2 carry exciting coils, supplied at 1KHz, and poles 3 and 4 carry search coils whose output voltage is rectified in synchronism with the excitation. When the probe is put on a steel plate that is free from stress no output is produced because the two poles with the search coils are on areas of equal magnetic potential. When the plate is stressed an output voltage v is produced in the search coils. If the probe is rotated on the stressed plate this voltage changes sinusoidally with the rotation angle θ, with a period of 180° (i.e. $v \propto \sin 2\theta$). Its peak amplitude corresponds to the difference of the principal stresses.

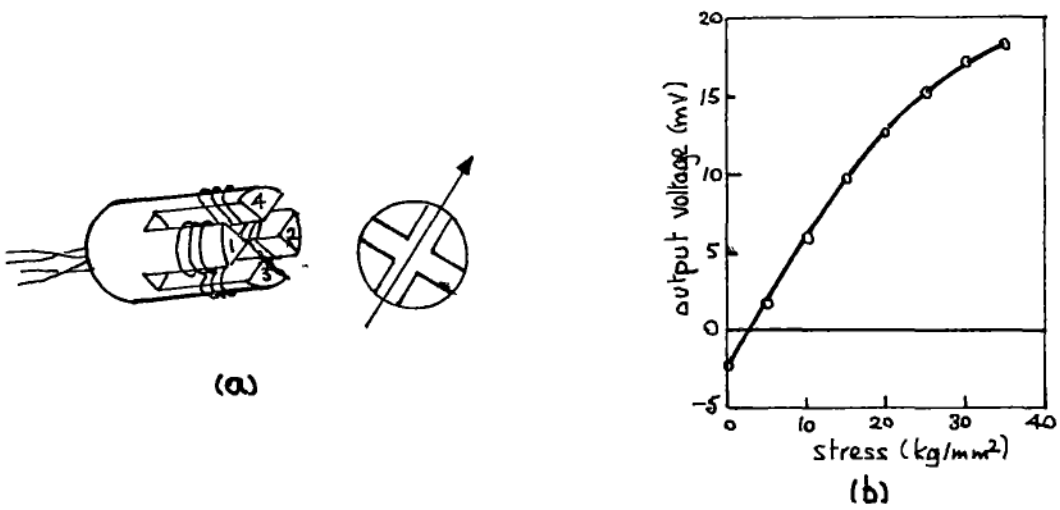

Figure 1.20 Stress measurement of Abuku and Takizawa [A7]: (a) probe, (b) probe calibration on 0.49% carbon steel.

Figure 1.20b shows a calibration of the probe for uniaxial tensile stress on a piece of 0.49% carbon steel (steel type S45C). There is a small negative voltage at zero applied stress, which suggests some residual stress or residual magnetic anisotropy.

The probe was also used to look at the residual stress resulting from uniaxial plastic deformation of the same steel. Sample size was 70mm x 25mm x 5mm. Figure 1.21a shows the stress vs. strain diagram, and 1.21b the corresponding output voltage of the magnetic probe. Nominal stress was calculated from the applied force divided by the cross sectional area. At various stages of deformation the tensioning force was released and then re-applied, and this resulted in hysteresis loops on both graphs. The negative voltage means that compressive residual stresses were induced in the sample by plastic tensile deformation.

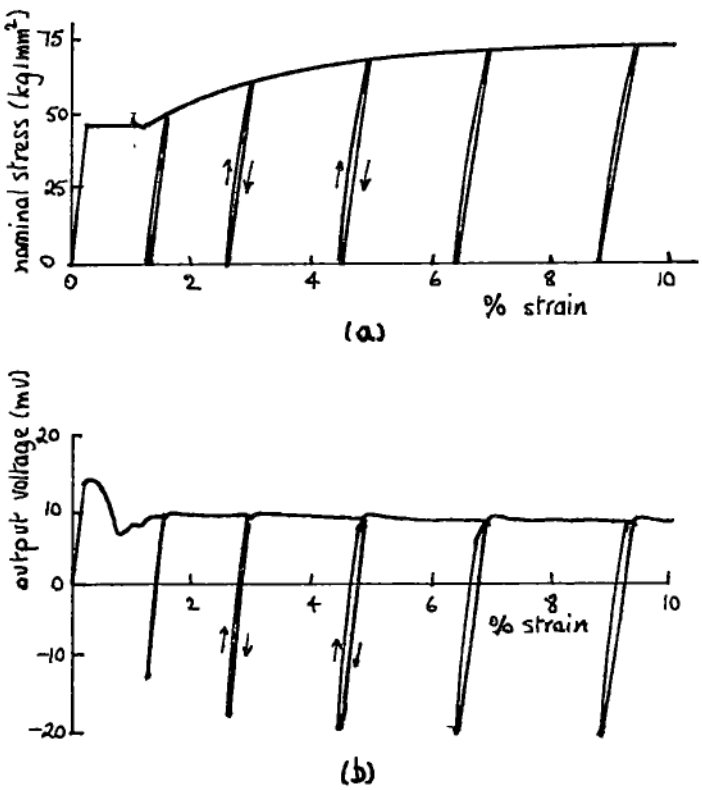

Figure 1.21 Plastic deformation by uniaxial tension on 0.49% carbon steel: (a) stress vs. strain (b) probe output vs. strain, [A7].

After this test, layers were removed from the surface by electrolytic polishing, and stresses were measured by the magnetic probe and by X-ray diffraction. Figure 1.22 shows the results. The stress was measured, by the

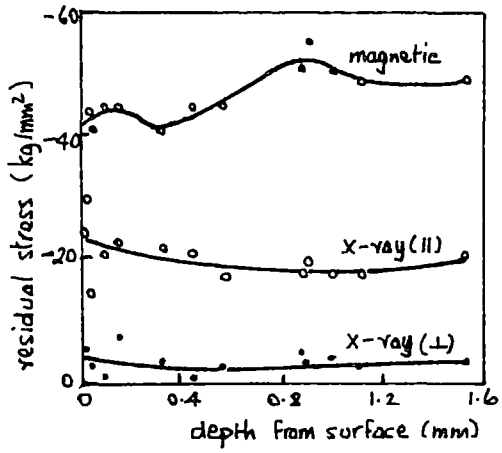

Figure 1.22 Residual stress distribution under the surface measured by magnetic and by X-ray methods. No correction has been made for the effect of the stress relief due to the polishing, [A7].

X-rays, parallel and perpendicular to the original direction of tension. The magnetic method (which gives the difference between the principal stresses) gave stresses of about 3 times the X-ray values. The same test on pure iron (0.01% carbon) gave very good agreement (2%) between the magnetic and X-ray stress-difference values.

The authors suggest that (for the 0.49% carbon steel) there is residual compression in the ferrite grains, balanced by residual tension in the cementite grains (surrounding the edges of the ferrite). Because the magnetostriction effect in ferrite is much greater than in cementite, the magnetic method measures a resultant compression. The X-rays measure compression because the stress gradients at the cementite boundaries are so high that the X-ray peaks are blurred. In contrast, in the pure iron with negligible cementite, both methods give almost identical results.

(2) H. Yamada et al [Y1,1981] describe an almost identical kind of probe with which they measured the depth of hardening on a structural alloy steel (type SNCM9). Figure 1.23 shows the basic arrangement. The cores are machined from 45% Permalloy. The exciting coils are wound with 800 turns (total for both) and carry 5mA at a frequency that is varied between 40Hz and 400Hz. The R.M.S. output voltage V_d from the coils on the detector core varies sinusoidally as the whole assembly is rotated on a magnetically anisotropic steel surface, just as in the previous case.

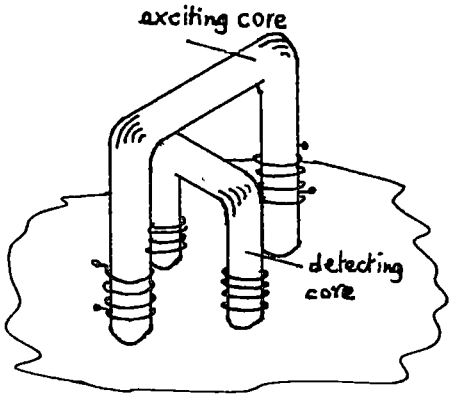

Figure 1.23 Yamada et al [Y1]: basic structure of magnetic anisotropy sensor.

An interesting aspect of this work is the use of a superimposed D.C. field (of about 6000A/m compared to 800A/m of the A.C. field). This reduces the dependence of V_d on the surface finish but still gives sensitivity to stress. Results are given to show how V_d varies with the depth of hardening, but these do not add anything of significance in the context of M.S.A. and so are not included here.

1.9 Recent Chinese research into magnetic stress analysis

As a result of correspondence with Mr.C.Ligong of Shanghai Jiao Tong University, Shanghai, I received a paper by Z.Haosen [H2,1984], describing some M.S.A. that was carried out in the Department of Materials Science and Engineering.

Neither the transducers or the electronics are described. However, the principle of the former seems to be the measurement of the inductance or impedance of a coil around a core whose magnetic circuit is completed by the steel under test. The coil is supplied with constant current, and if its reactance is much larger than its resistance, the change in voltage ΔV applied to the coil is proportional to the change in permeability $\Delta\mu$. ΔV is then converted to a corresponding current ΔI. Presumably the coil carries alternating current, since later on the fact is mentioned that the measuring depth is about 1.5mm at 50Hz.

The permeability is measured in two perpendicular directions, giving currents ΔI_x and ΔI_y - referred to from now on as I_x and I_y. Figure 1.24 shows how I_x and I_y vary with stress σ on a test sample of steel. Both uniaxial tensile and compressive stresses are applied. The type of steel is not specified. Figures 1.25a and 1.25b show the corresponding results for biaxial stresses. Figures 1.25c, d and e show the shape of the samples for the biaxial stress tests, and it is interesting to see that the one for the tensile - tensile test (1.25c) is almost identical to those I used for the same kind of test (see chapter 6). The thickness of the steel is not stated.

Polynomial curves are then fitted (by regression analysis) to the curves of figures 1.25a and b to obtain the following formulae for σ_x and σ_y in terms of I_x and I_y. Eight coefficients are used, and the equations are of the form

$$\sigma_x = A_1I_x + A_2I_y + A_3I_x^2 + A_4I_y^2 + A_5I_x^3 + A_6I_y^3 + A_7 + A_8I_xI_y$$

$$\sigma_y = B_1I_y + B_2I_x + B_3I_y^2 + B_4I_x^2 + B_5I_y^3 + B_6I_x^3 + B_7 + B_8I_xI_y$$

The A and B coefficients differ for different types of steel.

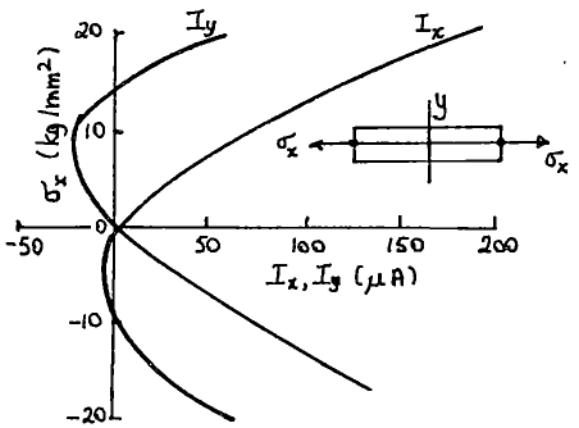

Figure 1.24 Haosen et al [H2]: stress σ_x vs. transducer output I_x (magnetisation parallel to stress) and vs. I_y (magnetisation perpendicular to stress)

Figure 1.26 shows a practical application: residual stresses, measured magnetically, on a pressure vessel (presumably at a weld).

The paper concludes that by making the two measurements at right angles to each other, and using the two equations, absolute values of

biaxial stresses can be calculated. There is no estimate of what the error in the technique might be, or of confirmation of the stress pattern of figure 1.26 by some other means.

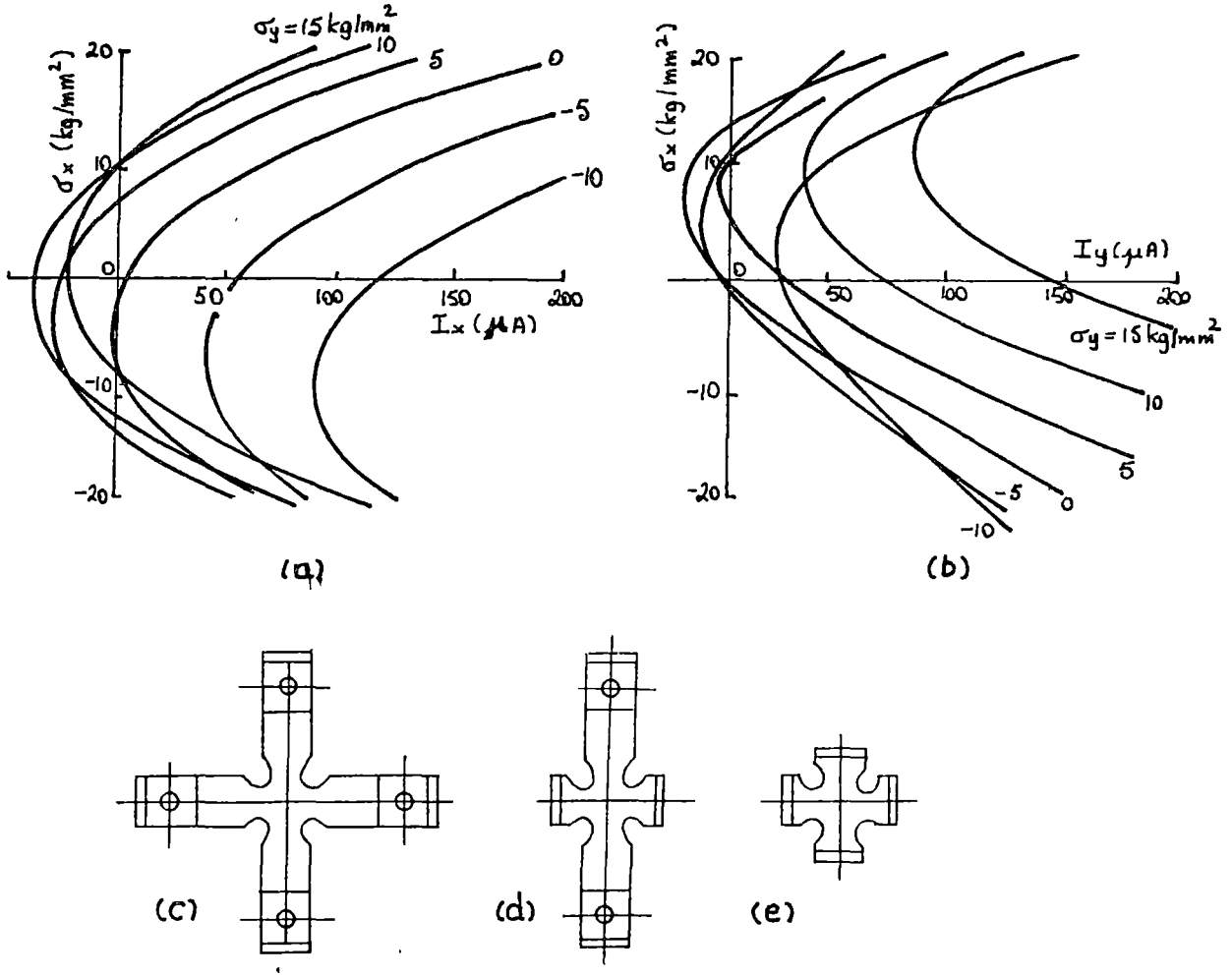

Figure 1.25 Biaxial stresses: (a) σ_x vs. I_x for various values of σ_y, (b) σ_x vs. I_y for various values of σ_y, (c) shape of sample for mild steel for tension-tension, (d) tension-compression, (e) compression-compression, [H2].

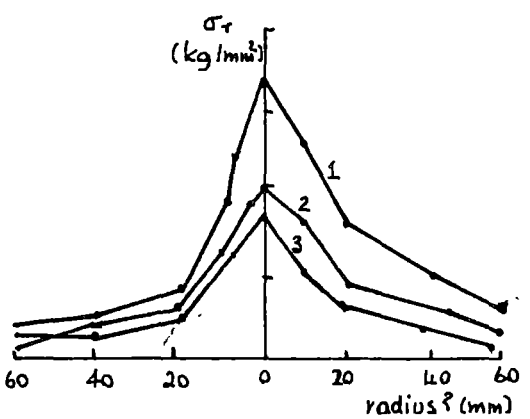

Figure 1.26 Residual stress σ_r vs. distance (radius?) from a weld in a pressure vessel, [H2].

1.10 Barkhausen noise

Gardener et. al. [G1,1971] of the Southwest Research Institute, San Antonio, Texas, have related Barkhausen noise (B.N.) to surface stress. Figure 1.27a shows the magnetising core and the signal coil on a steel sample that can be stressed as required; 1.27b shows the "electronically processed" Barkhausen signal during one complete cycle of magnetisation. Figures 1.28a, b, and c show relations between various B.N. signal parameters and applied stress. No details are given of the type of steel, the field strengths, the excitation frequency, the amplifier band-width, or of what the electronic processing involved.

A later paper by Barton et. al. [B4,1979] (also from the Southwest Research Institute) describes equipment for the routine testing of bearing races for the B.N. "signature". Figure 1.29 is a schematic representation of the stress measurement. Again, very little detail is given.

Some recent B.N. measurements are described by Kings [K2,1982], of the British Steel Corporation. He tested transformer laminations rather than structural steel. The idea is that since residual stress affects the core losses, then if the B.N. can be related to the stress it could be the basis of a quick check on the stress in the lamination. The patterns of R.M.S. noise over a cycle of magnetisation are not shown here since they are very like the trace of figure 1.27b. The distribution of noise pulses was found to be almost Gaussian. This attribute suggested the use of the standard deviation of amplitude as a means of quantifying the effects of stress in various regions of the magnetisation cycle. Figure 1.30 shows how the B.N. varies within the three regions of the B vs. H loop, for 3% Si-Fe. The maximum applied field was 800A/m, at a frequency of 0.15Hz.

Barkhausen noise has been used to detect plastic deformation of steel, and this is described in a paper by Karjalainen and Moilanen [K3,1980], of Finland. Figure 1.31a shows their transducer for magnetising the steel and detecting the B.N. The sample is 3mm thick 0.16% carbon steel. After

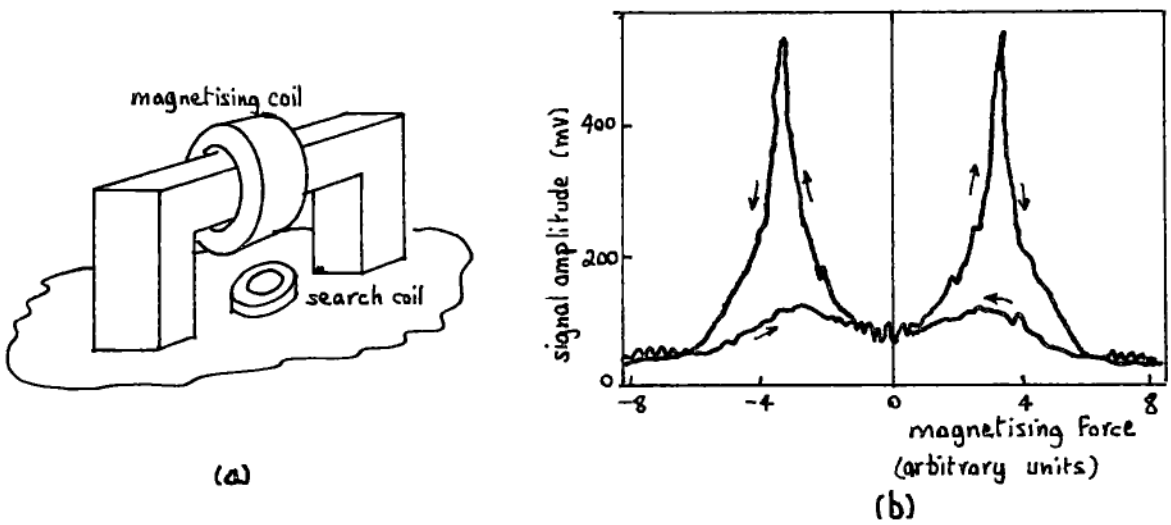

Figure 1.27 Gardner et al [G1]. Barkhausen noise measurement: (a) Magnetising core and coil, and signal coil on a steel sample, (b) "electronically processed" Barkhausen signal for one complete cycle of magnetisation.

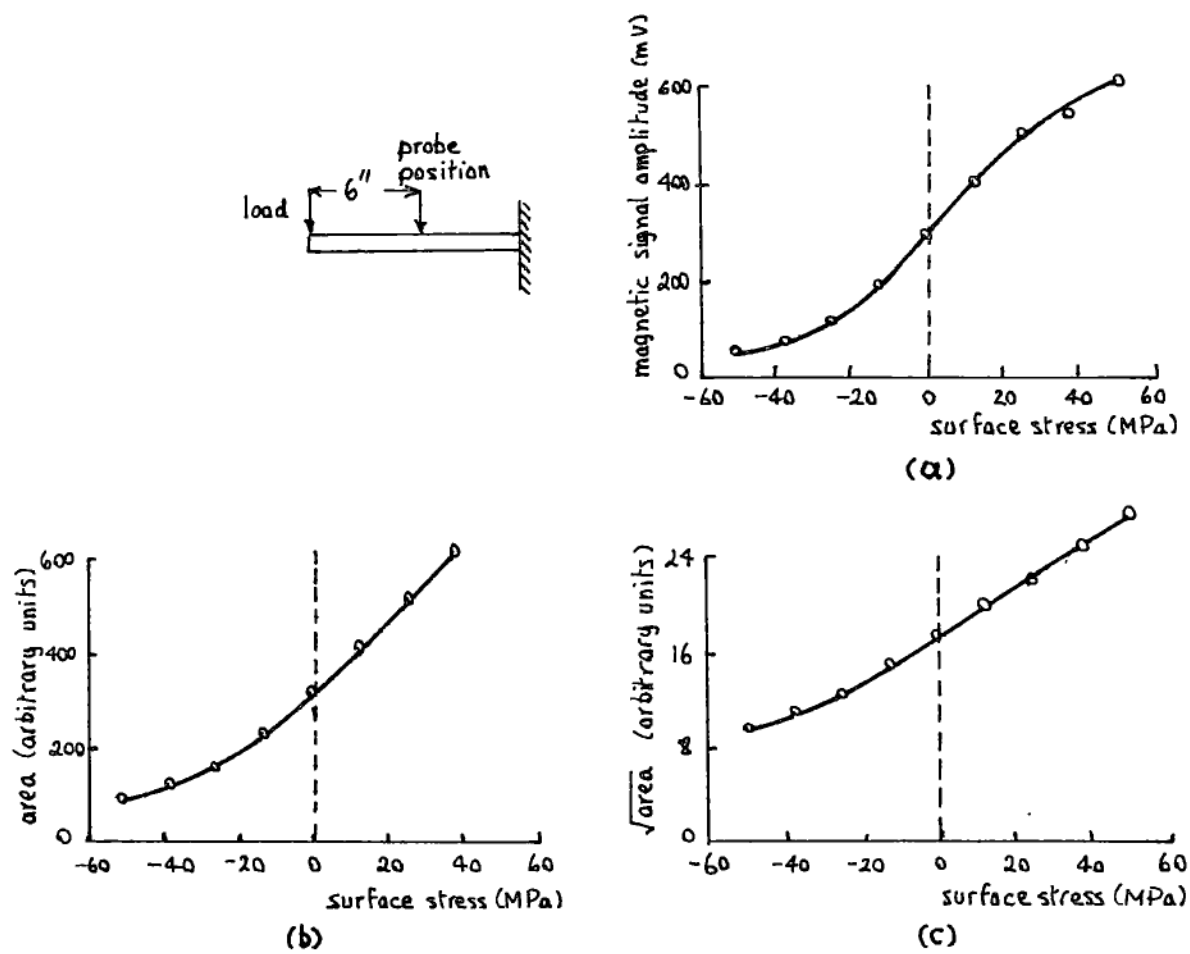

Figure 1.28 Correlation of Barkhausen signal parameters with the nominal surface stress of a loaded cantilever beam specimen: (a) signal amplitude vs. stress, (b) area under signal curve (see figure 1.27b) vs. stress, (c) area vs. stress, [G1].

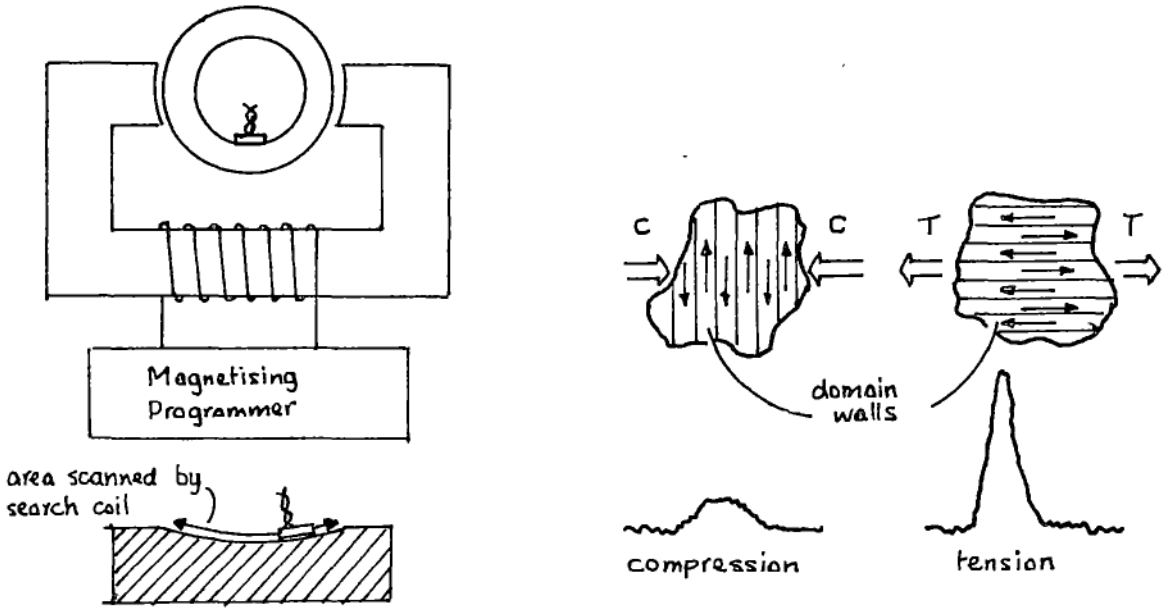

Figure 1.29 Barton et al [B4]: Barkhausen noise measurement on bearing races.

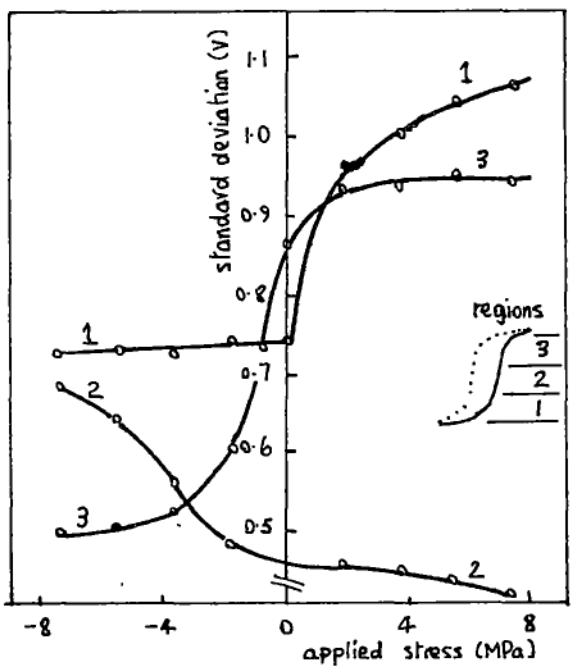

Figure 1.30 Kings [K2]: standard deviation of Barkhausen noise emanating from three regions of the magnetisation cycle, and its variation with stress, for transformer steel.

annealing at 890°C followed by slow cooling, conventional measurements give a lower yield strength of 280MPa. The B.N. is measured with an R.M.S. voltmeter of effective passband 2kHz to 100kHz. In the test the steel is stressed to a certain level, the load is released, and the B.N. is measured for magnetisation parallel (noise amplitude B_p) or transverse (B_t) to the axis of tension. Figure 1.31b shows the difference between B_p and its value B_{po} at zero stress, and also between B_p and B_t. There are slight changes in the B.N. before the yield point (280MPa), but at this point ($B_p - B_{po}$) decreases and ($B_p - B_t$) increases considerably. The change in ($B_p - B_t$) at the yield point is quite clear.

Ruuskanen and Kettunen [R3,1980] describe their use of the mechanical Barkhausen noise, as well as ordinary B.N., to detect the fatigue limit in commercial purity iron (0.004% carbon). The mechanical B.N does not need the steel to be magnetised and is produced when the stress in it changes. No details are given of the transducer. Figure 1.32 shows how the mechanical B.N. occurs during only part of a stress cycle at lower values of stress, but that it occurs during all of the cycle at higher stresses above the fatigue limits.

(Note that the mechanical B.N. is not quite the same thing as acoustic emission, which is the ultrasonic noise produced in materials as the stress in them changes. Both may be produced by the same phenomena - movement of domain walls - but they are detected differently).

A lot of information, including some theory, on the measurement of B.N. is in a paper by Saynajakangas [S3,1974], (also from Finland). His particular interest is the relation between B.N. and the size of the grains in steel, rather than stress, but the transducers and the measurement techniques are the same.

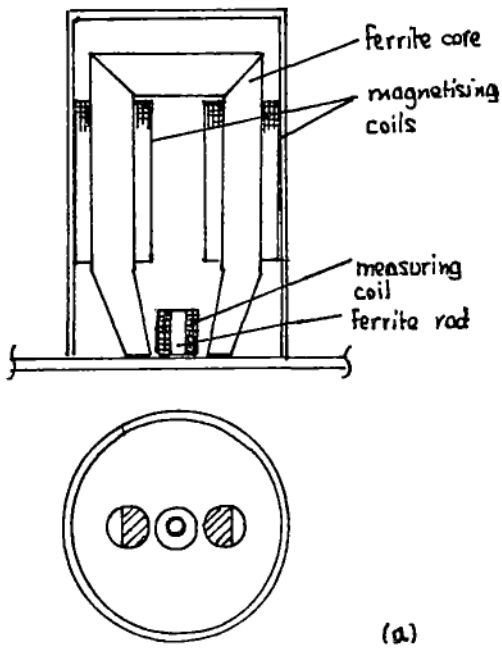

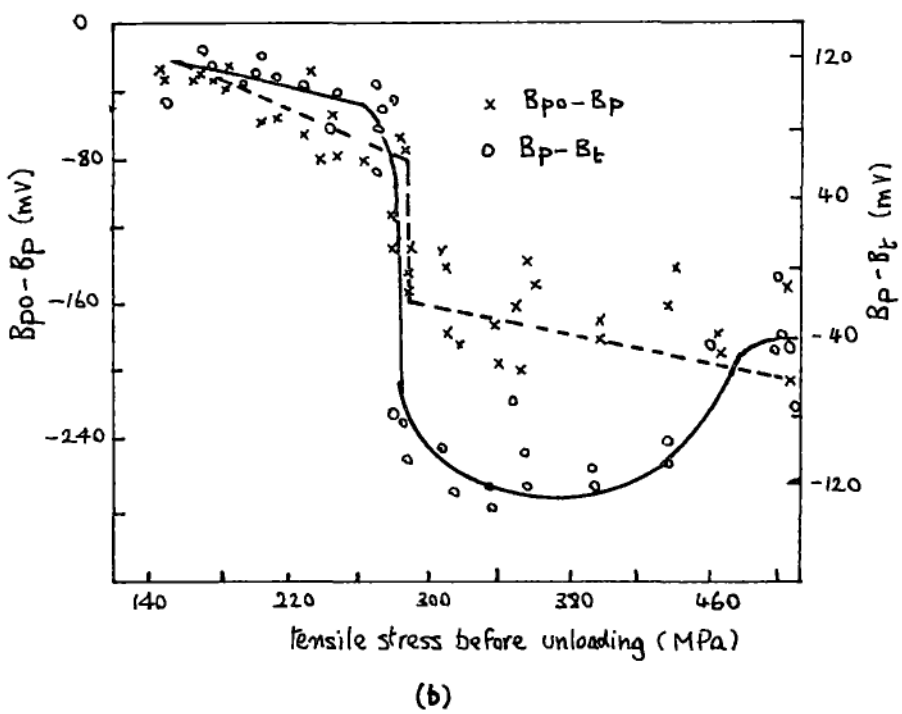

Figure 1.31 Karjalainen and Moilanen [K3]: Barkhausen noise and plastic deformation for mild steel: (a) transducer details, (b) B.N. for magnetisation parallel (B_p) and transverse (B_t) to the axis of tension.

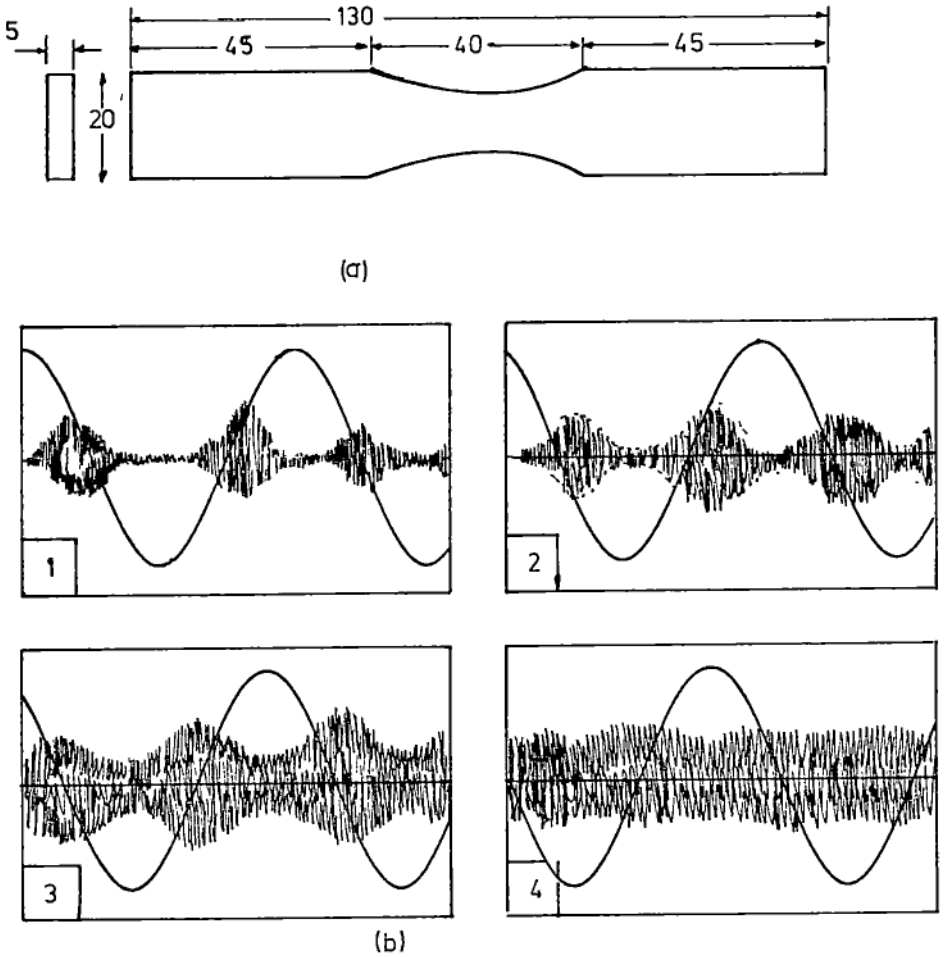

Figure 1.32 Ruuskanen and Kettunen [R3]: mechanical Barkhausen noise: (a) dimensions of fatigue test specimens, (b) mechanical B.N. bursts induced during cycling at constant peak applied stresses, of amplitude (1) 70MPa at 15Hz, (2) 90MPa at 15Hz, (3) 120MPa at 10Hz, (4) 180MPA at 3Hz.

1.11 Stress in buried pipelines

This section and the next one deal with the measurement of magnetic properties to detect stress in particular items: firstly in gas pipelines, and secondly in railway lines. They are included because the techniques involved differ somewhat from those already dealt with.

Atherton et. al. [A2,1983; A4,1984] of the University of Kingston, Ontario, Canada, describe their measurement of residual magnetic field of a steel pipe and its variation with applied stress. The aim of this work is to compare the magnetic field around a gas pipeline before and after it has been buried. A change in the field pattern could indicate that the stress

has been altered, perhaps by soil movement; since the pipe would also be stressed by the pressure of the gas in it, any extra stress could be dangerous.

Preliminary (laboratory) measurements were made, with a magnetometer, on 100mm diameter pipes at distances up to 3m from the pipe. They found that the residual magnetism of a particular pipe is not greatly affected by its orientation (i.e. the earth's magnetic field could be ignored) but is significantly affected by an applied stress produced either by bending or by internal pressure. The magnetisation patterns are complicated and are not shown here. A pattern can be thought of as a "signature" for a particular pipe, and it is the change in the signature that is significant rather than the signature itself.

A slightly different method of detecting stress changes by means of the corresponding change in magnetic properties is also being studied. The inside of gas pipelines is checked periodically by an inspection instrument called a pig. This travels slowly through the pipe, magnetising it, and recording the leakage flux as a guide to internal defects such as cracks or corrosion. (Eddy current techniques are also used at the same time). Corrosion on the outside of the pipe decreases the thickness of the metal and so could cause local changes of stress. Atherton [A3,1983] has looked at how such stress can alter the residual magnetism of the pipe after it has been magnetised by an inspection pig. Since the corrosion of interest is on the outside of the pipe and the effect of it is detected on the inside, he calls this technique stress-shadow magnetic inspection.

1.12 Stress in railway lines

If continuously welded rail gets too hot it may buckle due to thermally induced compression in it. A recent technique developed by the Polish State Railways uses the change in coercivity as a guide to the stress in the rail. Details of this are confidential and nothing had been published up to mid 1984. Mr R. Lewis, of the British Railways Board Research Department, prepared the following description for me.

"The method is based on the elastomagnetic effect and relies on measurement of the coercivity both along the rail axis (H_{cp}) and vertically at right angles (H_{cn}). The difference between these two values of coercivity is sensibly linear with respect to the force in the rail, when measured on the web of the rail. Since the value of coercivity is independent of air gap (a parameter that cannot be controlled on rusty rail), this is the parameter chosen. The measured quantity is $2H_c = H_{c1}-H_{c2}$ where H_{c1} and H_{c2} are the positive and negative values of coercivity of the B vs. H loop. The measuring system employs search coils to detect the point of zero flux and this causes the current in the magnetizing coils to be sampled and hence the coercivity noted. Figure 1.33a shows the coil and C-core measuring H_{cn}. For H_{cp} the core is rotated through 90°. The magnetic flux passes through the rail and there is therefore no problem of penetration. The coils are arranged in a feedback system, as shown in 1.33b, which ensures that the flux density is sinusoidal. An induction level of 1 Tesla consumes 85 watt. Figure 1.34a shows the way in which tensile and compressive stresses affect the B vs. H loop. Peak flux density is kept constant. We define the differential relative permeability as $\Delta H_c = H_{cp}-H_{cn}$. H_{cp} and H_{cn} tend to vary non-linearly with stress, but ΔH_c is sensibly linear, as shown in figures 1.34b and c. These graphs are for open hearth steel before heat treatment".

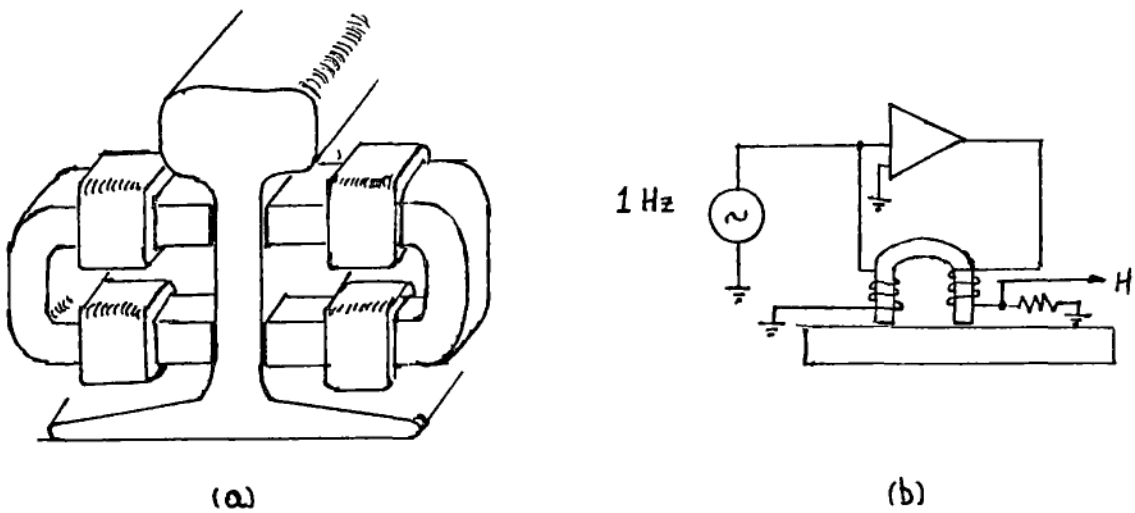

Figure 1.33 Magnetic measurement of stress in railway lines: (a) position of magnetising C-cores on the web of the rail for measuring H_c, (b) feedback to ensure sinusoidal flux density.

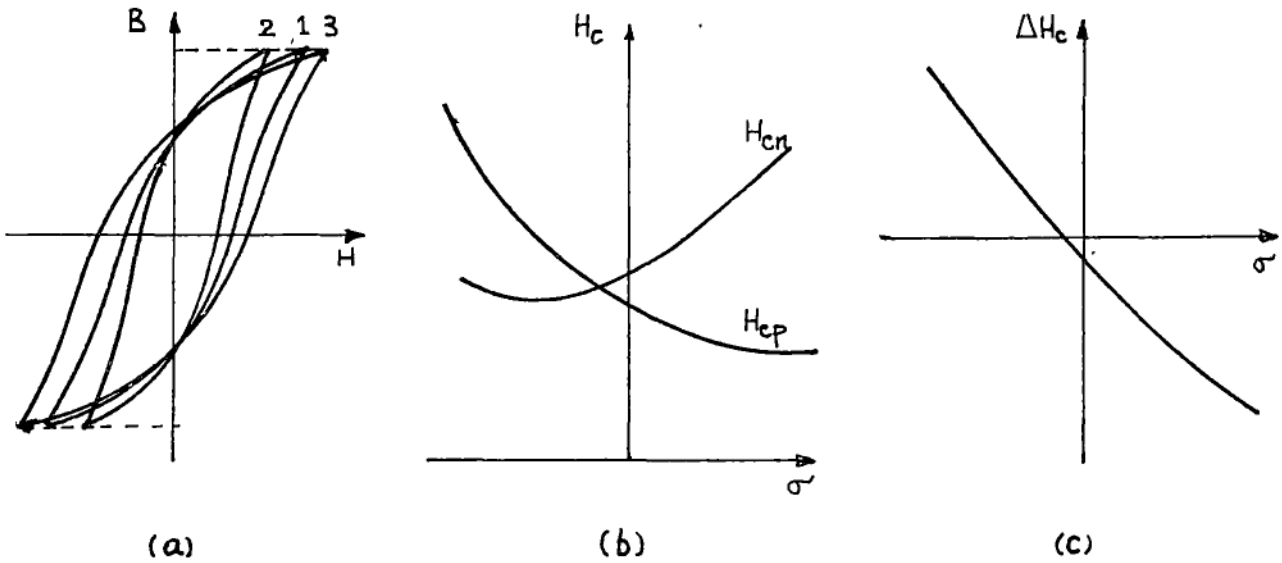

Figure 1.34 The effect of stress on the coercivity H_c of rail steel: (a) B vs. H loops at constant peak flux density but different stresses: (1) no stress (2) tension (3) compression, (b) H_c vs. stress σ for magnetisation parallel (H_{cp}) and perpendicular (H_{cn}) to the axis of the rail, (c) differential coercivity ΔH_c ($=H_{cp}-H_{cn}$) vs. stress.

1.13 Stress estimation by means of a combination of magnetic properties

The previous sections have dealt mainly with the relation between one particular magnetic property and stress. Recent research in Germany by Theiner and Altpeter [T1,1983] has studied the use of combinations of magnetic properties in order to estimate stress. As an example, figure 1.35 shows the relations between (a) coercivity H_c vs. stress σ, (b) Barkhausen Noise M_{max} vs. σ, and (c) incremental permeability μ_{inc} vs. σ, for different hardnesses (HV10) of SA508Cl2 steel. The differing hardnesses imply differing microstructures, obtained by heat treatment, for steel of the same composition. The point is that since M_{max} and μ_{inc} depend on microstructure as well as stress, the effect of these two variables must be separated. Since H_c does not vary significantly with stress its value can be used, for this steel, to determine the microstructure. Once this is done μ_{inc} and M_{max} can be used together to estimate the stress. (Note that the units used for μ_{inc} are A/m, which is puzzling).

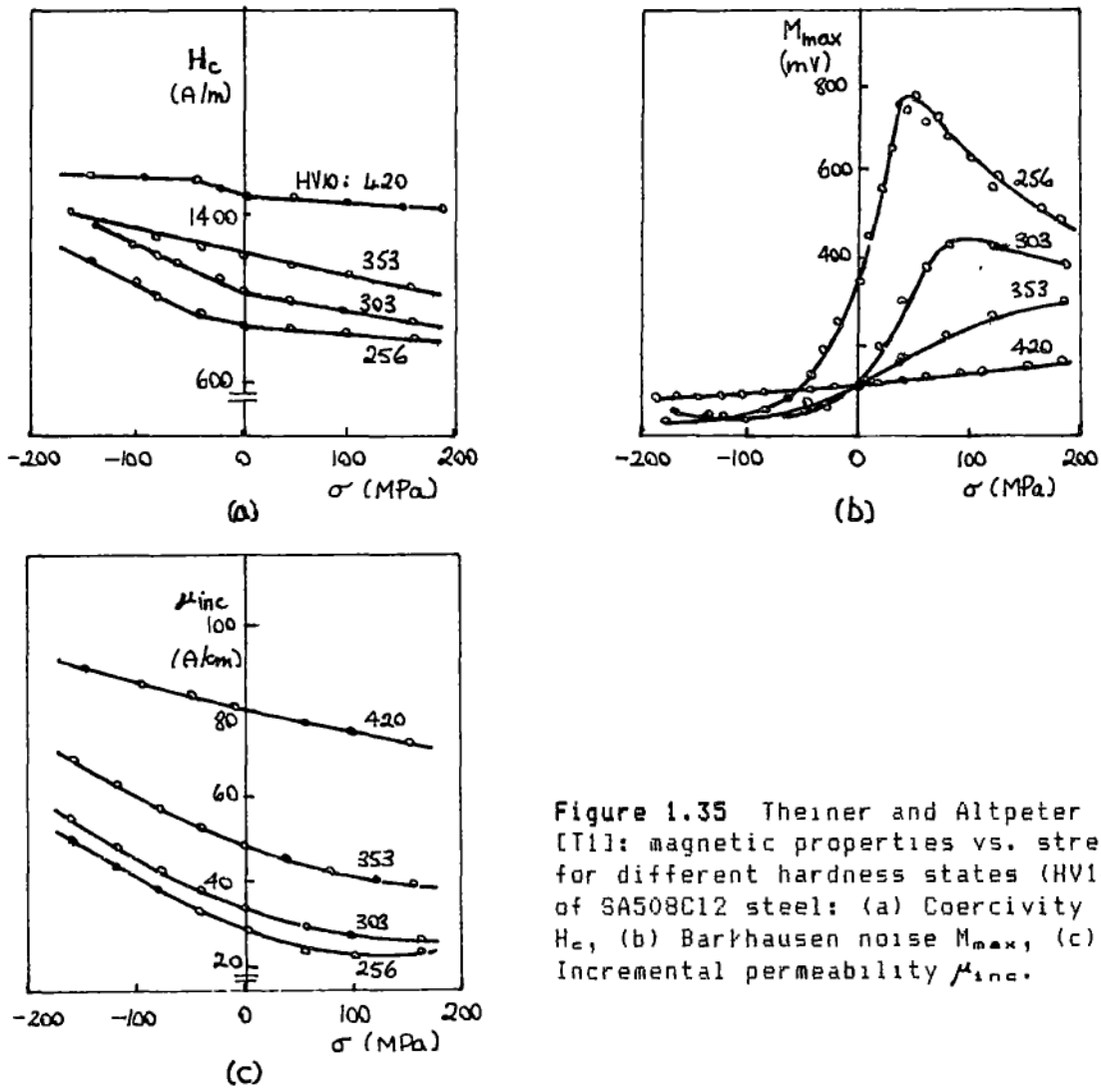

Figure 1.35 Theiner and Altpeter [T1]: magnetic properties vs. stress for different hardness states (HV10) of SA508C12 steel: (a) Coercivity H_c, (b) Barkhausen noise M_{max}, (c) Incremental permeability μ_{inc}.

A companion paper by Hauk et. al. [H3,1983] makes a comparison between X-ray, ultrasonic, and magnetic techniques of measuring stress. Each method tends to give a different result. This is not to imply that two, or even all, methods are wrong; the problem is that they look at different combinations of macro and microstresses. Cullity [C4] first drew attention to anomalous results of X-ray and magnetic stress measurements, but only recently have other attempts been made to explore and understand what is going on.

CHAPTER 2

INTRODUCTION TO PART II AND SUMMARY OF ITS CONTENTS

The aim of my research was to develop an instrument, for use in industry, that would measure stress in steel. The review of magnetic stress analysis in part I shows that there have been several attempts to do this (or, at least, to relate magnetic properties to stress), often for a particular application rather than for general use. What has been conspicuous is a lack of theory to go with experiment.

I was impressed with the one exception to this - the torquemeter of Barton and Ionides - on two accounts: (1) it is supported by theory that agrees with the experimental results to within 10%, and (2) the particular means that is used for detecting stress is a true null method. By this is meant that B and H are parallel in the absence of anisotropy (caused by stress) and so the output of the search coil is zero (figure 1.7). Only when H is not parallel to B does the search coil give an output. By comparison, for example, the change in reluctance (due to stress) tends to be quite small compared to the unstressed value. Worse still, its measurement with a U-core includes a dominant component of reluctance that depends on the air-gap; something that is notoriously difficult to keep constant or to allow for in other ways. With this in mind I adapted Barton and Ionides' method to work from one side of a flat piece of steel.

Figure 2.1 shows the essential parts. Alternating current in the magnetising coils around the poles of the U-shaped core sets up flux in the core and in the steel. The direction of the magnetic field at the surface is detected by a sensor that is usually a search coil. The coil's axis is fixed at 90° to the axis of the U-core. On isotropic steel the field H at the surface of the steel is at $\theta = 0°$; still parallel to the axis of the core as shown in figure 2.2a. The search coil has zero voltage induced in it.

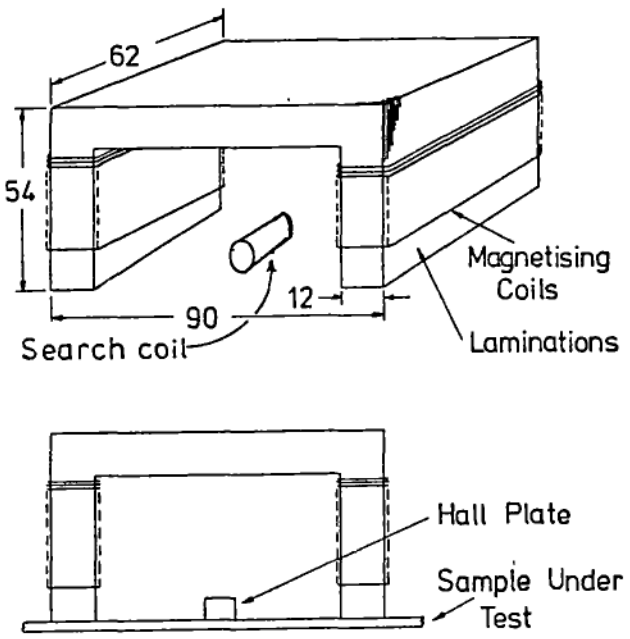

Figure 2.1 Prototype transducer for magnetic stress analysis.

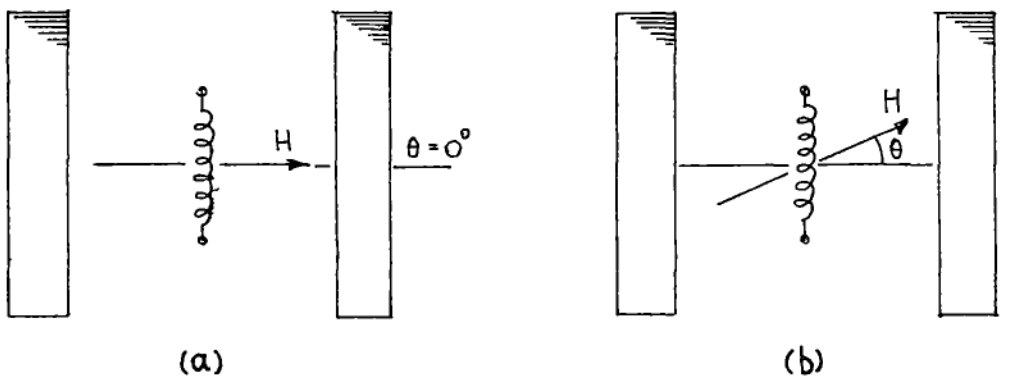

Figure 2.2 Detection of rotation of magnetic field H.
(a) steel isotropic: search coil output is zero,
(b) steel anisotropic: output is proportional to $H\sin\theta$.

Anisotropy in the steel causes a shift θ in the direction of H, that is detected by the voltage induced in the search coil, as in figure 2.2b. I called this layout the rotation rig.

Tests with the rotation rig on mild steel that was under tension to make it anisotropic showed a much larger rotation ($\theta >> 2^{o}$) than Barton and Ionides had measured. Also, the waveform of the voltage in the search coil was distorted and could not be explained. Further study of these two

aspects led to the derivation of a simple equation relating θ and the permeabilities in the direction of principal stresses, which was verified experimentally by tests on a silicon iron lamination and on mild steel sheet. This work is described in chapter 3; it also forms the basis of paper RL1. (The topics in chapter 3 have been selected from RL1 so as to show only the essential aspects of what was done; more details are in RL1). In this case the use of stress was only to vary at will the anisotropy of the steel. As such this work is not part of the main aim of the research, since the anisotropy could in theory have been produced by a means other than stress.

Chapter 4 describes some of the equipment and instrumentation used to obtain B vs. H data, including some large Helmholtz coils that cancelled out the earth's magnetic field to better than 1%. A "local" method of measuring B vs. H loops (i.e. that works from only one side of the steel) called the C-core rig is also described. This is rather an approximate technique compared to the conventional permeameter but it did enable changes of B vs. H loops to be compared, and avoided drilling small holes in the steel under test.

The rotation rig was then refined from the original one of figure 2.1, the main aim being to make it much smaller so that it would look at as small an area of steel as possible and thus give greater resolution of stress gradients. At the same time the signal processing was improved. Chapter 5 describes this work and also provides a comparison of the characteristics of different designs of rotation rig on thin mild steel sheets and on thick mild steel sections. (The distinction between thick and thin steel is that the flux penetrates through thin steel with little attenuation but eddy currents in the thick steel cause significant attenuation). Chapter 5 also gives results of the rotation rig on steel at different temperatures.

Chapter 6 presents results obtained with the rotation rig for biaxial stresses; some B vs. H data is also given. The biaxial stress tests were

crucial in showing that the rotation rig output depends on the difference between the principal stresses, and that by itself it cannot measure absolute values of stress.

Chapter 7 gives some stress patterns that were measured with the rotation rig on a disc of steel compressed across a diameter, and compares them with the theoretical pattern. The results from the rotation rig are closely analagous to those of photoelastic modelling.

At this stage enough testing had been done to show that the rotation rig worked within its stated limitations, and so a prototype instrument was built. Further development was hampered somewhat by the lack of a quantitative theory between stress and rotation rig output or, more fundamentally, between stress and magnetisation. This led to my measuring (rather more accurately than C-core rig would allow), B vs. H curves and loops on mild steel under biaxial compression and tension for magnetisation parallel and perpendicular to stress. Search coils for this were threaded through small holes drilled in the steel in order to measure the change of the flux in the steel, but magnetisation was still by means of a U-core. This technique gives an accuracy in between that of the C-core rig and the permeameter.

About this time (1983) some new theory was proposed that involved the anhysteretic B vs. H curve, and so I repeated the tests in order to measure B vs. H curves for anhysteretic conditions. These are all described in chapter 8. (I also put forward, rather tentatively, an analysis to explain the measurements in the context of existing magnetomechanical theory. By no means all the effects could be predicted quantitatively, but one important aspect could. This is dealt with in chapter 13).

Chapter 9 looks at some tests on steel strained to beyond its yield point. Also given is a comparison between rotation rig and Barkhausen Noise measurements on steel as it was strained into the plastic region.

CHAPTER 3

MEASUREMENT AND THEORY OF ROTATION OF MAGNETISATION IN ANISOTROPIC STEEL

3.1 Theory of rotation of field strength

Tests with the U-core and search coils of figure 2.1 on mild steel and silicon steel (both under tension) showed that when they were magnetised parallel or normal to the direction of tension there was no shift in the direction of the field strength. The fact that the flux did not change its direction was checked by threading fine wire through 0.7mm diameter holes 30mm apart in each sample to form search coils that measure changes of flux parallel (SCp) and normal (SCn) to the tension, as shown in figure 3.1. On reversing the current in the magnetising coils of the U-core there was no significant voltage induced in SCn when the sample was magnetised parallel to the tension (ϕ = 0°), and none in SCp when magnetised normal to the tension (ϕ = 90°).

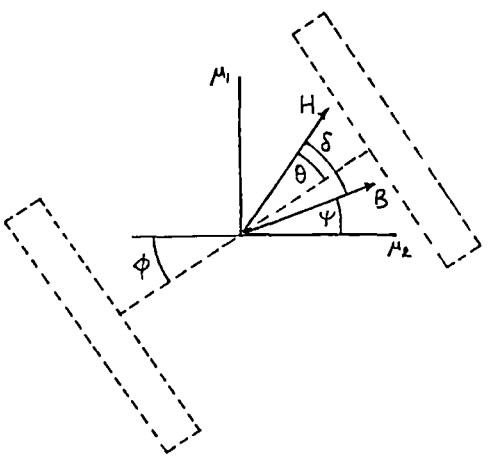

Figure 3.1 Positions of search coils and Hall plates relative to the poles of the U-core and to the tension direction.

Experiment showed, then, that there are two orthogonal directions, sometimes known as the principal directions [B5], such that along them B and H are related by the equations

$$B_1 = \mu_1 H_1, \quad B_2 = \mu_2 H_2$$

Correction: the drawing parts of figures 3.1 and 3.2b should be swapped.

(Tests on some strongly grain-orientated silicon steel showed that maximum and minimum permeabilities were not at right angles even when no tension was applied. The reason for this has not been adequately explained, but it is discussed in RL1)

Suppose that μ_2 is in the direction of maximum permeability and μ_1 is in the direction of minimum permeability, as shown in figure 3.2. If flux density B exists at angle ψ to the μ_2 direction it can be resolved along the principal directions

$$B_1 = B\sin\psi, \quad B_2 = B\cos\psi$$

and so

$$H_1 = (B/\mu_1)\sin\psi, \quad H_2 = (B/\mu_2)\cos\psi$$

The resulting field H is at an angle $(\psi+\delta)$ to μ_2, where

$$\tan(\psi+\delta) = (\mu_2/\mu_1)\tan\psi \qquad (3.1)$$

or

$$\tan\delta = [(\mu_2/\mu_1-1)\tan\psi/[1+(\mu_2/\mu_1)\tan^2\psi] \qquad (3.2)$$

If $\psi = 45^\circ$, equations 3.1 and 3.2 simplify to

$$\tan(45^\circ+\delta) = \mu_2/\mu_1 \qquad (3.3)$$

or

$$\tan\delta = (\mu_2/\mu_1-1)/(\mu_2/\mu_1+1) \qquad (3.4)$$

It follows from equation 3.2 that $\tan\psi$ has its maximum value when

$$\tan^2\psi = \mu_2/\mu_1 \qquad (3.5)$$

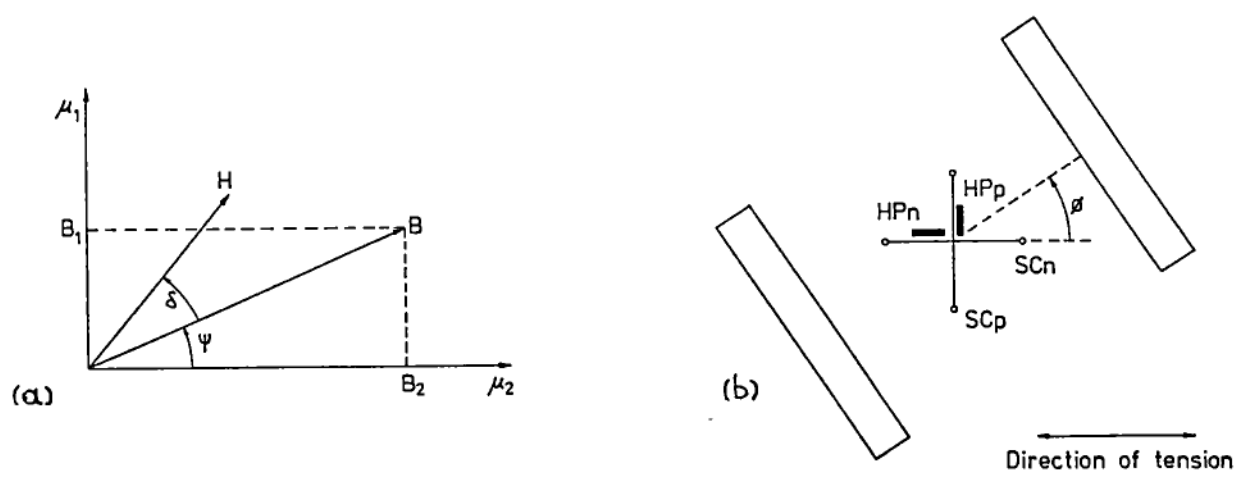

Figure 3.2 (a) Directions of B and H relative to the direction of maximum permeability μ_2, (b) the different angles used in the analysis of the rotation of magnetisation.

Equations 3.1 to 3.5 are now examined in detail to see what they imply. Firstly, in order to give a feeling for the numbers involved, values of δ are tabulated below for ψ between 0° and 90°, with μ_2/μ_1 taking the values 1.5, 4, and 10.

ψ°	μ_2/μ_1		
	1.5	4	10
		δ°	
0	0	0	0
10	4.8	25.1	50.4
20	8.6	35.5	54.6
30	10.9	36.6	50.2
40	11.5	33.4	43.2
50	10.8	28.2	35.2
60	8.9	21.8	26.7
70	6.4	14.8	17.9
80	3.3	7.5	9.0
90	0	0	0

Secondly, these points follow from the analysis:

(1) When an anisotropic ferromagnetic material is magnetised cyclically in a non-principal direction, B and H are in different directions. The ordinary scalar B vs. H loop cannot completely describe the relation between B and H; directions as well as amplitudes are necessary.

(2) When a flux density of known amplitude and direction exists the analysis requires that the value of μ_2/μ_1 relevant to the components B_1 and B_2 (see figure 3.2a) be known in order to calculate the amplitude and direction of H. If a number of B vs. H loops for the principal directions have been measured it should be possible to obtain correct values of μ_2/μ_1.

This becomes rather involved, one difficulty being that the direction of B may itself vary as the B vs. H loop is traversed, and will not generally be known. Clearly things are simplified if μ_2/μ_1 is constant for all values of flux density, which implies linear B vs. H "loops" of zero area. The directions of B and H should then be constant at all points on the B vs. H

loop. These criteria were very nearly satisfied by the silicon steel, but rather less so by the mild steed. Results of tests on both materials, that appear to verify the analysis, are given in section 3.2.

Note: The angle θ (defined in figure 2.2) through which the field is rotated relative to the U-core axis is not the same as the angle δ between B and H referred to in this analysis. B may not be parallel to $\theta = 0°$. Measurements to obtain the shift in direction of B as well as H are described in section 3.2; figure 3.2b shows the various angles involved.

3.2 Experimental verification of equation 3.2 with μ_2/μ_1 constant, ψ variable

The situation here is that the angle δ is measured only at the tips of a B vs. H loop (i.e. at the maximum values of B and H attained for the particular loop). B is kept constant in amplitude but its direction ψ relative to the principal direction μ_2 is varied by moving the core of the rotation rig at different angles ϕ to the direction μ_2.

Prediction of δ

The silicon steel, under tension, has almost constant permeability, for all necessary values of flux density, in both principal directions ($\phi = 0°$ and $90°$). Figure 3.3 shows the initial B vs. H curves for these directions (from the loci of tips of B vs. H loops). These were obtained using the U-core for magnetisation, and with two search coils SCp and SCn through holes in the sample and two Hall plates HPp and HPn, as shown in figure 3.1. (The U-core is not a conventional permeameter arrangement, and details of some errors associated with it are described in chapter 4). The value of μ_2/μ_1 varies from 5.6 to 7.1 and a mean of 6.35 is used to predict the variation of δ with ψ from equation 3.2: the result is shown in figure 3.4. (The dashed lines show the predicted curves for the extreme values of μ_2/μ_1 = 5.6 and 7.1).

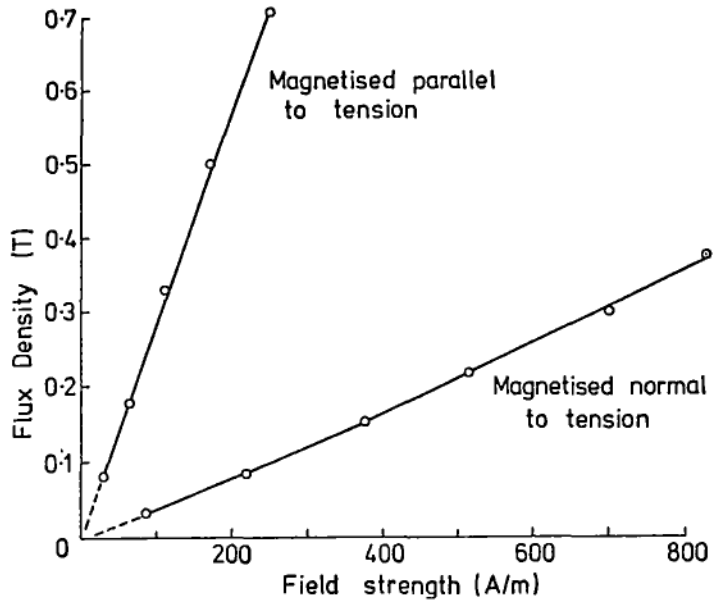

Figure 3.3 Initial B vs. H curves for silicon steel under 107MPa tension.

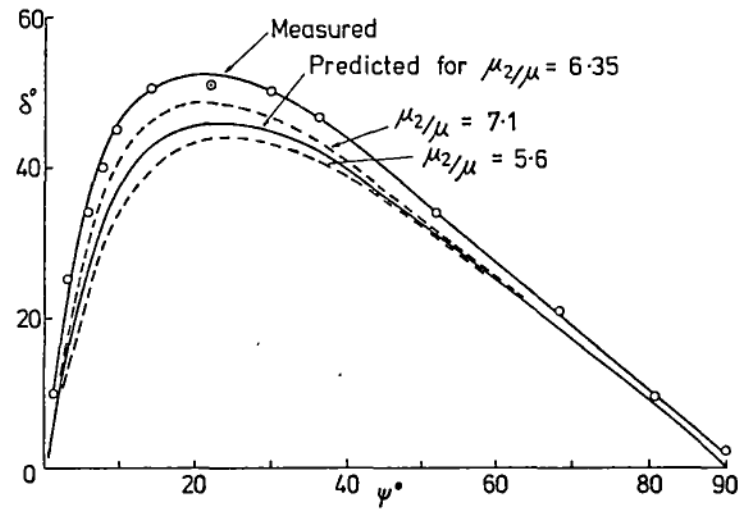

Figure 3.4 Verification of equation 3.2 for silicon steel: predicted and measured values of δ as ψ is varied.

Measurement of δ

The U-core was also used to measure δ for different values of ψ. The resultant flux density vector $B \angle\psi$ is calculated from the vector sum of B_1 (measured with SCn) and B_2 (measured with SCp). Unless $\phi = 0°$ or $\pm 90°$ the direction of B differs from ϕ, and is shifted towards the μ_2 direction (of maximum permeability).

The resultant magnetic field vector $H\underline{/\psi+\delta}$ is calculated from the two Hall plate voltages. In general the direction of H differs from ϕ and is shifted away from the μ_2 direction. The measured direction (δ) of H relative to B is also shown in figure 3.4.

Equations 3.1 and 3.2 predict only the angle of H relative to B. Figure 3.5 shows the measured directions of B and H for the silicon steel as the pole angle ϕ is varied. The actual directions of B and H depend on the geometry of the equipment. Constraints, such as would occur when a sample is in the form of a long thin strip (as in a permeameter) and B and H are forced to be parallel, would render equations 3.1 and 3.2 meaningless. The central part of the sample between the poles of the U-core is presumably free from such constraints.

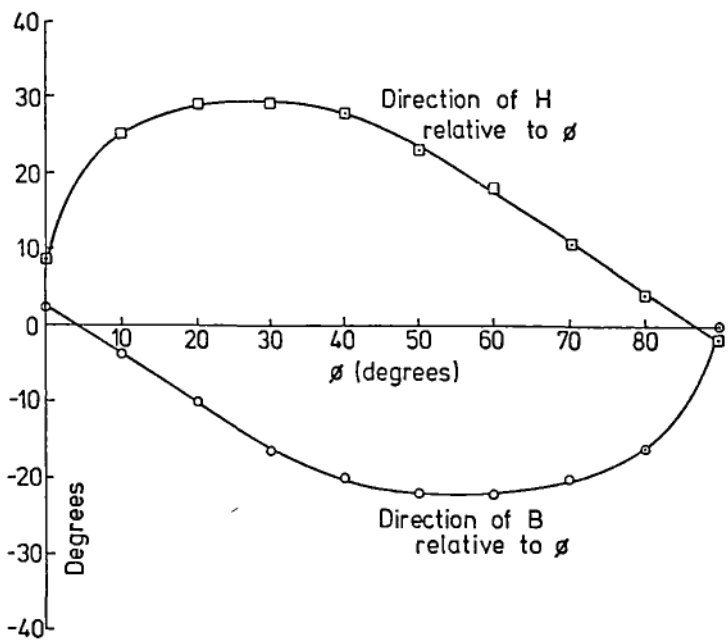

Figure 3.5 Silicon steel: measured directions of B and H relative to the poles of the U-core when they are at a varying angle ϕ to the direction of tension.

3.3 Experimental verification of equation 3.3 for a B vs. H loop of silicon steel

The situation here is that the position of the core is kept at an angle that makes the direction of B at the peak of a B vs. H loop at 45^{o} to the μ_2 direction, and the sample is then taken through a B vs. H loop. μ_2/μ_1 varies widely for both the mild steel and the silicon steel. The time-integrated outputs from the two search coils and the outputs from the two Hall plates were displayed one at a time, on an X-Y plotter, against the magnetising current. For identical values of magnetizing current, the direction and magnitude of B and H could then be calculated as the B vs. H loop was traversed.

Predicted direction of H

A peak value ($\hat{B}$) of 0.33T at 45^{o} to the μ_2 direction was chosen as the starting point. This required B vs. H loops measured in the principal directions with their peak values of $0.33\cos45^{o} = 0.33\sin45^{o} = 0.235$T in each direction. Figure 3.6 shows these loops, measured with the U-core. Figure 3.7 shows the predicted directions of B and H (dashed line). Note that in assuming the direction of B, the sense in which it switches from 45^{o} to the opposite direction is not known: it is drawn changing clockwise from 45^{o} to -135^{o} to agree with its measured directions.

Measured directions of B and H

Trial and error showed that the poles of the U-core had to be at 67^{o} to μ_2 to give B at 45^{o}. All four plotter traces are very thin loops of almost constant slope; figure 3.8. From these traces the direction of B was found to be 45^{o} (as required) and that of H 74^{o}, i.e. $\delta = 29^{o}$ for most of the perimeter of the B vs. H loop (the exception is at low values of B and H), as shown in figure 3.7. It can be seen that as B goes through its minimum value its direction relative to μ_2 decreases and turns clockwise through

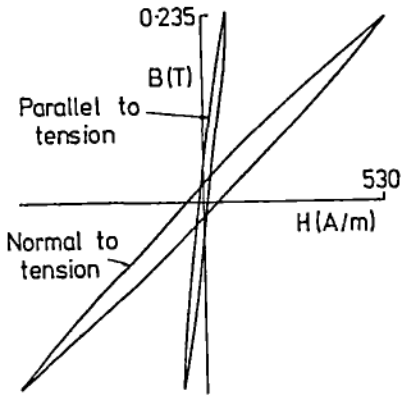

Figure 3.6 Silicon steel: B vs. H loops for the principal directions.

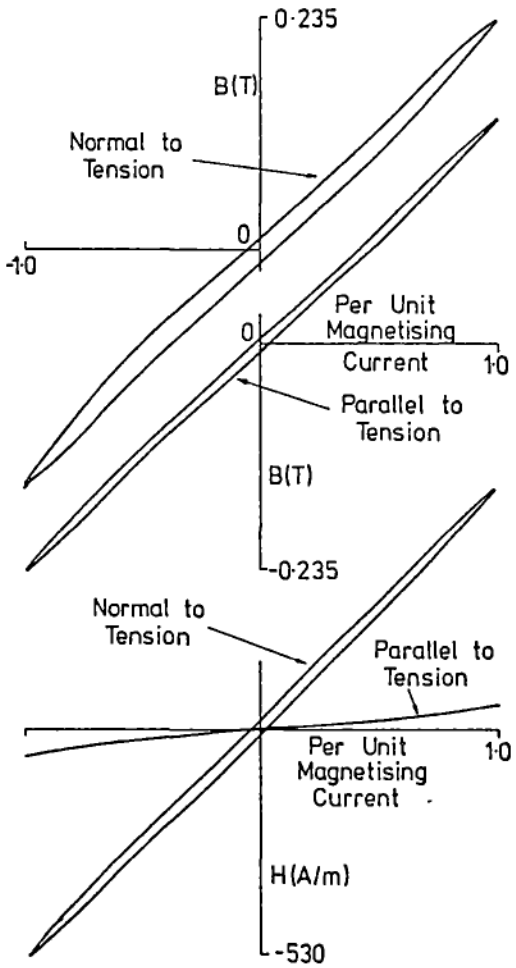

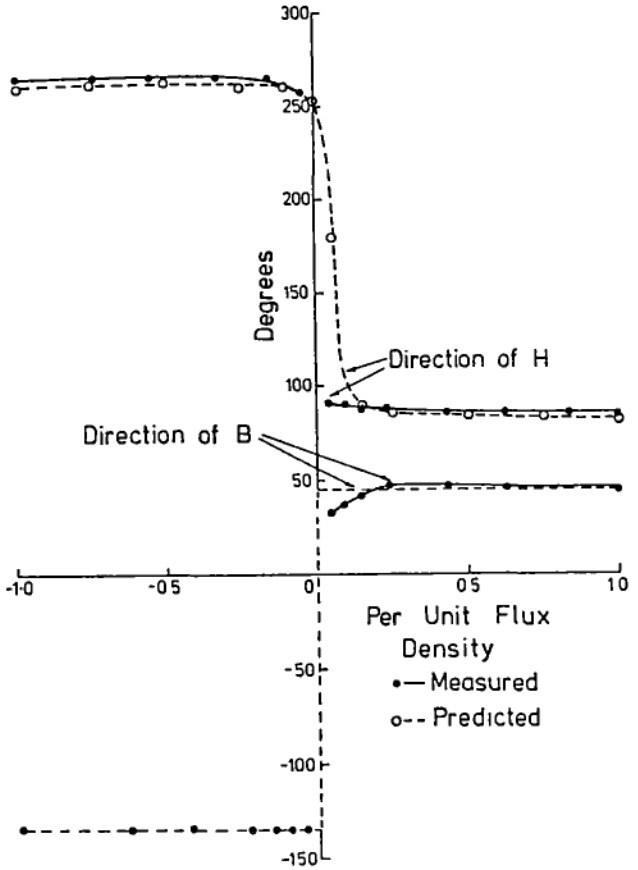

Figure 3.7 Silicon steel: predicted (- - -) and measured (——) directions of B and H for a B vs. H loop. The peak value of B was set at 45° to the tension.

Figure 3.8 Silicon steel: variation of B and H parallel and perpendicular to tension for a B vs. H loop.

180°, whilst the angle of H increases and turns anticlockwise through 180°. Hence as B increases to its peak negative value, δ is the same as it is for the peak positive value of B, but B and H have rotated in opposite sense to get there.

3.4 Experimental verification of equation 3.3 for a B vs. H loop of mild steel

Figures 3.9, 3.10, and 3.11 for the mild steel correspond to figures 3.6, 3.7, and 3.8 for the silicon steel. A peak flux density of 1.13T at 45° to the μ_2 direction was chosen, requiring B vs. H loops of 0.80T (peak) measured in the principal directions (figure 3.9). One problem is that since the angle between B and μ_2 is not constant over most of the B vs. H loop, then only one B vs. H loop for each principal direction is inadequate. Since μ_2/μ_1 varies with ψ, good agreement between measured and predicted directions of H should not be expected under these conditions. In the event, there was reasonably good agreement.

An interesting result from the XY plotter traces (figure 3.11) is that the magnitudes of B or H are never zero (but the components in the principal directions pass through zero in order to reverse). This is worthy of further study. Thus in figure 3.10 the measured values of B and H are shown as discontinuous at values of B below ±0.1 per unit.

3.5 Qualitative explanation of the directions of B and H for a B vs. H loop of mild steel

Figure 3.12 shows (on the left) B vs. H loops in the principal directions for mild steel. As the loops are traversed from peak positive to peak negative the following ranges of values of δ can be predicted:

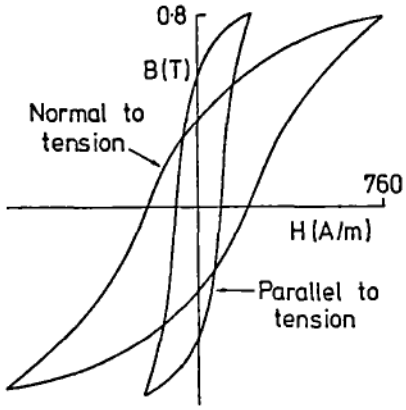

Figure 3.9 Mild steel: B vs. H loops in the principal directions.

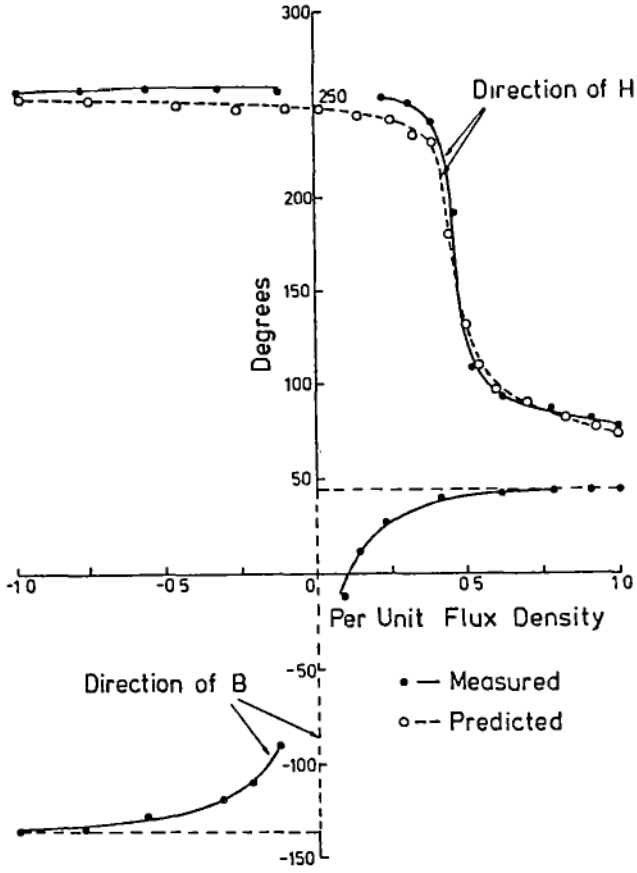

Figure 3.10 Mild steel: verification of equation 3.3; predicted (- - -) and measured (——) directions of B and H for a B vs. H loop. The peak value of B was set at 45° to the tension.

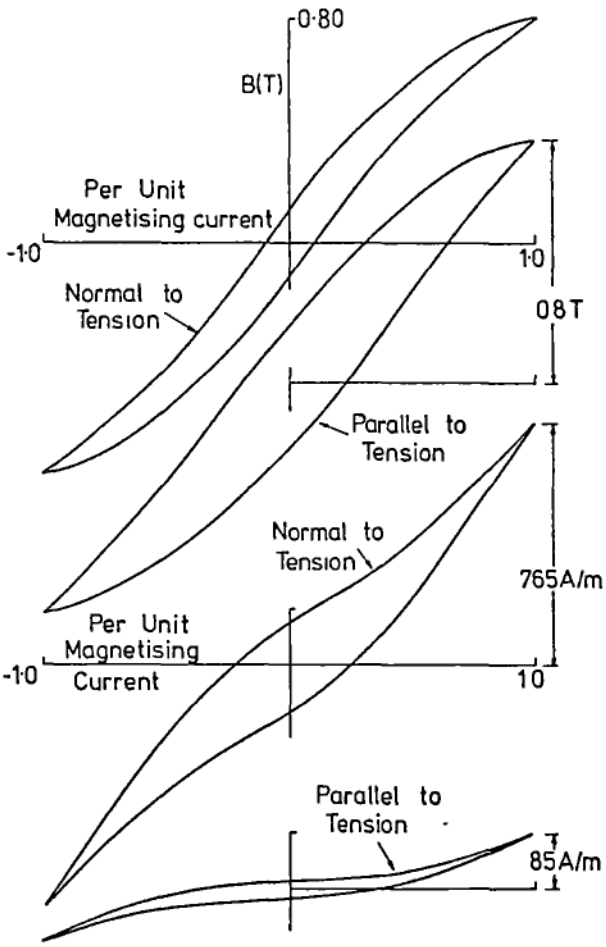

Figure 3.11 Mild steel: variation of B and H parallel and perpendicular to tension for a B vs. H loop.

Points A to C:

H_1 and H_2 are both positive and $H_1 > H_2$. Hence $0° < \delta < 45°$.

Points C to D:

H_1 positive, H_2 negative, and $H_1 > |H_2|$. Hence $45° < \delta < 90°$.

Points D to E:

H_1 positive, H_2 negative, and $H_1 < |H_2|$. Hence $90° < \delta < 135°$.

Points E to F:

H_1 and H_2 are negative, and $|H_1| < |H_2|$. Hence $135° < \delta < 180°$.

Points F to G:

H_1 and H_2 are negative, and $|H_1| > |H_2|$. Hence $180° < \delta < 225°$.

Between points A to G, B is positive. After point G, B goes negative.

Points G to J:

H_1 and H_2 are negative, and $|H_1| > |H_2|$. Hence $0° < \delta < 45°$.

The remaining set of six vector diagrams are the same as the first set turned through 180°.

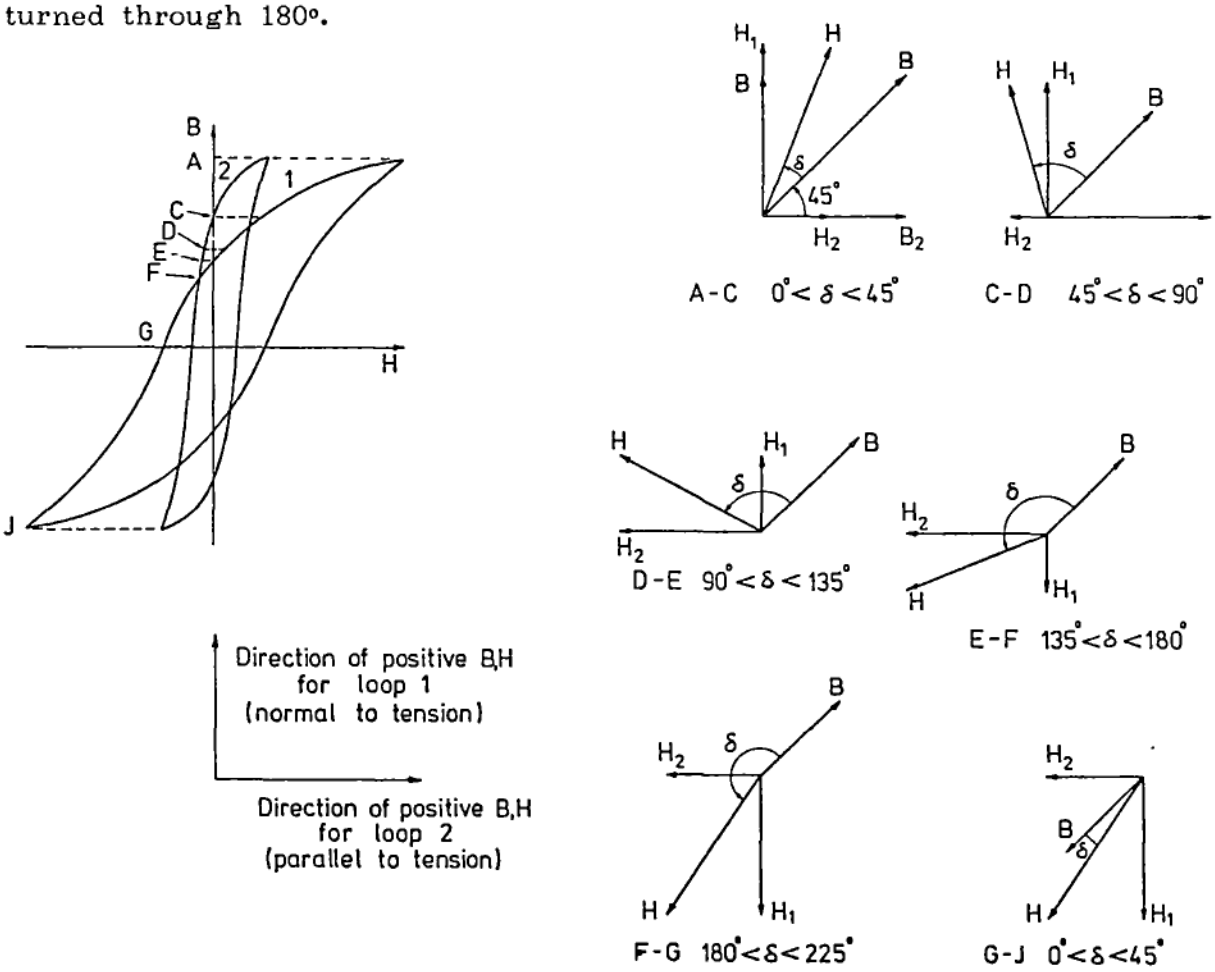

Figure 3.12 Mild steel: qualitative prediction of δ from the B vs. H loops for the principal directions.

3.6 Representation of the B vs. H vector relationship

Measurements on the mild steel sample show that neither B nor H become zero at any stage of the B vs. H cycle. One cannot therefore draw a conventional B vs. H loop on cartesian co-ordinates, since this forces B and H to pass through zero, and of course does not show their directions.

An alternative would be to use polar co-ordinates. The two curves in figure 3.13a show the measured values of B and H vectors for mild steel. The peak value of B is at 45° to the principal directions. Pairs of points with the same number, one on each curve, show corresponding values of B and H for one half of a B vs.H loop. Figure 3.13b shows the predicted values of B and H in the same manner. The line for B is now straight, corresponding to the assumption that B is constrained to be at 45° to the (principal) direction of maximum permeability.

3.7 Conclusions

(1) When an anisotropic homogeneous ferromagnetic material is magnetised at an angle ϕ to the direction of maximum permeability μ_2, the field strength H in the material is rotated by an angle δ relative to the flux density. δ is related theoretically to μ_1, μ_2, and ϕ by equation 3.2

$$\tan \delta = (\mu_2/\mu_1 - 1)\tan \psi / [1-(\mu_2/\mu_1)\tan^2 \psi]$$

in which μ_1 is the minimum permeability and is assumed to be in a direction perpendicular to μ_2. The criterion for applying equation 3.2 is that the permeability in intermediate directions vary sinusoidally from the μ_2 to the μ_1 direction.

(2) Equation 3.2 has been verified experimentally for samples of non-grain-orientated silicon steel and mild steel, both of which had been made anisotropic by tensioning them. The mild steel has significant remanence and coercivity when magnetised to about the kneepoint of the magnetisation curve, and equation 3.2 predicts that the angle between H and B in this case would vary by over 180°; this too was verified by measurement.

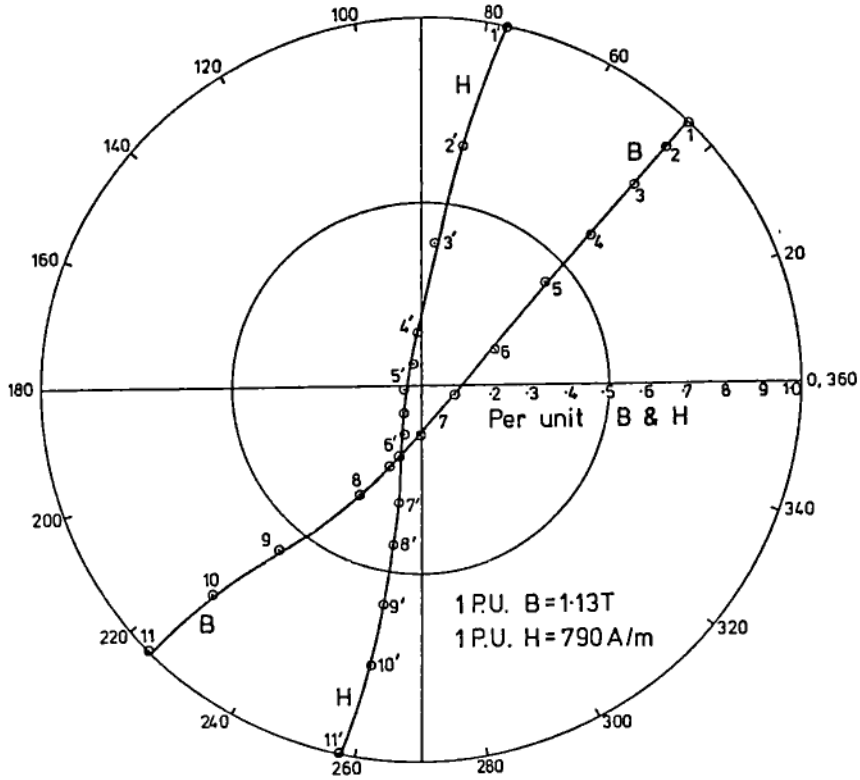

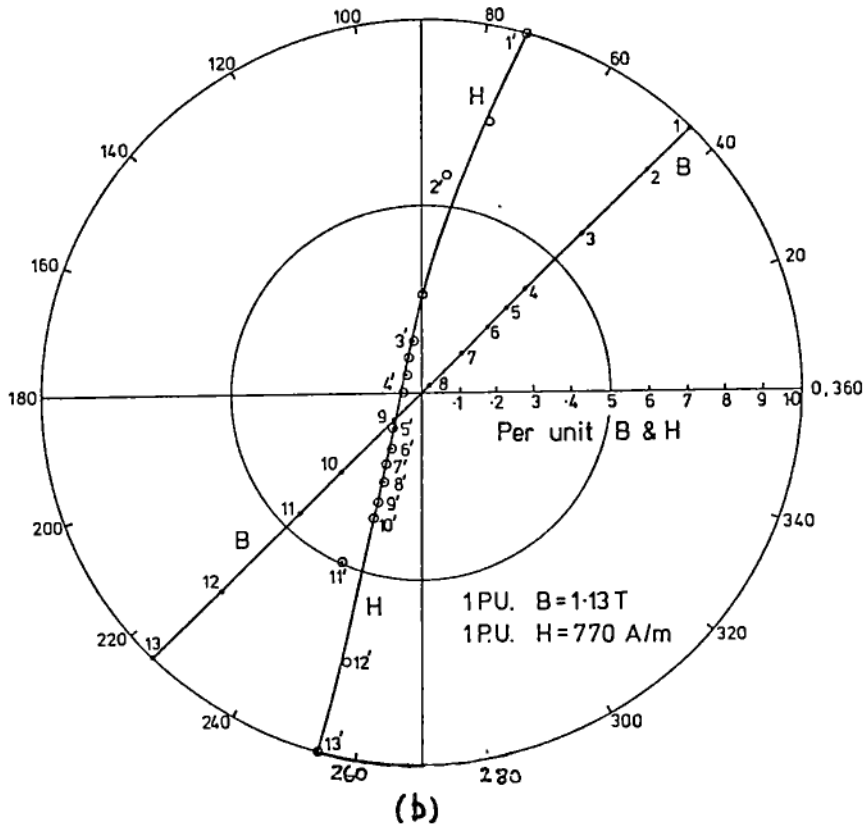

Figure 3.13 Mild steel: B vs. H loop drawn in polar coordinates. (a) measured, with the peak value of B at 45° to the tension, (b) predicted, with B assumed to be always at 45° to the tension.

CHAPTER 4

EQUIPMENT AND INSTRUMENTATION FOR B vs. H MEASUREMENTS

4.1 The C-core rig

Introduction

The accepted way to measure a B vs. H loop is with a permeameter. This requires in general that the sample be long and thin and have a search coil wound around it to measure change of flux. However, in order to make measurements of magnetisation at different directions on a stressed steel sample, a means of working from only one side of the sample is needed.

Wilkins and Drake [W2,1965] describe such a "local" method for the measurement of power losses at 50Hz in transformer laminations. The essential parts are shown in figure 4.1a. The three C-shaped cores are assembled from 0.2mm thick Mumetal laminations. Not shown are two search coils that are wound intimately with the magnetising coils but only on the central core. The outer cores act as guards to prevent the flux in the central core and in the laminations from spreading out sideways, so that the magnetic conditions in the lamination under the central core are substantially uniform.

The power loss in the shaded part of the lamination and in the central core is given by $VI\cos\phi$ (V = search coil voltage, I = current in the magnetising coil, ϕ = phase angle between them) measured with a suitable wattmeter. The use of a search coil in this way is known as the shadow coil technique, and excludes the copper loss of the magnetising winding. The loss just in the core is measured separately and then subtracted from the total to give only the loss in the lamination. The authors say that this method has an error of about 2% compared to the standard Epstein square method.

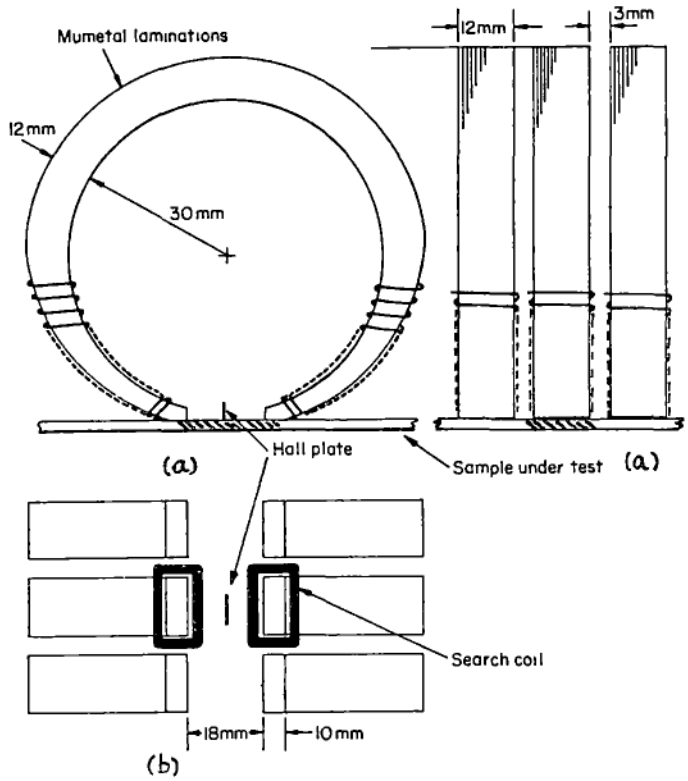

Figure 4.1 (a) The local loss tester of Wilkins and Drake, (b) Its modification to form the C-core rig in order to measure B vs. H curves.

Development of the C-core rig

I hoped to adapt this equipment to measure B vs. H loops. First attempts to make a local tester from mild steel cores of the same shape as above, and also from U-shaped cores of silicon steel, were a failure. Fortunately I was eventually able to get 150 of the specially shaped laminations from Mr. Drake at the National Physical Laboratory, U.K.

Modifications for B vs. H measurement were: (1) a Hall plate was fixed between the poles of the central core to measure field strength; (2) two search coils, each of 200 turns of 44 B&S wire, were put around the pole faces of the central core (instead of, previously, over the magnetising coils) to measure the flux entering the sample. These are shown in figure 4.1b which is the view from underneath. The air-gap between the poles and the lamination has to be as small as possible and so the three cores were

clamped together and their pole faces were carefully ground flat to within 0.01mm. The whole assembly was pressed lightly against the thin sample of steel while a measurement was taken. I called this local B vs. H tester the C-core rig (C.C.R.). The basis of this method, then, is that the flux through the search coils is approximately the same as the flux in the sample; hence the flux density can be inferred from the cross-section of the sample between the poles. The field strength at the surface of the sample is equal, to within 5%, to the value inside it.

Performance

The B vs. H loops are not exact; they contain errors when compared with "reference" results from a permeameter. The errors result partly from the flux that fringes through the air on the far side of the sample to the core faces but mostly from flux in the sample that spreads out sideways, despite the guard cores.

Figure 4.2a shows an example of initial B vs. H curves for untensioned mild steel, obtained with the C.C.R. on a 150mm wide sample, and also with the permeameter (using in the latter case a narrower sample, 52mm x 500mm). It can be seen that the flux density from the C.C.R. is greater than that from the permeameter by a factor that varies from 2.0 at low strengths to 1.3 between 300 and 600 A/m. At field strengths above 600A/m the Mumetal cores begin to saturate and apparent flux density in the sample increases rapidly relative to the (true) permeameter value. (The C.C.R. curve has also been drawn rescaled in this figure so that the lengths at 600A/m on the B axis are equal. The rescaled curve and the permeameter one are similar above 250A/m). Thus for values of H between 250 and 600A/m the values of B from the C.C.R. are greater than the permeameter values by a factor of about 1.3. Figure 4.2b shows the corresponding B vs. H loop. The C.C.R. flux density has again been rescaled to be equal to the permeameter value at 600A/m.

The errors in the C.C.R. can be summarised thus: it "sees" either too much flux or slightly too low a field strength, or both, by a factor (that varies with the value of field strength) of up to 2.

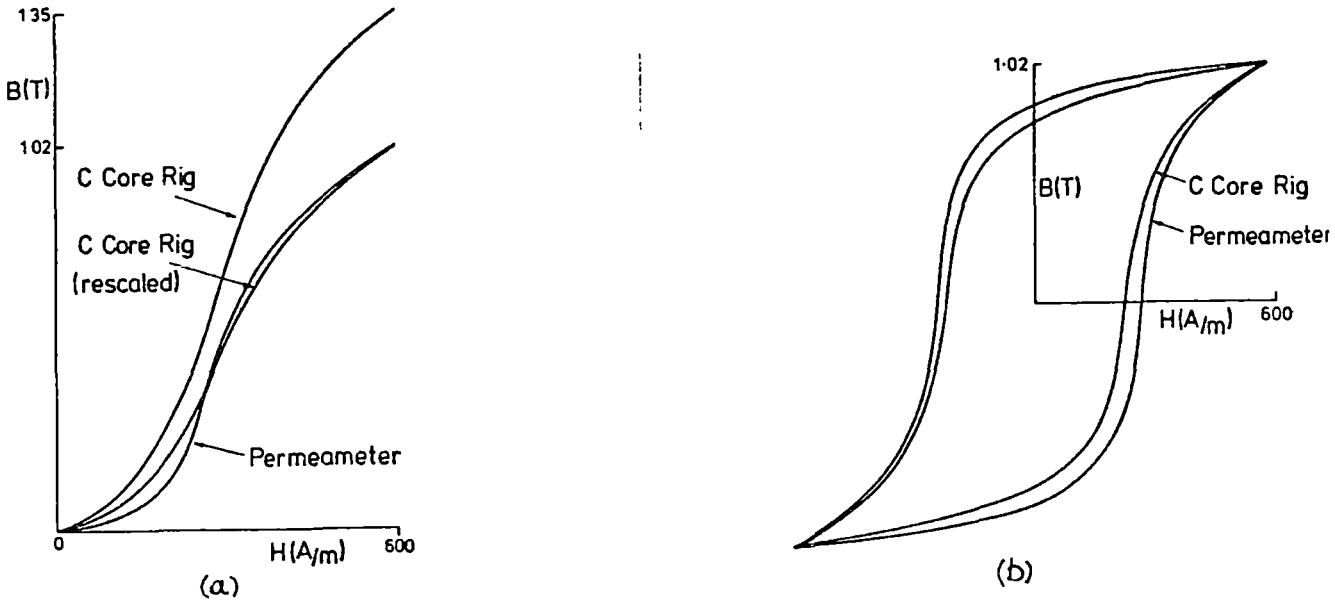

Figure 4.2 Comparison between the permeameter and the C- core rig on mild steel: (a) initial B vs. H curves, (b) B vs. H loop.

Tests to discover the source of error

(1) The effect of varying the air gap between poles and sample.

Figure 4.3 shows values of B and H as the air gap is varied from 0 to 0.15mm. The sample is a 52mm x 350mm long piece of steel 0.42mm thick. This test was not intended to contribute directly to an understanding of the errors - it was merely to establish the sensitivity of B and H to small variations in the air gap such as would occur if the sample was not quite flat.

(2) Core flux and sample width.

A 0.34mm thick silicon iron lamination was cut into samples of width varying from 50mm to 150mm. Figure 4.4 shows the B vs. H curves for

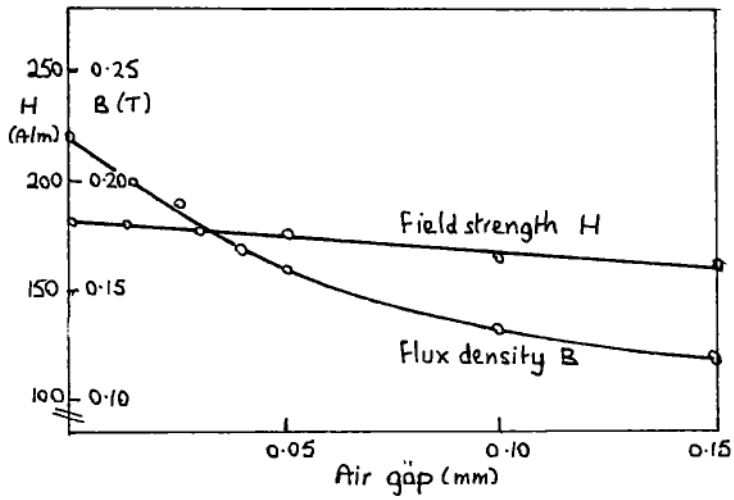

Figure 4.3 The effect of varying the air gap between the C-core rig and the sample.

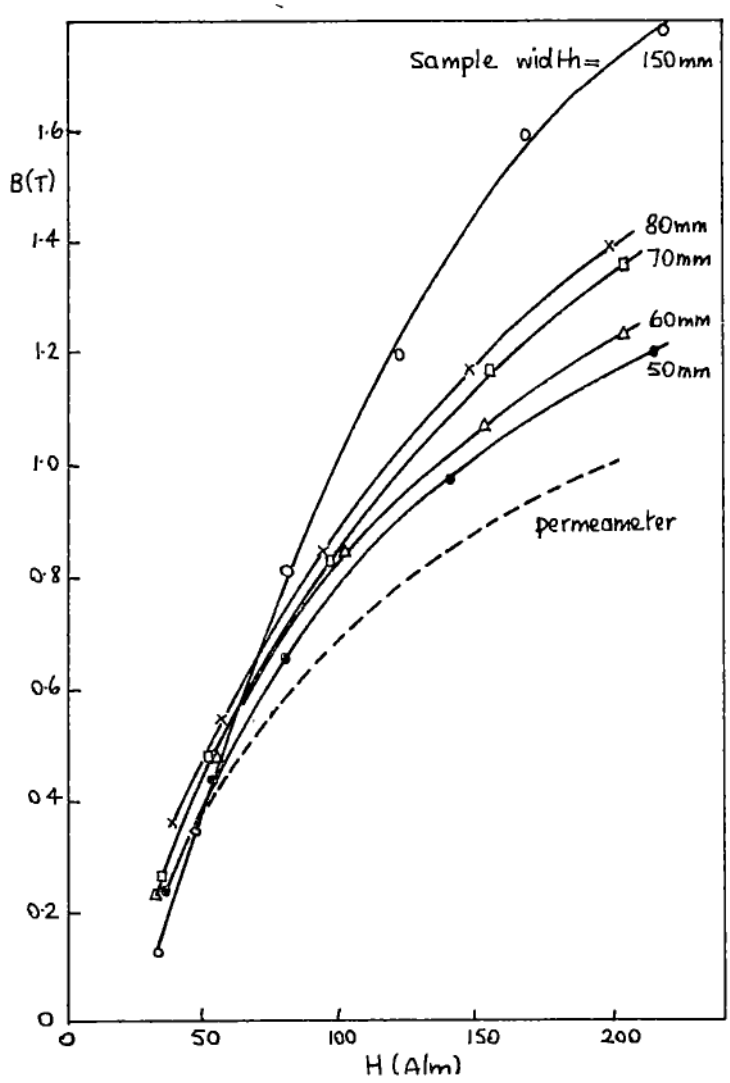

Figure 4.4 C-core rig: B vs. H curves for different widths of silicon steel. A reference curve from the permeameter is included for comparison.

different widths, plus a reference curve from the permeameter. At 160A/m the 150mm wide sample gave a flux density of 1.67 times the reference (permeameter) value, and even the 50mm wide sample gave a flux density of 1.14 times the reference value.

Conclusions

Some flux through the search coils fringes the far side of the sample from the poles, but calculation of possible paths suggests that this adds no more than 2% to the total flux in the search coils. The bulk of the extra flux must therefore spread out sideways in the sample. The guard cores are probably not wide enough, but no more laminations are available to test this by making the outer cores wider.

Despite the poor quantitative agreement between B vs. H loops from the C.C.R. and from the permeameter, there is similarity in their shapes. For example figure 4.5 shows pairs of B vs. H loops for a mild steel sample 0.42mm thick and 52mm wide, obtained with the C.C.R. and with the permeameter. For each peak value of H the loops have been scaled to be the same height or B-value. Figure 4.6 shows the same for a silicon steel sample 0.34mm thick and 52mm wide.

The C.C.R. cannot be relied upon to give B vs. H data to an accuracy of better than 50%. This is disappointing; however it was used in later tests for determining whether or not the permeability is higher in one direction than in another and for obtaining comparative shapes of B vs. H loops.

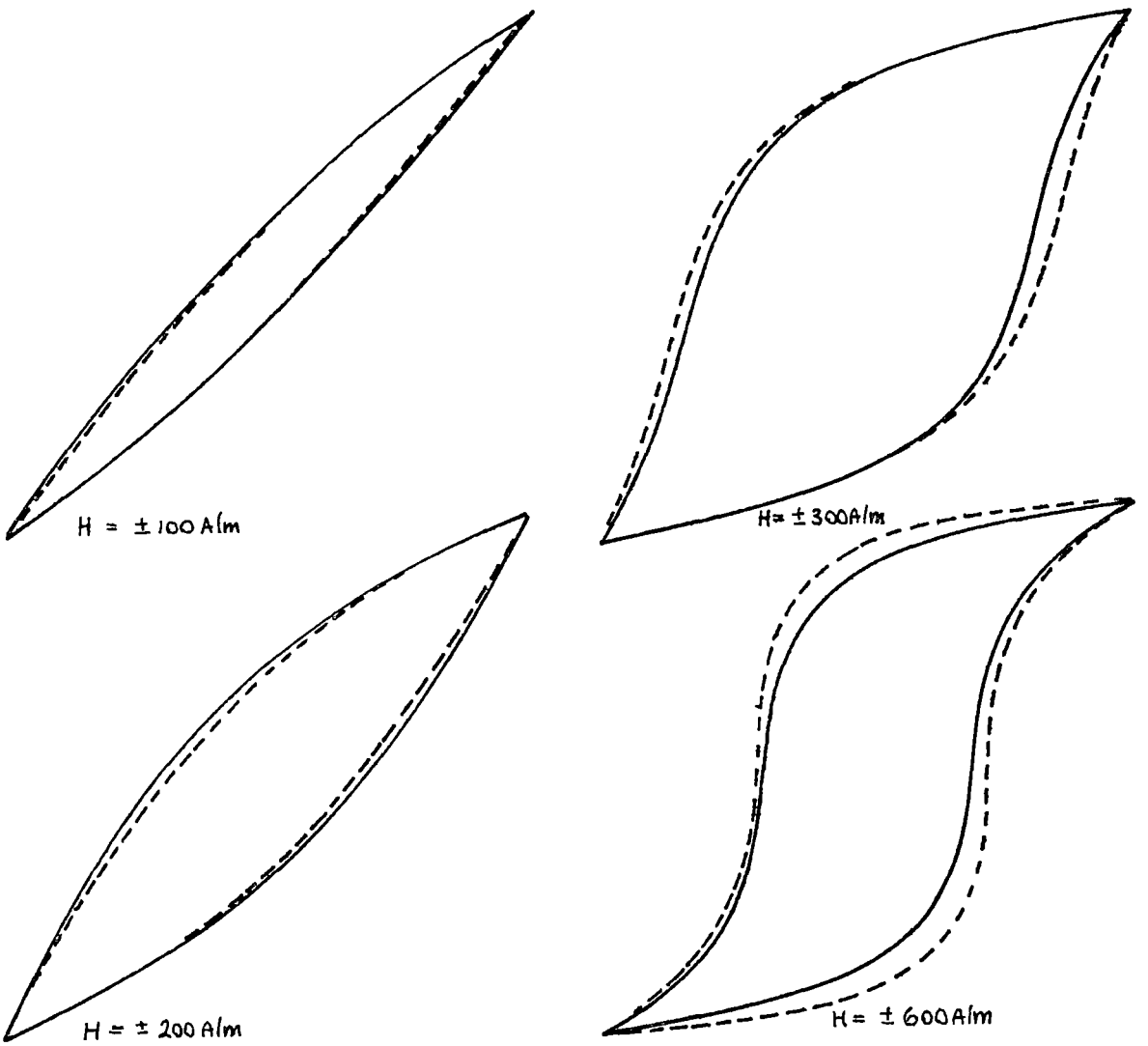

Figure 4.5 B vs. H loops for a mild steel sample, obtained with the C-core rig (——)and with the permeameter (- - -). The C.C.R. results have been rescaled to the same size as the permeameter ones.

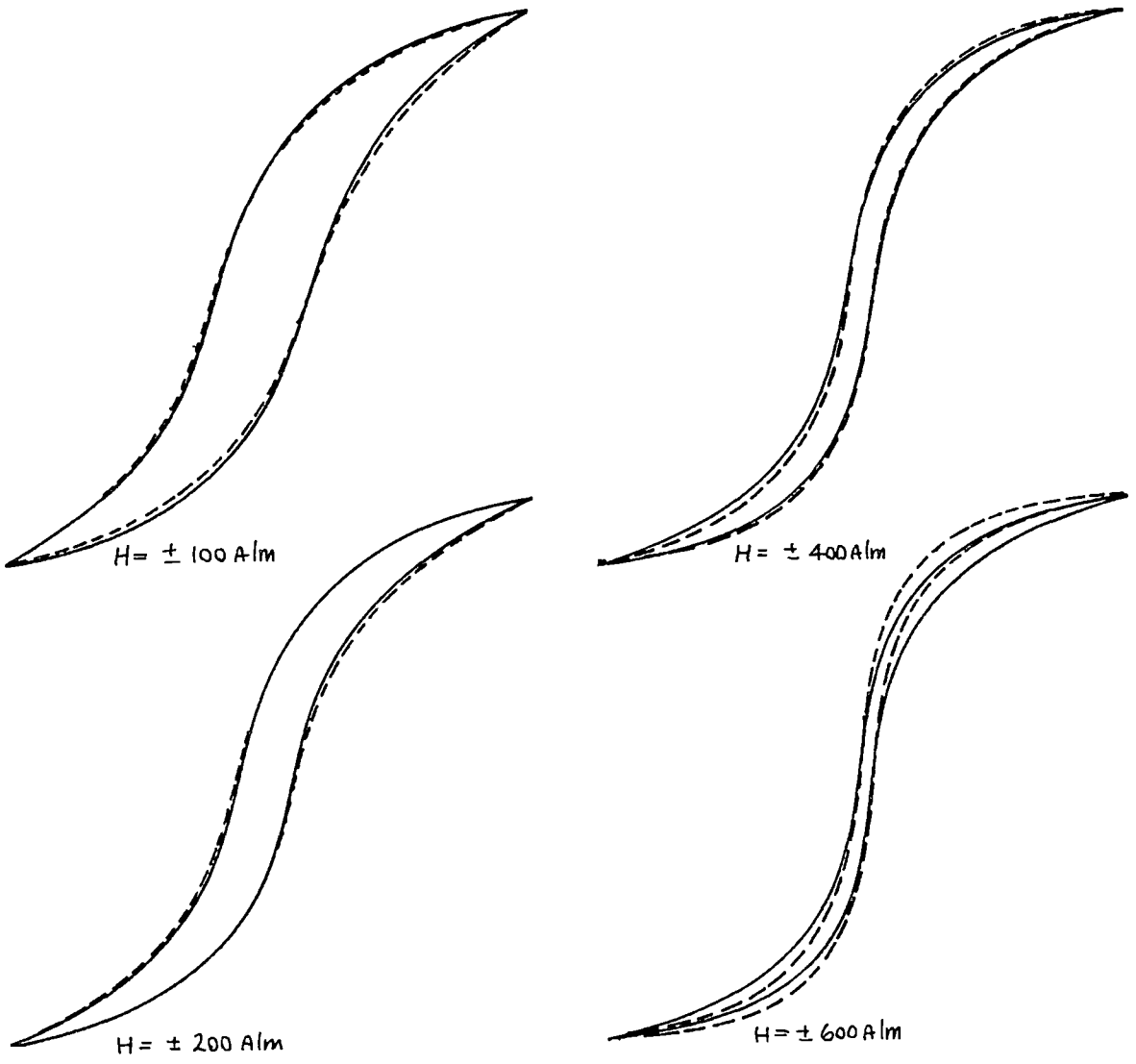

Figure 4.6 B vs. H loops for a silicon steel sample obtained with the C-core rig and with the permeameter. The C.C.R. loops have been rescaled.

4.2 The permeameter

In order to estimate the accuracy of the C-core rig it must be compared with results obtained by a method of known accuracy. The standard means of measuring a B vs. H loop is by means of a permeameter such as is shown in figure 4.7. The general criteria for producing uniform flux and field in a sample - which are the aims of a precision permeameter - are [A5]:

(1) The ratio of the length to diameter of the magnetising coil and the ratio of the length of the magnetising coil to the axial length of the test region should both be as large as possible.

(2) The reluctances of the yoke and of the specimen-to-yoke joints should be small compared with that of the specimen.

(3) If necessary extra M.M.F. should be concentrated at the joints to compensate for their reluctance.

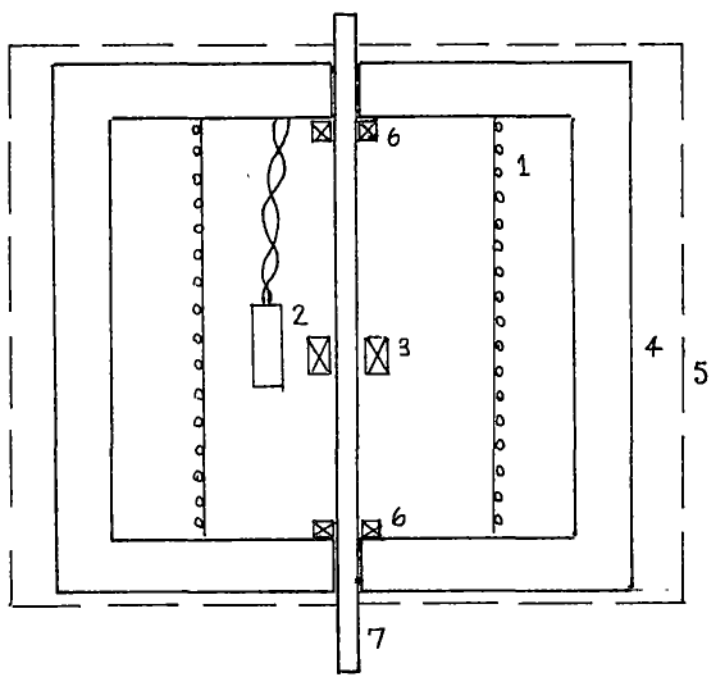

Figure 4.7 The National Physical Laboratory permeameter. 1=magnetic field coil, 2=oersted meter probe, 3=flux measuring coil, 4=Mumetal yoke, 5=Mumetal shielding, 6=compensating coils, 7=rod-shaped specimen.

These criteria are for B vs. H measurements of the highest accuracy (with an error of less than 0.1%) and my requirements were rather less stringent, even for a standard against which to compare the local method of testing. However, the permeameter layout I eventually used was made with these criteria in mind, and is shown in figure 4.8. The error in flux or field measurements is estimated at 1%.

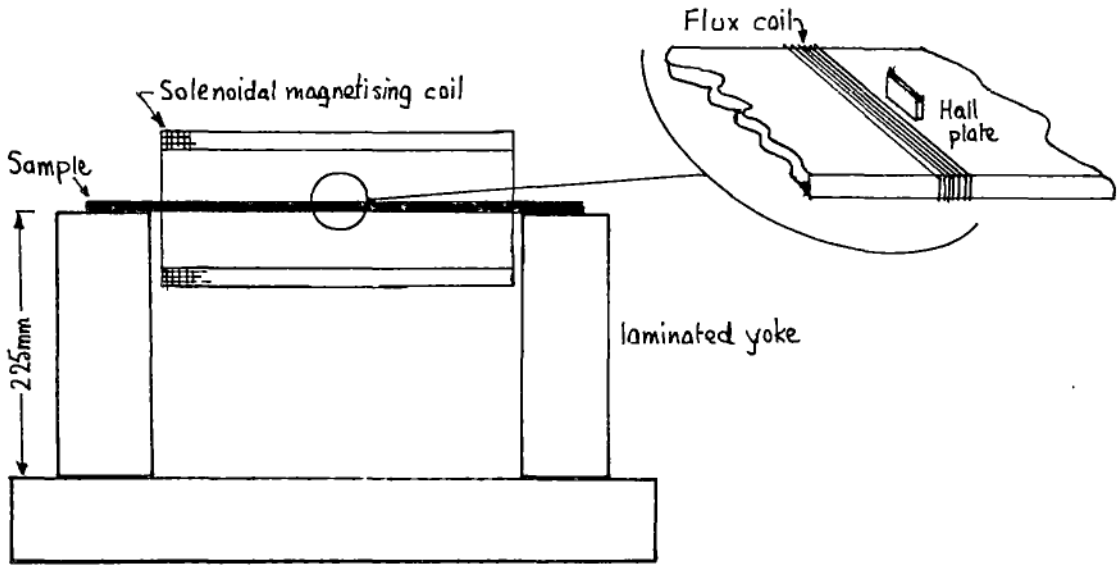

Figure 4.8 Permeameter used for "reference" B vs. H data.

4.3 Measurement of field strength

Values of field strength between 10 and 1000A/m were required to be measured in conjunction with the permeameter, the C-core rig, and the U-core. A Hall plate was used in preference to an air-cored coil, mainly because it occupies less space. Field strength H is related to Hall voltage V by (approximately) H[A/m] = 2.2V[μV]. The limit of useful measurement (set by random drift in the HP425A microvoltmeter and in the Hall plate supply) is $\pm$0.5μV on the 10μV scale, and thus a field of about 5A/m could be measured with an error of $\pm$5%. Figure 4.9 shows the circuit for the Hall plate supply, which includes a circuit to zero the output voltage in the absence of an applied field.

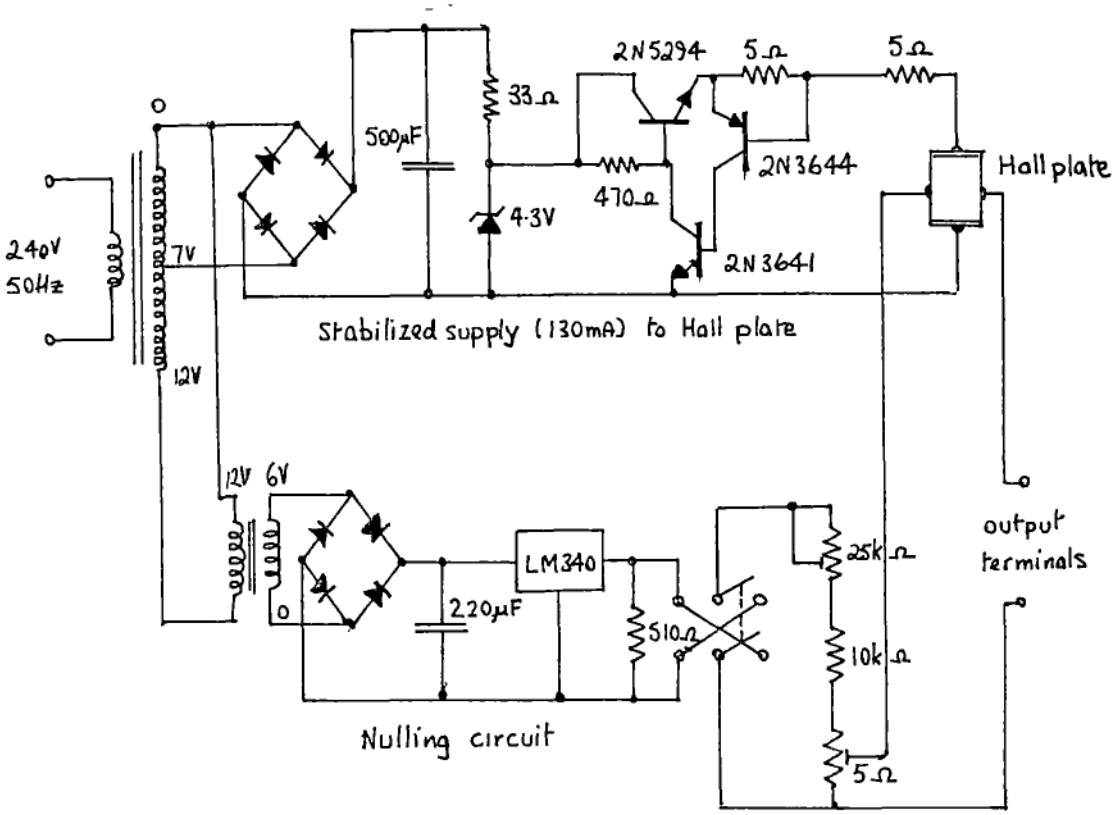

Figure 4.9 Hall plate circuit.

The Hall plates were bought from F.W.Bell Inc. Each had to be calibrated with its own D.C. supply. This was conveniently done with a pair of Helmholtz coils, shown in Figure 4.10a. (Two identical circular coaxial coils separated axially by a distance equal to their radius are known as Helmholtz coils. Their usefulness is that they provide a magnetic field that is uniform to within 1% inside a sphere of 1/3 of the coil radius). Direct current for these coils was obtained from a rectifier and smoothing circuit - figure 4.10b. Maximum current (before heating significantly altered the coil current more rapidly than it could be re-adjusted) was 0.5A. These coils were themselves calibrated by means of a carefully made solenoid consisting of 370 turns of 18 B&S wire in a single layer of 401mm axial length and mean radius 56mm. The field at the centre was calculated to be 11.17±0.05 gauss/amp. This solenoid was fitted inside the Helmholtz coils,

with a Hallplate inside the solenoid used as a null detector. The currents in the Helmholtz coil and the solenoid were adjusted until, on reversal of both currents, no change occurred in the Hall voltage. The reason for not calibrating the Hall plates directly from the solenoid was that one of the Hall plates was on the end of a long thin strip of bakelite and this would have to be bent more than was desirable to get it into the right place inside the solenoid.

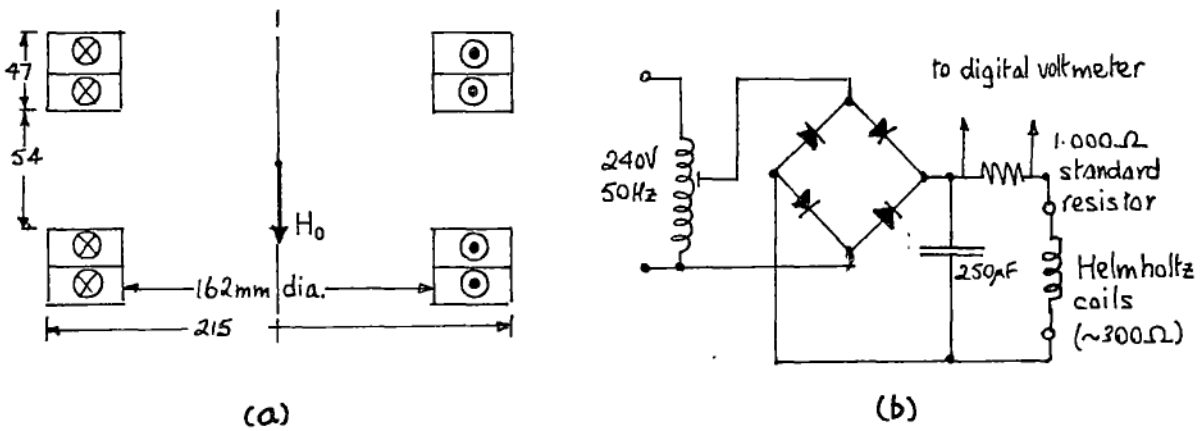

Figure 4.10 Helmholtz coils for calibrating Hall plates: (a) dimensions of coils, (b) D.C. power supply.

4.4 Measurement of flux density

Analogue integration

Flux density was calculated from the change of flux due to reversal of the magnetising current, which in turn was calculated from the time-integral of the voltage induced in a search coil wound round the sample. Figure 4.11 shows the analogue integrator used for this purpose. Integrator output

$$v_o = 1/(RC) \int v_i dt + (dE_o/dt).t$$

$$= 10 \int v_i dt + \text{error term}$$

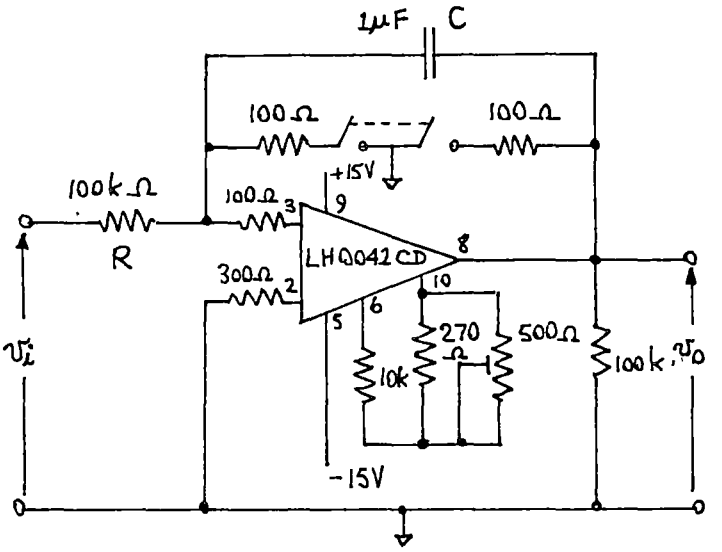

Figure 4.11 Analogue integrator with FET amplifier. $v_o = 10\int v_i\,dt$.

The error term causes the output to drift, which sets a limit to the sensitivity of the integrator. Examining the cause of the drift in more detail [B6]:

$$dE_o/dt = |V_{os}/RC| + |I_b/C|$$

where V_{os} is the input offset voltage and I_b is the input bias current.

Clearly the lower are V_{os} and I_b the less is the drift. The LH0042C is a FET-input operational amplifier that has $V_{os}<4mV$ and $I_b<15pA$. Hence, with R = 100KΩ and C = 1μF,

$$dE_o/dt = (40 + 0.015)mV/sec \cong 40mV/sec$$

However, use of the offset voltage nulling circuit enabled a drift of 100μV/sec to be achieved - but this took patience and time to attain and could not be held for more than a few seconds. The sensitivity of this integrator was limited to an output voltage change of 1mV with an error of 0.1mV (i.e. 100±10 Wb-turns). This was not a serious limitation for permeameter work as the flux coil could be wound with as many turns as was necessary to achieve an adequate voltage change, but it was not sensitive enough for the C-core rig (where there was no space to increase the number of turns) and which could in consequence only measure to (0.05±0.005)T.

Digital integration using a voltage to frequency converter and a pulse counter

The Analogue Devices 460L voltage to frequency converter gives, nominally, 10^5 pulses per volt-second of input; thus it gives 100 pulses per millivolt-second. The pulses are counted with a Data Precision 4740 counter which, over a 10 second period, counts the 100 pulses and displays a frequency of 100/10 = 10Hz with a resolution of 0.1Hz. This combination was tested for accuracy by supplying the 460L with a steady voltage of (100±0.1)μV. The counter displayed a frequency of (10±0.2)Hz, i.e. a ±2% error. Looked at the other way, the digital integration has a sensitivity 5 times better than the analogue integration for the same error, and there is also no time wasted in zeroing the output voltage drift. Figure 4.12 shows the power supply, precision adjustment, and calibration circuits for the 460L.

However, it turned out that the sensitivity of the analogue integrator could be greatly improved with the addition of an amplifier - described next - such that the still-present problem of drift was outweighed by other advantages in comparison with the digital integration.

4.5 Amplifiers

In order to use an XY plotter to draw B vs. H loops, variable gain D.C. amplifiers are needed for the B and H signals. These were made up using an LM321H low noise preamplifier and then an LM741 second stage, as shown in figure 4.13. Maximum gain is about 300. Amplifier performance criteria are: (1) low noise below 10Hz and (2) low drift of the integrator output voltage when the amplifier is used as a preamplifier for the integrator.

In order to check these the gain was set at 100 and the input resistor at 100Ω, and the 425A voltmeter used to monitor the output voltages. Results were:

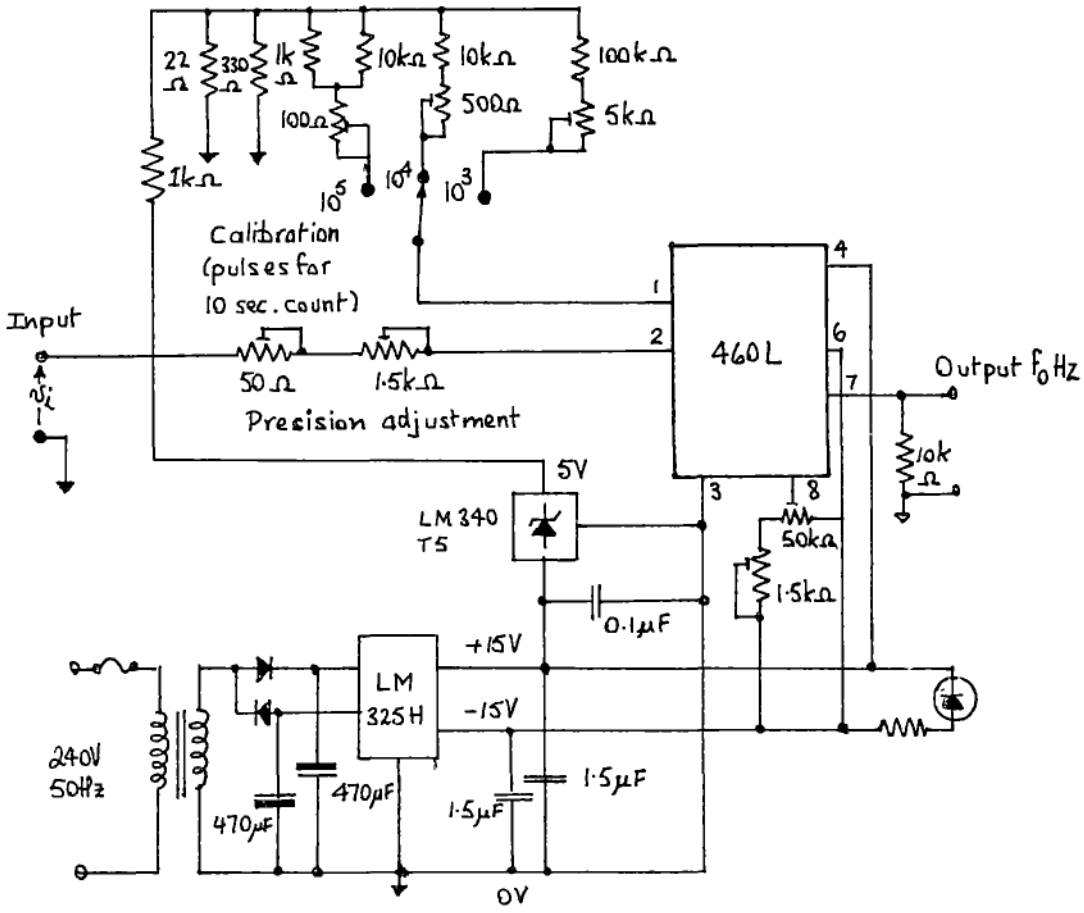

Figure 4.12 Digital integrator using a voltage to frequency converter. $f_o[Hz]=10^5 V_{in}[V]$.

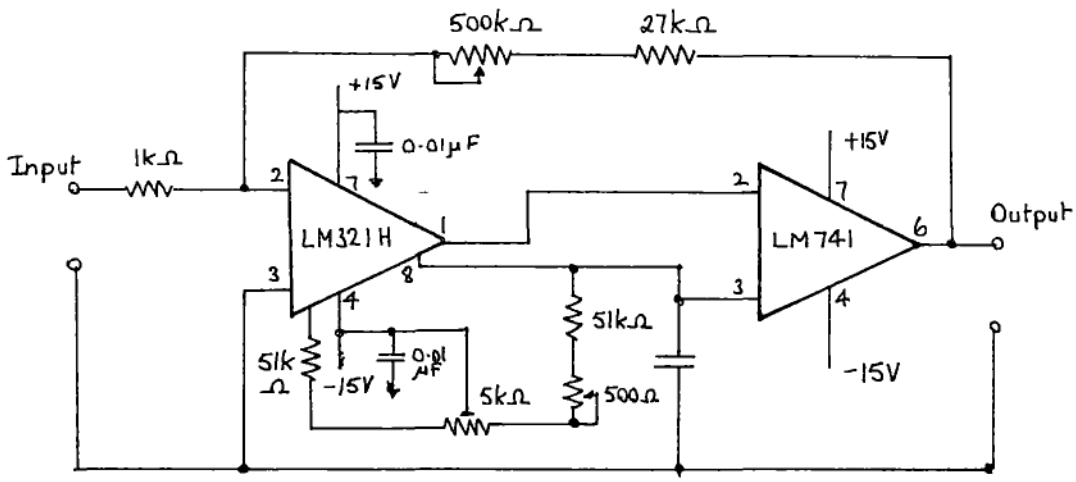

Figure 4.13 Low noise D.C. amplifier.

(1) Random noise (amplifier only) = ±20μV

(2) Integrator drift (when supplied by the amplifier) = 200μV/sec. Since the lowest drift of the integrator by itself is 100μV/sec, the amplifier together with the integrator gives a sensitivity 50 times better than the integrator alone; the limit for ±10% error is 2μWb-turns. (This compares well with a Scalamp fluxmeter that has a resolution of 200μWb-turns for a ±10% error). It is also 10 times better than the voltage to frequency converter, and in fact the latter was rarely used as it had the additional disadvantage that it could not be combined with an XY plotter.

4.6 Noise in leads

The signals from the Hall plate are in the D.C. microvolt range and so it was important to reduce any low frequency noise. A comparison of coaxial and twisted leads was made. In one case 2m lengths of each were laid on the bench near various transformers and leads carrying 50Hz currents, and in the other case longer lengths (20m of coaxial, 9m of twisted) of each were run from the central bench (inside the 2.6m demagnetising coils) to the instrument bench.

The noise was measured, with a wideband RMS voltmeter, for different values of terminating resistance. In both cases the coaxial cables were better than the twisted ones, and for source resistances of 100Ω or less the wideband noise (for coaxial cables) was less than 100μV. The same conditions, but measuring noise on the 425A voltmeter (which has a low pass filter) gave a noise of only 0.2μV.

4.7 Control of magnetising current

In order to draw B vs. H loops on the XY plotter a smooth controlled change in magnetising current is needed, and so a transistor controller was built for this purpose. It was in fact used for all permeameter and C-core rig tests. Figure 4.14 shows the circuit. The potentiometer was turned by hand. Equal positive and negative coil currents were ensured by using a reversing switch rather than by a more complicated push-pull circuit.

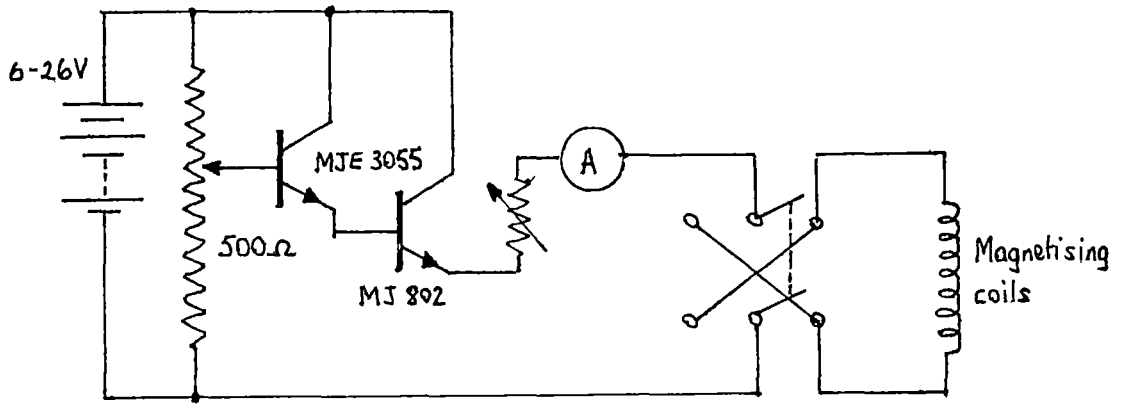

Figure 4.14 Magnetising current controller.

4.8 The 2.6 metre demagnetising coils

The earth's magnetic field is of the order of 50A/m, which is similar to the applied field at the low end of the B vs. H measurements. Thus it might be useful to cancel out the earth's field where the permeameter or the C-core rig was to be used. Three mutually perpendicular components of the earth's field were measured with a gaussmeter on the bench where the B vs. H measurements would be made; results were: vertical 44A/m, N-S 18A/m, E-W 1A/m.

The three components of field were cancelled out by means of three pairs of Helmholtz coils. They were not circular but square with the corners cut off - almost octagonal in fact. Because each coil needed different ampere-turns (80, 33, and 2) but the same power supply was to be used for all three, some extra (adjustable) resistances were needed in series with each coil. These were calculated assuming that a battery supply of about 50V would be used. In practice, the battery voltage fluctuated from minute to minute because other people took current from it, and so instead the mains from a Variac transformer was rectified and smoothed. Final adjustment of the three series resistances to give cancellation of all components of the earth's field was done using a magnetometer as a guide to zero field conditions.

The residual field could be cancelled to less than 0.10A/m (i.e. less than ·2% of the earth's field) in all three directions inside a sphere of 0.1m radius, and to less than 0.45A/m (less than 1% of the earth's field) inside a sphere of 0.4m radius.

Figure 4.15 shows the circuit that supplied the Helmholtz coils. The correct current was maintained by reading the voltage across a standard 0.1000Ω resistor; adjustments to the current in the individual pairs of coils was never needed. (The large number of resistors is due to the use of some existing ones, rather than buying new ones specially).

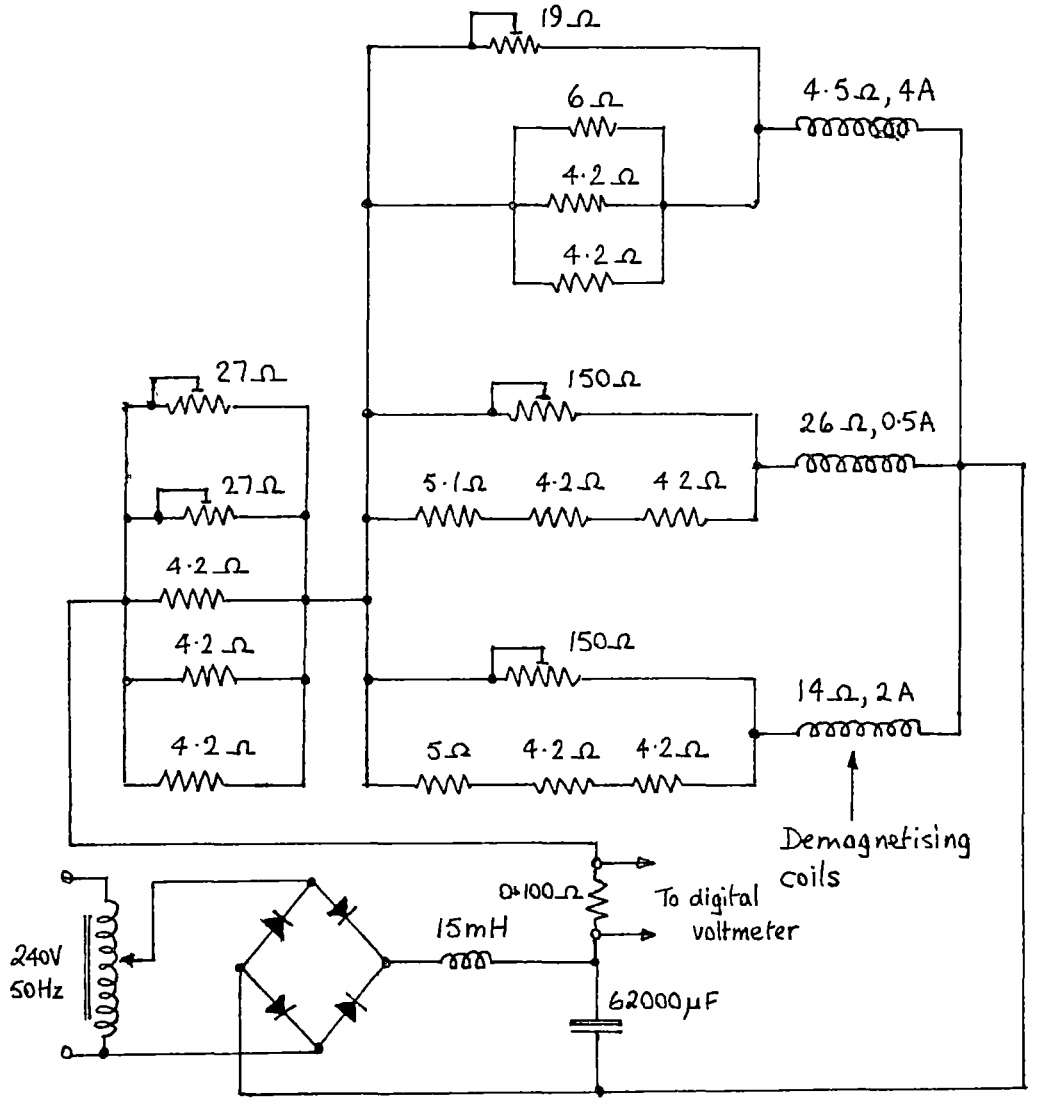

Figure 4.15 Power supply and adjusting resistors for the 2.6m demagnetising coils.

4.9 A final comment

An obvious criticism of most of this instrumentation is that it belongs to the pre-digital era. It is true that far more refined ways of collecting and displaying data are available, but my attitude was that I wanted a few results as quickly as possible, rather than a lot of results later, and I was not prepared to spend time improving this aspect of the project at the expense of less time devoted to other aspects.

Another criticism could be that the methods of measuring B vs. H loop are rather approximate, with errors of several tens of percent. The counter argument to this is that they did the job they were designed to do, again without much development time spent on them. Also, their accuracy was adequate to show the trends in the change of magnetic properties with stress; and, in any case, no quantitative theory was available to justify the effort involved in significantly improving the accuracy.

CHAPTER 5

DEVELOPMENT OF THE ROTATION RIG

5.1 Introduction

This chapter describes different designs of the rotation rig and also gives measurements that show its characteristics on stressed mild steel. The first version of the rotation rig was the U-core of chapter 3. This used a Hall plate to sense field strength for B vs. H loops; the current in the coils on the U-core was varied slowly and steadily by hand (aided with a transistor controller) i.e. essentially D.C. conditions. In order to measure anisotropy, and hence stress, by means of the resulting rotation of magnetic field (and to make it the basis of an instrument), A.C. magnetisation is more convenient in that a search coil can be used instead of the Hall plate. The former has the advantage of robustness, cheapness, and not needing its own power supply; also its sensitivity is adequate. A.C. magnetisation has other advantages that are dealt with later.

Figure 5.1a shows how, for $\mu_2 > \mu_1$, the field H at the surface of anisotropic steel is rotated away from the μ_2 direction by some angle θ (when $\mu_2 = \mu_1$, B and H are parallel to each other and point along the axis of the core; $\theta = 0^o$). There are two ways of sensing this change:

(1) Rotate the search coil until the voltage V_n induced in it is zero (or a minimum); this gives θ directly, as in figure 5.1b.

(2) Fix the search coil, so that V_n varies as $\sin\theta$, as in figure 5.1c.

If it is fixed, the whole assembly and search coil with its very fine wires can be potted and thus made quite durable. A rotatory search coil is mechanically weaker and more complicated. The choice was in fact simple: use the fixed search coil. The actual angle θ may then be obtained by putting another fixed search coil at right angles to the first one: $\theta = \tan^{-1}(V_n/V_p)$ where V_n and V_p are the voltages induced in the search coils

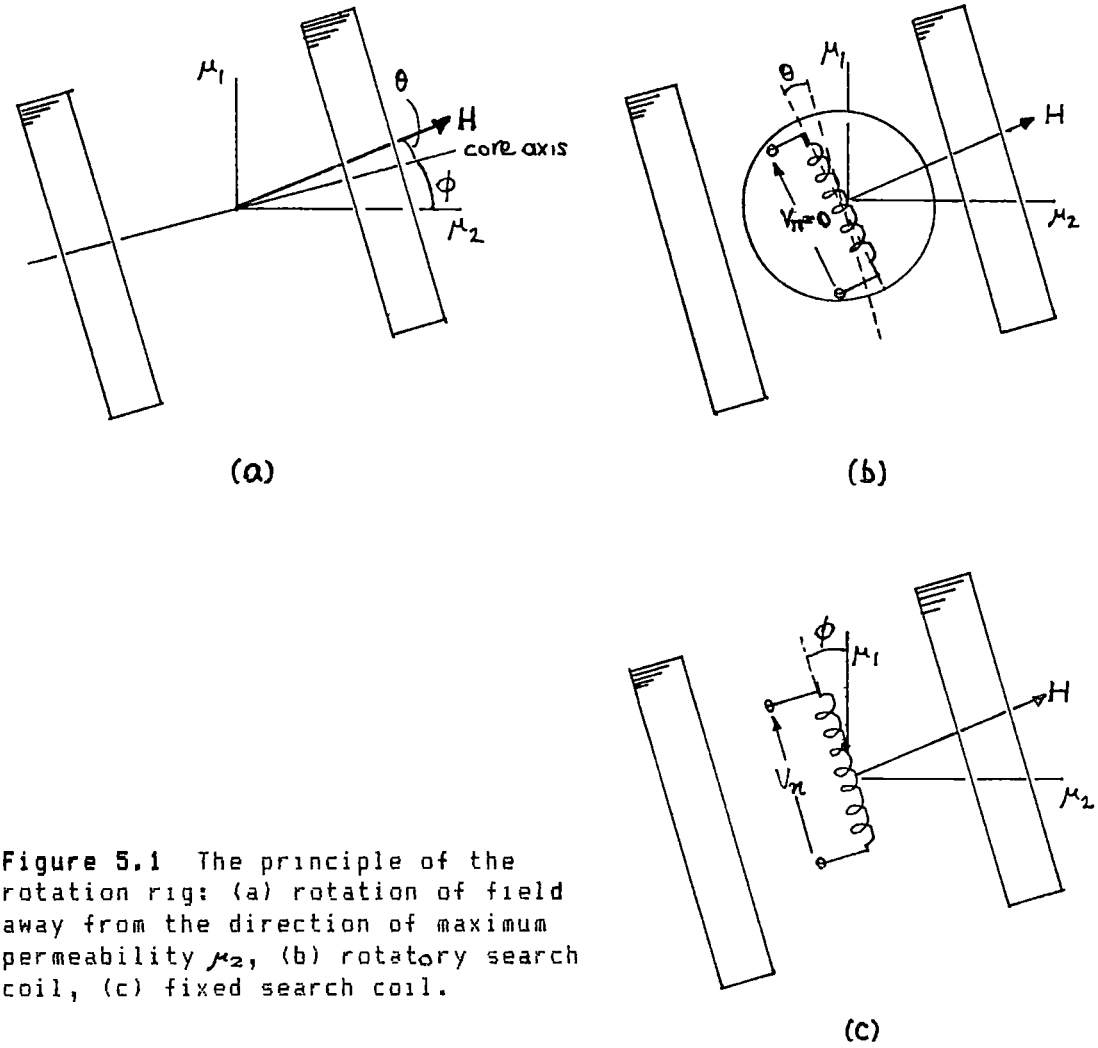

Figure 5.1 The principle of the rotation rig: (a) rotation of field away from the direction of maximum permeability μ_2, (b) rotatory search coil, (c) fixed search coil.

normal (SCn) and parallel (SCp) to the axis of the core. (Chapter 3 shows that when μ_2/μ_1 varies around the B vs. H loop, θ changes correspondingly, so with A.C. magnetisation the value of V_n will represent some kind of averaging of θ).

The layout and dimensions of the first rotation rig are shown in figure 5.2a. I called it the Small Rotation Rig (S.R.R.). Excitation was at 50Hz, monitored by the value of the current in the coils that in turn was related linearly to the field strength (details of this are in section 5.4).

Figure 5.2b shows the very simple instrumentation that went with it. A reason for the integrator is that it gives an output waveform that is the

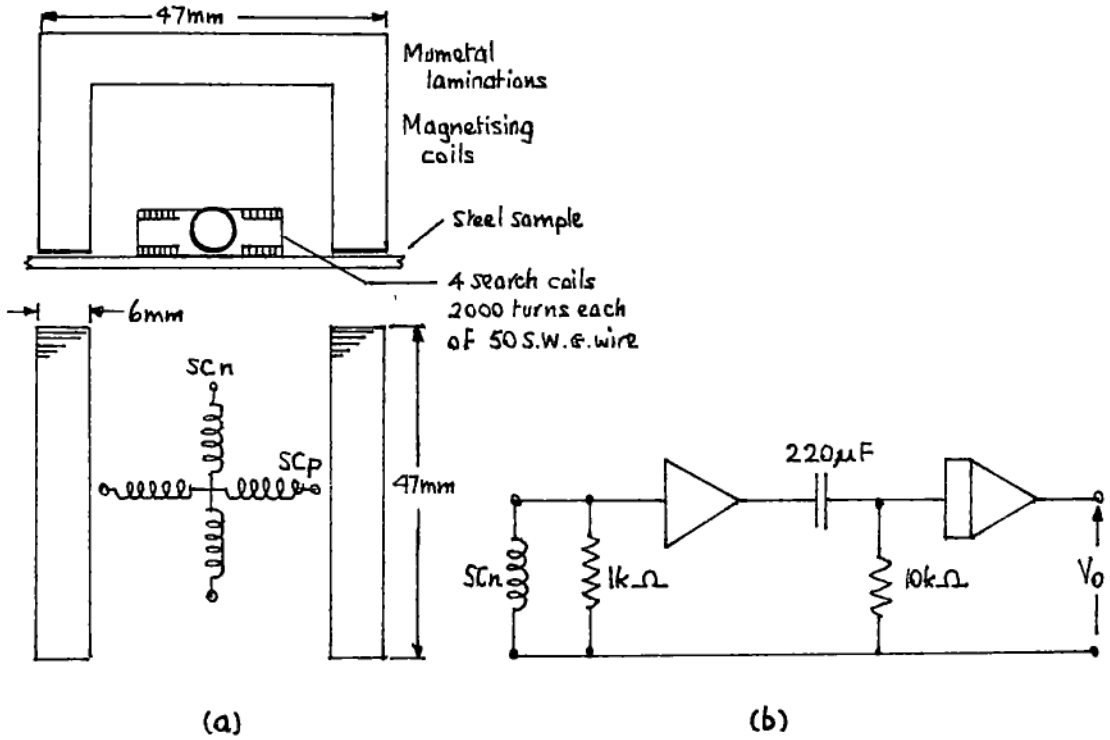

Figure 5.2 The small rotation rig (S.R.R.): (a) core and coil dimensions, (b) signal processing.

time-variation of the magnetic field, rather than its time-derivative. In this case the integrator output voltage is proportional to the component of magnetic field parallel to the axis of the search coil. The 1kΩ resistor in parallel with the search coil reduced the source impedance and hence the noise at high frequencies, and the 220μF capacitor blocked any D.C. offset voltage from the amplifier and hence reduced the output drift of the integrator. The overall voltage gain at 50Hz was about 10. Any voltage in the search coil above a minimum (noise) value indicated rotation of the magnetic field, and it was possible to tell whether the rotation was clockwise or anticlockwise by the phase of the voltage. V_o was read by means of a true RMS voltmeter (an HP 3400A).

As far as making the cores and search coils went there were no

problems; no particular precision was needed to assemble them, except to position the SCn search coil. It is essential, for all the rotation rigs, that the voltage V_n is as small as possible (ideally zero) when the field is straight between the poles. This was achieved by monitoring V_n with the U-core in air - not on any steel - and whilst the potting compound hardened the position of SCn was adjusted so that V_n remained a minimum. In this way V_n for $\theta = 0^o$ could be made as low as $0.005V_p$.

5.2 Tests with the small rotation rig on mild steel

The steel sample for the first two tests described here was a 900mm length of hot-rolled mild steel bar, presumably 250 grade. Its cross section was 4" by 1/2", i.e. a thickness of about 12mm. It was bent by means of the arrangement shown in figure 5.3. The applied load was known from the deflection of a proving ring on top of the upper spreader and was varied by tightening two tie bolts linking the top of the proving ring and the base. The stress in the beam was initially calculated from the curvature of the middle part of it, but since this agreed to within 5% with the value calculated from the load and the dimensions of the beam and supports, the value of the load itself was subsequently always used to give the stress on the upper and lower faces of the beam.

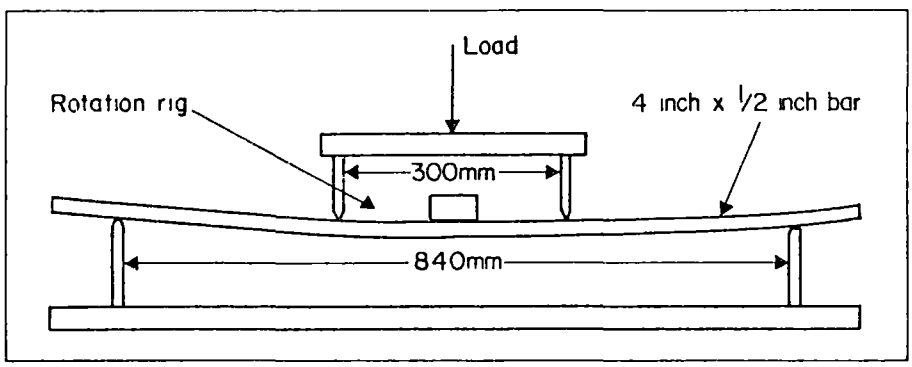

Figure 5.3 Bending arrangement for the 12mm steel bar.

(1) Output voltage vs. angular position of the core

The S.R.R. was rotated at a fixed spot on the upper face of the bar, which was loaded to a stress of 150MPa at the surface. Figure 5.4 shows the search coil voltage V_n versus the angle ϕ that the rig was turned through. The phase of V_n altered by 180° as ϕ went from positive to negative and this is shown as a change of sign of V_n on the graph (although the A.C. voltmeter always read positive). Maximum output was for $\phi = \pm 45°$.

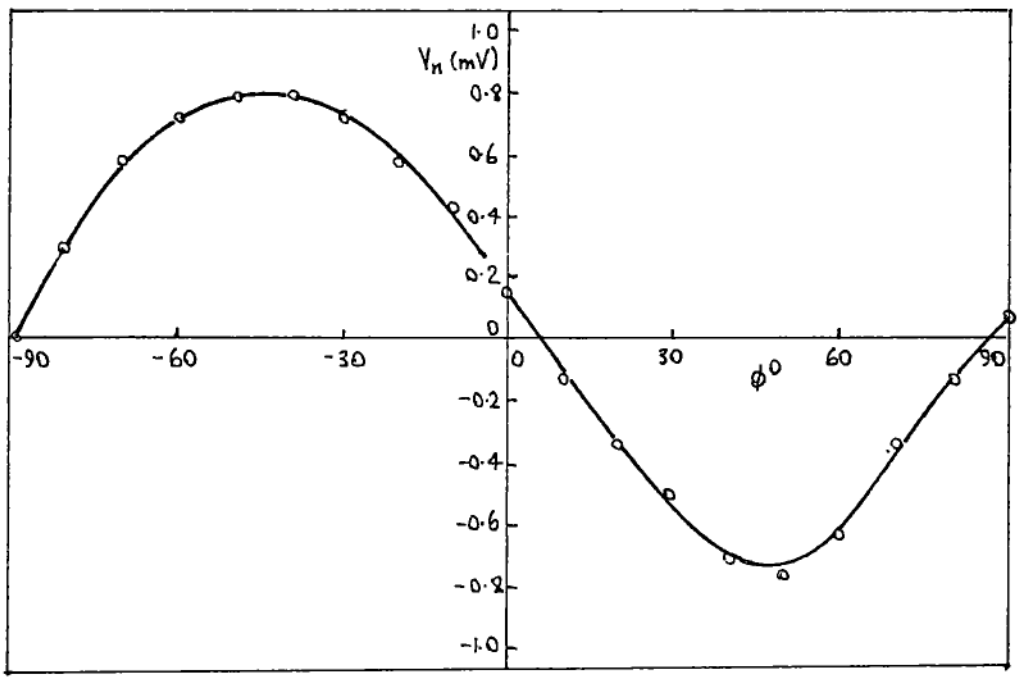

Figure 5.4 Ratio of search coil voltage V_n vs. magnetising core angle for the Small Rotation Rig (S.R.R.) on a 12mm mild steel bar under 150MPa compression.

(2) Output voltage ratio vs. stress for various magnetising currents

Figure 5.5a shows the variation with stress of the ratio V_n/V_p, denoted by R_v, for the lower face of the bar in tension. The maximum stress was slightly less than the upper yield point of 250 MPa. Figure 5.5b shows the corresponding result for the upper face of the bar in compression. The S.R.R. was positioned with its poles at 45° to the direction of stress. The four curves on each graph show the effect of different values of field strengths. If V_n were plotted instead of R_v the voltages for the same

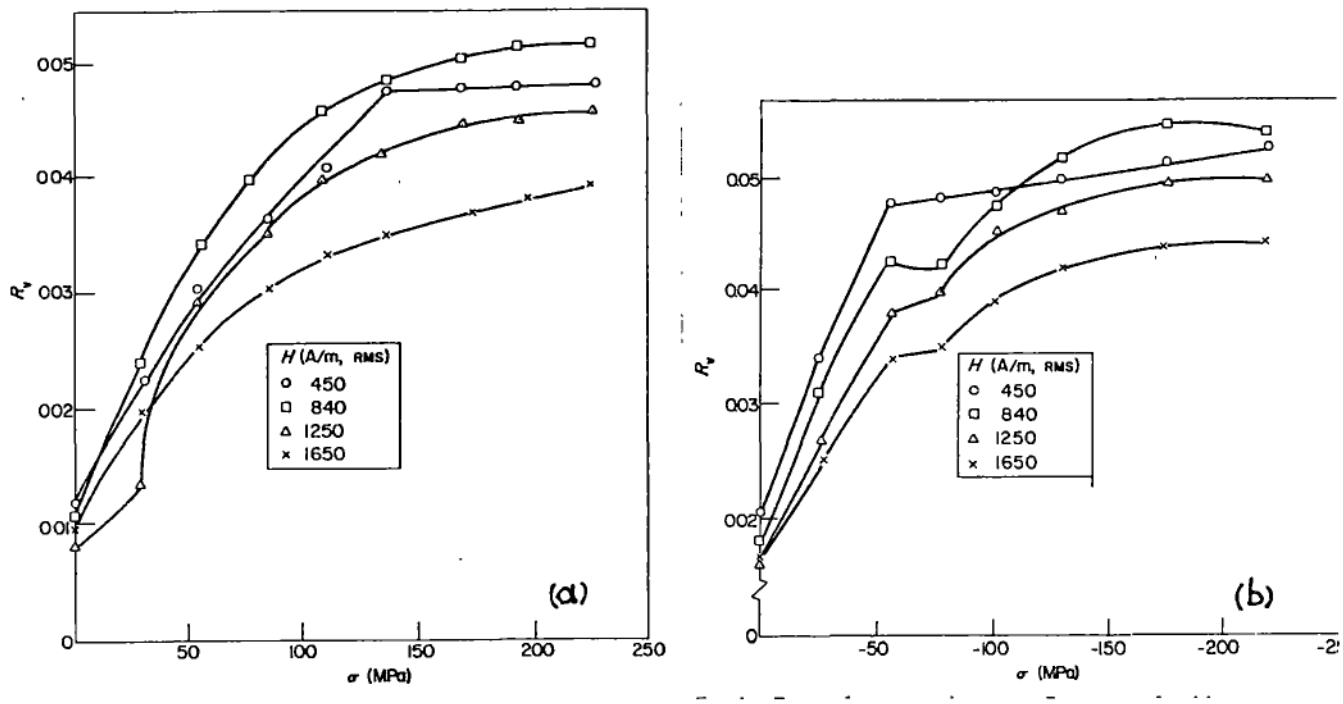

Figure 5.5 Ratio of search coil voltages R_v vs. stress σ for 12mm mild steel: (a) tension, (b) compression.

stress would vary widely. Dividing by V_p removes the effect of the differing flux density in the sample and means that differences in R_v are caused by differing shapes of B vs. H loops. The value of R_v at zero stress was higher for the compression face than for the tension one and may be due to residual stress. Also, there was always some noise picked up in SCn that got through to the voltmeter despite the use of a low-pass filter. The minimum value of R_v was never less than 0.005, corresponding to $V_n = 50\mu V$. The maximum value of V_n, at the highest magnetising current, was 1.2mV. This rather poor signal to noise ratio could be improved by more attention to signal processing.

(3) R_v vs. stress at different temperatures

For this test a piece of 0.42mm thick mild steel (annealed to remove residual stress) was tensioned whilst heated to different temperatures up to 165°C. Figure 5.6 shows the rather crude way in which the steel was

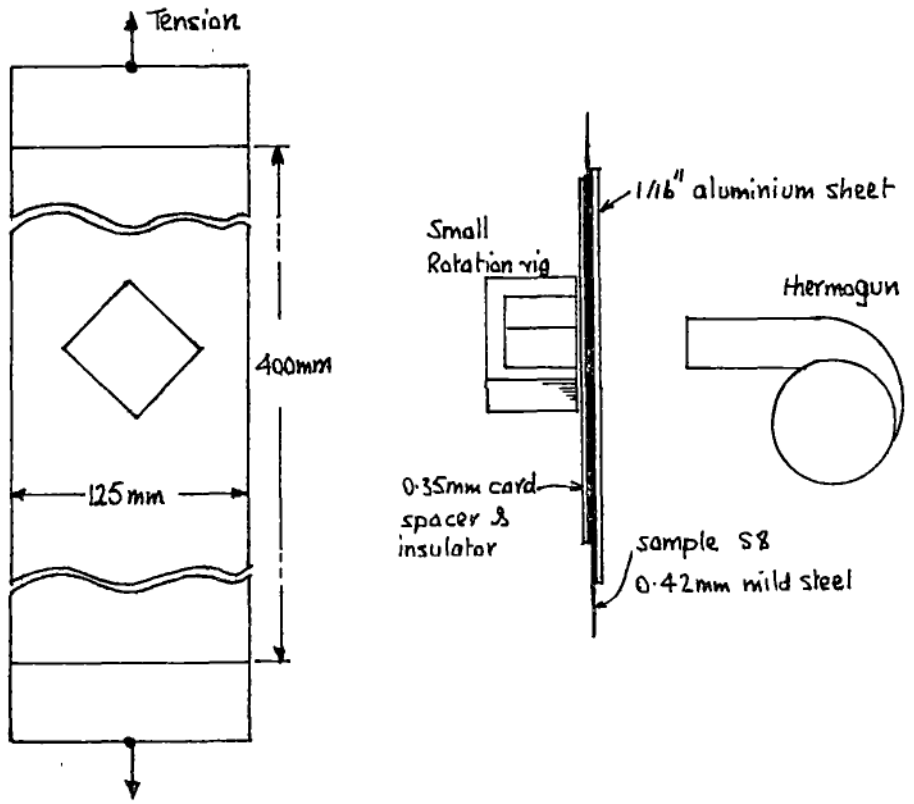

Figure 5.6 Equipment for testing the sensitivity of the rotation rig on steel at different temperatures: the S.R.R. on a thin mild steel sample.

heated. The thin aluminum sheet spread out the heat somewhat. The S.R.R. was partly insulated from the warm steel by a 0.35mm cardboard spacer and as a result its sensitivity was decreased. Figures 5.7a-e show the results. The last figure, 5.7e, compares the "calibration" at 20°C and 165°C for a fairly sensitive value of magnetising current (equivalent to a field of 800A/m off the steel). In order to speed up taking readings the integrator was omitted.

The graphs show that the general effect of the increasing temperature is to reduce R_v slightly for stresses above 40MPa. Below 40MPa there is peculiar, unexplained, behaviour.

The aim of testing at different temperatures was to find out whether stress or strain affects the magnetic properties. At constant stress, the strain increases linearly with temperature. The coefficient of thermal expansion of steel is about 7×10^{-6} so a temperature rise of 120°C would cause 840 microstrain. This strain is equivalent to that due to a stress, at

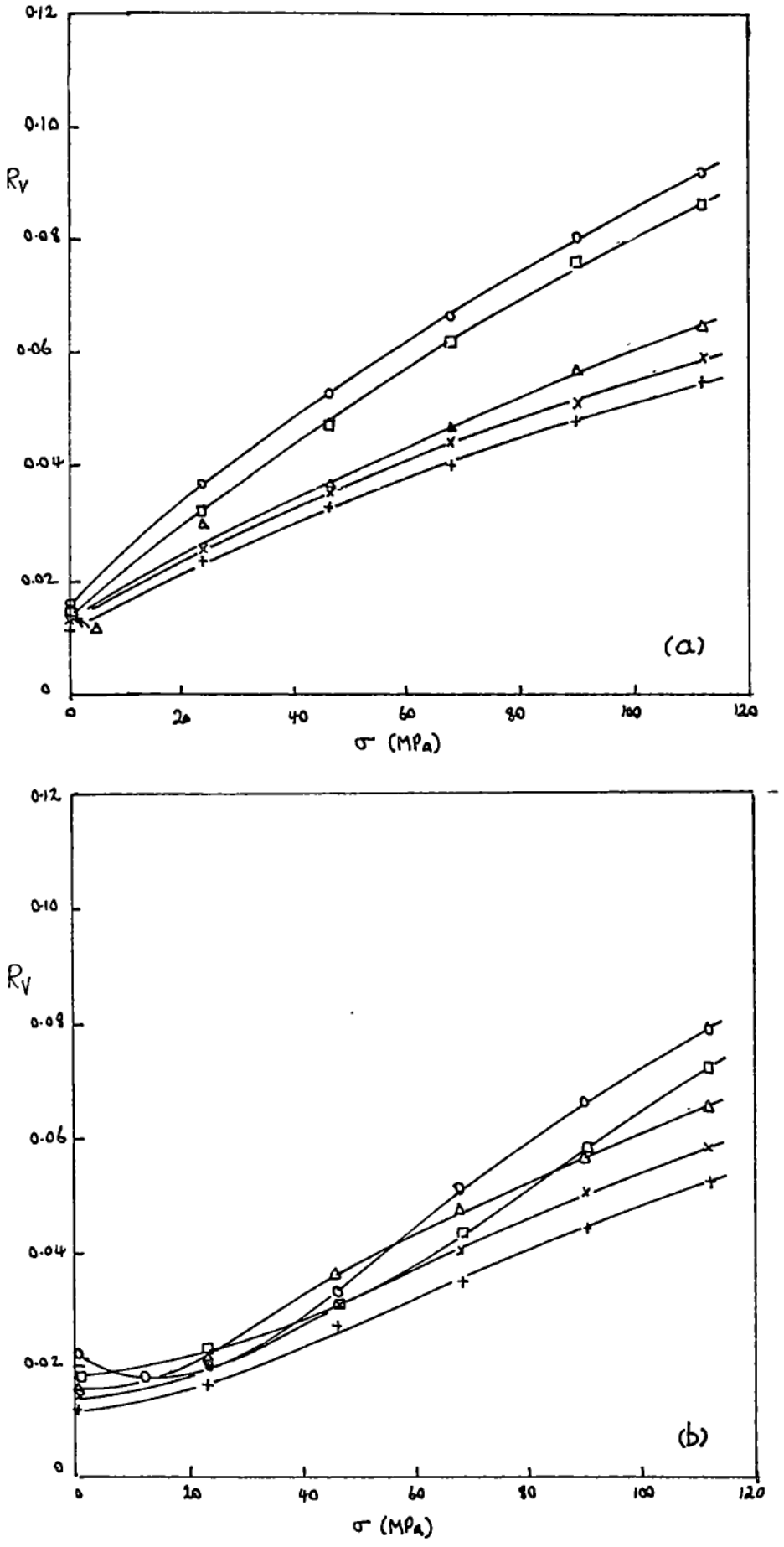

Figure 5.7 R_v vs. stress for the S.R.R. on 0.42mm mild steel, at different temperatures and field strengths: (a) 25°C, (b) 85°C. o:400A/m, □:800A/m, Δ:1250A/m, x:1700A/m, +:2200A/m

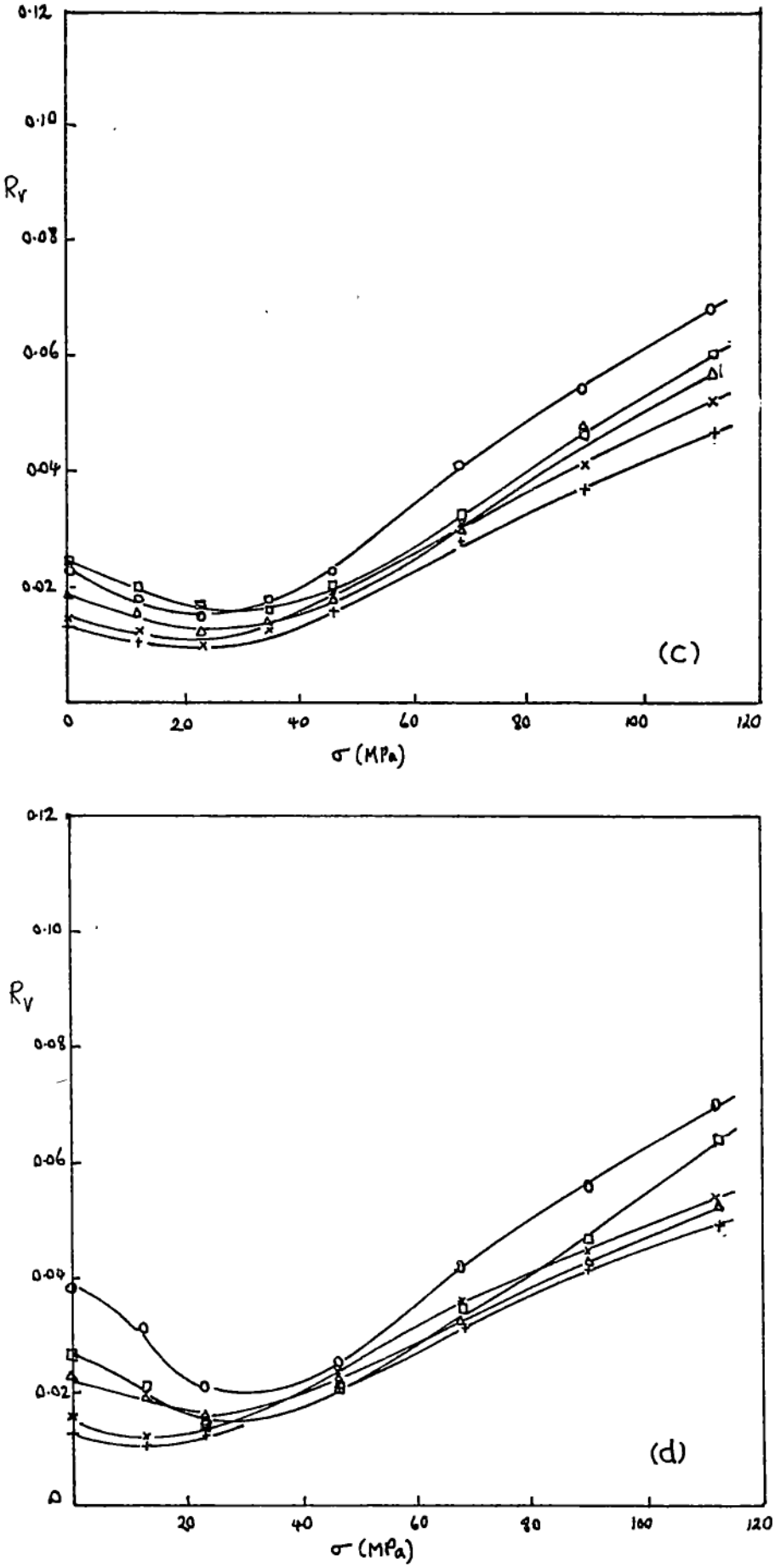

Figure 5.7 (continued) (c)120°C, (d) 165°C.

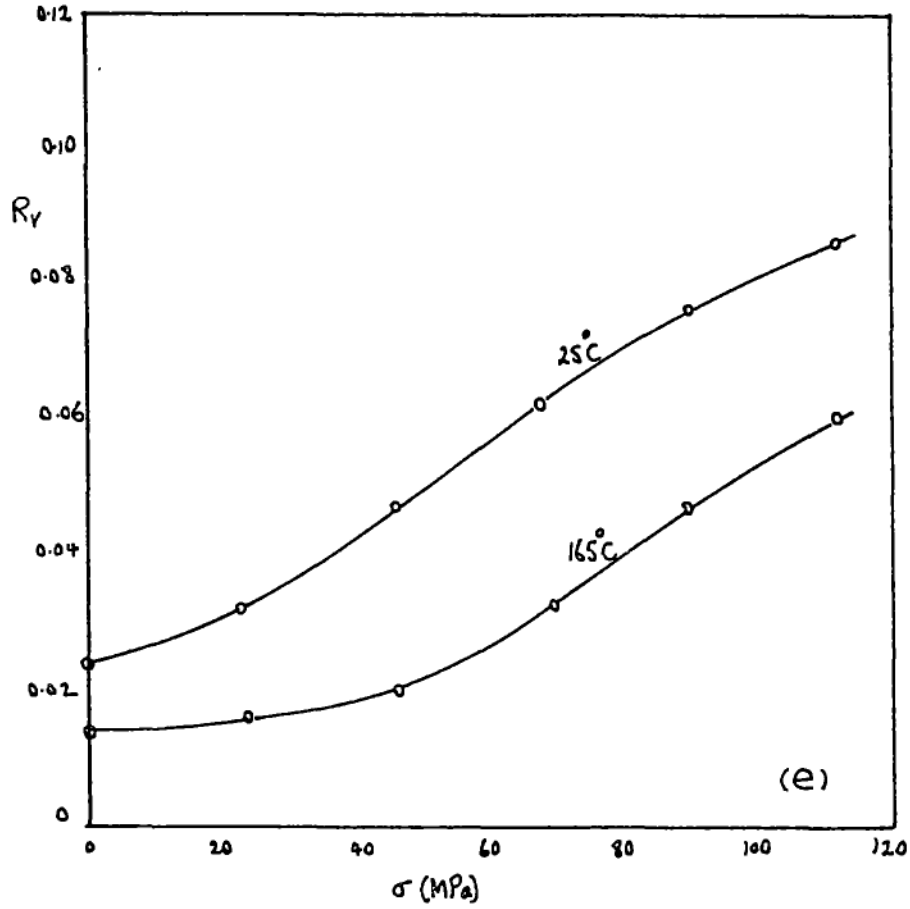

Figure 5.7 (continued) (e) comparison for 25°C and 165°C for field strength H=800A/m.

constant temperature, of 175MPa. Figure 5.7e gives results for 25°C and 165°C. If the rotation of field were dependent on strain I would expect for the same stress higher values of R_v at the higher temperature - the opposite of what occurs. However this is not conclusive evidence that the rotation depends only on stress; the results merely show that temperature has an effect. Since the amount of rotation depends on the difference between permeabilities parallel and normal to the stress, all figure 5.7e shows is less difference between permeabilities at the higher temperature. Possibly permeabilities in both directions are slightly decreased at 165°C, since the decrease of saturation magnetization due to this temperature would be about 5%. This might be hard to check since measurement of the B vs. H loop requires use of a Hall plate, which is extremely sensitive to temperature.

(4) Rotation rig measurements at different frequencies

All tests with the rotation rig were with 50Hz magnetising current, for the obvious reason of convenience. Although the voltage induced in the search coil depended primarily on the shapes of the hysteresis loops in the two principal directions, it may, especially with a thick steel sample, be affected by eddy currents in the sample. In order to study this, measurements were made at different frequencies, above and below 50 Hz.

The classical depth of penetration d and the thickness of the steel control eddy current behaviour. d is usually defined from $d = (2\rho/\mu\omega)^{1/2}$ metres in which ρ = resistivity in Ω-m, μ = permeability in H/m, and ω = frequency in rad/sec.

Although permeability can vary widely, and hysteresis makes an analysis very difficult, the order of magnitude of d may be estimated as follows. At the peak of a B vs. H loop for a particular mild steel sample (number S8), $\mu = \mu_o\mu_r$ = 0.7T/300A/m. If $\rho = 20\times10^{-8}\Omega$-m and ω = 314 rad/sec, then d = 0.75mm. Sample S8 is 0.42mm thick and as this is less than d one would expect that eddy currents would not significantly prevent the penetration of the magnetic field through the sample (not until the sample thickness is 4d is the field attenuated to less than 1% by the opposing field of eddy currents).

The small rotation rig was used on sample S8 with the search coil axis fixed at right angles to the poles. The field strength was kept at 800A/m at frequencies from 50Hz to 0.1Hz. The integral of the search coil voltage altered by less than 3%. The magnetic field on the far side of the sample also remained constant in amplitude at 10% less than the value on the search coil side of the sample and was the same as the decrease in field with no sample present. An increase of frequency, up to 700 Hz, did not (surprisingly) alter the integral of the search coil voltage, even though at 700Hz the field on the far side of the sample had halved its amplitude (at 700Hz, d = 0.2mm).

To conclude: eddy currents do not significantly alter the results with the rotation rig on thin steel, which means that any convenient frequency can be used. (An obvious reason for not choosing 50Hz is that 50Hz noise may then be filtered out). However if the steel is 4d = 3mm thick or more, then as far as eddy currents are concerned it is infinitely thick. Measurement show that R_v for thin steel is about twice as much as for thick steel. Different thicknesses inbetween d and 4d give different R_v values (all for the same stress). In order that R_v be unaffected by thickness it is important to use a frequency that gives a depth of penetration of less than 0.2 of the thickness of the steel. Since most structural steel is more than 3mm thick, the frequency should be above 50Hz. This is another advantage of A.C. magnetisation compared to D.C.

5.3 Improvements to the rotation rig

Disadvantages of the small rotation rig

(1) It used 50 Hz magnetization (from the mains) and so interference from other mains equipment could not be eliminated adequately. For example, the off-sample signal V_n was about 50μV under good conditions but was more usually about 100μV, compared with a maximum output, at the yield point of steel, of 1.6 mV (SCp set at 10mV; H=500A/m). This I judged to be too low a signal to noise ratio.

(2) It was not possible to distinguish (easily) the phase of the SCn signal relative to that of the magnetising current. A knowledge of the phase was essential to determine the direction of rotation of the field, and hence the sign of the principal stress (tensile or compressive).

(3) It was too big. It needed a flat area on the steel of 70mm x 70mm. Also the two SCn coils together were 20mm long and so averaged the rotation of the field, and hence stress measurement, over an area of 20mm x 20mm.

The very small rotation rig (V.S.R.R.)

Figure 5.8 shows the arrangement of this core and coils. A standard C-core with its laminations already glued inside each other was used instead of laminations stacked in the other direction (as in the S.R.R.). It was compact and already had flat squared-off pole faces. A possible problem was that the width of the core was 10mm and its length was 25mm, compared with the 47mm x 47mm of the S.R.R. The relatively narrow width of the C-core gave a less uniform magnetic field between the pole faces but this did not apparently affect its performance.

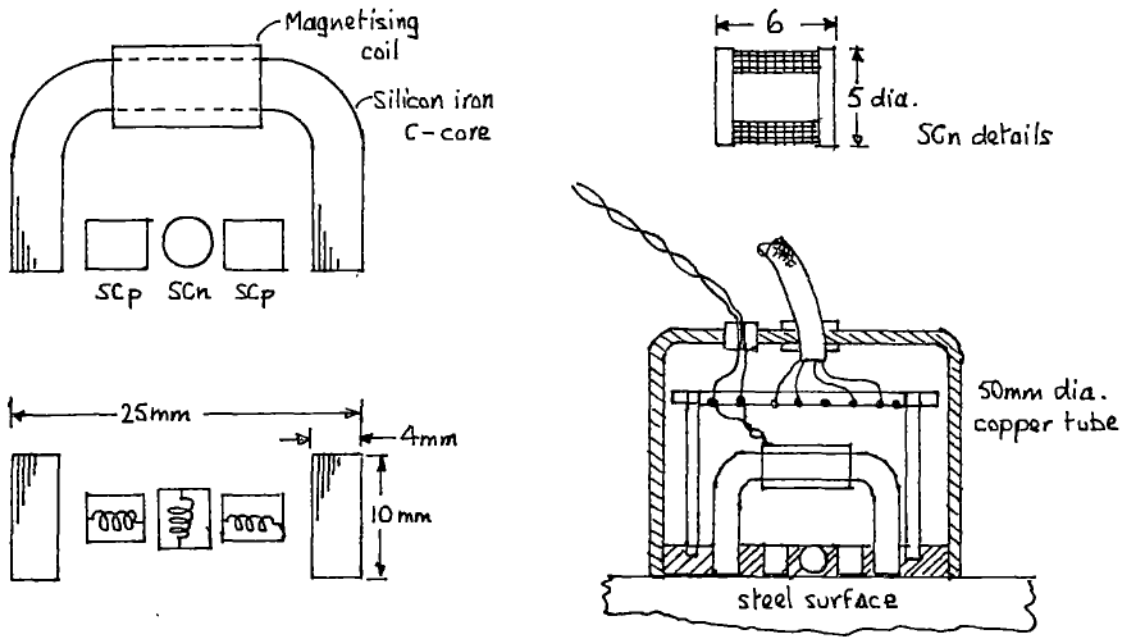

Figure 5.8 The Very Small Rotation Rig (V.S.R.R.). The magnetising coil has 200 turns of 30B&S wire, search coil SCn has about 2000 turns of 48 B&S wire, and SCp both have about 1500 turns of 48 B&S wire.

(The different directions of the stacking of the laminations have more implications than would appear. Wilkins and Drake [W2] used a stack of laminations to measure the losses in uncut electrical sheet steel; their equipment was the model for the C-core rig described in chapter 3. At first they made the cores from a toroid wound from a continuous strip by grinding away a segment of the toroid. They found it "impossible to derive

any detailed information of the power loss of the steel under test. There appeared to be an over-riding variable factor which masked and confused the significance of the results; this was attributed to the reluctance of the gaps between the strips which, it was thought, had the effect of altering the pattern of the flux between the yokes, for each material under test. Satisfactory yokes were subsequently designed to be free of radial discontinuities and were made up from ring laminations". This was in my mind when designing the V.S.R.R. with the C-core. When in use it did give some inconsistency in readings - no more than about 2% at maximum signal - which the S.R.R. did not have. Possibly it was caused by the effect that Wilkins and Drake noticed).

The coils had to have as many turns as possible which meant using fine wire. The smallest size in stock, 50 B&S, proved too fragile and so 48 B&S was eventually used. It was only 0.03mm in diameter, was difficult to see, and made the job of coil winding and connections delicate and slow. The whole core and coil assembly was inside a 50mm diameter copper cover, with 10 degree intervals marked on the outside, so that the angle it was turned through could be estimated to 2°. (The S.S.R. was in a square box, which made angular measurement awkward).

Signal processing

The main aim here was to use a phase sensitive filter. This effectively means multiplying the search coil signals by a reference square wave derived from the same source as the magnetising current. Any signal frequencies other than the reference are completely eliminated, and the filter output voltage has a direct component whose polarity depends on the phase of the signal relative to the reference. For example, an inphase (0°) signal might give a positive component, a 180° signal would then give an equal negative component, and a 90° signal would give zero.

Figure 5.9 shows the circuit. The oscillator is described in National Semiconductor Applications Note AN29-8 of February 1973. The more usual Wein Bridge circuits have more complicated stabilising methods and are more temperamental. The frequency was set at 68Hz, which is clear of any harmonics of the mains. The power amplifier will give up to 0.5A which is more than enough for the needs of magnetising current. The signal coils are connected to the control box via a 4-core screened cable, which is kept separate from the twisted pair carrying the magnetising current. This separation is better at reducing interference than having the high current leads with the signal leads, although not as neat.

The basis of the phase-sensitive filter is the MC14016B FET switch. Its "on" resistance is 300 ohm; "off" resistance 10^{12} ohm. The reference signal is obtained from the oscillator via a phase-shifting network and two operational amplifiers without feedback. One is inverting, and the other non-inverting, to give outputs 180° apart. The square wave output of +15V is clamped at +5V and -0.7V by zener diodes before going to the control inputs of the FET switch.

A simple voltage divider from the supply is adequate to back off the off-sample signal in SCn (V_n) to within 1μV. Without any back off, V_n is 30 μV when the SCp signal V_p is 30mV. Maximum V_n reading on thick steel, at yield, is about 1.4mV. (Figure 5.9 actually shows the circuit for later rotation rigs R.R.6 and R.R.7. The circuit described here differs only slightly; not enough to justify a separate circuit diagram).

Rotation rig R.R.4.

The slight inconsistency in readings from the V.S.R.R. that may have been caused by the radial air gap in the C-core was a nuisance and so yet another small rotation rig was built. It is shown in figure 5.10 and was named Rotation Rig number Four (R.R.4). It used a core of Mumetal laminations of the same proportions as the S.R.R, and could be plugged in

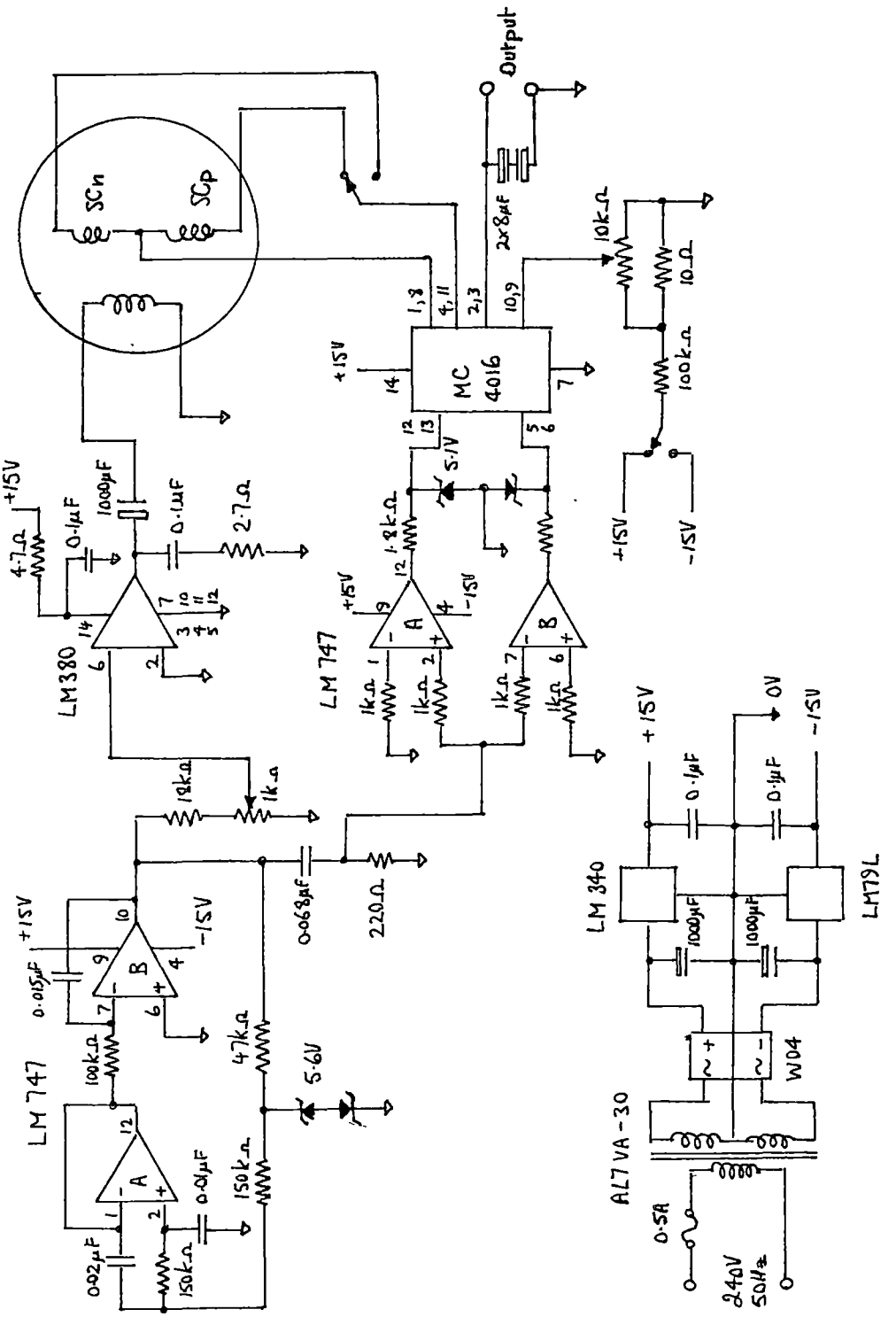

Figure 5.9 Magnetising current supply (68Hz) and phase sensitive filter for the V.S.R.R., R.R.6, and R.R.7 rotation rigs.

to the circuit of figure 5.9. The inconsistency in V_n readings (of the V.S.R.R.) appeared to be absent, and in fact a comparison between the three rotation rigs showed R.R.4 to be the best.

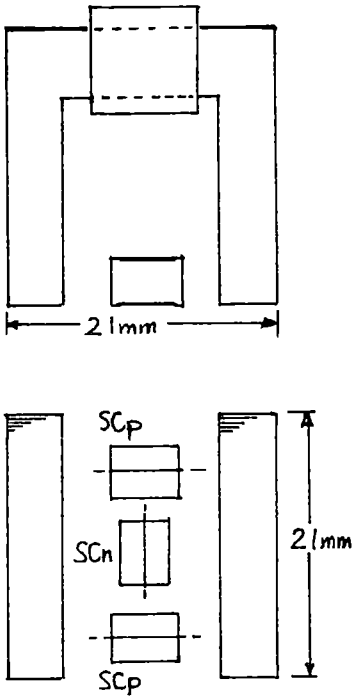

Figure 5.10 Dimensions of the rotation rig R.R.4. Coils SCp and SCn are the same as for the V.S.R.R.

Use of the rotation rig: Rv and differences of principal stress

A steel sample in uniaxial stress is used as an illustration. Firstly, the sample in tension. Figure 5.11a shows the rotation rig on the steel with its poles at angle ϕ to the direction of (principal) stress. As ϕ is altered the output voltage of the rotation rig varies as shown. (Voltage does not in theory vary sinusoidally with angle - see chapter 3). The maximum positive reading is when the principal stress (tensile) lies at about 45° anticlockwise to the pole axis.

Secondly, the sample in compression. Figure 5.11b shows that the maximum negative reading is when the principal stress is at about 45° anticlockwise to the pole axis. However, when ϕ = 135°, maximum positive reading occurs and this case is the same as for the same stress in tension. The rotation rig cannot distinguish between tension and compression. All it

does is to show that the more positive principal stress lies at about 45° anticlockwise to the pole axis at maximum positive reading.

However, any ambiguity over this is quickly resolved for a particular rotation rig. It can be placed on a sheet of steel that is flexed to make one side in tension, and when the rotation rig is rotated on it, the sign of V_n can be checked with the direction of principal (tensile) stress. The behaviour for the more general case of biaxial stress is dealt with in chapter 6.

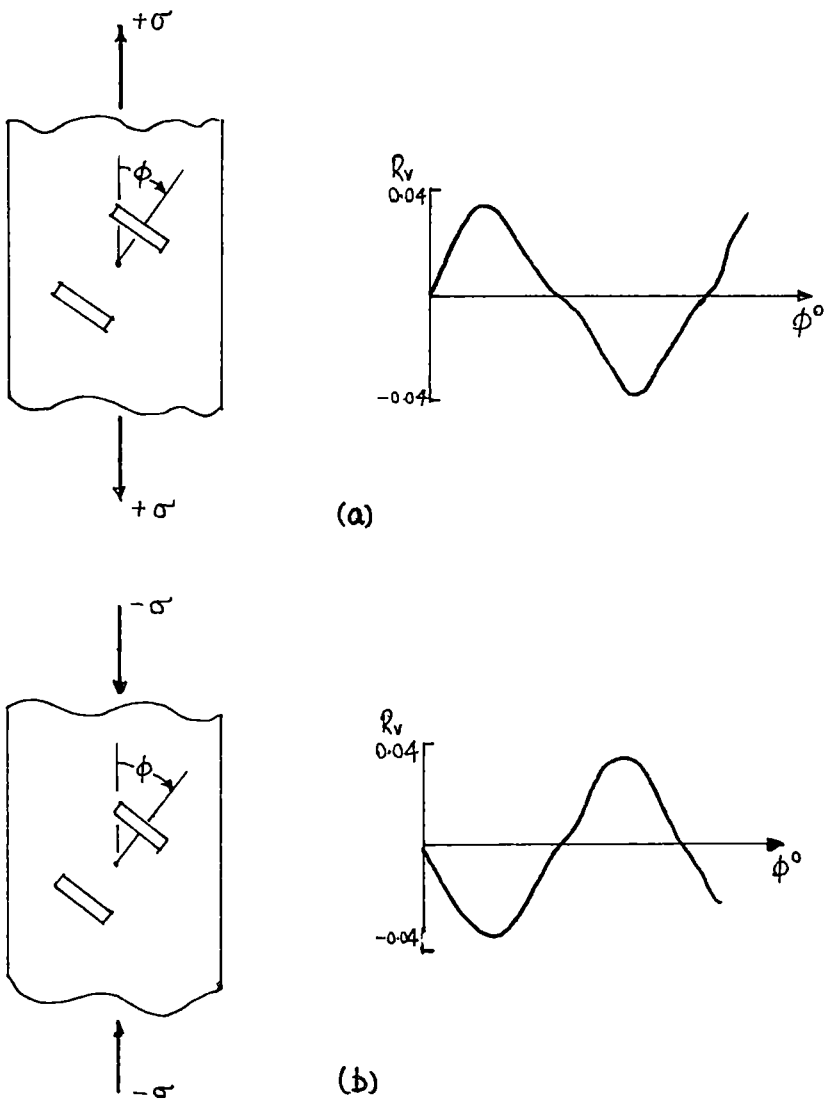

Figure 5.11 The sign of R_v and possible ambiguity between readings for tension and compression.

5.4 Comparison of the three rotation rigs

This section gives a comparison of the R_v vs. σ (σ = stress) curves of the Small Rotation Rig (S.R.R.), the Very Small Rotation Rig (V.S.R.R.), and Rotation Rig number Four (R.R.4). They have different sized cores, and search coil size relative to core size. These are shown, full size, in figure 5.12. The detailed geometry is arbitrary in that the pattern of the magnetic field and of the eddy currents in the steel samples is not completely known, and maybe a "better" result could be obtained with a different core and coil arrangement.

Two samples of annealed mild steel were used for the comparison: a 400mm x 0.42mm piece of sheet and a 1000mm x 102mm x 12mm piece of bar.

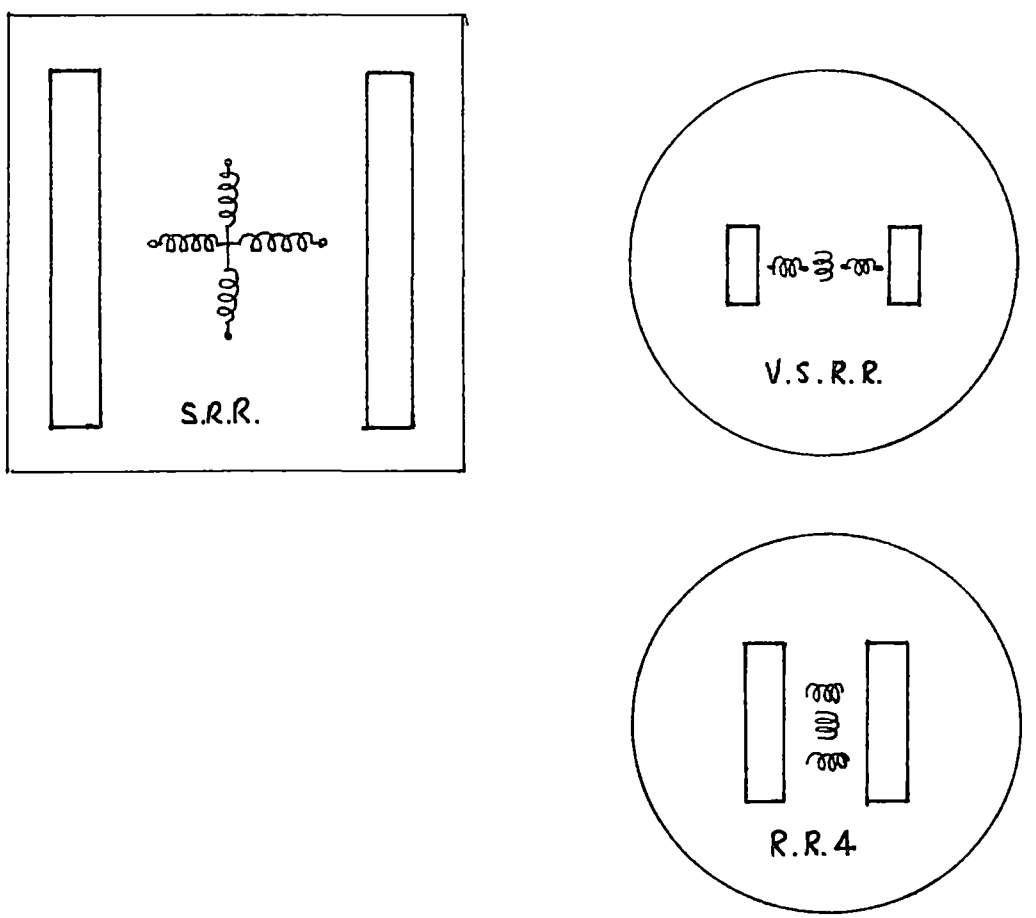

Figure 5.12 A comparison of the actual sizes of the three rotation rigs.

The significance of the setting of the applied field

Figure 5.5 shows the effect of four different values of field strength on the R_v vs. σ curves for the S.R.R. The sensitivity and shape do not vary much. Maximum sensitivity occurs in the region of the "knee" of the B vs. H curve for mild steel, at about 500A/m and 1.1T. The R_v vs. σ curves for the V.S.R.R. and for R.R.4 are also rather insensitive to the applied field. As a result any one value of field would probably give an R_v vs. σ curve that would be typical of the particular rotation rig, but I preferred to test with two different values of field.

Figure 5.13a shows how the magnetic field strength parallel to the surface of the steel is related to the voltage V_p induced in SCp. (This graph is given here since in some later chapters values of V_p rather than field strength are given). Field strength was measured with a Hall plate, placed as sketched in figure 5.13b, with the rotation rig off the steel. The field is not uniform over the area of the Hall plate so the readings represent average values. When the probe is placed against the steel V_p decreases by up to 50%, indicating that the field seen by the SCn coil is reduced. Figure 5.13c is the B vs. H loop for annealed mild steel, and may be used to relate the V_p reading on the steel to the flux density in the steel - but only very approximately.

Tests and presentation of results

Maximum tensile stress was 184MPa for the thin sample and 200MPa for the thick one. (For each the yield point was about 260MPa). Stress was calculated from the applied force divided by the cross sectional area of the sample.

Several graphs are shown of the same tests but with the data treated in different ways to bring out different aspects. Figures 5.14, 5.15, and 5.16 show R_v vs. σ curves for the S.R.R., V.S.R.R., and R.R.4 respectively.

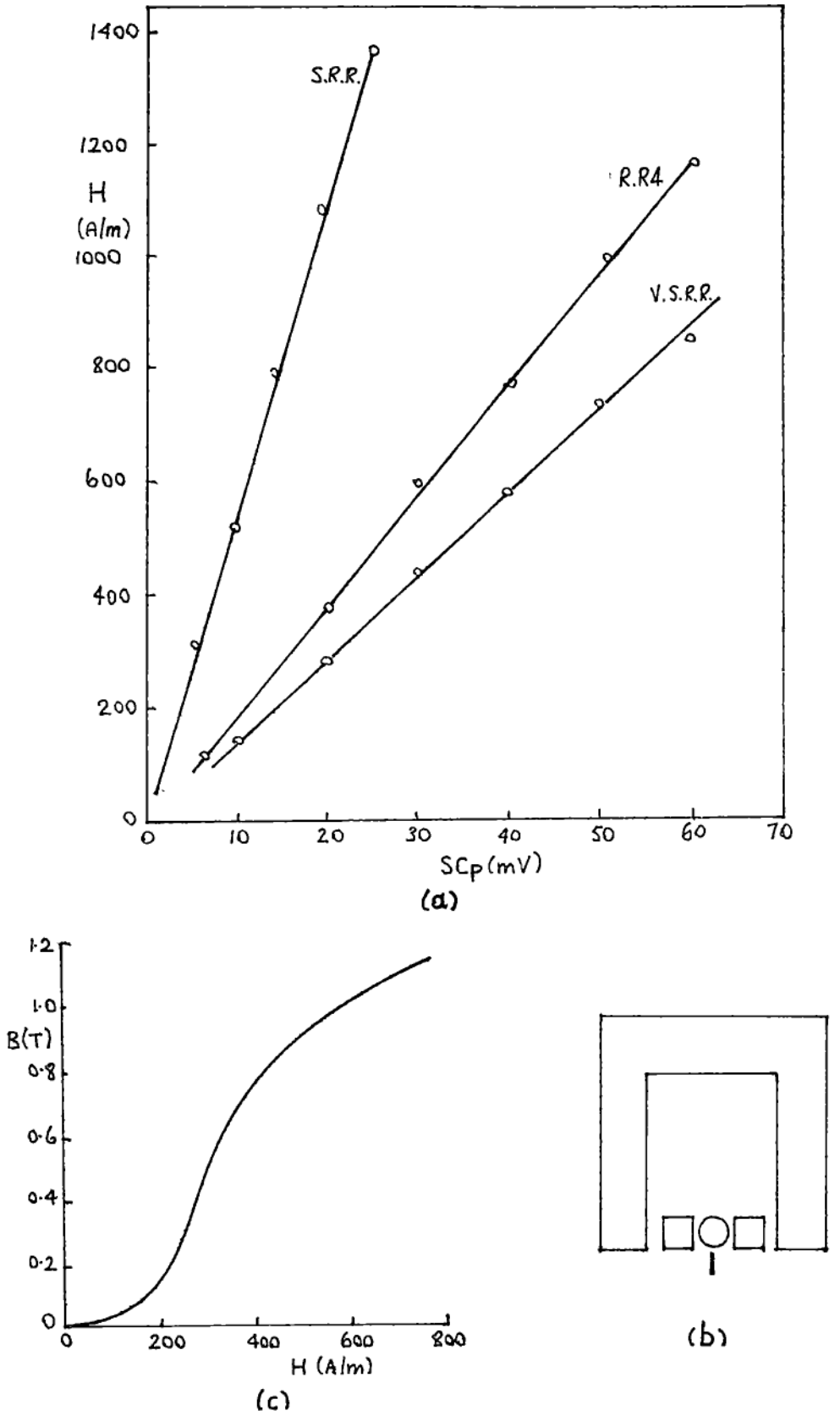

Figure 5.13 (a) field strength H vs. voltage V_p induced in SCp coil, (b) position of the Hall plate for relating the off-steel field strength to Vp, (c) B vs. H curve for the 0.42mm mild steel sample used for the comparison of the three rotation rigs.

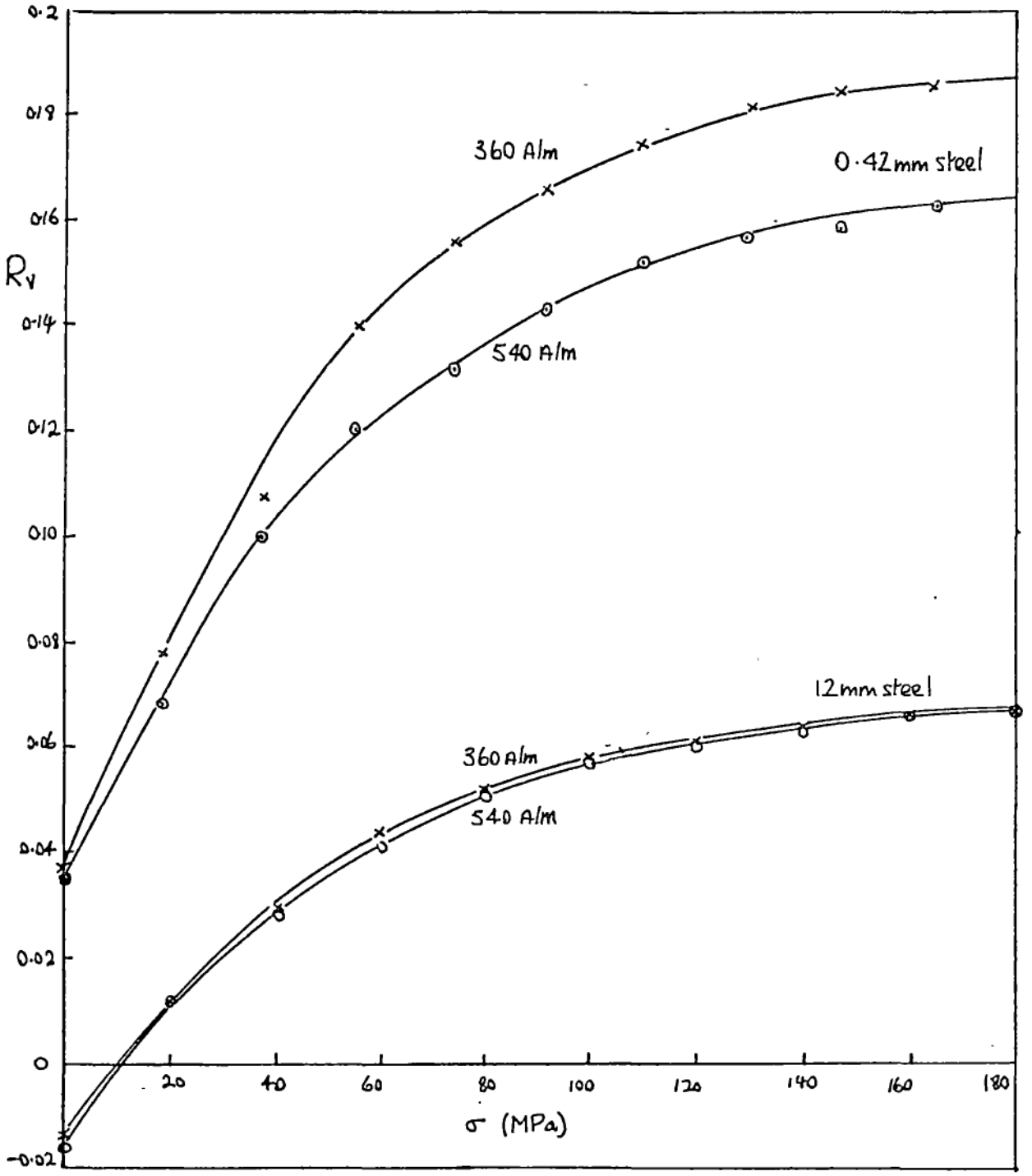

Figure 5.14 R_v vs. σ for the S.R.R. on thin (0.42mm) and thick (12mm) mild steel.

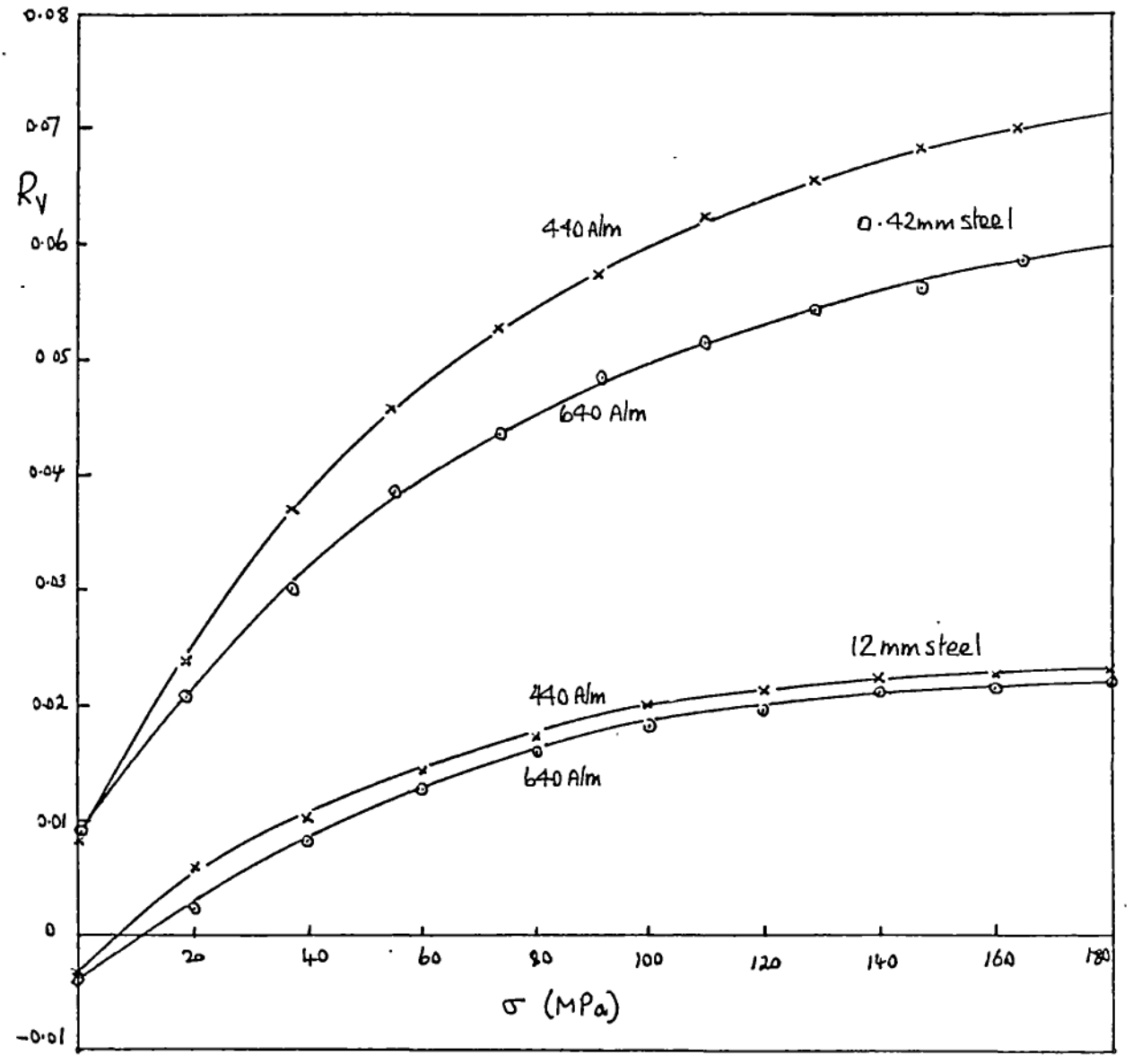

Figure 5.15 R_v vs. σ for the V.S.R.R. on thin (0.42mm) and thick (12mm) mild steel.

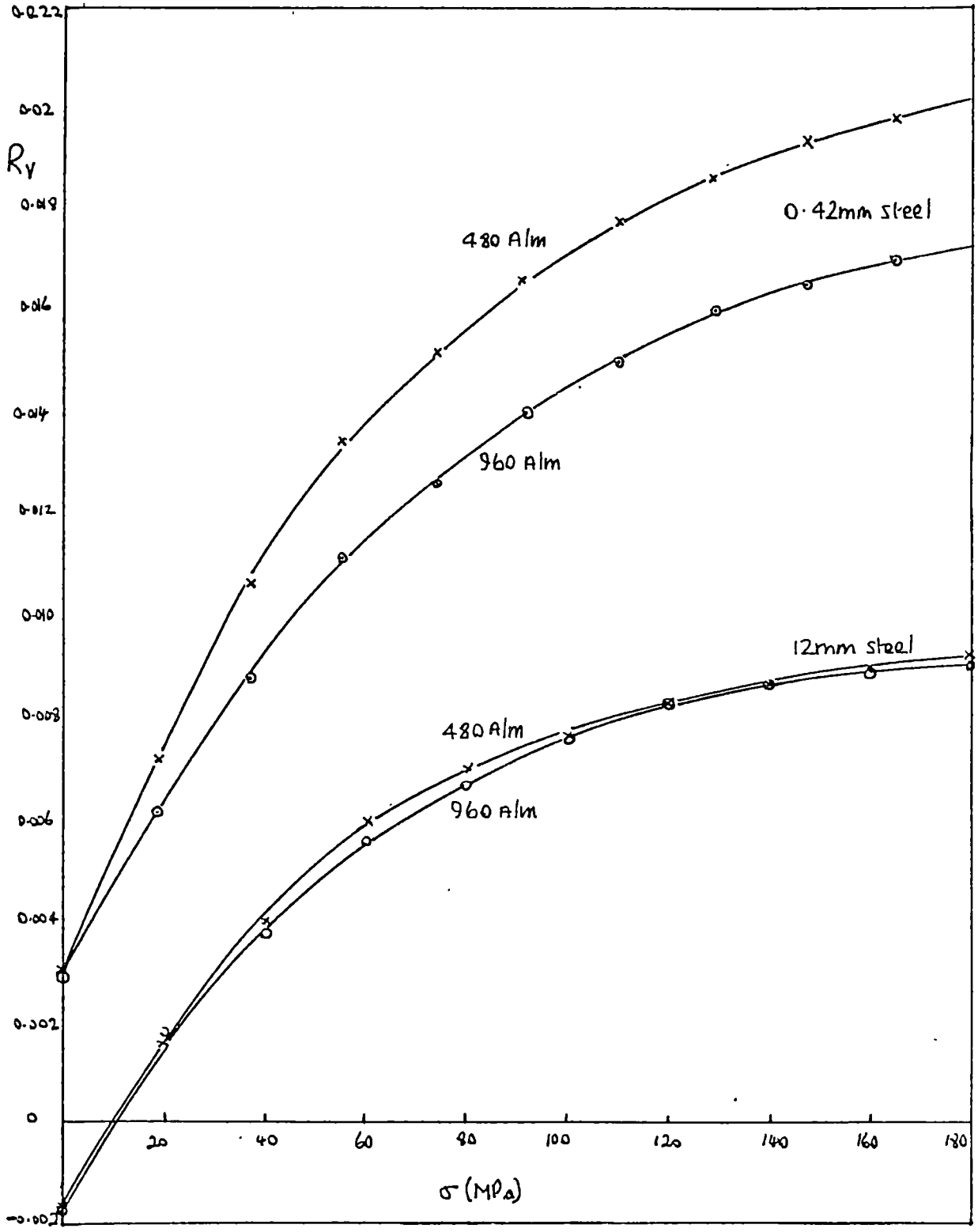

Figure 5.16 R_v vs. σ for R.R.4 on thin (0.42mm) and thick (12mm) mild steel.

In order to compare the shapes of the curves at different magnetizing currents and on the two samples, the R_v values have been scaled to be equal to 1.00 at 100MPa for all tests. Figures 5.17, 5.18, and 5.19 are the corresponding graphs for the S.R.R., V.S.R.R., and R.R.4. Finally, figure 5.20 compares the scaled curves for each rig for the thin sample, and figure 5.21 does the same for the thick sample.

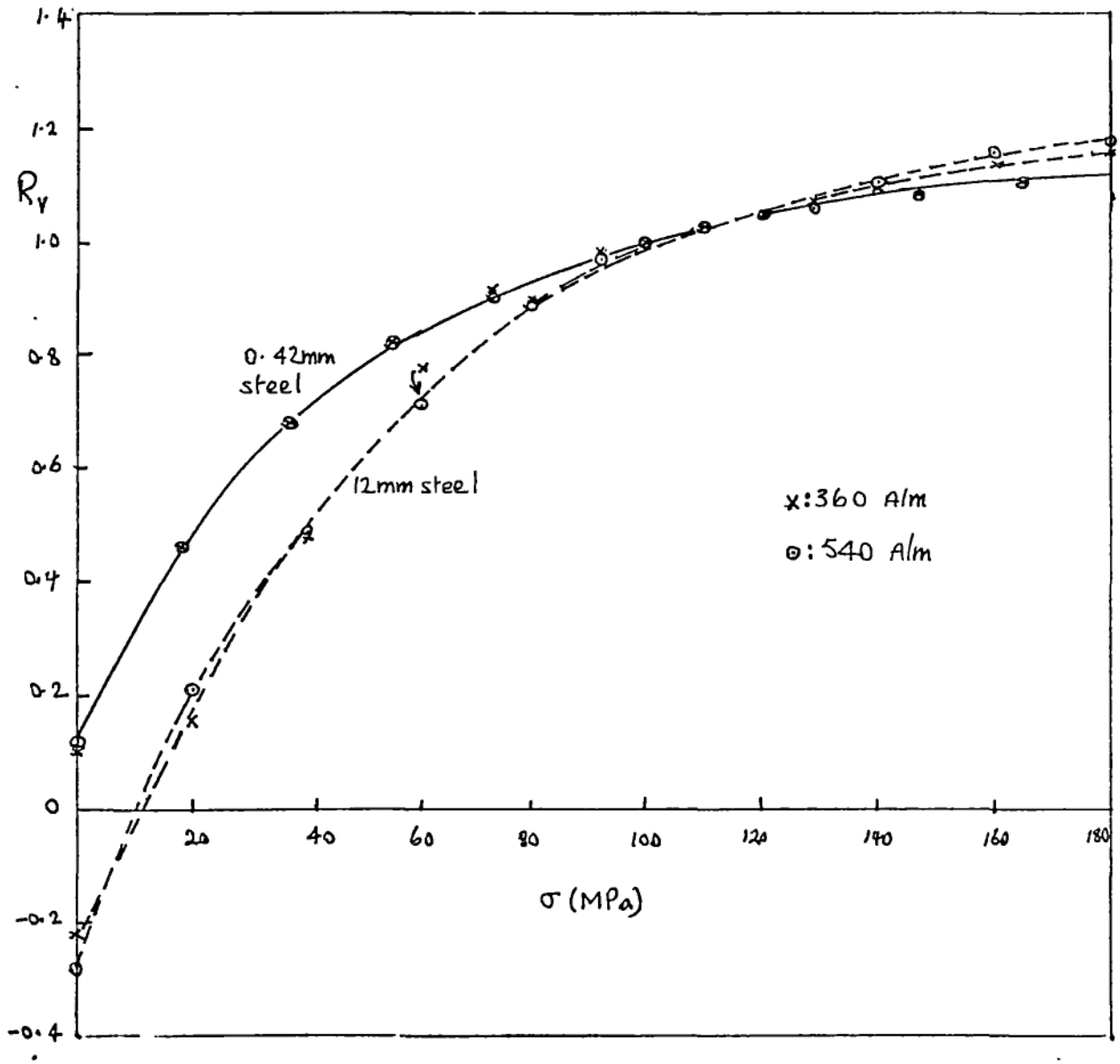

Figure 5.17 R_v (scaled to 1.00 at 100MPa) vs. σ for the S.R.R. on thin and on thick steel.

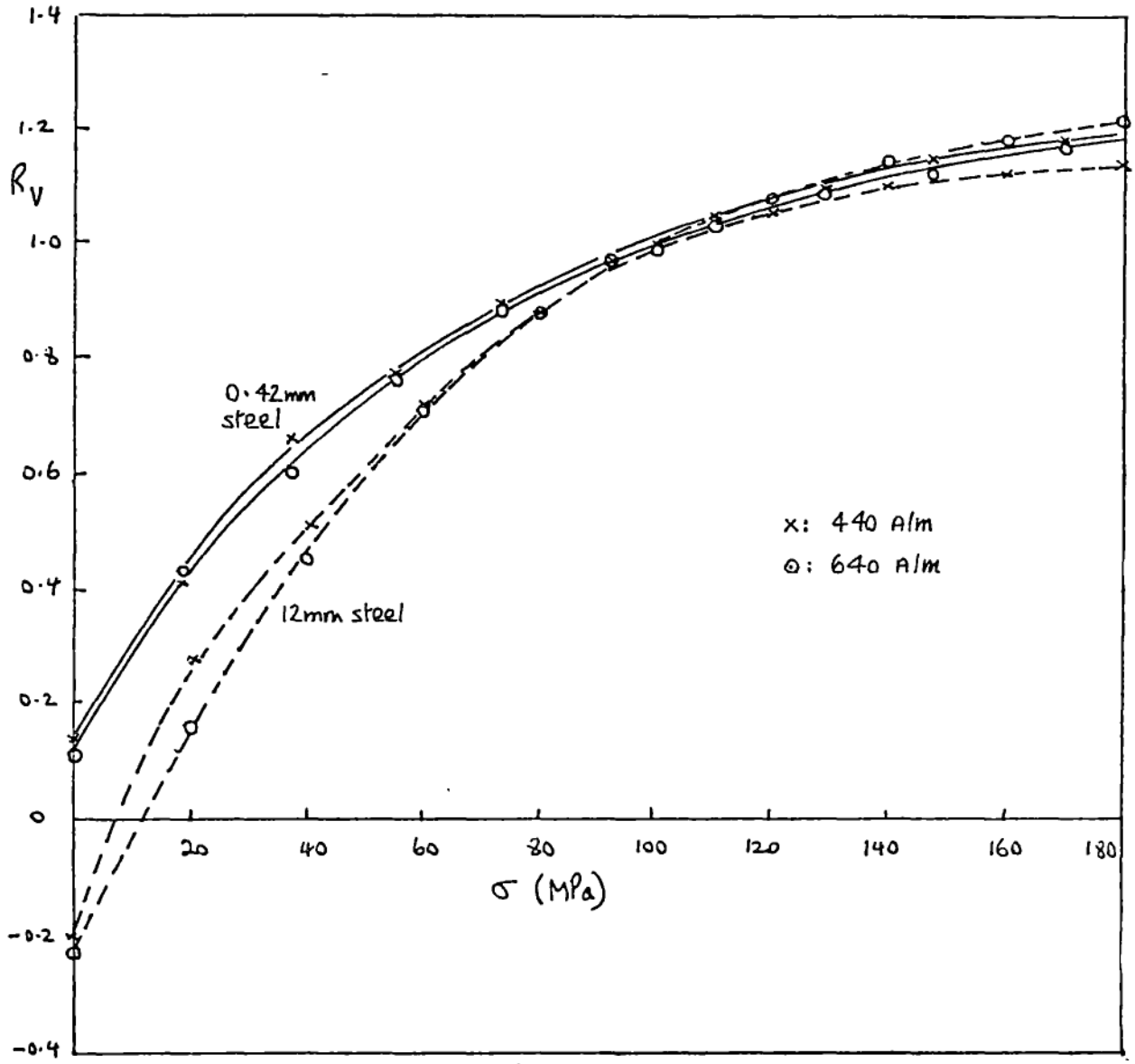

Figure 5.18 R_v (scaled to 1.00 at 100MPa) vs. σ for the V.S.R.R. on thin and on thick steel. (The spread in the four curves at the R_v=1.00 value shows up the random error in the readings with this rotation rig).

A note about the use of rotation rigs and how R_v was obtained may be useful. When using the V.S.R.R. or R.R.4, I always turned it from +45° to -45° to the stress axis so that the reading changed from, say, positive maximum to negative maximum. The readings were often not quite the same but by using the algebraic difference between them (denoted by $\hat{V}_n$) the effect of any residual signal in SCn could be eliminated (assuming it was in

phase with the wanted signal, and it did appear to be). R_v was then calculated from $\hat{V}_n/2V_p$. The output of the S.R.R. was A.C. but the phase change in SCn in going from +45° to -45° was of course still there, and so for these tests the sum of the two maximum readings was used to calculate R_v.

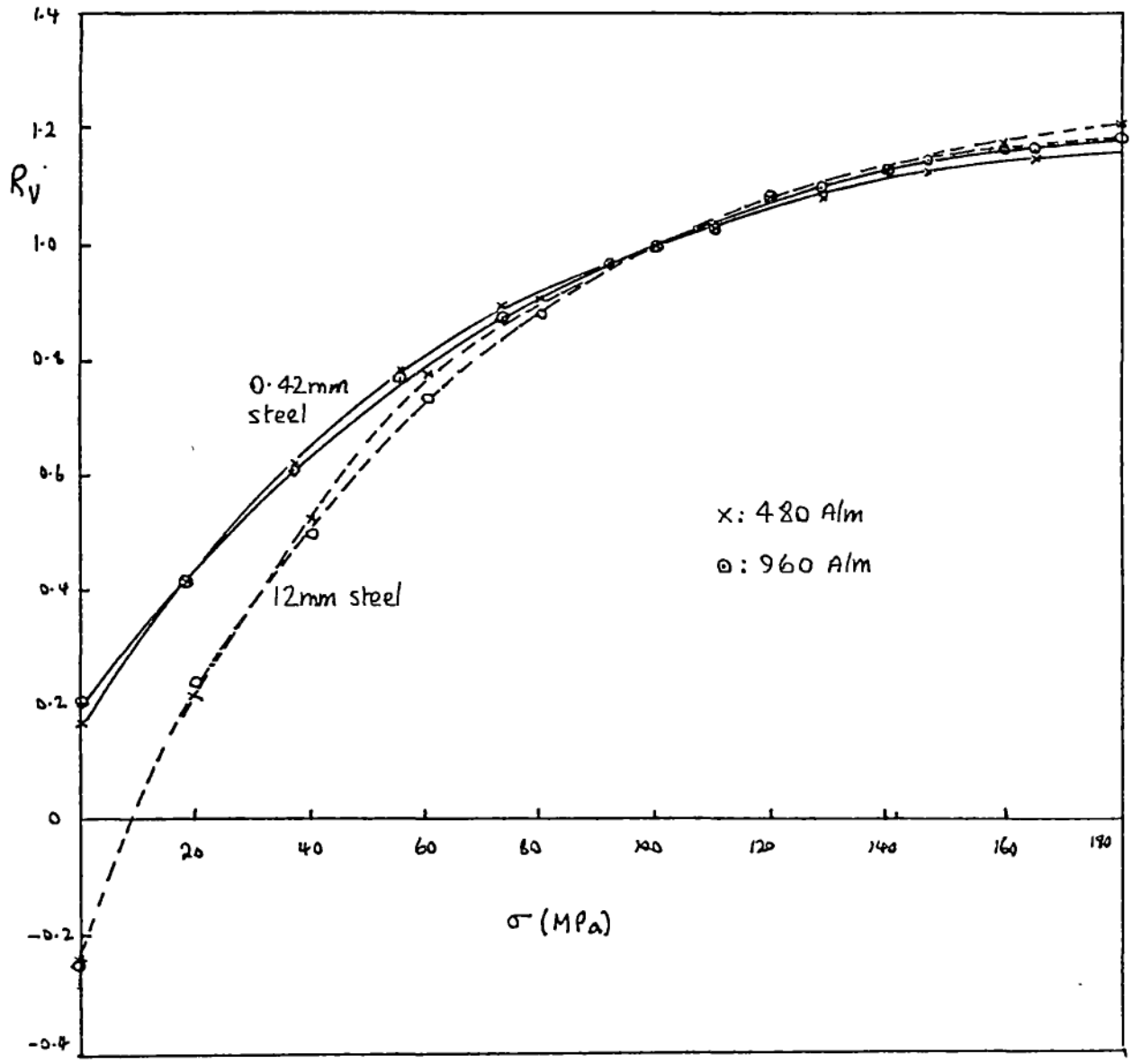

Figure 5.19 R_v (scaled to 1.00 at 100MPa) vs. σ for R.R.4 on thin and on thick steel.

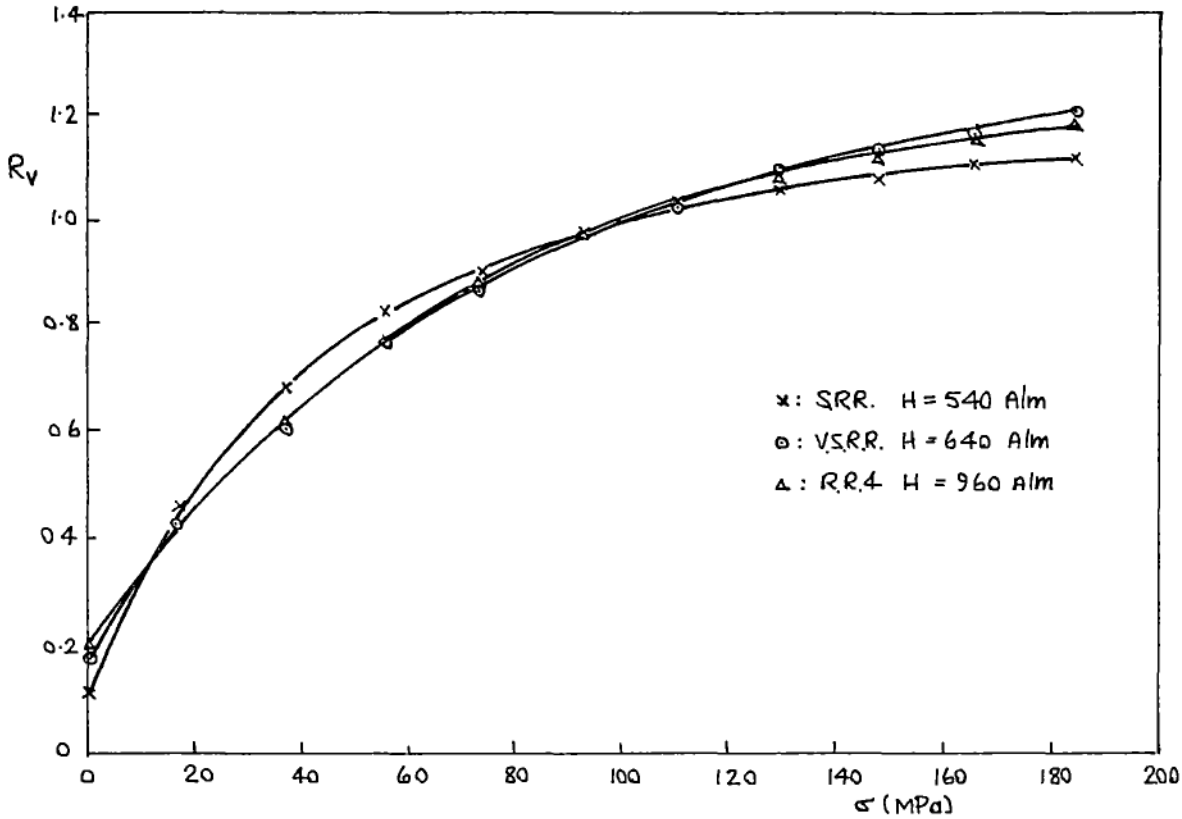

Figure 5.20 (upper) Comparison of scaled R_v values for the 0.42mm steel.
Figure 5.21 (lower) Comparison of scaled R_v values for the 12mm steel.

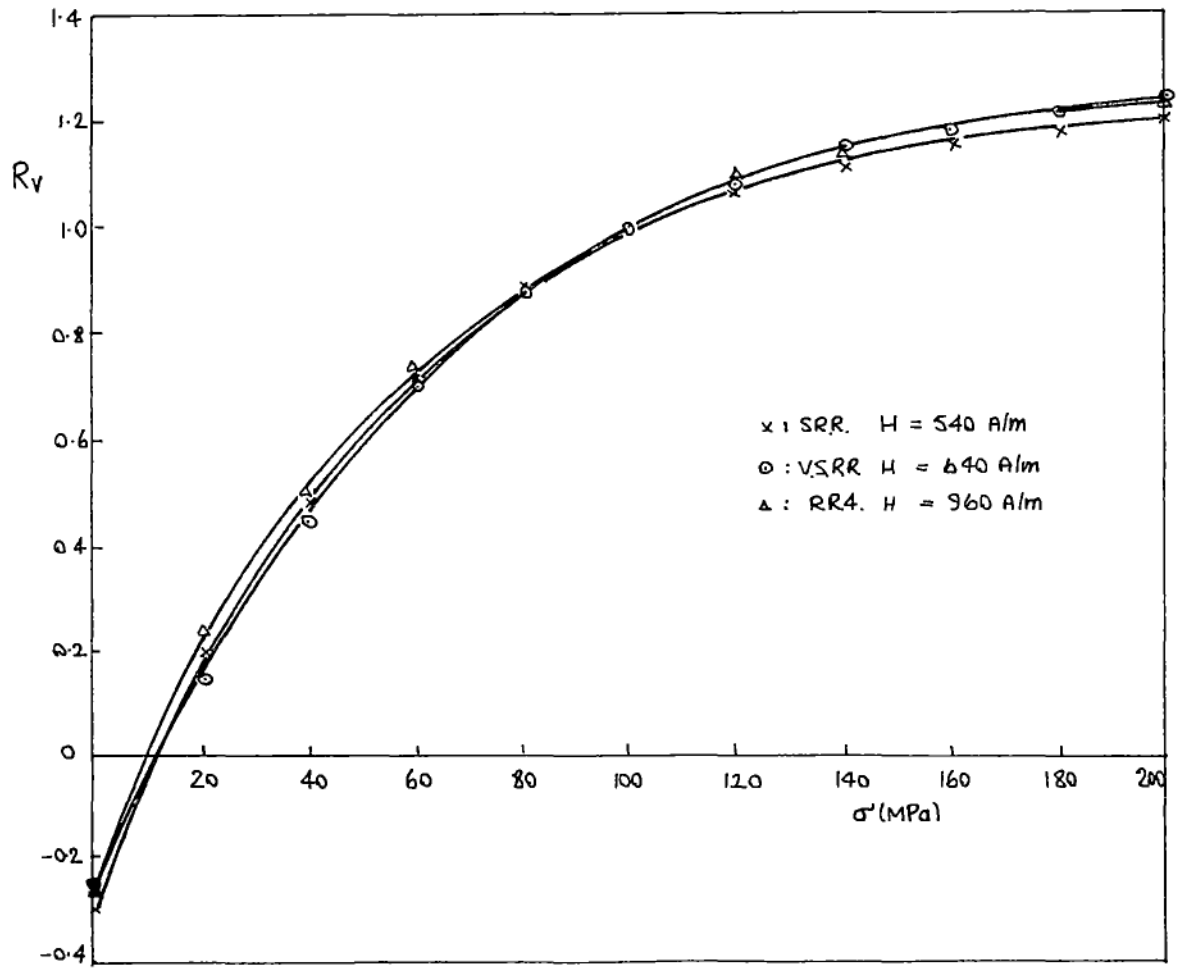

Discussion

Figures 5.14, 5.15, and 5.16 show that:-

(1) The lower SCp value always gives increased sensitivity on the 0.42mm sample (about 20% higher than for the higher SCp value), but makes very little difference on the 12mm sample.

(2) The 12mm sample decreases the sensitivity by at least 50%.

(3) At zero applied stress, the 0.42mm sample appears to have residual tension but the 12mm sample has residual compression (negative R_v values). A negative R_v is assumed for the S.R.R. when on the thick sample.

Figures 5.17, 5.18, and 5.19 show that, superficially, all four curves for a particular rotation rig are nearly coincident for stresses above 100 MPa. But this is deceptive, since the total change in (scaled) R_v values between 100 and 200 MPa is about 0.2 compared with the 1.0 change between 0 and 100 MPa. R.R.4 has the least spread of values (4%) but there is not too much to choose in this respect between the three rigs. In comparison, the error in the meter reading is about 1% of SCn at stresses between 100 and 200MPa.

It is interesting to see that the effect of the residual stress (or texture) has apparently disappeared at high applied stress, and in fact five of the six curves for the 12mm sample (that has residual compression) have greater R_v values than the six curves for the 0.42mm sample that has some residual tension.

5.5 Rotation rig probes R.R.6 and R.R.7.

R.R.4 was completed in 1981; it worked well but one drawback was that it needed a 50mm diameter flat area for a reading and could not measure nearer than 25mm to an obstacle. In 1983 I designed two more probes. R.R.6 was 18mm in diameter - as small as could be made with the existing coil-winding facilities. It turned out not to work too well on thick steel. The roughish surface of the test bar, plus the fact that bending (in order to

stress it) made it slightly curved, caused the probe to rock slightly on the bar as I rotated it and the readings to vary randomly by about 10%. Even a 25mm thick guide for the probe failed to prevent all rocking, and the readings still varied. One reason might be due to the fact that the SCn coil occupied all the space between the poles of the core, and was too sensitive to variations (caused by rocking the probe or surface unevenness) of flux next to the poles of the core.

R.R.7 was designed so that the SCn coil occupied only about a third of the space between the poles, and in this respect it was similar to R.R.4. The U-core had to be larger so that the SCn coil did not have to be made smaller. This probe ended up 25mm in diameter, and it could thus be used to within 12mm of an obstacle. Figure 5.22 shows the dimensions of both probes and details of the coils in them. Both probes had a 0.2mm (an arbitrary thickness) paper spacer glued to the faces of the poles. This made an effective air gap between the poles and the steel and greatly reduced the variation of flux caused by uneven steel surface. Figure 5.9 shows the circuit diagram for the magnetising current supply and the filter.

(The missing number in the series is R.R.5. This was exactly the same as R.R.6 except that the magnetizing coil was accidentally wound to be too low an impedance. It could not be used with the same electronics as R.R.6 and R.R.7).

Figure 5.23 shows the test results for R.R.7 on thin (0.42mm) steel and thick (12mm) steel. The magnetising current was set to be the same for both; the output voltage and hence the sensitivity of the probe on the thick steel was about half the value for thin steel (at high stresses). Figures 5.24a-d are curves of R_v vs. stress for 12mm thick steel for both tension and compression. The sensitivity is greatest for the lowest field strength of 1000A/m and lowest for the highest field of 3500A/m. However, the bad feature of these curves, namely their non-linearity, is not as

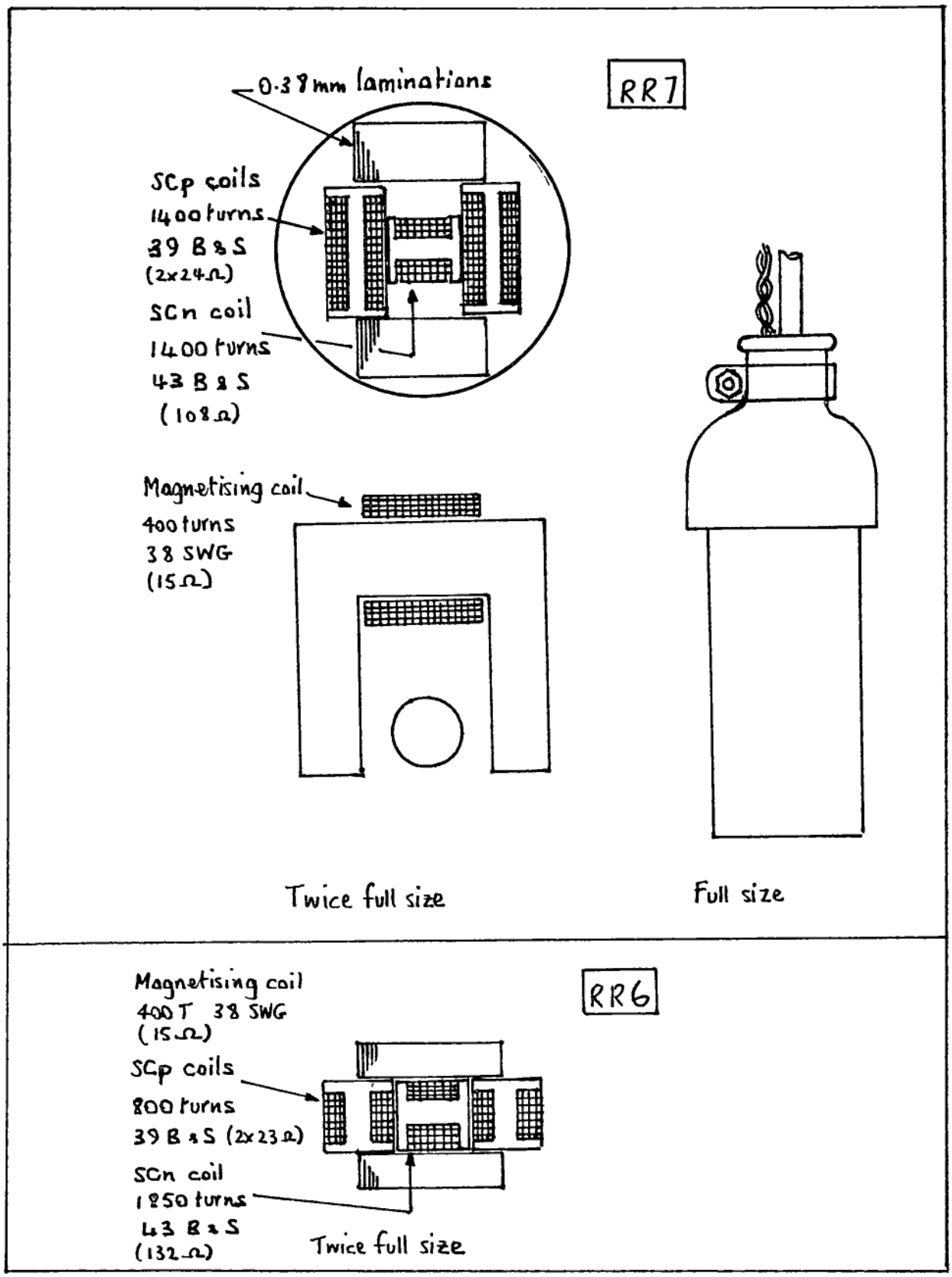

Figure 5.22 Layout and dimensions of rotation rig probes R.R.6 and R.R.7.

marked at the high field strength. This, together with the fact that the actual SCn reading is larger at the higher field strength, suggests that R.R.7 be used in future with as high a field as possible. The limit is about 3500A/m with the circuit of figure 5.9 but it would be useful to increase this if it led to a more linear characteristic.

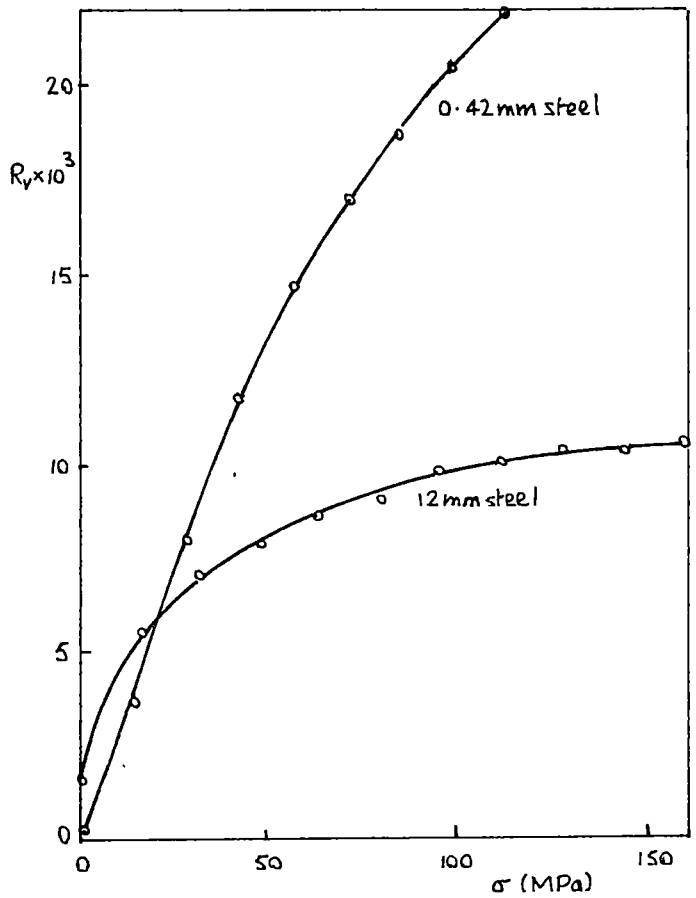

Figure 5.23 R_v vs. for R.R.7 on 0.42mm and 12mm mild steel. H=1500A/m in the off-steel position.

5.6 Correction of R_v for an air gap

If the surface of the steel is rough or slightly curved, or there is paint on it, R_v (or V_n) is affected; in general it is decreased. It can be corrected to allow for what is effectively an increased air gap by making use of a corresponding change in V_p. V_p is quite sensitive to the size of the air gap but is insensitive to stress. R_v is affected by both. Thus the value of V_p (or its average as the probe is rotated) can be used to correct R_v.

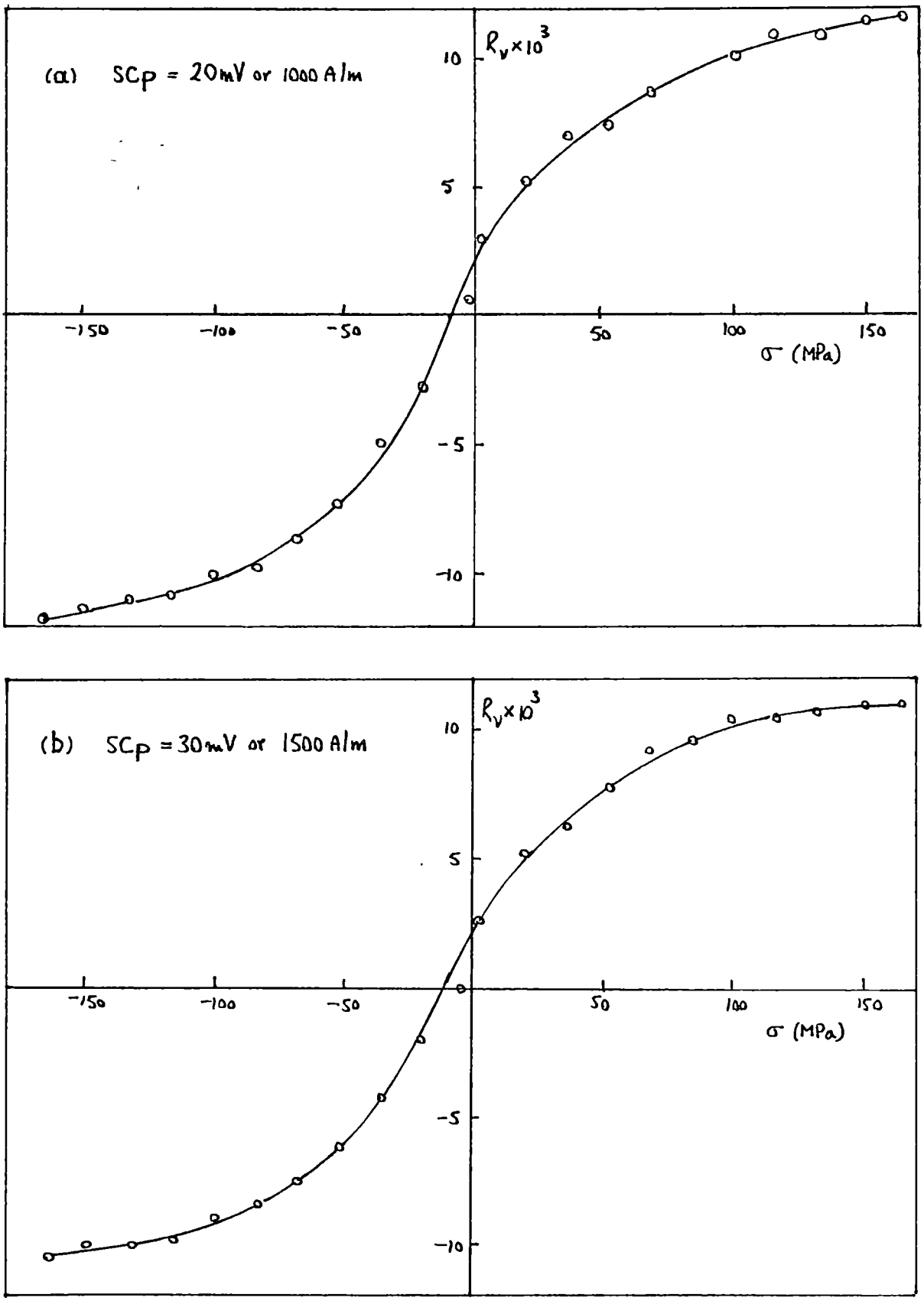

Figure 5.24 R_v vs. σ for R.R.7 on 12mm steel.
(a) H=1000A/m, (b) 1500A/m.

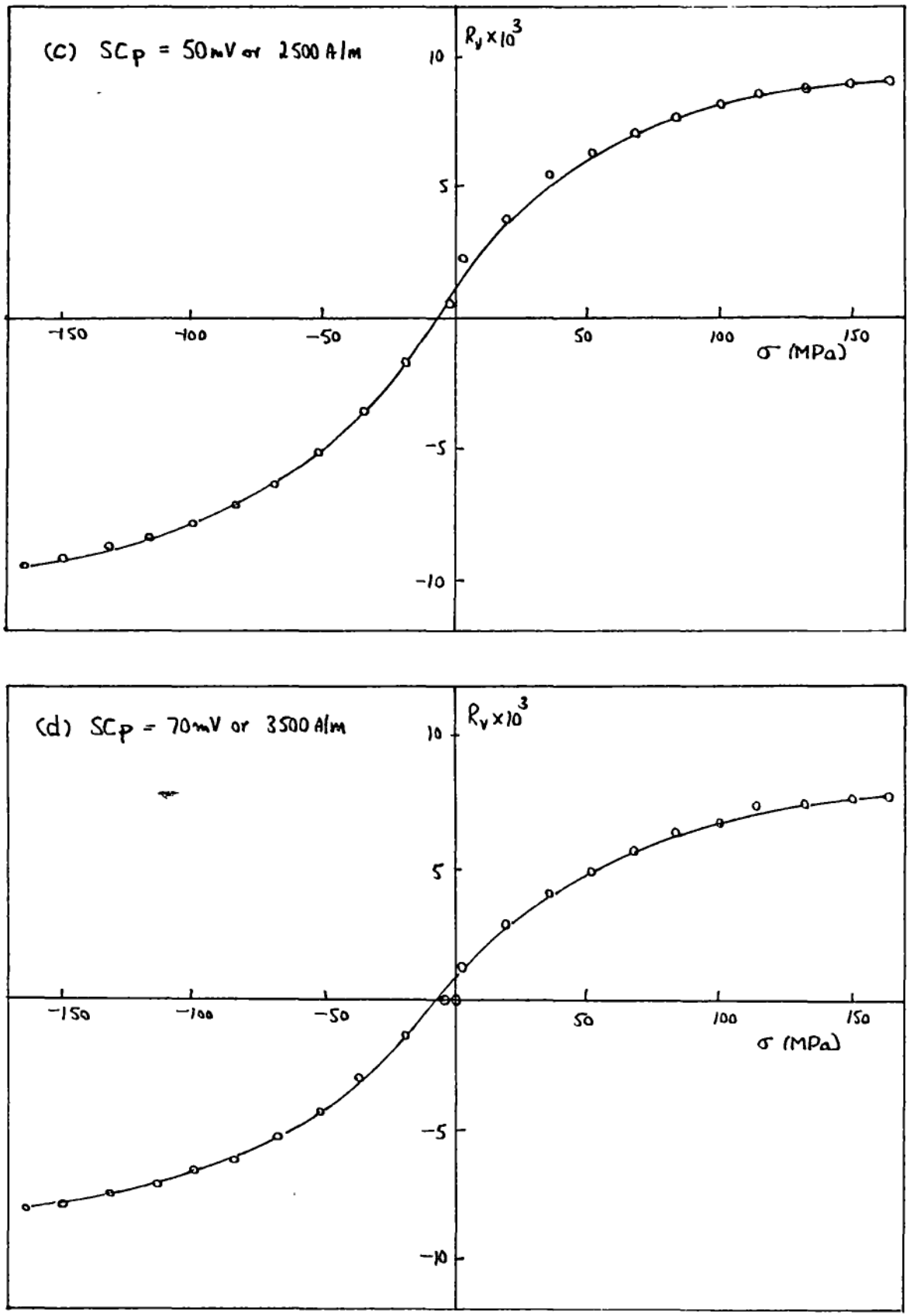

Figure 5.24 (continued) H=(c) 2500A/m, (d) 3500A/m.

As an example, an air gap of 0.12mm increases V_p (for R.R.7 on the 12mm steel bar) from 29mV to 33.5mV but decreases R_v from 0.085 to 0.070, i.e. it causes a 16% increase in V_p and a 19% decrease in R_v. Also, the percentage change in R_v due to change of air gap is almost independent of the actual value of R_v. Ideally, the calibration curves of R_v vs. stress should be done under conditions of minimum air gap on a flat sample, unlike those of figure 5.3 where the steel is curved by bending. Typically, on a smooth flat piece of steel, V_p is 28mV (when set at 50mV in air). A correction graph such as figure 5.25 can then be used. For small changes in air gap (<0.5mm) a linear correction is adequate.

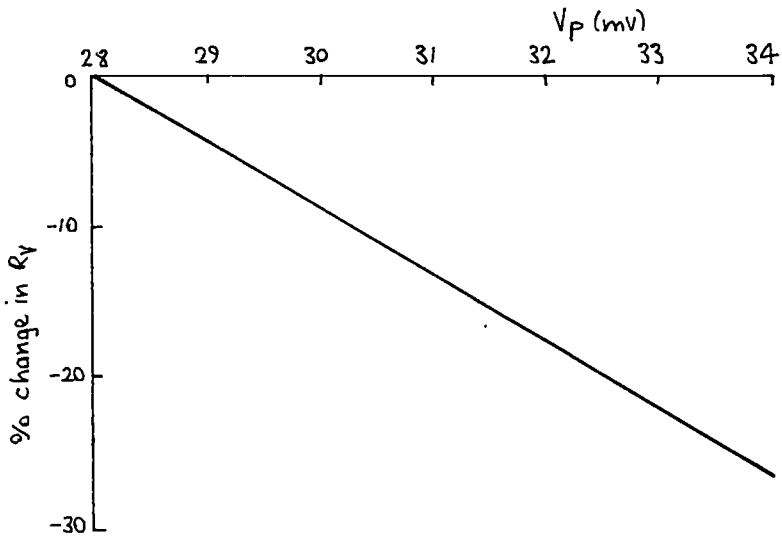

Figure 5.25 Illustrating the correction of R_v for a varying air gap (the calibration curves of figure 5.24 were obtained for V_p=29mV).

5.7 Conclusions

Later chapters deal with other tests with the rotation rig that bring out other features of it. For this reason, a summary of the main characteristics of R.R.7 are left until chapter 16.

CHAPTER 6

BIAXIAL STRESSES

Since the cause of rotation of magnetisation is magnetic anisotropy that results from directional differences in stress, there would logically be no rotation for equal biaxial stresses. This was shown to be the case by a test in which biaxial tensions were applied to mild steel.

6.1 Equipment

The sample and the tensioning equipment are shown in figure 6.1. In order that the tensions could be set independently of each other, the horizontal force was applied via a frame that was suspended on springs from the vertical tension frame. The whole of the tensioning equipment was used inside the 2.6m demagnetising coils.

The cross-shaped sample was copied from one used by Basak and Moses [B8,1978] for their measurement of stress and rotational loss in silicon steel. (The same shape was also used for M.S.A. research with biaxial stresses at Shanghai University). The idea behind this particular shape is that different stresses can be set up almost independently of each other in the centre of the cross by altering the tension applied to each axis.

6.2 The use of resistance strain gauges with biaxial stresses

A single gauge should ideally respond only to longitudinal strain but in practice it is affected slightly by transverse strain. The particular gauges used here (Micromeasurements type CEA-06-250-UW) had a transverse sensitivity of 0.001 of the longitudinal value. Thus, for an accuracy of measurement of the order of 10 microstrain, transverse sensitivity can be ignored.

Strains ϵ are related to stresses σ by

$$\epsilon_x = \sigma_x/E - \nu\sigma_y/E$$

and $$\epsilon_y = \sigma_y/E - \nu\sigma_x/E$$

where E = Young's modulus and ν = Poisson's ratio. Hence

$$\sigma_y = E(\epsilon_y + \nu\epsilon_x)/(1 - \nu^2)$$

and $$\sigma_x = E(\epsilon_x + \nu\epsilon_y)/(1 - \nu^2)$$

The gauges were stuck onto the opposite face of the cross to the rotation rig. In order to set up the desired values of σ_x and σ_y the corresponding values of ϵ_x and ϵ_y were calculated from these two equations and the tensioning handles were turned until the strain gauge meter read ϵ_x and ϵ_y.

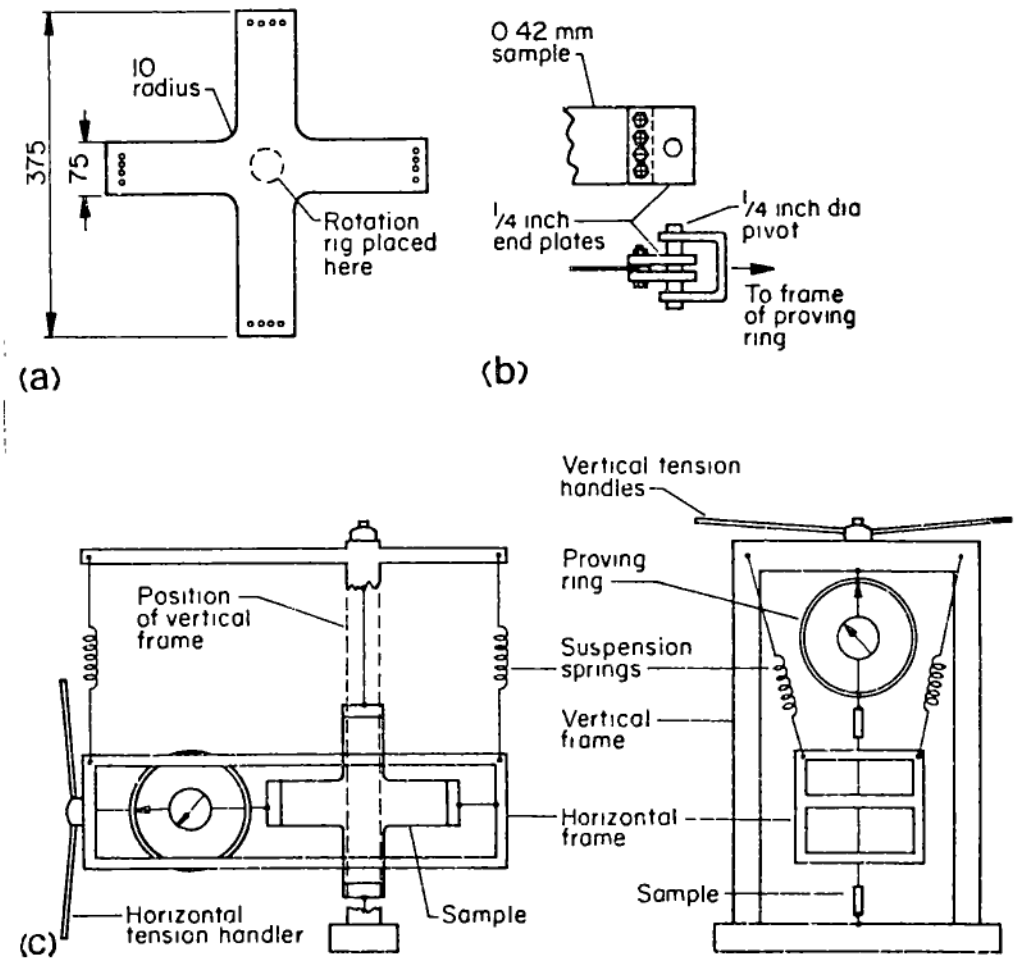

Figure 6.1 Equipment for the biaxial tension test: (a) 0.42mm thick mild steel sample, (b) arrangement for holding the sample, (c) test rig.

6.3 Anisotropy in the steel at zero load

The cross-shaped samples were cut from 0.42mm galvanised mild steel sheet. The galvanising was removed with hydrochloric acid and they were then annealed at 580°C. Rotation rig R.R.4 was used for the measurements, with V_p set at 25mV (H = 500A/m).

Readings with no load on the sample are given in figure 6.2 for eight orientations of R.R.4. A pair of readings separated by 180° (for example 2 and 6) should ideally be equal. The fact that they were not was probably a result of slight unevenness on the steel and a lack of exact symmetry in the rotation rig itself. The biggest difference in this instance was for positions 3 and 7 or 4 and 8, which each gave an R_v value of 0.0008. This corresponded to a stress difference of about 5MPa. However, it may also have been due to some texture that was not removed by the annealing.

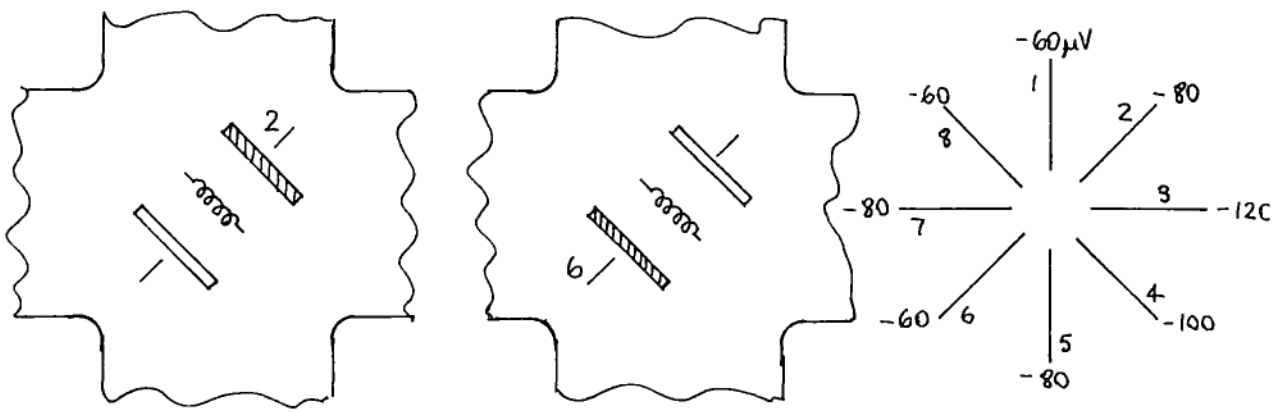

Figure 6.2 Rotation rig R.R.4 readings on the unloaded sample, showing the residual anisotropy.

6.4 R_v vs. stress for tension in each axis: results and discussion

Figure 6.3 gives the R_v value when the Y axis stress was fixed at various values (0 to 125MPa in steps of 25MPa) and the X axis stress was varied. Figure 6.4 is the corresponding graph of R_v vs. stress difference $\sigma_y - \sigma_x$. Figures 6.5 and 6.6 are the corresponding curves when the X axis stress was fixed and the Y axis stress was varied. The results should presumably be identical. There is some difference at low stresses, probably attributable to the high sensitivity of the rotation rig at low stresses and to the random error of $\pm 20\mu V$ in V_n readings. The latter corresponds to an error in stress of ±3MPa. A curious effect is that in figures 6.4 and 6.6 there are larger scatters for negative R_v than for positive R_v. I cannot explain this and do not know whether or not it is significant.

A few days later I repeated the test with the sample turned through 90°. Figures 6.7 and 6.8 are the graphs. They show that there was some residual stress that gave a negative R_v value, which was consistent with the earlier tests since the X and Y axes had been swapped round. Also, the scatter in the stress differences in figure 6.8 is slightly less than before and is in general greater for positive R_v than for negative R_v. However, the slope of the curve in figure 6.8 is considerably less (the earlier result from figure 6.6 is shown here by the dashed line) which suggests that the steel had changed magnetically over the five days that elapsed between the tests. The first tests, figures 6.3 - 6.6, were done one day after annealing. It was as though the steel had become slightly harder magnetically with time.

One way to examine the results is to ask: suppose $R_v = 0.004$; what does this mean? Referring to figure 6.8: the cluster of points on the graph at $R_v = 0.004$ was obtained by drawing a horizontal

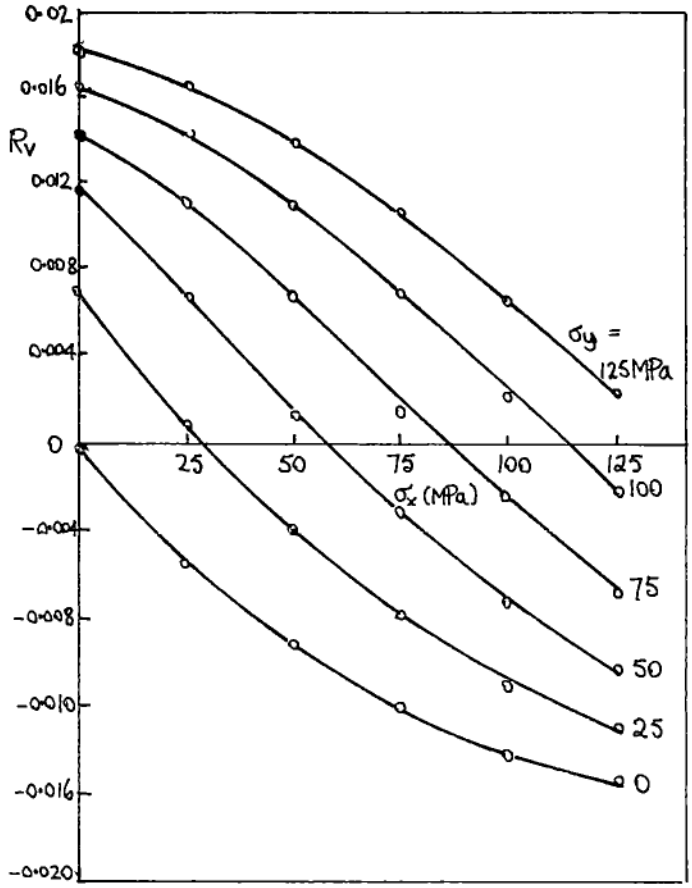

Figure 6.3 R_v vs. σ_x with σ_y held constant; 0.42mm mild steel.

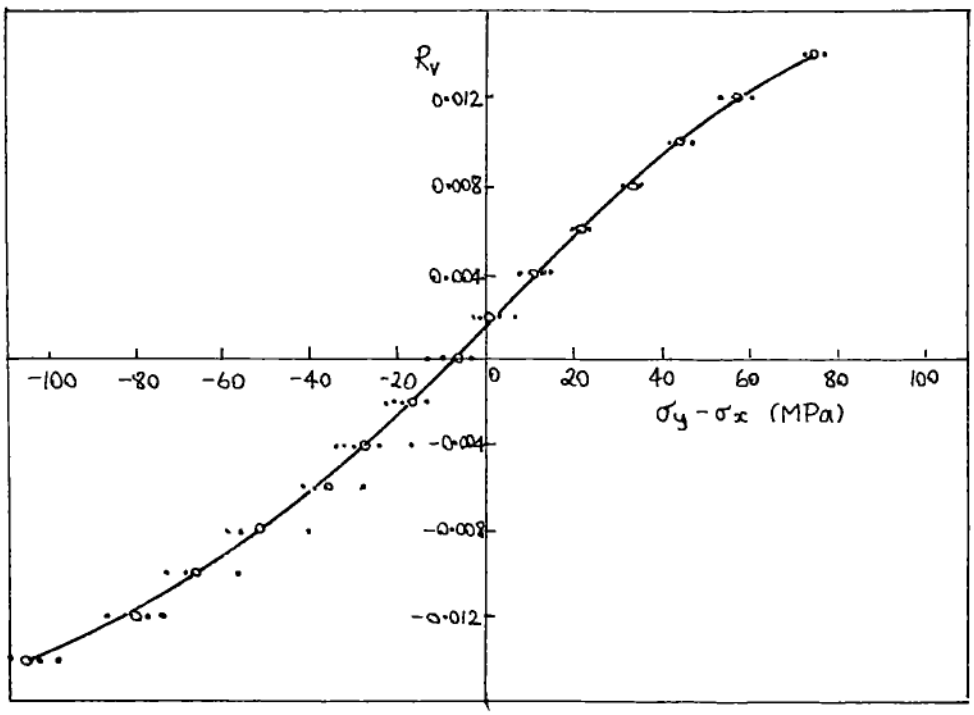

Figure 6.4 R_v vs. $\sigma_y - \sigma_x$, from figure 6.3. o=mean value, •=individual point.

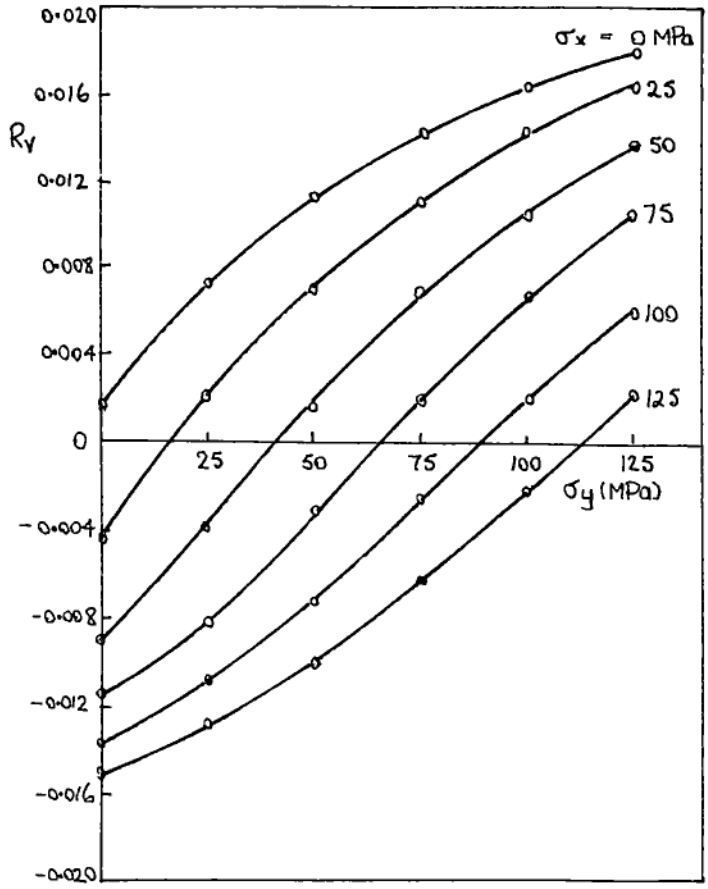

Figure 6.5 R_v vs. σ_x with σ_y held constant; 0.42mm mild steel.

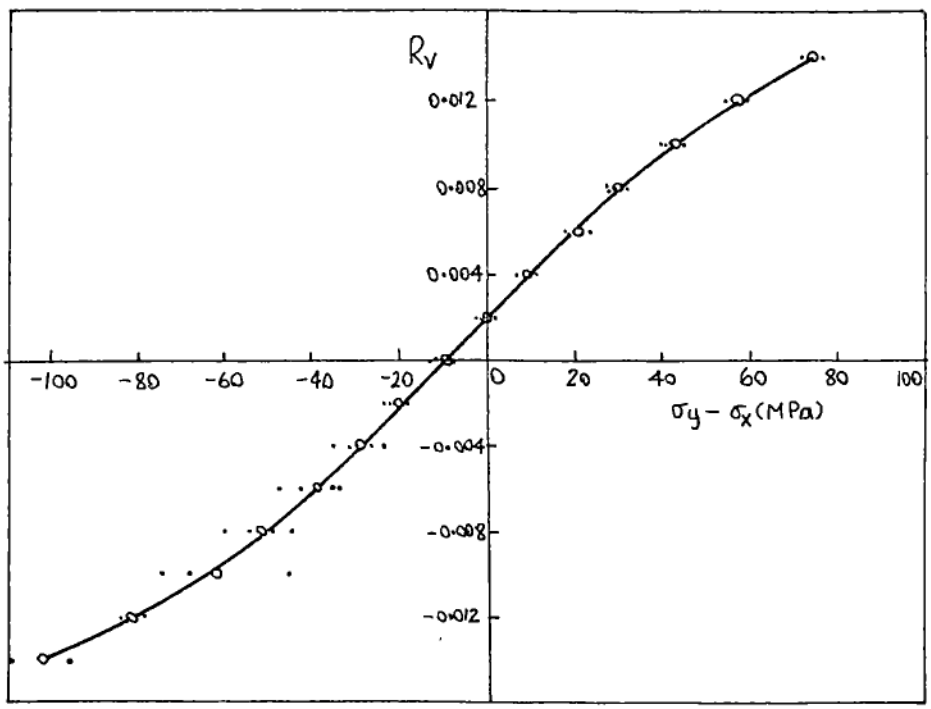

Figure 6.6 R_v vs. $\sigma_y - \sigma_x$, from figure 6.5. o=mean value, •=individual point.

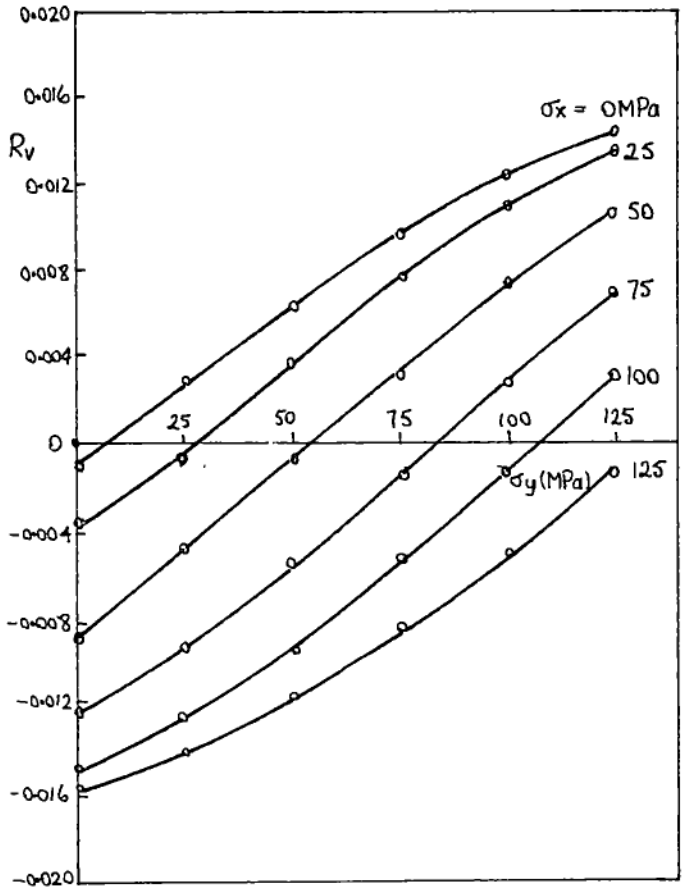

Figure 6.7 R_v vs. σ_y with σ_x held constant; 0.42mm mild steel. Test done 6 days after annealing, with X and Y axes reversed.

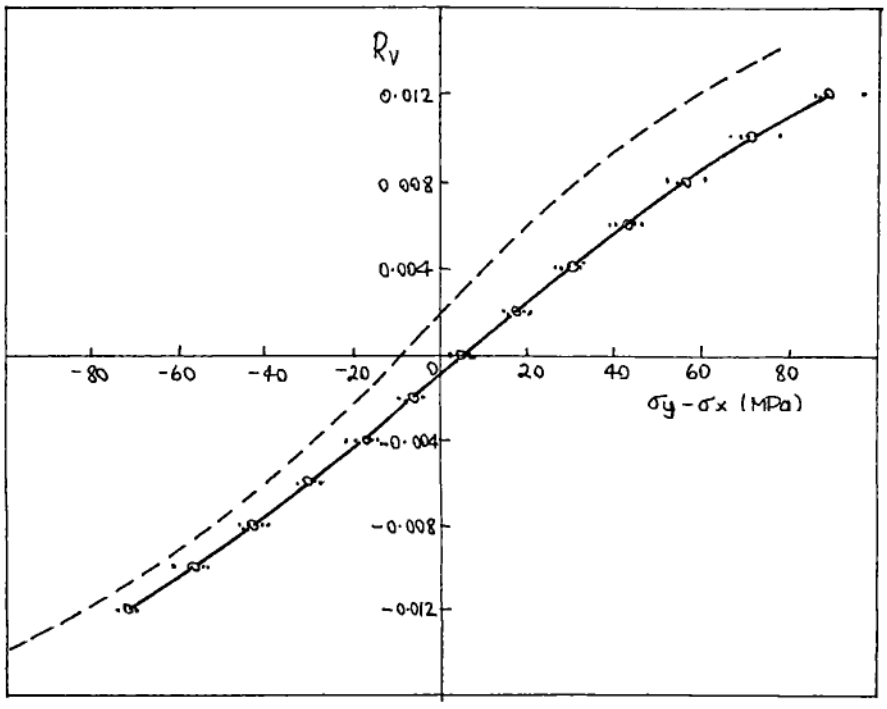

Figure 6.8 R_v vs. $\sigma_y - \sigma_x$, from figure 6.7. o=mean value, •=individual point. The dashed line is from figure 6.6 (1 day after annealing).

line at R_v = 0.004 on figure 6.7 and noting the differences in principal stresses where the curves intersect the line. R_v = 0.004 indicates an average stress difference of +30MPa, and that the more positive (tensile) principal stress is about 45° anticlockwise to the axis of the rotation rig. The curve of figure 6.8 is drawn through the average values of stress differences.

It seems reasonable to deduce from figure 6.8 that, as a first order effect, the rotation rig responds to the difference in principal stresses. The discrepancies of a few MPa may or may not be significant but would at any rate seem to be a second order effect.

6.5 Steel in biaxial tension and compression

This was an attempt to extend the range of stresses applied to the cross-shaped sample to cover tension in one axis and compression in the other. The sample was the same shape as before but was glued to a 12mm piece of particle board to give it stiffness in compression. A similar piece of steel was glued to the other side of the wood to minimise the risk of buckling. Compression in the vertical (Y) direction was by means of a Shimadzu testing machine (which had the necessary rigidity) and the same sprung frame as before was used to tension the sample in the horizontal (X) direction.

Previous tests showed that the wood by itself could be strained elastically up to 0.6% (which was more than enough to take the steel to its yield point) and that its modulus of elasticity was the same to within 1% along each axis. However there were problems in measuring the stress in the centre of the sample.

The strain gauges could not now be put on the opposite side of the steel to the rotation rig since the steel was glued to the

wood. Instead I put strain gauges where the rotation rig would go and also on each arm of the cross. My intention was to relate the arm gauge readings to the centre gauge ones, then remove the central gauges, put the rotation rig there, and rely on the arm gauges. Consistent readings could not be obtained with the pair of gauges that were in compression, and eventually I abandoned the test.

However, a short while earlier I had done similar measurements (i.e. tension and compression together) but had rejected them since I had made a (systematic) error in relating the strain gauge readings to stress. These results are shown in figures 6.9 and 6.10; the corresponding tension/tension results are included. Note that the values of stress are all too high by a factor of about 1.4, and that the V.S.S.R. was used instead of R.R.4.

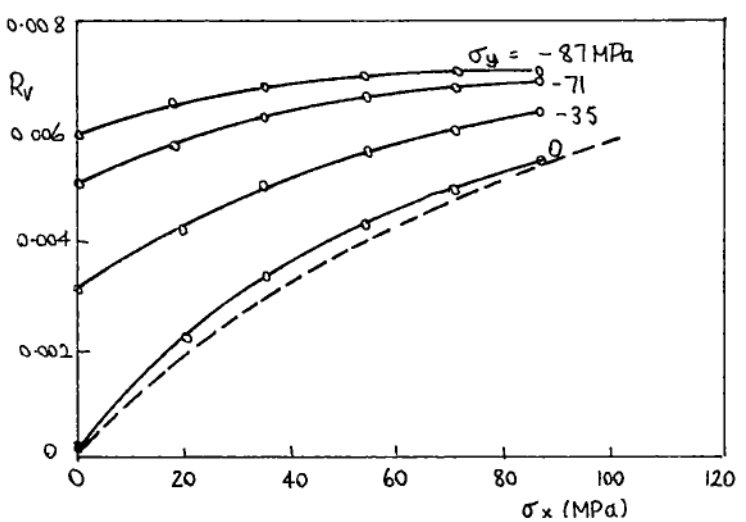

Figure 6.9 R_v vs. σ_x (tension) with σ_y (compression) held constant.

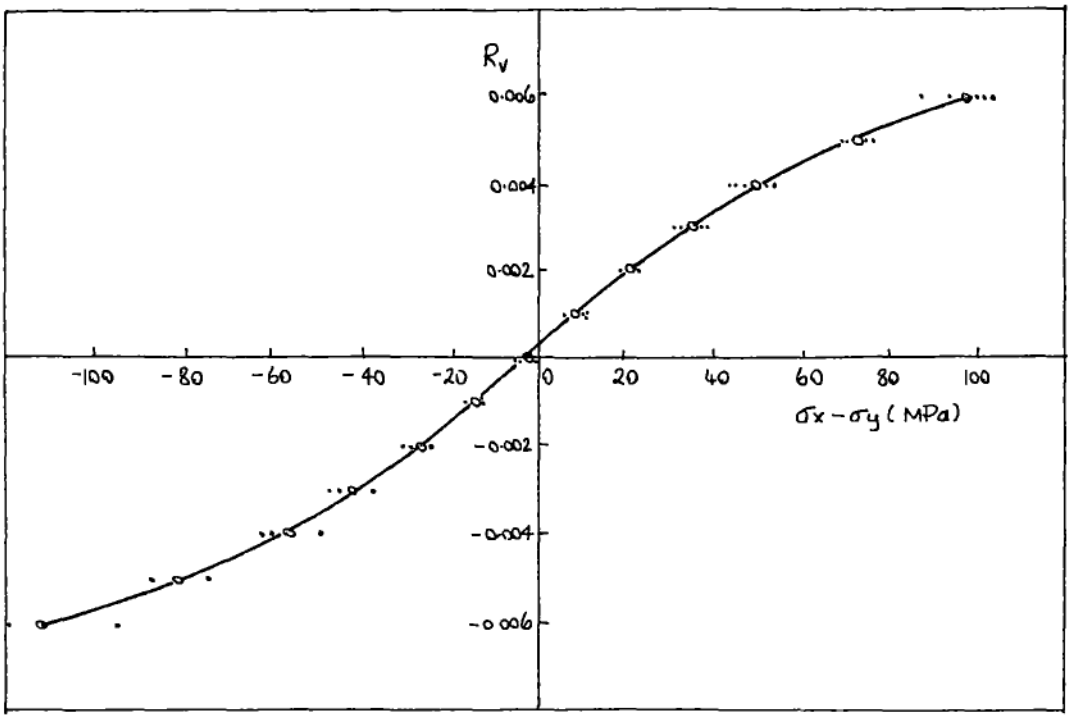

Figure 6.10 R_v vs. $\sigma_x - \sigma_y$, from figure 6.9.

6.6 B vs. H loops for biaxial tension

These were measured with the C-core rig at the centre of the cross-shaped sample, in the direction of each axis (B_x and B_y) and also at 45° to an axis (B_{45}). Figure 6.11 shows some of the loops. Peak field strength was kept at 230A/m. B_x remained almost constant for magnetisation parallel to the larger tension σ_x, whereas B_y was reduced for all but equal tensions in each axis. The loops for $\sigma_x = \sigma_y = 0$ are also included. (These results have the same error in stress as those in figures 6.9 and 6.10 but this does not invalidate the trends in the shapes and sizes of the B vs. H loops).

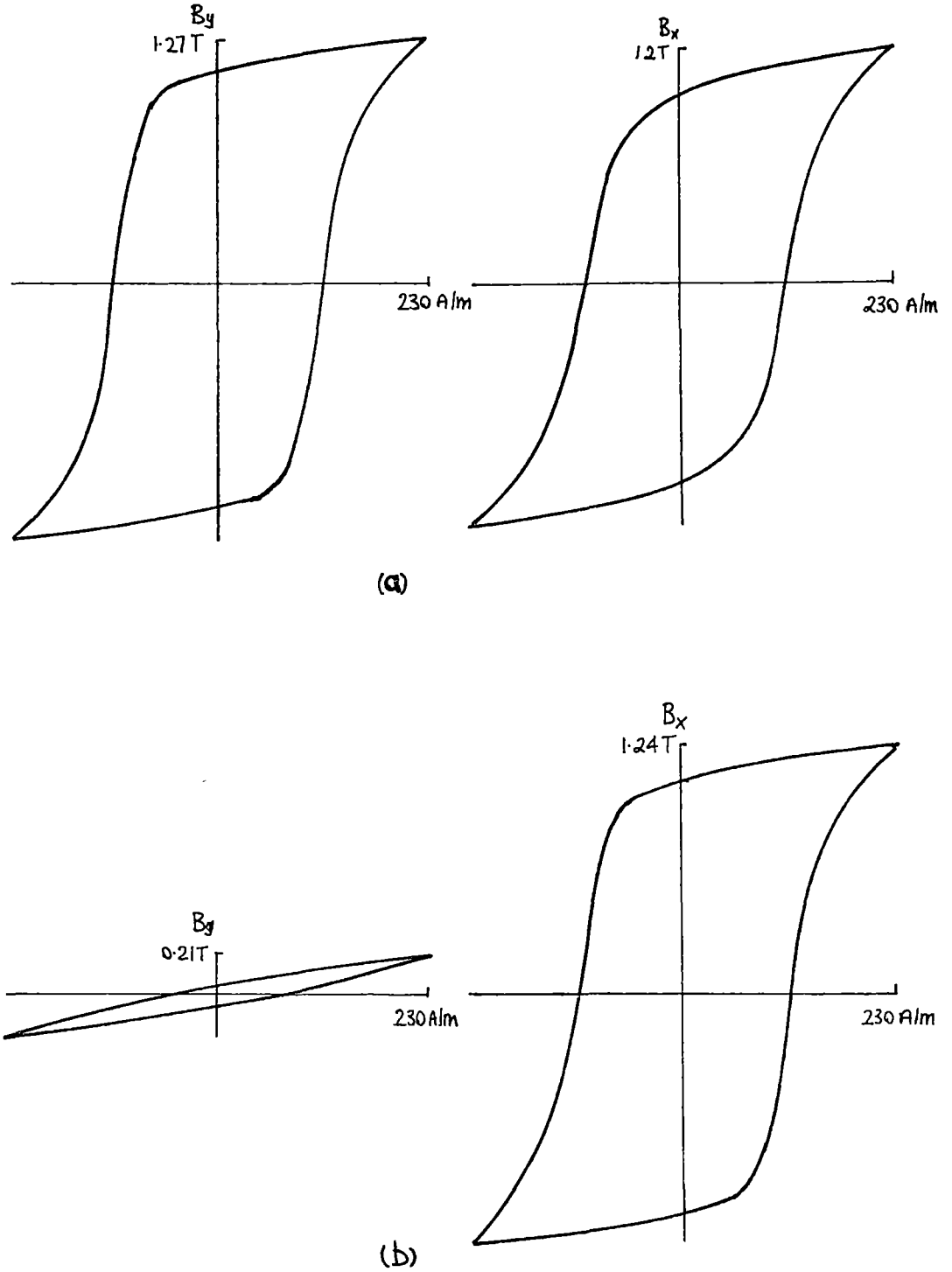

Figure 6.11 B vs. H loops for biaxial tensions. Peak field is 230A/m. (a) σ_x=0, σ_y=0. (b) σ_x=184MPa, σ_y=0.

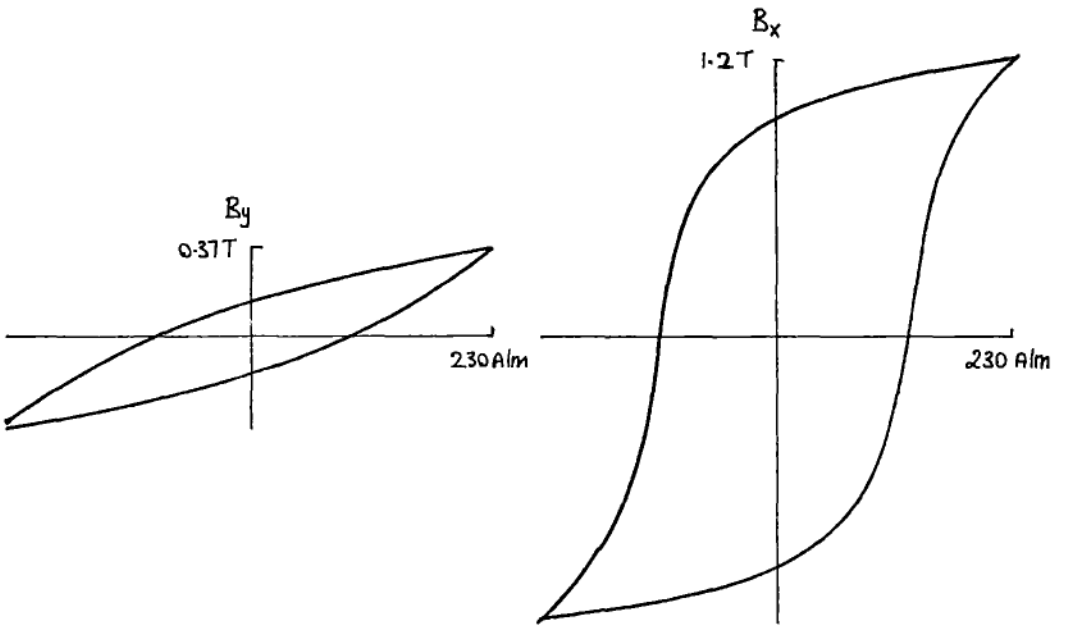

(c)

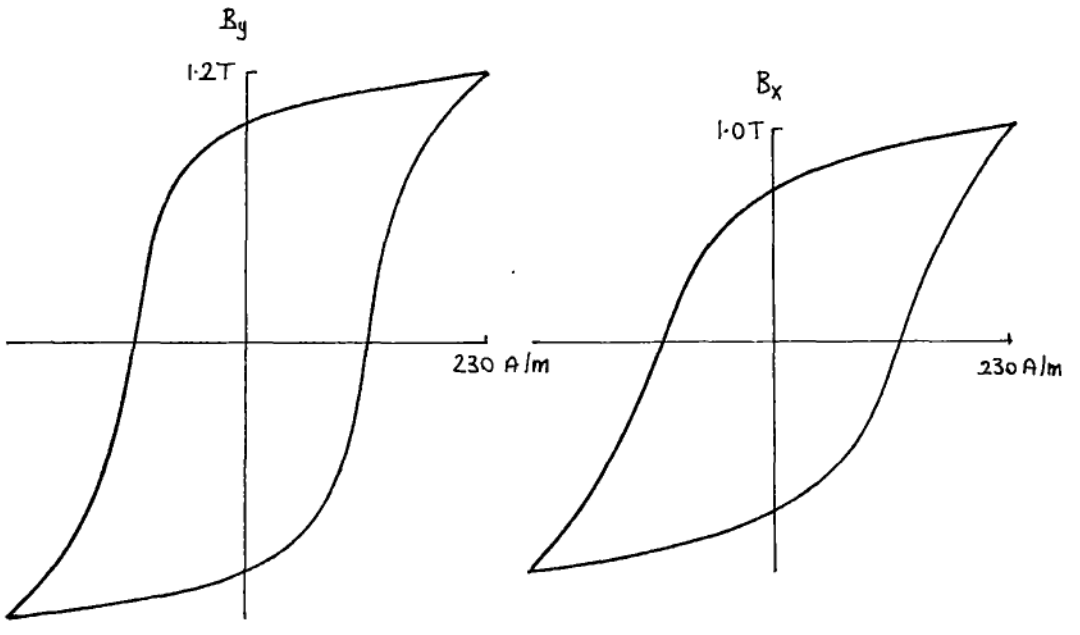

(d)

Figure 6.11 (continued) (c) σ_x=184MPa, σ_y=92MPa. (d) σ_x=184MPa, σ_y=184MPa.

Figure 6.12 shows the variation of heights of the three loops (B_x, B_y, and B_{45}) for different stresses up to 184MPa. Peak field strength was again 230A/m. The graph for uniaxial tension is included so that the slight differences of height for biaxial stress can be compared with the large differences for the uniaxial stress. Ideally the upper three curves should be coincident but, even at zero stress, it was never possible to measure identical B vs. H loops in different directions. There was always some anisotropy in the steel that could not be removed by annealing. However, disregarding this imperfection in the steel, figure 6.12 does show that the steel appeared isotropic for equal biaxial stresses; thus there was no rotation of the magnetic field and the output voltage of the rotation rig was zero.

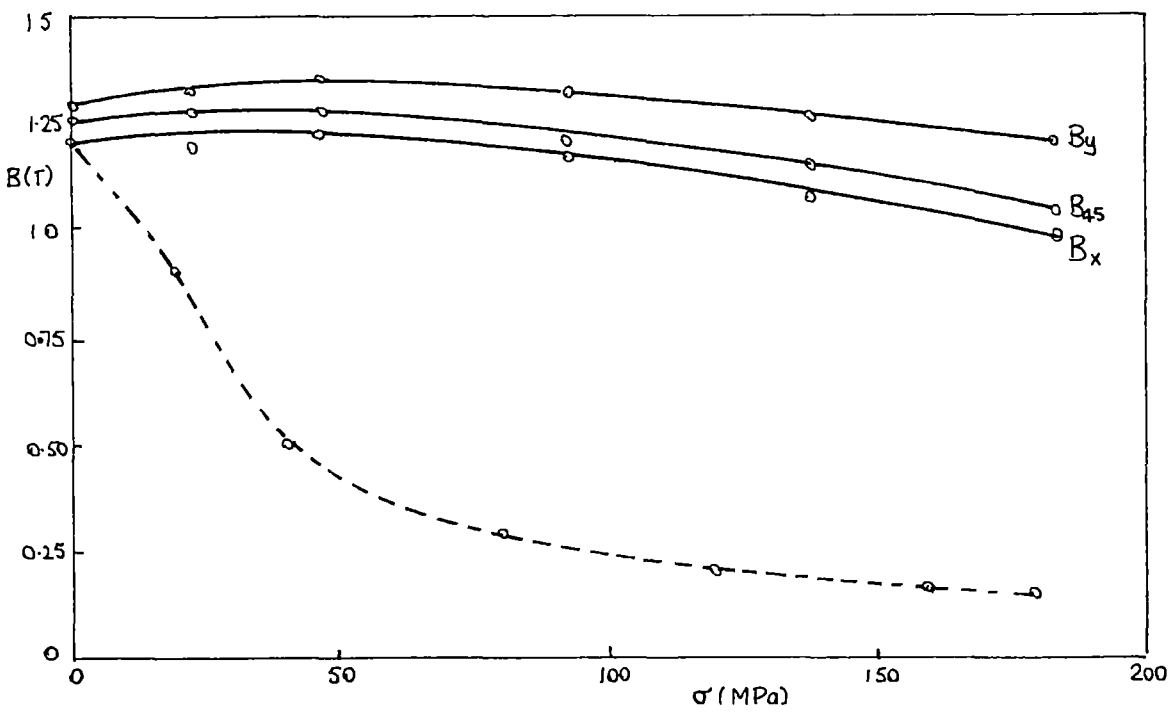

Figure 6.12 Heights (B-values) of B vs. H loops vs. stress for equal biaxial tensile stresses. Peak field is 230A/m. The dashed line shows B for magnetisation perpendicular to uniaxial tension.

CHAPTER 7

MEASUREMENT OF THE STRESS PATTERN IN A STEEL DISC COMPRESSED AT THE ENDS OF A DIAMETER

7.1 Introduction

All previous tests have been in the nature of calibrations with uniform applied stresses. A more stringent test of the rotation rig would be to use it on a non-uniform pattern of stress. Of course, the pattern would have to be known by some other means - either by an alternative measurement or by calculation - so that the accuracy of the rotation rig could be determined. Such a test on a disc and its results are described in this chapter.

Several points were kept in mind whilst choosing the shape of the test piece: (1) it should be easy to make and test, (2) the stress pattern should be available analytically, (3) the steel should be kept below its yield point, and (4) in general tensile stresses should be greater than compressive ones, since the calibration for the rotation rig using a separate test piece is easier for tension than for compression.

Figure 7.1a shows one shape - a hole cut in a rectangle - that meets all these requirements. (Such a test piece was used by Kino et. al. [K4,1980] for acoustic measurement of stress). However it was in practice a failure. The steel sheet was too big to anneal (it was 1600mm x 400mm) and although hot-rolled sheet was used for this very reason, the residual stresses masked the applied ones almost everywhere. The steel also buckled at the top and bottom of the hole, where the stress was compressive, because it was only 1.2mm thick. Thicker steel, although less liable to buckle, would have been much more trouble to machine, heavy to handle, and require massive end plates to cope with the forces needed to give an adequate stress around the hole.

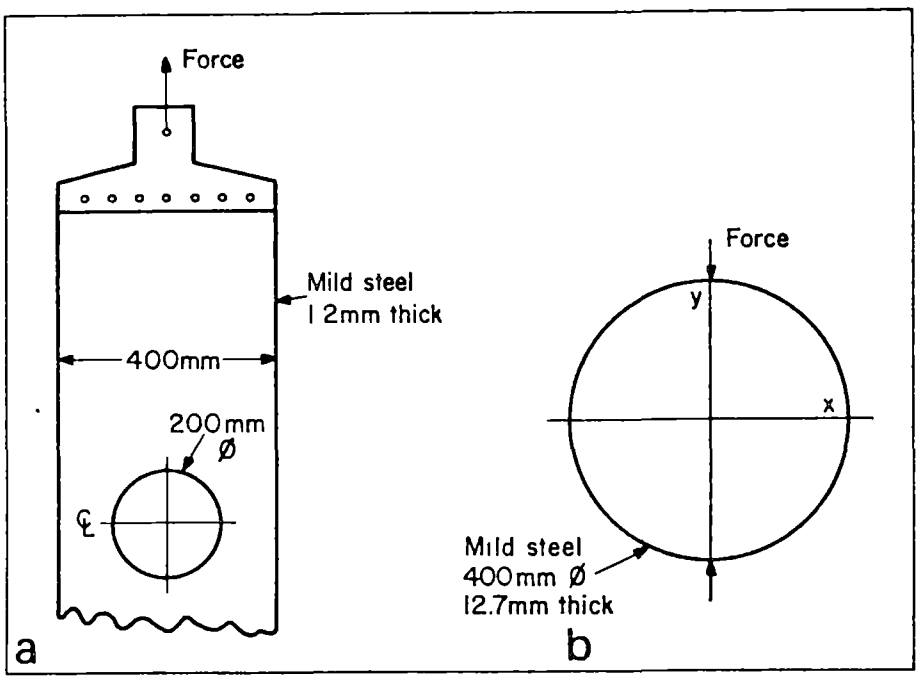

Figure 7.1 Test pieces for non-uniform stress pattern: (a) hole in a rectangle, (b) disc.

Instead of this I chose a disc, to be compressed at the ends of a diameter: figure 7.1b. It was flame-cut from 12.7mm (1/2") mild steel plate and its edge was machined to 400mm diameter. This shape did not meet points 3 and 4 in the list, but the portions of the disc that yielded were around where the load was applied and where the rotation rig probe would not reach. Also, a compression calibration test was done to a high enough value of stress without difficulty. However, the fact that the steel did yield must have caused some discrepancy (of unknown amount) between the actual stress pattern and the theoretical one and in this respect the disc was still unsatisfactory.

7.2 Theoretical stress pattern

An exact analytical solution is available for the stresses in the disc. The load is assumed to be applied uniformly along a line across the edge of the diameter (which is the Y axis) as in figure 7.2. In this way the problem is two dimensional; there is no variation of stress through the thickness of the disc.

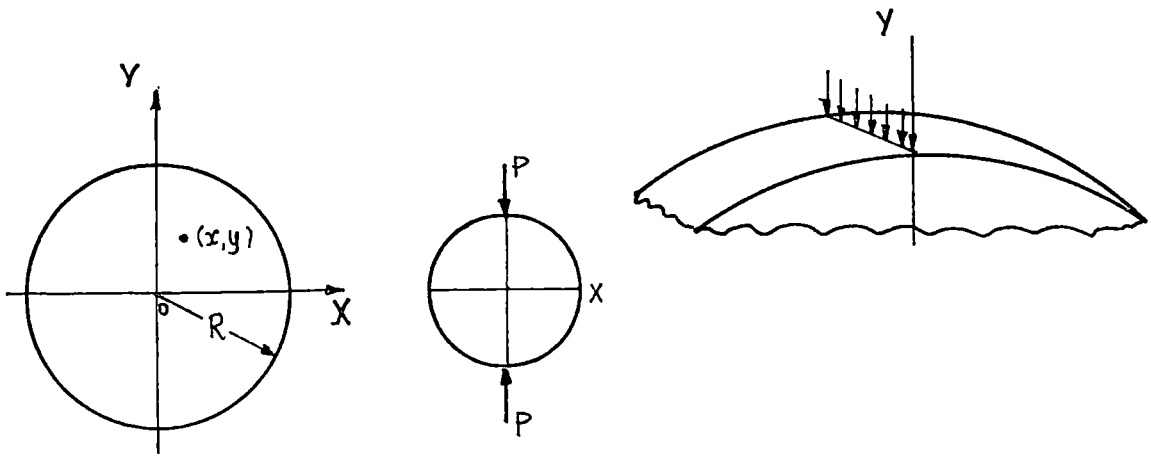

Figure 7.2 Coordinates for the analysis of the stresses in the disc.

The original analysis is by Michell [M2,1900] but it is rather hard to follow as the notation is old-fashioned. A (relatively) more up-to-date presentation is by Frocht [F1,1948]. He gives the components of stress at a point (x,y) as

$$\sigma_x = -\frac{2P}{\pi t}\left[\frac{(R-y)x^2}{r_1^4} + \frac{(R+y)x^2}{r_2^4} - \frac{1}{2R}\right]$$

$$\sigma_y = -\frac{2P}{\pi t}\left[\frac{(R-y)^3}{r_1^4} + \frac{(R+y)^3}{r_2^4} - \frac{1}{2R}\right] \qquad (7.1)$$

$$\tau_{xy} = \frac{2P}{\pi t}\left[\frac{(R-y)^2x}{r_1^4} - \frac{(R+y)^2x}{r_2^4}\right]$$

where $r_1^2 = x^2 + (R-y)^2$

$r_2^2 = x^2 + (R+y)^2$

t = thickness of the disc

R = radius of the disc

P = load applied

The rotation rig gives R_v values that depend on the difference in principal stresses, $\sigma_1 - \sigma_2$; thus values of these are required as functions of x and y.

At this stage it is useful to look at the photoelastic effect. Very briefly, it enables interference fringes, called isochromatics, to be produced, whose shape is the locus of constant difference between

principal stresses. For this technique a plastic model of the disc is compressed. The plastic must be translucent and stress-sensitive; Araldite will do. Circularly polarised light is shone through the disc and the series of fringes are viewed through a quarter wave plate and an analyser. Figure 7.3 shows a set of such fringes (called isochromatics) for a disc loaded along a diameter. Other types of fringes (isoclinics - see later) can also be produced by suitable modification of the polariser and analyser.

There is thus a (limited) analogy between the rotation rig and the photoelastic effect. Although I did not make a photoelastic model of the disc to verify the rotation rig results, it seemed sensible to use the rotation rig to produce the fringes or contours of constant stress-difference and then to compare the rotation rig results with the theoretical stress pattern. As it turned out, Michell's theoretical analysis does not apply near the load points where yielding occurs. Thus the actual pattern was not known exactly).

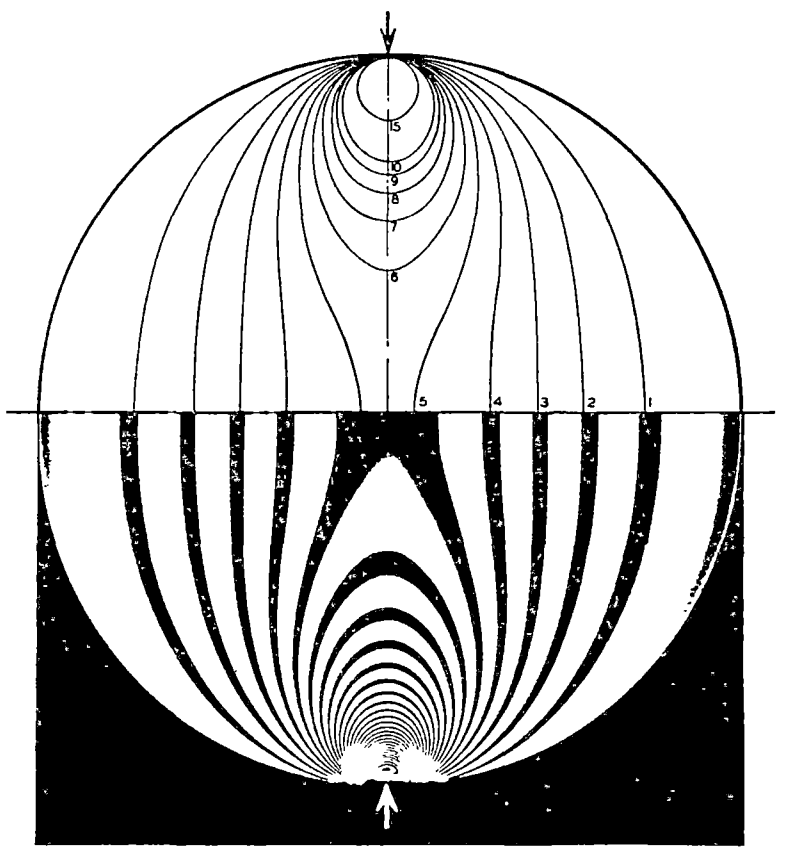

Figure 7.3 Isochromatic fringes. Upper half circle: theoretical loci of fringes. Lower half circle: fringes produced in a photoelastic model. [from Frocht, F1].

Continuing the analysis: the principal stresses σ_1 and σ_2 are related to their x and y components by

$$\sigma_1 = 0.5(\sigma_x + \sigma_y) + 0.5\sqrt{[(\sigma_x + \sigma_y)^2 + 4\tau_{xy}^2]}$$

$$\sigma_2 = 0.5(\sigma_x + \sigma_y) - 0.5\sqrt{[(\sigma_x + \sigma_y)^2 + 4\tau_{xy}^2]}$$

thus

$$\sigma_1 - \sigma_2 = \sqrt{[(\sigma_x - \sigma_y)^2 + 4\tau_{xy}^2]} \qquad (7.2)$$

The definition of an isochromatic is $\sigma_1 - \sigma_2 = \Delta$, a constant.

Substituting from these equations gives

$$\frac{4PR}{\pi t \Delta} = \frac{(x_2^2 + y_2^2 + R^2) - 4y^2R^2}{R^2 - x^2 - y^2} \qquad (7.3)$$

At the centre of the disc $x = y = 0$ and then

$$\Delta = 4P/\pi tR$$

Frocht now introduces the fringe order n and the fringe value F: $\Delta = 2nF$. The left hand side of equation 7.3 becomes

$$\frac{4PR}{\pi t \Delta} = \frac{2PR}{\pi tnF} = \frac{K}{n} \qquad (7.5)$$

where $K = 2PR/(\pi tF)$

The value of F depends on the particular photoelastic model. I was not of course using a model but the K and the n are necessary to follow a graphical method that is described next. Equation 7.3 becomes

$$\frac{K}{n} = \frac{(x^2 + y^2 + R^2)^2 - 4y^2R^2}{R^2 - x^2 - y^2} \qquad (7.6)$$

This gives the relation between x and y co-ordinates for any fringes described by K/n = constant. Equation 7.6 can be re-arranged to give x in terms of y (or vice versa if required):

$$x^2 = -R^2 - y^2 - \frac{K}{2n} + \sqrt{\frac{K^2}{4n^2} + \frac{2R^2K}{n} + 4R^2y^2} \qquad (7.7)$$

Construction of isochromatics

Frocht gives a graph, from equation 7.7, which is reproduced here as figure 7.4. It is obtained by putting K = 2, R = 1. I used it in this way. Suppose P = 100kN. From equation 7.4, $\sigma_1 - \sigma_2 = \Delta = 50.1$MPa at the centre of the disc. From the graph n = 5.1. To draw a fringe for, say, 70MPa, the value of n is 5.1 x 70 / 50.1 = 7.13. A horizontal line drawn for n = 7.13 intersects the curves y = 0.6, 0.7, 0.8, 0.9 at corresponding values of x of about 0.12, 0.165, 0.18, 0.15. These give the co-ordinates of the 70MPa contour.

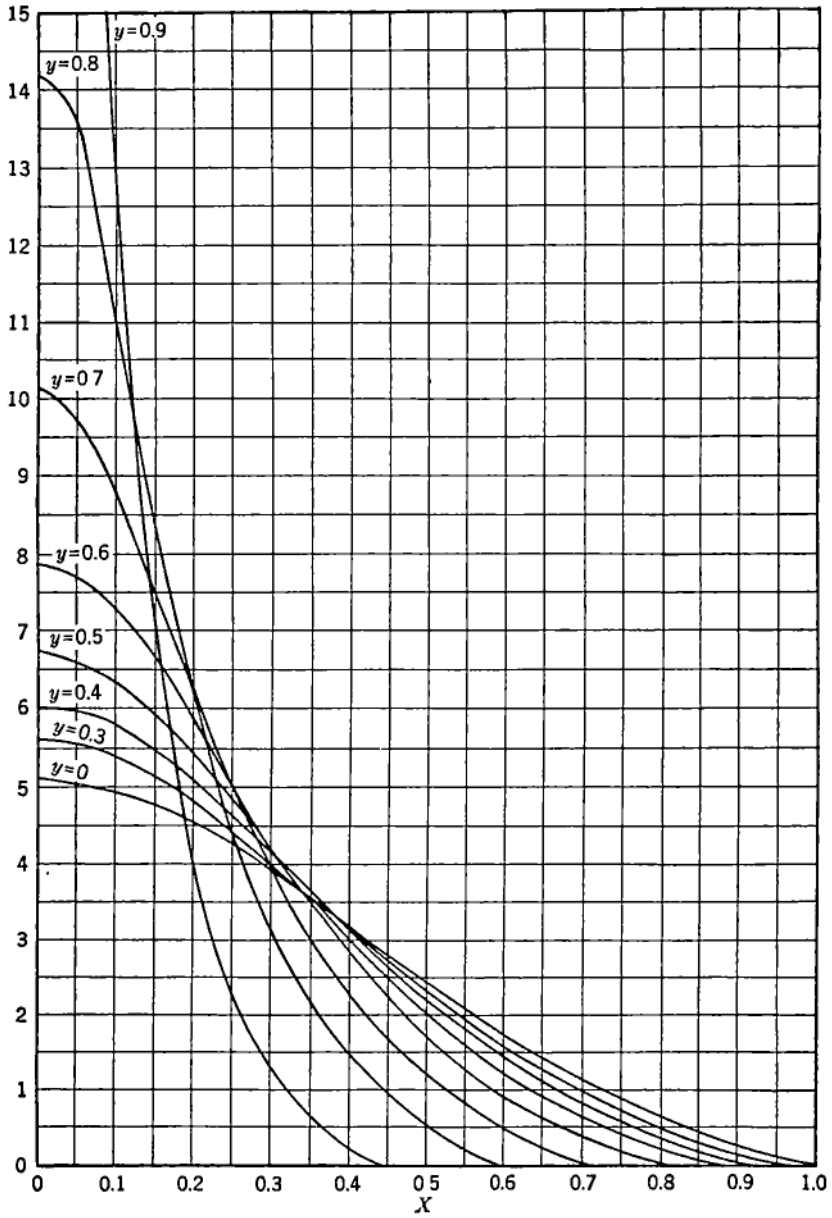

Figure 7.4 Values of fringe order n as a function of x, for constant values of y, from equation 7.7 [F1].

Construction of isoclinics

The photoelastic techniques can also display fringes that are loci of constant direction of principal stress. These are called isoclinics. The rotation rig will also give these. When the probe (search coil) axis is in the direction of a principal stress its R_v reading is zero. Thus to plot isoclinics for an angle θ_o the probe is held at this angle to the X axis and is moved about on the disc until the R_v reading is zero. Its position is then on the θ_o isoclinic. Frocht shows that the equation of the isoclinic is

$$x^2 - 2xy.\cot\theta_o - y^2 + R^2 = 0 \qquad (7.8)$$

He also shows how to fix three points B, P, and V on the isoclinic. Referring to figure 7.5, point B is where the load is applied and where the isoclinic makes an angle θ_o to the X axis. The isoclinic is parallel to the X axis at P. Distance OV = $R\sqrt{\sin\theta_o}$ and lies on a line through the intersection of BE and PE. The isoclinic can be drawn quite accurately through these three points. Figure 7.5 shows the isoclinic for $\theta_o = 20^o$. There is of course symmetry between the top and bottom halves of the disc.

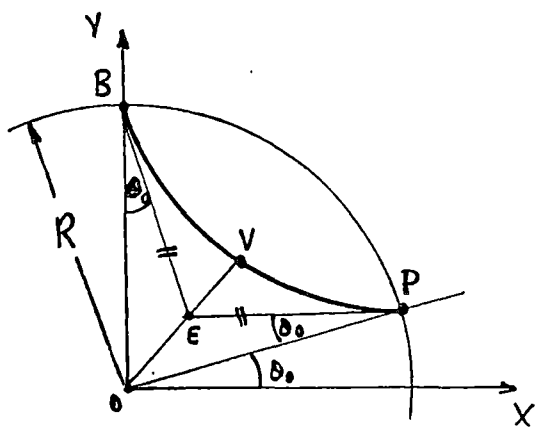

Figure 7.5 Construction of an isoclinic [F1].

7.3 Annealing and residual stresses

After machining, the disc was given a stress-relief anneal of 2 hours at 570° followed by slow cooling. The rather low temperature was because the disc was too big to go in the usual oven at 650°C and so was put in a glass annealing oven; 570°C was the temperature for glass. However, although this treatment had in the past reduced residual stresses in other samples of steel to about 5MPa (measured magnetically), this time they stayed at several times this value. Figures 7.6a and 7.6b show the isochromatics for applied loads of 70kN and 120kN.

They show that the measured contours were very distorted and of no use for a comparison with the theoretical ones. At this stage I had not done a calibration test on the steel and so the contours are marked with an (approximate) stress-difference from some previous tests.

The rotation rig cannot distinguish between a signal that results from stress or from magnetic texture (i.e. a non-random orientation of the grains). Since a temperature of 570°C (although rather lower than the accepted optimum of 650°C for mild steel) should still remove residual stress, it is likely that the particular plate from which the disc was cut had some texture which was not removed at that temperature. A disadvantage of annealing at higher temperatures is that the surface of the steel tends to end up rather uneven where some areas have oxidised more than others. Also, it may distort if it gets very soft. However, in this case a higher temperature had to be used.

The disc was reheated to about 870°C for several hours and then cooled slowly (I am grateful to the Ceramics Department of the University for the use of one of their pottery kilns for this). In the event, the disc stayed flat to within 0.2mm across a diameter, and the scale on the surface was uniform and left a smooth surface when it was chipped off. The rotation rig showed the average residual stress-difference (or equivalent texture) to be no more than 3MPa over the disc, with maximum stress-differences of 8MPa; these were only near the parts of the disc where the load would be applied and where there would be high resulting stresses anyway.

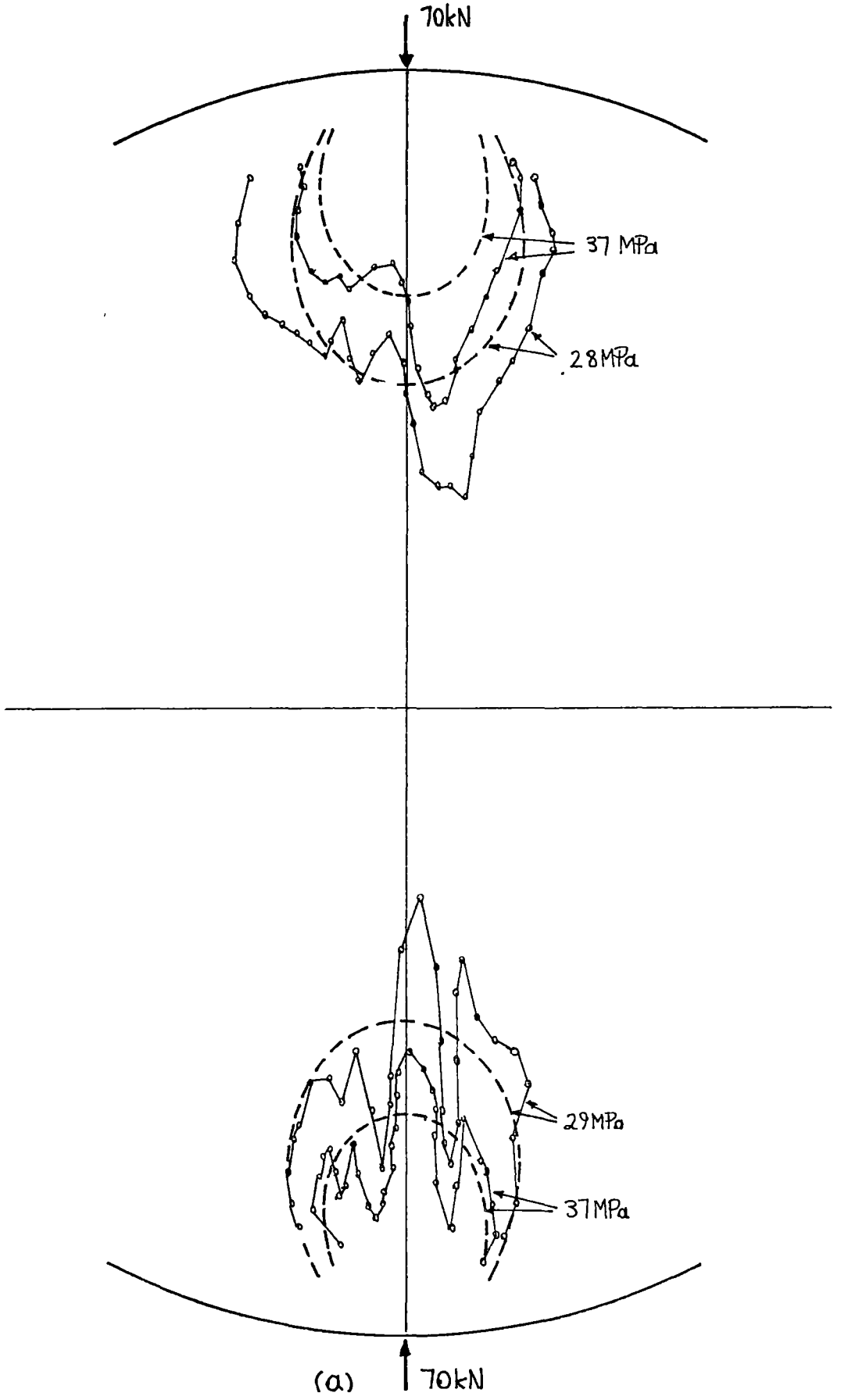

Figure 7.6 Isochromatics measured on the disc after it had been annealed at 570°C: (a) 70kNload.

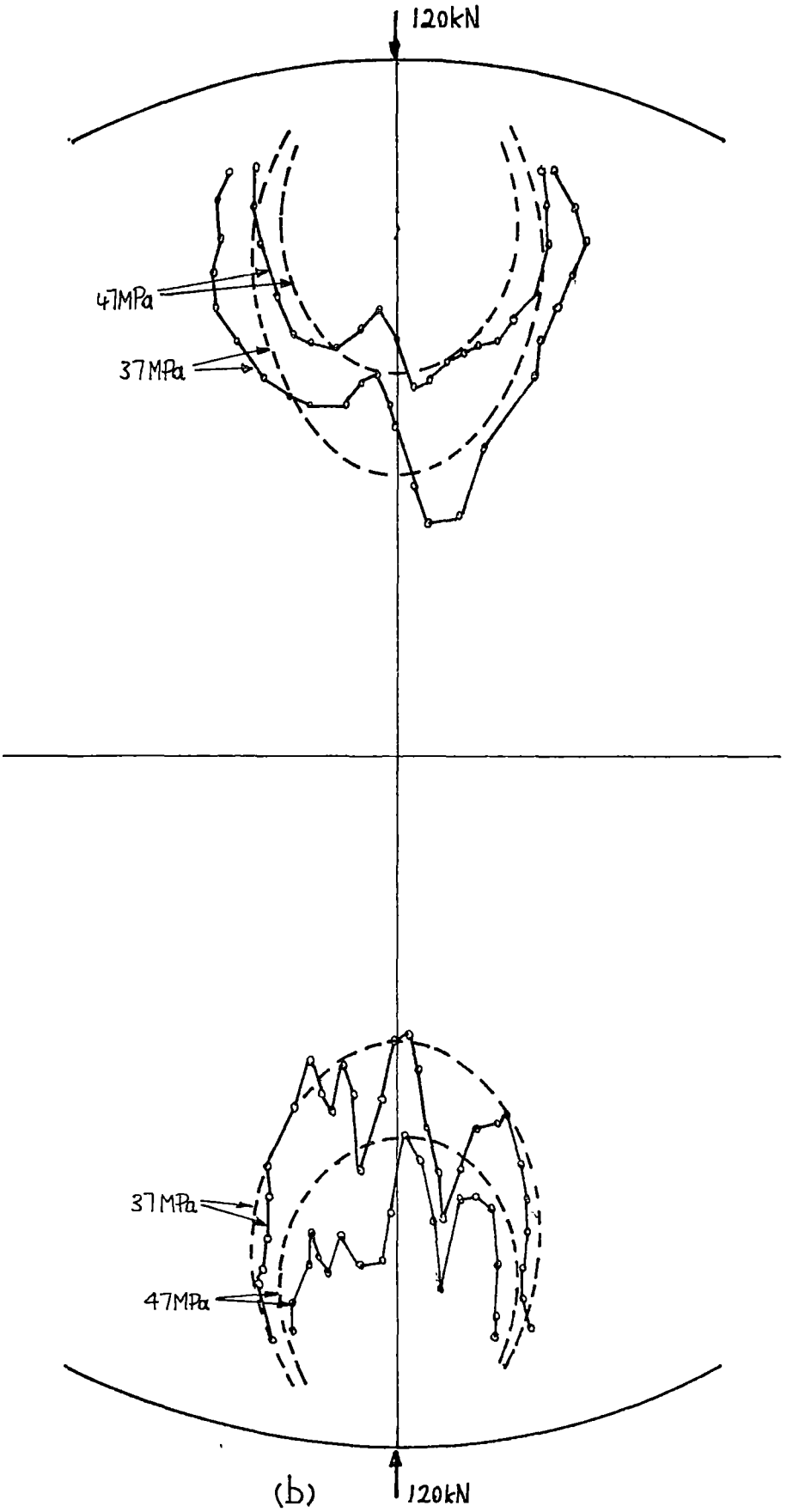

Figure 7.6 (continued): (b) 120kN load.

7.4 The calibration curve for the rotation rig

The sample for this was 50mm wide, cut from the same plate as the disc, and annealed in the same way. A calibration curve (i.e. of R_v vs. σ) was required for applied compression since in general the stress in the disc would be compressive. In using the results of this calibration test for the disc I assumed that the R_v vs. σ graph for uniaxial stress is the same as that for R_v vs. $(\sigma_x - \sigma_y)$ for biaxial stresses. Previous tests with biaxial stresses showed that this was only approximately the case, to within about 10% for the particular mild steel used, but I did not know how well this applied to all mild steels. The amount of error was unknown.

The results of tensile tests on the 50mm test piece are shown in figure 7.7a. The test was done one day after annealing and may not be accurate because I did not use strain gauges (which would have enabled the stress to be calculated to within 2%). Instead I calculated the stress from the applied load and the cross sectional area of the test piece. However, the actual stress at the surface on each side of the test piece may not have been the same as this because of uneven loading at its ends. No precautions were taken to force the line of action of the load to be along the axis of the test piece. However, the interesting part of the graph is the sudden increase of R_v at low values of tension, with no comparable effect two weeks later. The possible error in (calculated) stress would not by itself account for this. A repeat calibration two weeks later (using resistance strain gauges) is also shown. The sudden increase of R_v at low tension did not show up. Figure 7.7b shows the corresponding curves for compression. The difference in the two curves (one day and two weeks after annealing) is much less than for tension.

It appears that the magnetic properties of the steel had changed markedly with time: one day after annealing the steel was much more sensitive to low tensile stresses than it was several days later. The fact that magnetic properties can change with time was known many years ago

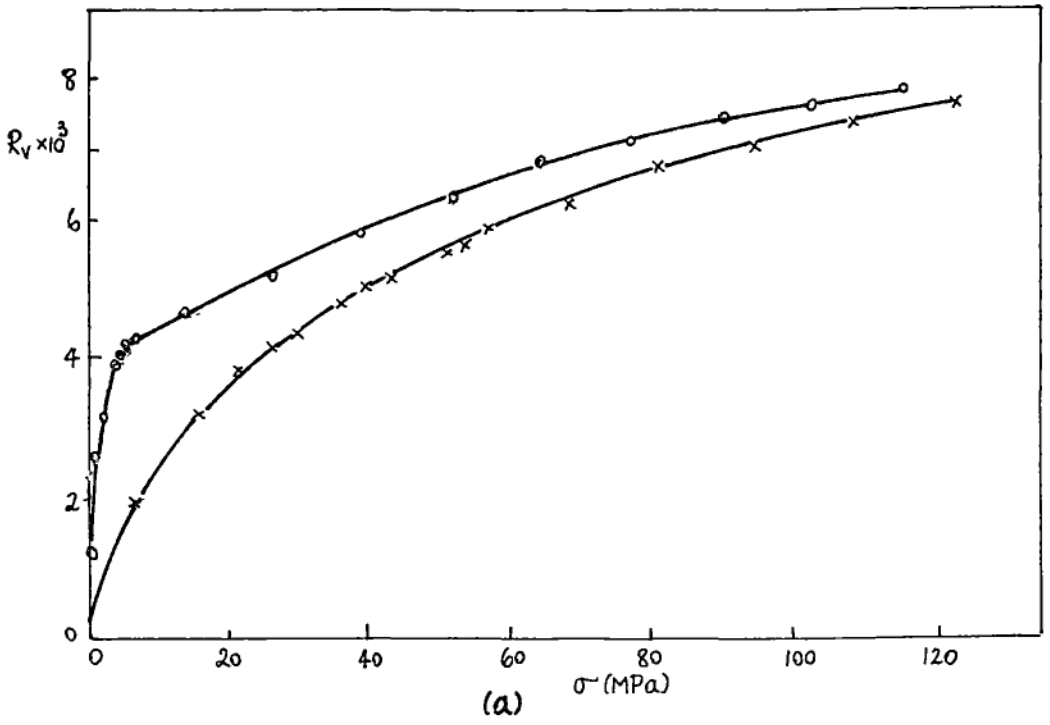

(a)

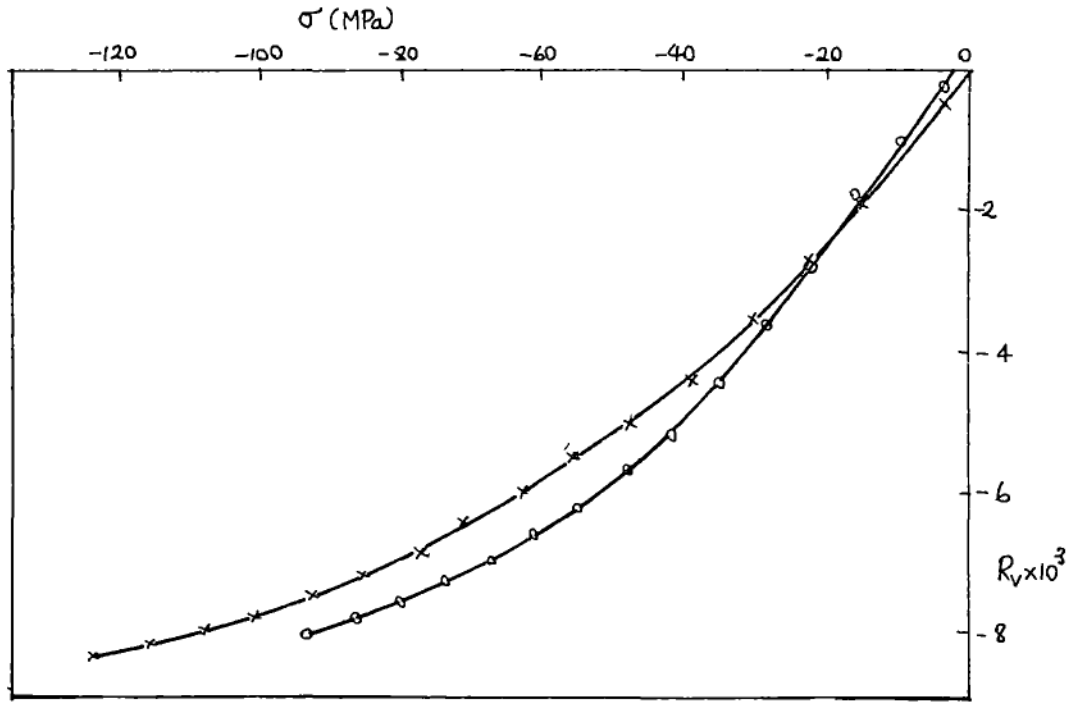

(b)

Figure 7.7 Calibration tests with R.R.4 for a test strip of steel: (a) tension, (b) compression. o = 1 day after annealing, x = 14 days after annealing.

and several authors of books on ferromagnetism refer to it. I had noticed a similar thing when doing measurements of B vs. H loops on newly-annealed mild steel. A qualitative explanation by Cullity is that annealing at 870°C causes grain growth in the steel; it also becomes very soft magnetically. In time the carbon atoms diffuse to the grain boundaries where they make the steel harder magnetically. Also, in very soft steels a low tension can completely re-arrange the domain orientations and give a much higher permeability [Craik and Wood,1970], whereas compression decreases permeability somewhat. In harder steels the changes of permeability with tension and compression (increase and decrease, respectively) can be about equal [Faunce,1970].

The useful measurements on the disc were done one or two weeks after annealing. Since the larger stress is compressive, the calibration curve of figure 7.7b (two weeks after annealing) was used.

7.5 Tests carried out

These are summarised in figures 7.8 to 7.13. Three different loads of 70, 100, and 140kN were used for the isochromatics. They show that the differences between measured and theoretical values are similar for all three. (The results for just one load might have been by chance, very good, and have given a false impression). Having shown this to be the case, I then measured isoclinics for a 100kN load only. Two different methods of loading were used; these are described in section 7.6.

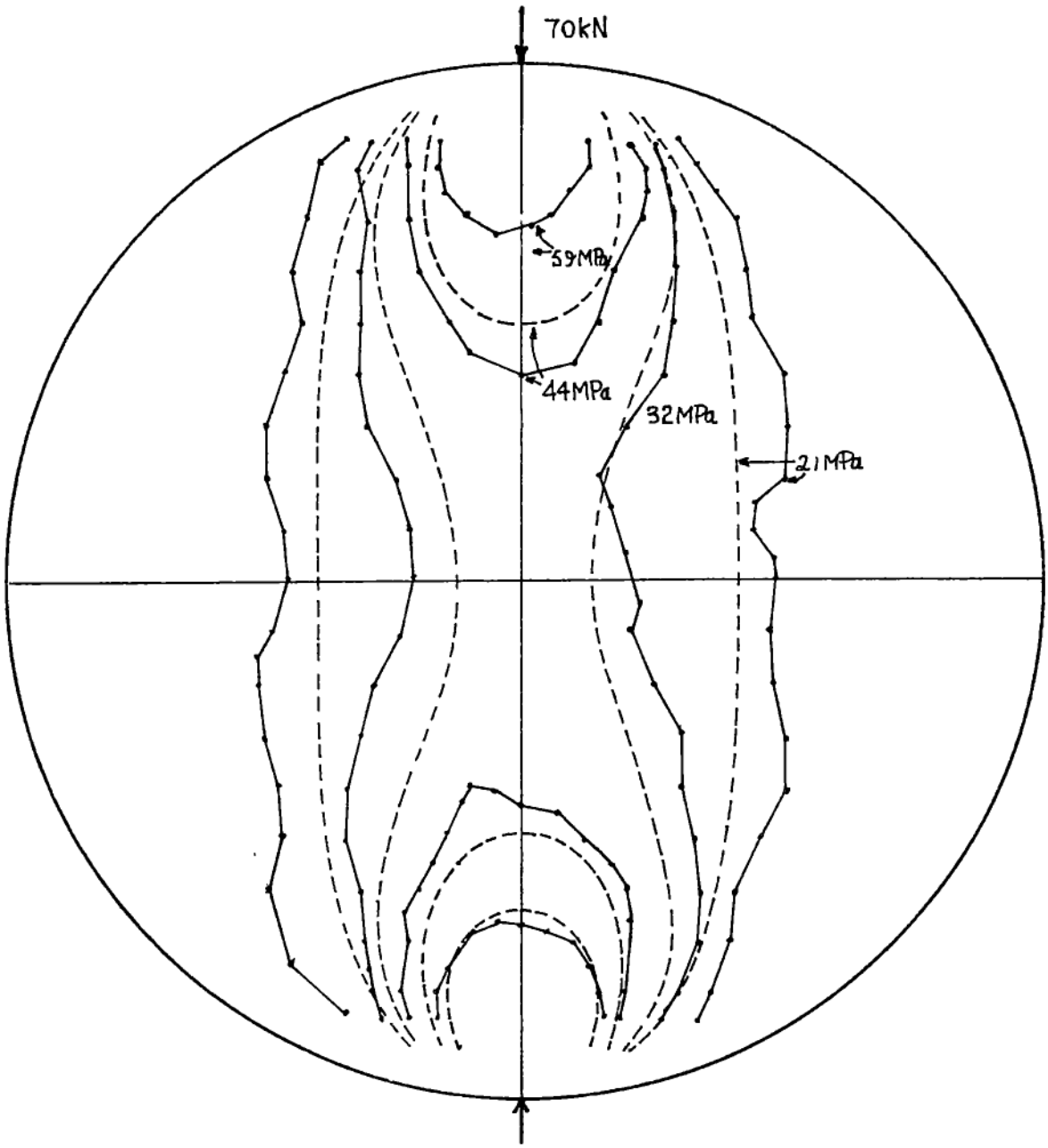

Figure 7.8 Isochromatics for 70kN load.

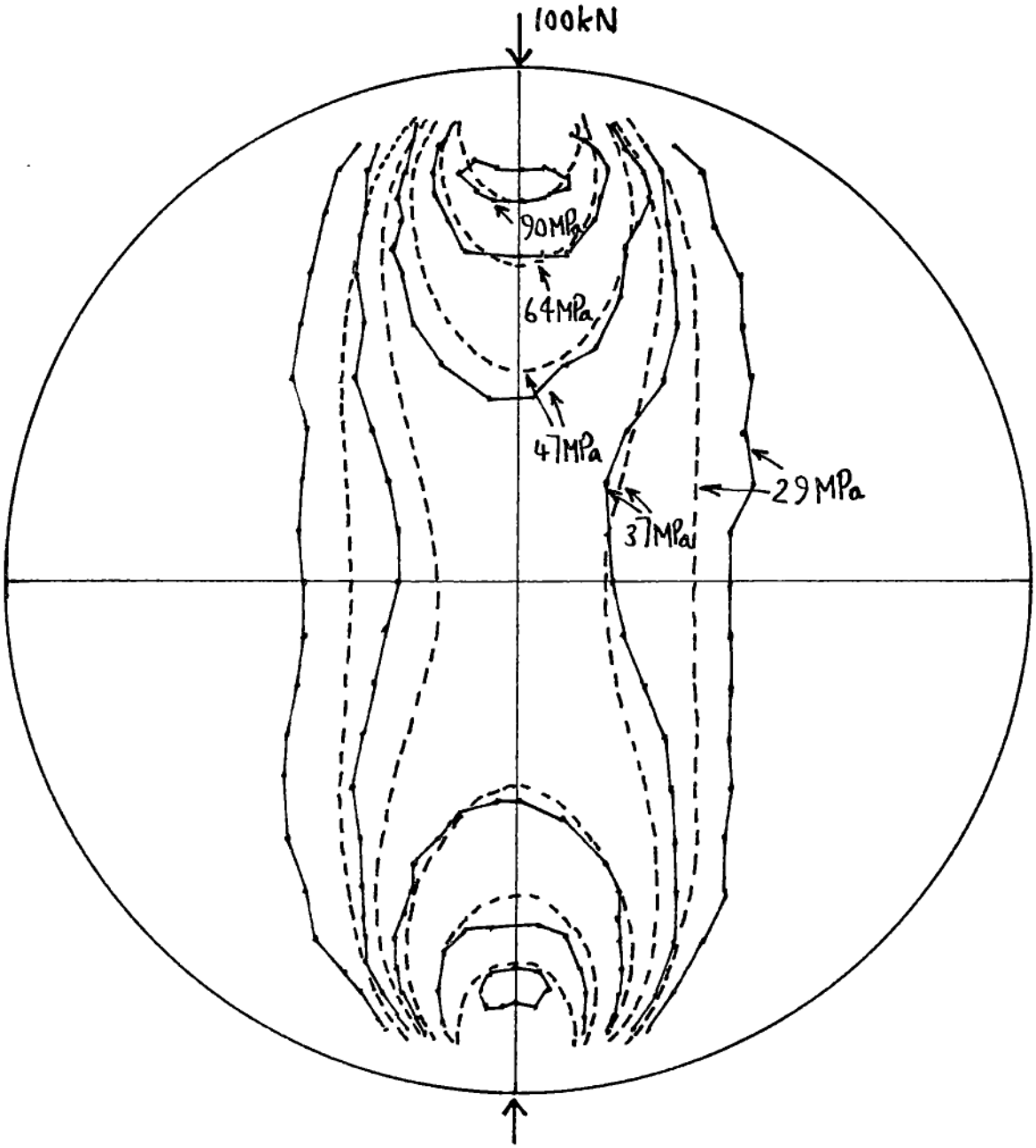

Figure 7.9 Isochromatics for 100kN load.

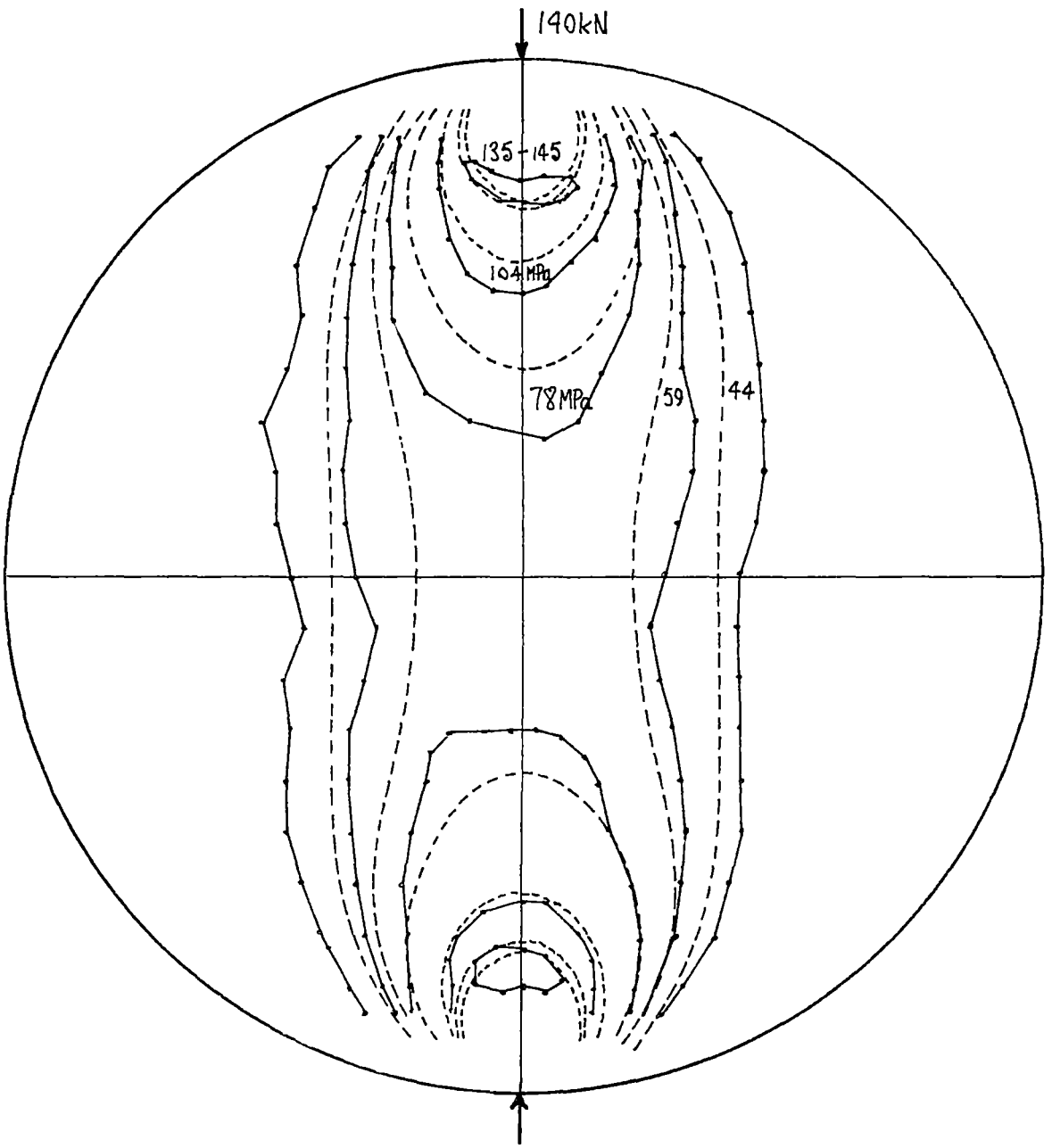

Figure 7.10 Isochromatics for 140kN load.

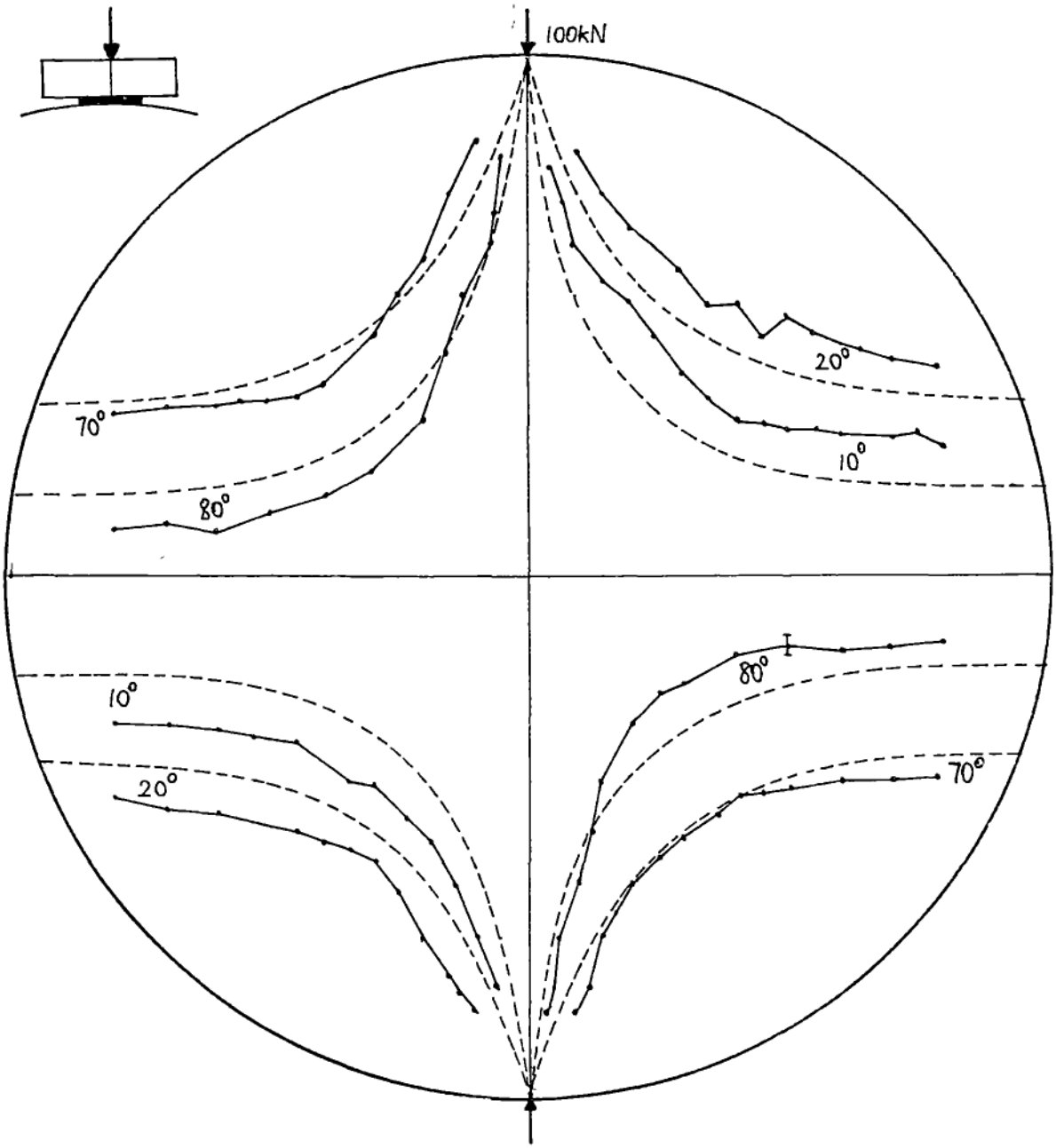

Figure 7.11 Isoclinics for 100kN load, with the load applied via a circumferential 3mm diameter rod.

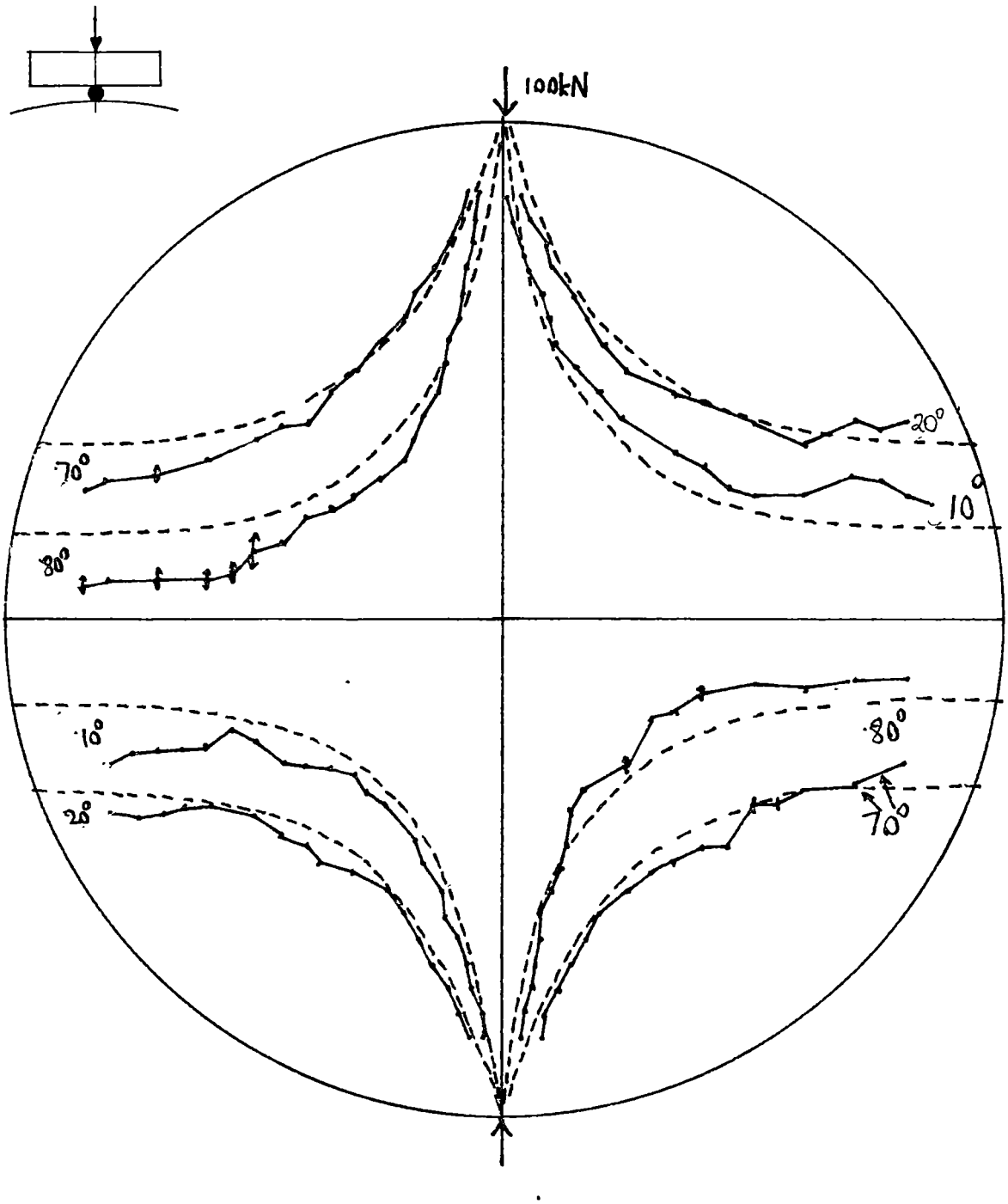

Figure 7.12 Isoclinics for 100kN load applied via an axial 3mm diameter rod.

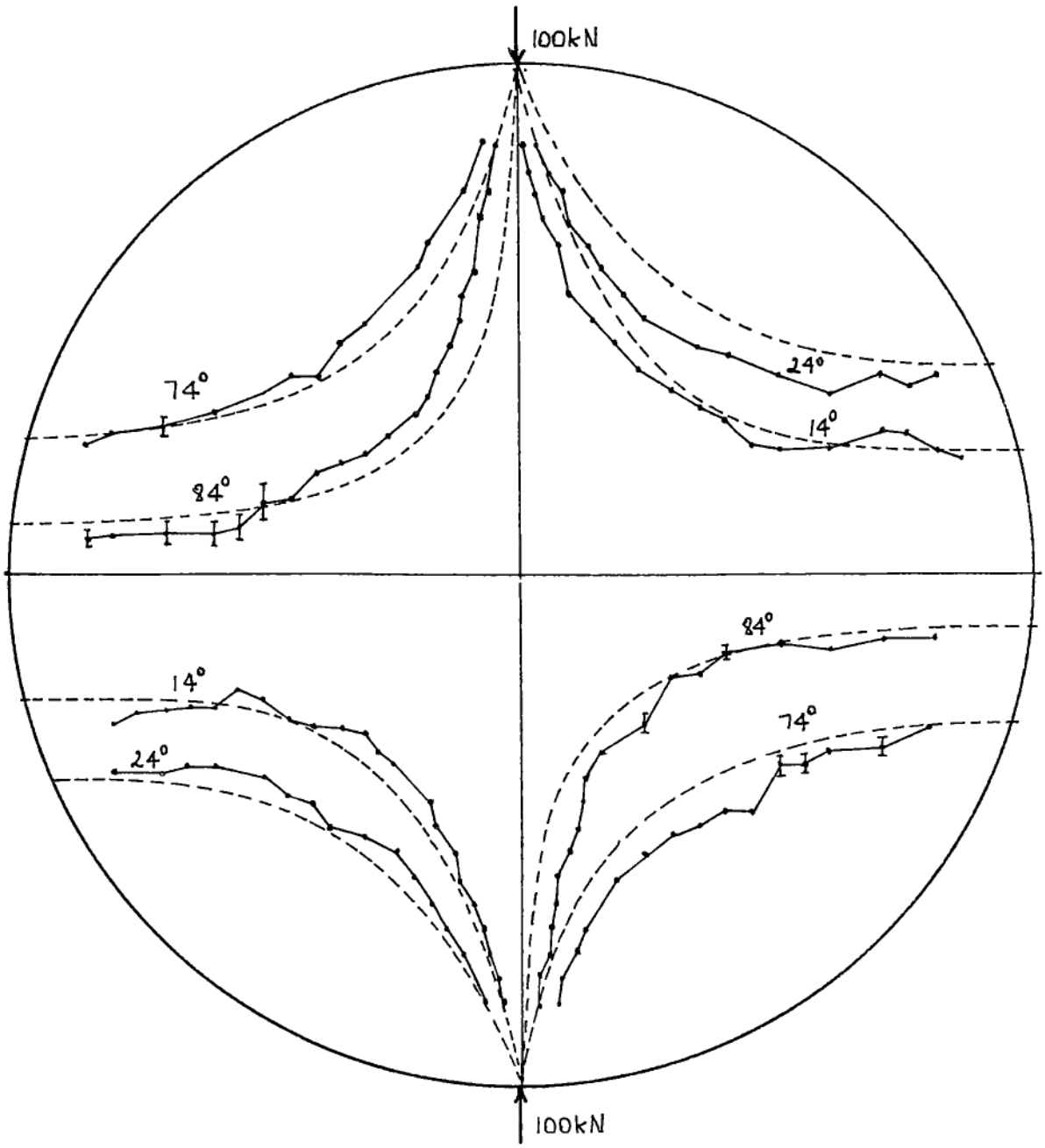

Figure 7.13 Corrected (for a 4° angular error in the scale on the rotation rig) isoclinics for figure 7.12.

7.6 Methods of applying the load to the disc

Circumferential groove

I filed a shallow groove about 40mm long around the edge of the disc, in the middle, and put a piece of 3mm diameter steel rod in it. The idea behind this was that the line of action of the load would pass centrally between the two faces and give equal stresses on each face. This was used for the 100kN load for isochromatics and for isoclinics.

Axial groove

This groove was filed perpendicular to the faces of the disc, exactly on the Y axis to ensure that the line of action of the load was along the diameter. This was used for the 70kN and 140kN loads for isochromatics and for a 100kN load for isoclinics.

The effect of these two methods is discussed in section 7.8; whether they achieved just what I intended is doubtful but they certainly caused a noticeable difference in the isoclinic stress contours. (A paper that is relevant to this type of problem is by Goodier [G2,1932]).

7.7 Discussion of the results: general comments

All contours were formed by joining up the points by straight lines. I judged this to be less subjective than drawing a smooth curve through them. Because of the difficulty of applying the load so as to get equal stresses on each face of the disc, the theoretical isochromatics are based on the (magnetically) measured stress-difference at the centre ($x = y = 0$) of the disc.

In general the measured isochromatics lie outside (or are greater than) the corresponding theoretical ones, rather more so for the low values of stress-difference than for the higher ones. For example, for the 100kN load (figure 7.9) the measured 29MPa contours lie inbetween theoretical

contours of 25 MPa and 20MPa: discrepancies of -14% and -32%. In the same way the discrepancies for the 88MPa isoclinic are -11% and +14%. (More details of these errors are in section 7.8).

Figures 7.9 and 7.10 show closed contours for the highest stress-difference. In theory all isochromatics pass through the line of application of the load and the stress tends to infinity at this point at the edge of the disc. In practice the steel yielded around where the load was applied. Previous work showed that R_v decreased (for the same applied stress) when the steel yielded). Thus the outer line of these closed contours would be within the yielded region. However the theoretical isochromatics would also be incorrect where yielding occurred.

In figures 7.11 and 7.12 the discrepancies between measured and theoretical isoclinics are least where the stress-differences are small, near the X axis. Although the distances between them are less at higher stresses, the relative discrepancies between them are actually larger, since the stress gradients are higher. This is probably due to yielding of the steel. There is also a skewed effect in that to get symmetry (which there should be) between the top and bottom halves of the disc the X axis must be turned anticlockwise by about 6°. This led me check the angle scale on the probe and I found there was an error on it of about 4°. Figure 7.13 shows the measured isoclinics of figure 7.12 but with the theoretical ones drawn for 14°, 24°, 74° and 84°; agreement between measurement and theory is now better.

7.8 Errors

This section gives a more detailed account of the errors between the measured and the theoretical results.

Isochromatics

Errors in the measured position of these arose due to:-

(1) The random residual stresses in the disc (indistinguishable from texture) of ±3MPa.

(2) Resolution of the voltmeter and the "fuzziness" of the R_v value. Fuzziness needs an explanation. Suppose that the probe is being rotated by hand at a spot on the steel to look for the highest values, positive and negative, of voltage. Rotation clockwise towards the positive maximum might give 0.40mV. Rotation anticlockwise might give 0.42mV. Turning the probe to and fro by 10° about the position of the maximum might give 0.41mV at the maximum. Turning it to and fro by 30° might give 0.40mV. More force to push the probe against the steel might cause 0.01mV change. The point is that the R_v value depends on how I used the probe, and although I tried to be consistent there was always an uncertainty of about ±0.01mV. This must be largely the result of magnetic hysteresis. All the readings on the disc were done with an HP425A microvoltmeter, set to either the 0.3mV or the 1.0mV range. It is a pointer meter with a resolution of 0.0025mV on the 0.3mV and 0.005mV on the 1.0mV range. So the error due to the limit of resolution was rather less than that due to hysteresis. (Later on I used an HP3466A digital multimeter, which was easier on the eyes and which had a maximum resolution of 0.001mV. On this range the last digit was never steady and I found it better to use a less sensitive range with a resolution of 0.01mV).

Taken together, points (1) and (2) gave errors ranging from ±12% for the 29MPa contour to ±6% for the 88MPa one. These figures are for the 100*kN* load, figure 7.9.

In order to compare these random errors with those actually existing between the measured and the theoretical contours, pairs of contours were drawn that enclosed each measured contour. Figure 7.14 shows these for the 100kN load, and the following table summarises the actual errors.

Measured contour (MPa)	Estimated (random) error (%)	Pairs of contours (MPa)	% difference relative to measured contour
29	12	20 & 25	-32 & -14
37	9	29 & 36	-22 & -3
48	8	40 & 50	-17 & +4
64	7	57 & 80	-12 & +9
88	6	80 & 100	-11 & 14

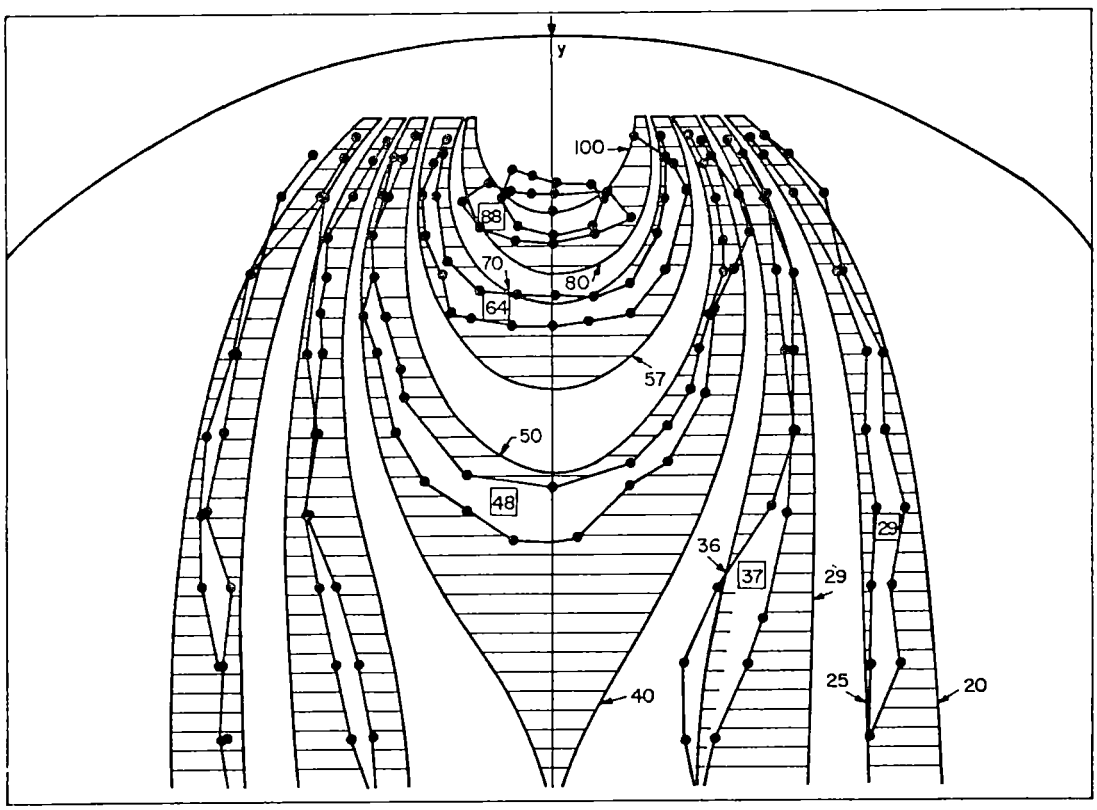

Figure 7.14 Pairs of theoretical isochromatics, for the 100kN load, that enclose the measured ones. (The disc has been "folded" so that the top and bottom sets of contours are both shown on the top half).

There are other errors which I cannot quantify.

(3) The calibration curve for the rotation rig was obtained for uniaxial compressive stress on a 50mm wide strip of steel cut from the same plate as the disc. In using this calibration I assumed that the R_v value for a particular uniaxial stress is equal to that for the same (numerical) difference in principal stresses $(\sigma'_x - \sigma'_y)$. Results of tests for biaxial stresses showed that there is a scatter in the values of $(\sigma'_x - \sigma'_y)$ for given R_v value that depends on the values of the principal stresses. This is of the order of 10% but is most unlikely to be the same for all mild steels. Thus the value of stress-difference assigned to a particular contour may be in error by at least 10%. Put another way, for a given stress-difference the position of the measured contour may be out by an equivalent amount.

Two things affect the position of the "true" contours and make them differ from the theoretical ones by an unknown amount. The (magnetically) measured ones may differ from the true ones by errors described in (1) - (3) above. The theoretical contours also differ from the true ones by errors described in (4) and (5).

(4) The method of applying the load to the disc. The following table gives the measured and theoretical stress-difference at the centre (x = y = 0) of the disc.

	Load (kN) =	70	100	140
$\sigma'_x - \sigma'_y$	theoretical	35	50	70
(MPa)	measured	34	39	67
	discrepancy	-3%	-22%	-4%
	loading groove	axial	circum-ferential	axial

The axial loading groove gave stress-differences close to the theoretical ones. A check with strain gauges showed that the circumferential groove gave a stress-difference on the other side of the disc that was correspondingly greater than the theoretical one. However, once I had allowed for these discrepancies by basing the theoretical contours on the measured value of stress-difference at the centre of the disc, the measured stress patterns were similar to the theoretical ones for all three loads.

(5) Yielding of the steel around where the load was applied.

St. Venant's principle suggests that the contours would be distorted over a region at the contact point about three times the length of the flattened perimeter of the disc. What was needed of course was an "accurate" (±5%) method with which the rotation rig results could be compared.

Isoclinics

Figures 7.11 and 7.13 show quite good agreement between measured and theoretical isoclinics for the two middle parts of the disc (i.e. between y = ±100mm). The corresponding exercise to that shown in figure 7.14, namely enclosing the measured isoclinics within pairs of theoretical ones, showed a spread of about ±5°.

However for the top and bottom parts of the disc the agreement is much worse; again I assume this to be mainly a result of the yielding of the steel. There is also a considerable difference here between figures 7.11 and 7.12. Figure 7.12, where the load was applied via the rod in the axial groove, has the measured contours closer to the theoretical ones than does figure 7.11. This seems reasonable, since the axial groove would concentrate the load on the diameter whereas the circumferential groove would tend to spread the load over 10 or 20mm around the edge. For both kinds of loading the faces of the disc were belled out by about 1mm where the load was applied; no doubt causing more departure from the theoretical case.

7.9 Conclusions

The discrepancies between measured and theoretical isochromatics are up to 20% (in round figures) for stress-differences between 40MPa and 100MPa; between isoclinics they are about ±5° for the middle parts of the disc (between y=±100mm). The random errors in measurement of the isochromatics range from ±12% (low stresses) to ±6% (high stresses. Other errors (of unknown amount) are described in the previous section. That these exist is a shortcoming of the disc test piece. They would have been largely avoided had the hole-in-a-rectangle test piece been used, but as already stated, this would have required considerably more effort. Overall, I think the results from these tests on the steel disc show the rotation rig to be a useful technique.

CHAPTER 8

B VS. H DATA FOR MILD STEEL, FOR MAGNETISATION PARALLEL AND PERPENDICULAR TO STRESS, FOR UNIAXIAL TENSION AND COMPRESSION

8.1 Introduction

Chapters 4 and 6 include descriptions of the use of the C-core rig, which is a local method (working from one side of the steel) of measuring B vs. H loops. I knew at the time that the C-core rig had a systematic error in it and could not be used to get accurate B vs. H data. However this error was acceptable for a comparison between B vs. H loops at different stress. Now, later, I wanted to have reasonably accurate results on which to base some theory and so I repeated the tests with, this time, search coils threaded through small holes in the steel in order to get more accurate values of flux density than were possible with the C-core rig.

These results were included in a paper [RL5] that was submitted for publication. One of the reviewers drew my attention to some recent work by Jiles and Atherton [J1,1984] that centred on the anhysteretic magnetisation curve. In this they also consider the effect of stress. The reviewer suggested that I repeat the B vs. H measurements for anhysteretic conditions. The results of this are in section 8.5; the B vs. H results of section 8.3 are for the measurement of the ordinary or hysteretic B vs. H loops.

8.2 Equipment

Mechanical details

An important feature is that the same piece of steel would be used for tension and compression. For the latter, since the steel was only 0.42mm thick, it had to be glued to hardwood to prevent buckling. Figure 8.1

shows the dimensions of the test piece and its mountings. For symmetry, to reduce bowing, an identical piece of steel was glued to the other side of the wood to make a sandwich. The side cheeks were glued as well as bolted to the sandwich. Experience showed that just bolting the side cheeks on did not prevent movement, and that too much force on the nuts to try to prevent this just squashed the wood. No trouble ever occurred when glue (standard two-tube Araldite) was used as well. The stress in the steel was calculated from readings of resistance strain gauges. These were glued on each face of the sandwich in order to detect uneven strains (and possible bowing in compression).

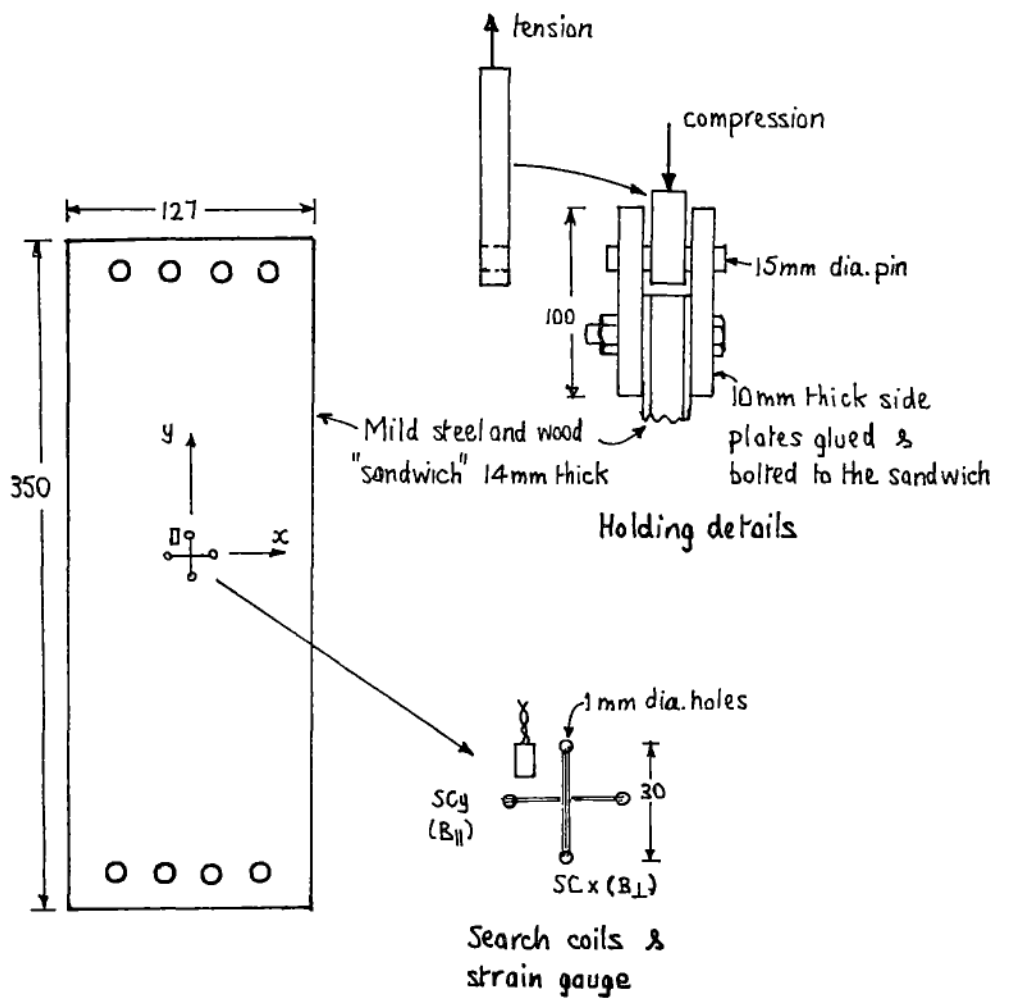

Figure 8.1 Details and dimensions (in mm) of the test piece.

Two pieces of mild steel, marked S44 and S45, were first annealed at 650°C to reduce residual stresses in them. Measurements with rotation rig number 4 (R.R.4) showed that S44 had about 5MPa left and S45 about 16MPa - hence S44 was used for magnetisation.

Magnetic details

The search coils were threaded through 1mm diameter holes bored right through the sandwich. Each had 17 turns of 47 B&S rayon covered wire. The size of the holes was a compromise: too large, and they would cause stress-concentration and hence differing magnetic properties over too much of the steel enclosed by the search coil; too small, and not enough turns of wire could be put through them. Figure 8.2 shows the theoretical change of stress around a hole. If, without holes in the steel, the (uniform) stress σ_y in the Y direction is σ_o, and the stress σ_x in the X direction is

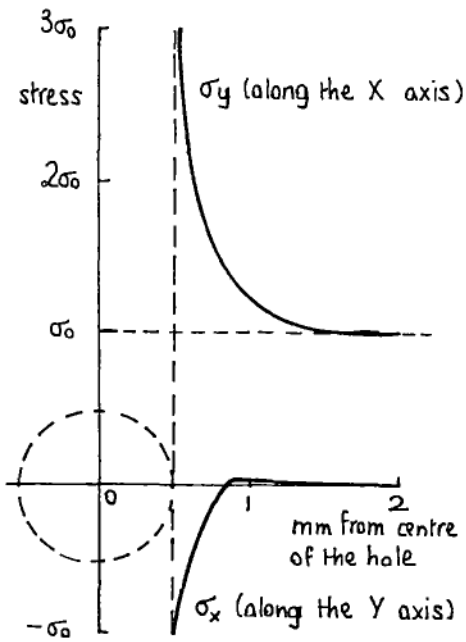

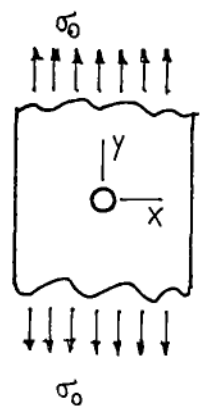

Figure 8.2 Stress concentration around a hole.

zero, then over 28mm inbetween the holes σ_y is near enough equal to σ_o and σ_x is near enough to zero [T2,1970]. Only for 0.5mm around the holes is the stress altered significantly. Thus about 97% of the steel enclosed by the search coil is at a uniform stress. At the edge of the hole $\sigma_y = 3\sigma_o$, and so if σ_o were 100MPa, there would be slight yielding. There would also be some change in flux density next to the holes but I assumed this effect to be very slight.

The M.M.F. was provided by the magnetising coil on the U-core, as shown in figure 8.3a. It was clamped lightly against the steel with one layer of 0.05mm tape between them. The magnetic field in the X and Y directions was measured with Hall plates. Measurements with the simple test pieces of figures 8.3b, c, and d showed that there was no detectable extra flux through the search coil, i.e. in figure 8.3c compared to 8.3d the steel on the far side of the wood did not carry significant flux, and neither did the wood itself. The same pieces of steel were used by themselves in 8.3b and glued to the wood in 8.3c.

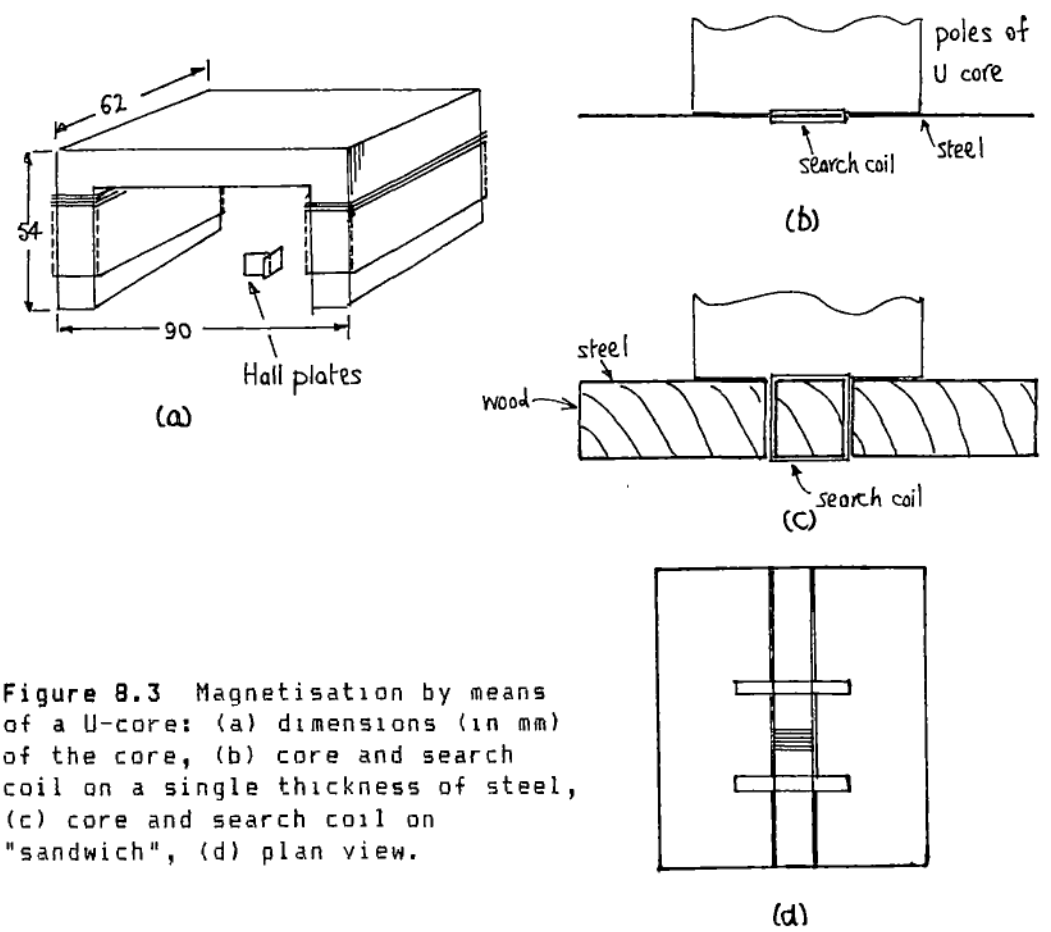

Figure 8.3 Magnetisation by means of a U-core: (a) dimensions (in mm) of the core, (b) core and search coil on a single thickness of steel, (c) core and search coil on "sandwich", (d) plan view.

Figure 8.4 shows the electrical equipment, used both for the permeameter and the U-core. (Chapter 4 describes much of this in more detail). All measurements were done inside a pair of 1.2m diameter demagnetising coils that cancelled out the vertical component of the earth's magnetic field to within 5%.

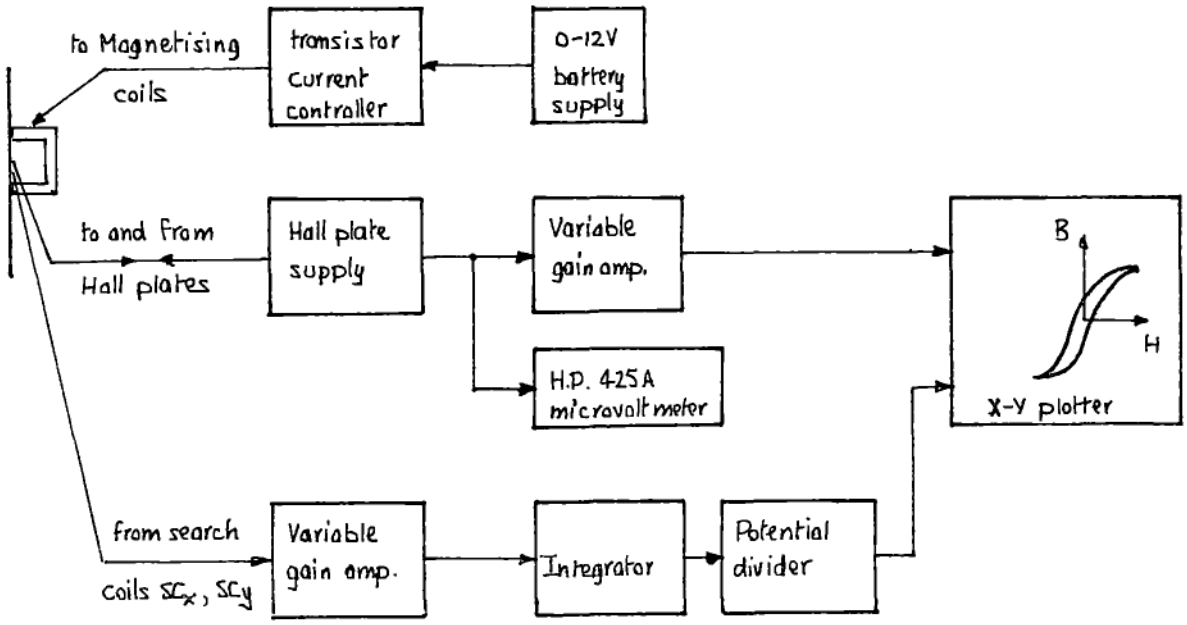

Figure 8.4 Electrical equipment for B vs. H loops.

Errors

Figure 8.5 shows B vs. H curves measured with the U-core in two directions at right angles to each other on the unstressed sample. $B_{\parallel}$ denotes the flux density for magnetisation parallel to the direction in which the stress would be applied, and $B_{\perp}$ denotes the same for the perpendicular direction. There are only slight differences between them for applied field values of 250A/m and 500A/m. Below 250A/m $B_{\parallel}$ and $B_{\perp}$ differ rather more. Thus the steel appeared almost isotropic for $250 < H < 500$A/m.

Also in figure 8.5 is a reference B vs. H curve for a test strip of the same steel, taken with the permeameter. It still differs (by between 27% and 7% for $100 < H < 600$A/m) from $B_{\parallel}$ for the U-core, but the difference is less than in the case of the C-core rig (up to 100%).

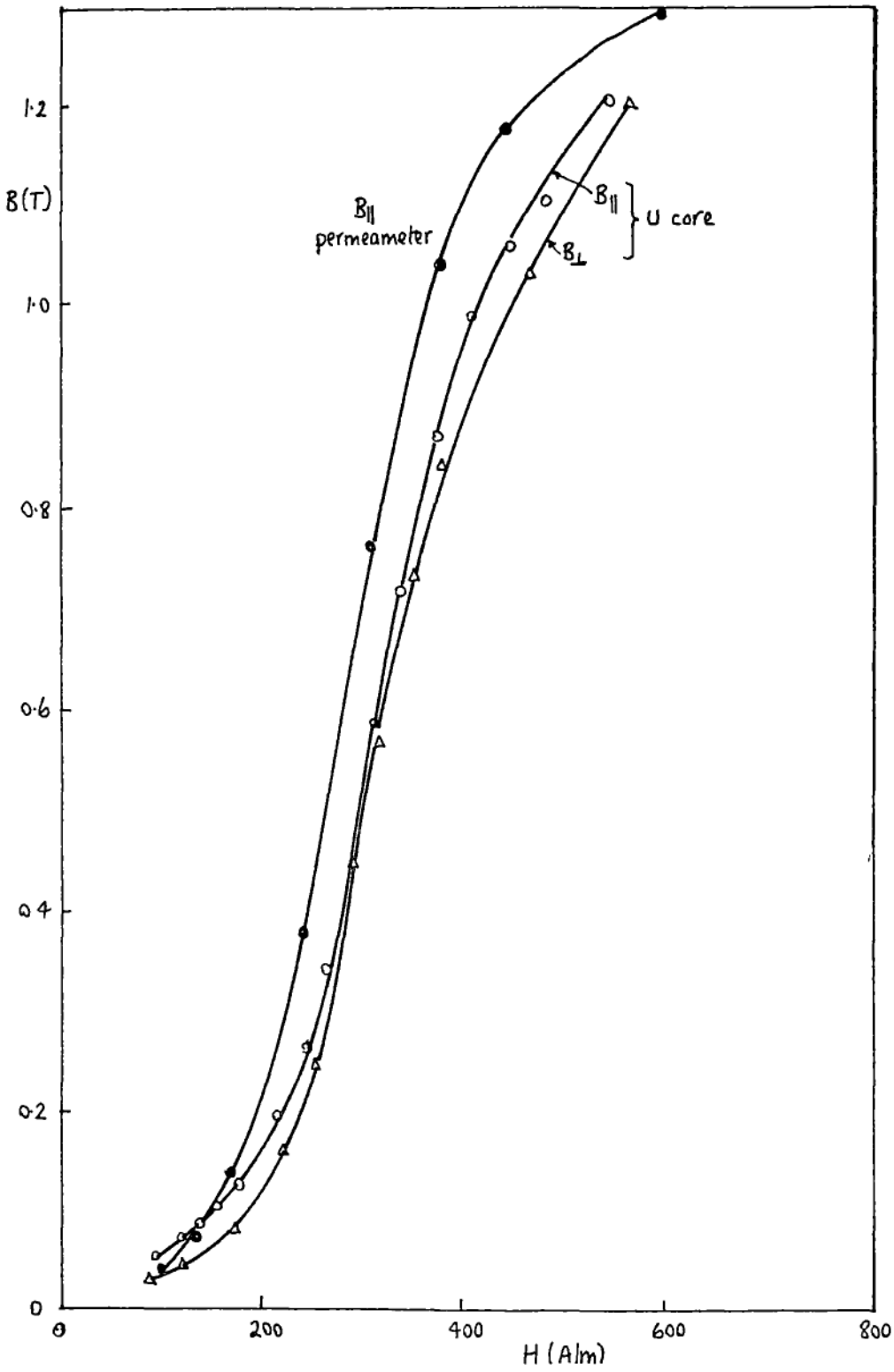

Figure 8.5 B vs. H curves for mild steel using the U core for magnetisation parallel ($B_{\parallel}$) and perpendicular ($B_{\perp}$) to the stress axis, and also the permeameter for a test strip in the parallel direction. No stress was applied for these results.

8.3 B vs. H results for hysteretic conditions

Measurements of B vs. H loops for four values of H between 100 and 600A/m were made for tensile and compressive stresses up to 120MPa. The heights of the loops are shown in figures 8.6a-d. The significant characteristics of these are:-

(1) Tension parallel to the applied field ($+\sigma,B_{\parallel}$) has little effect on flux density whereas parallel compression ($-\sigma,B_{\parallel}$) reduces the flux density considerably.

(2) Compression perpendicular to the field ($-\sigma,B_{\perp}$) has little effect but perpendicular tension ($+\sigma,B_{\perp}$) reduces the flux density considerably.

There is thus symmetry: $+\sigma,B_{\parallel}$ is similar to $-\sigma,B_{\perp}$ (flux density slightly affected) and $+\sigma,B_{\perp}$ is similar to $-\sigma,B_{\parallel}$ (flux density decreases considerably). It is tempting to write "the same" in place of "similar" and thus to make out that the differences are insignificant, perhaps due to some imperfections in the particular steel sample under test, but there is not enough evidence from these results to decide the matter.

The shapes of the B vs. H loops are not shown because their variation with stress is very similar to those shown in figure 6.11.

(One other shortcoming of the U-core that is presumably not exhibited by the permeameter is that in figure 8.6 the curve for, say, $B_{\parallel}$ is not continuous where it crosses the zero stress axis. When a test with tension had been completed, the U-core was taken off the steel whilst different end pieces were put on the sample so that it could be loaded in compression. On replacing the U-core, the flux density (for the same H as before) usually differed. This fact does not unduly decrease the worth of the results, but was a rather irritating aspect that had to be tolerated).

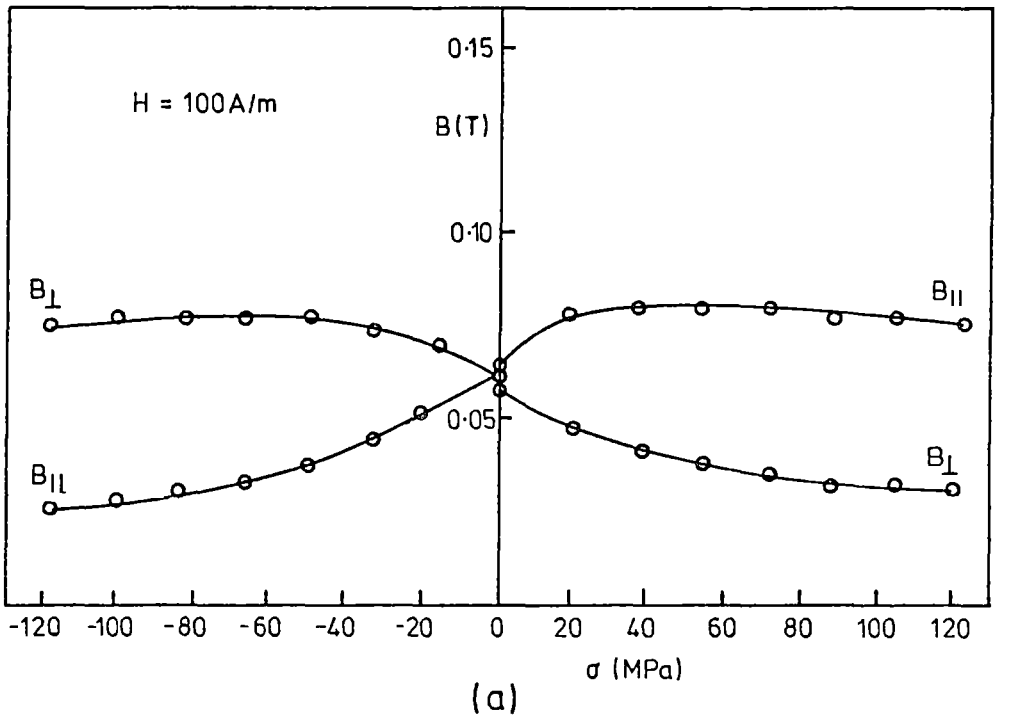

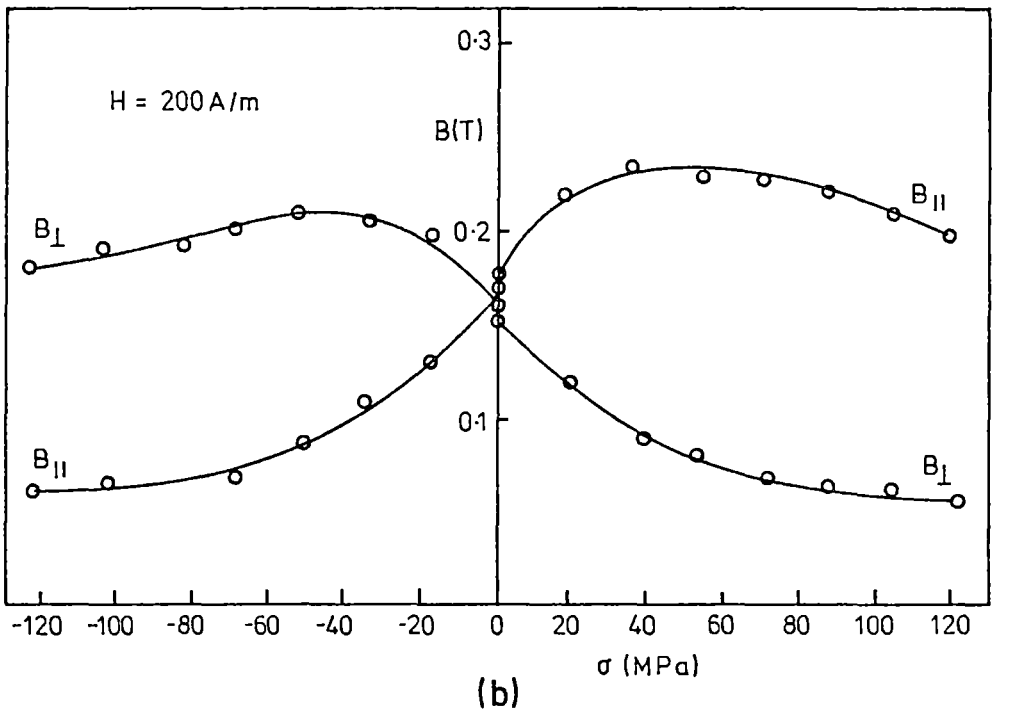

Figure 8.6 Values of peak flux density vs. stress for constant peak field H; hysteretic conditions. H = (a) 100A/m, (b) 200A/m. Stress was held constant whilst H was varied.

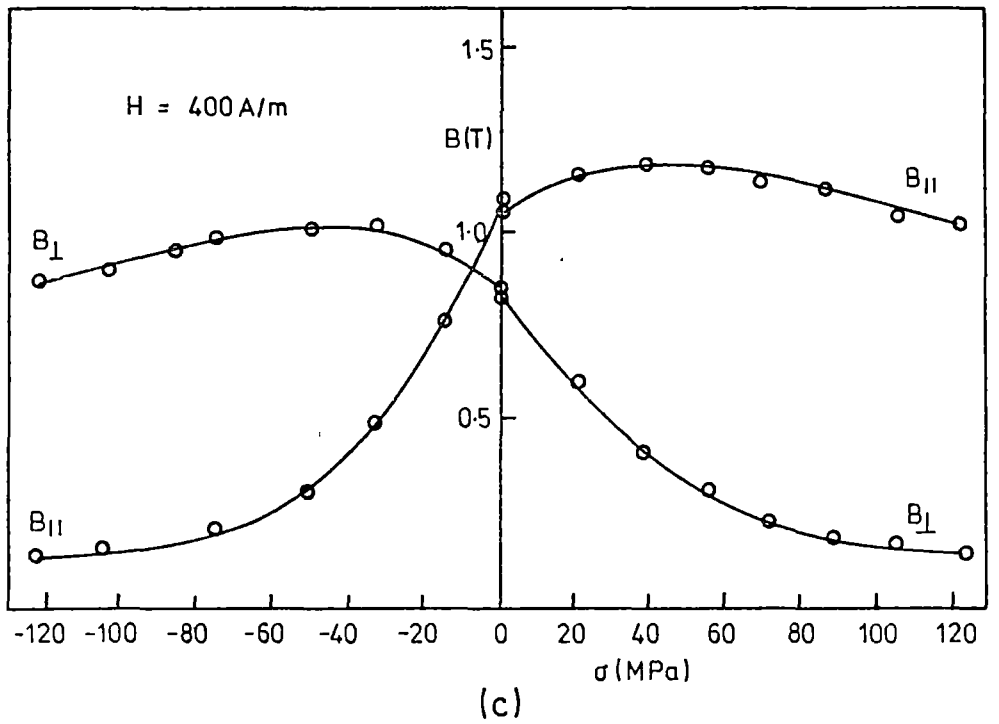

(c)

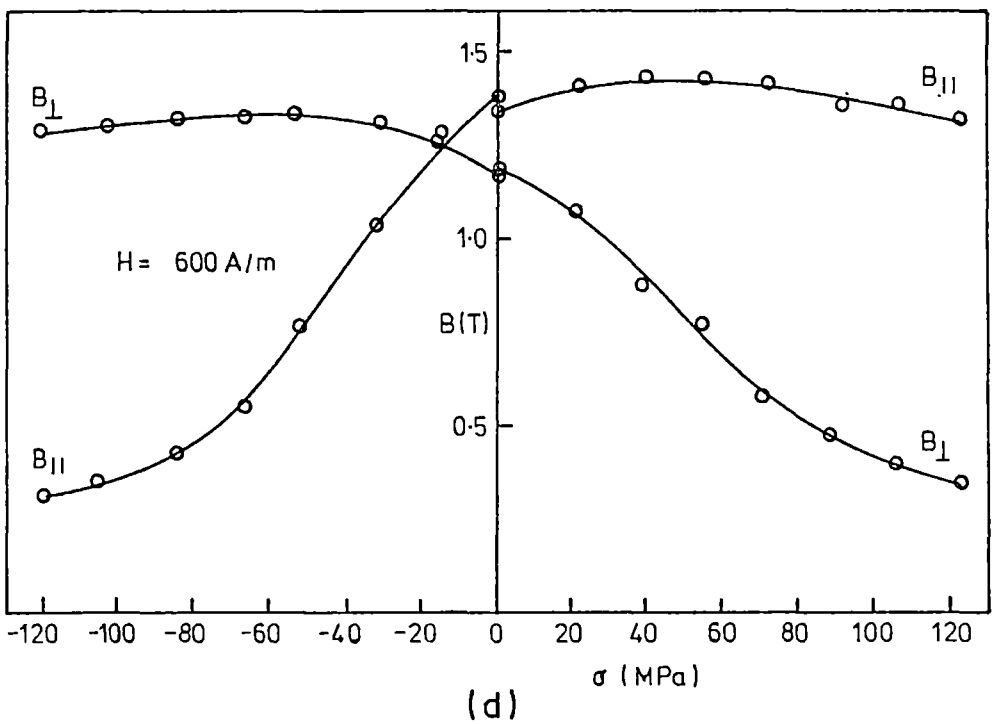

(d)

Figure 8.6 (continued): (c) H = 400A/m, (d) 600A/m.

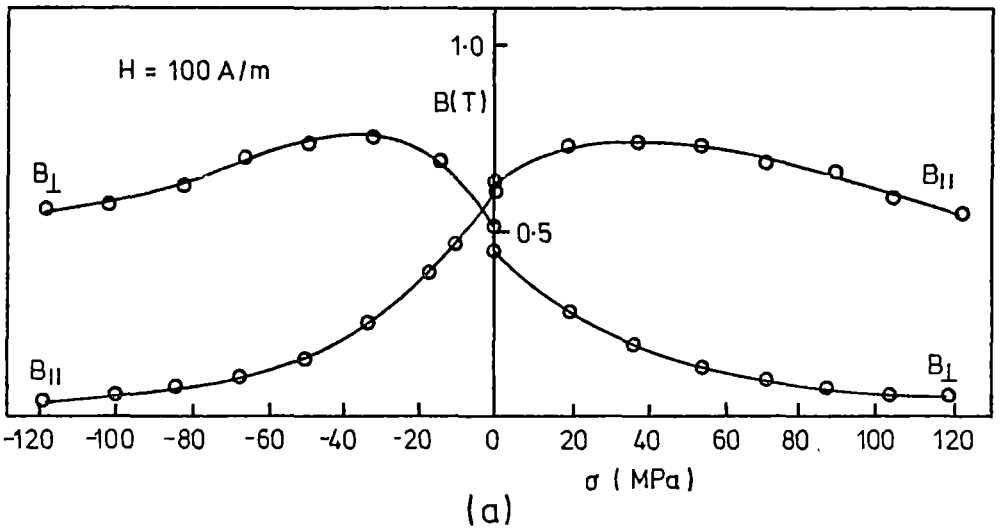

(a)

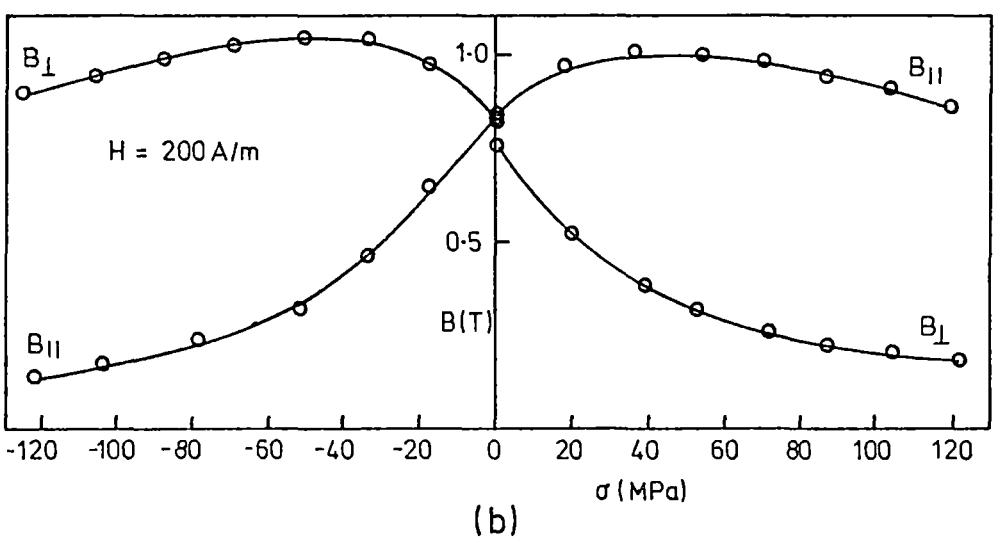

(b)

Figure 8.7 Values of peak flux density vs. stress for constant peak field H; anhysteretic (ideal) conditions. H = (a) 100A/m, (b) 200A/m. Stress was held constant whilst H was varied.

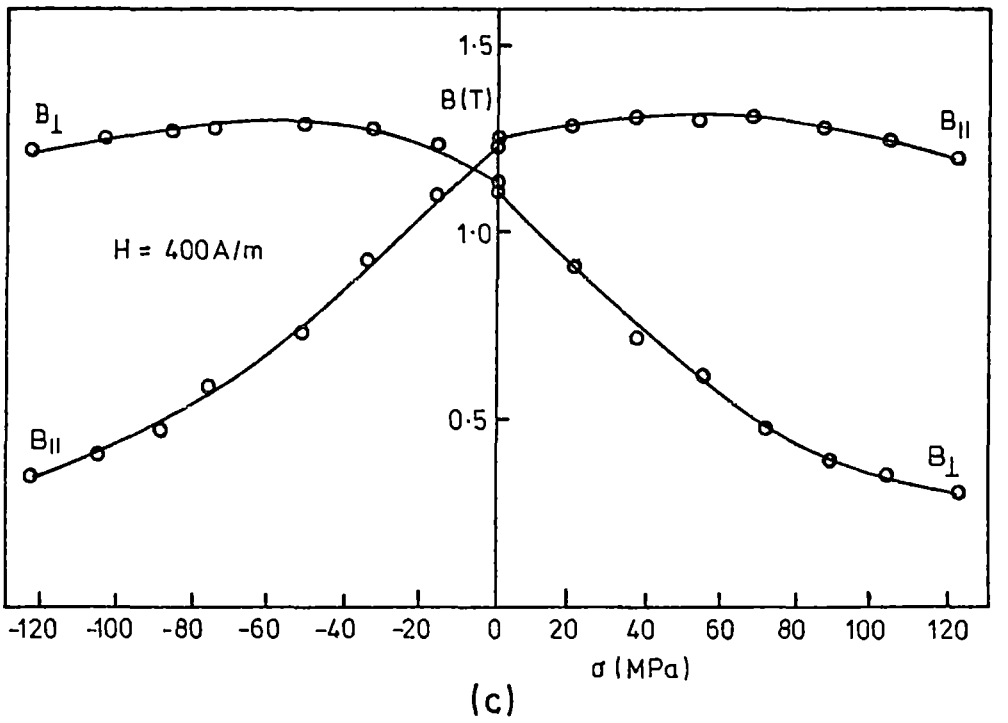

(c)

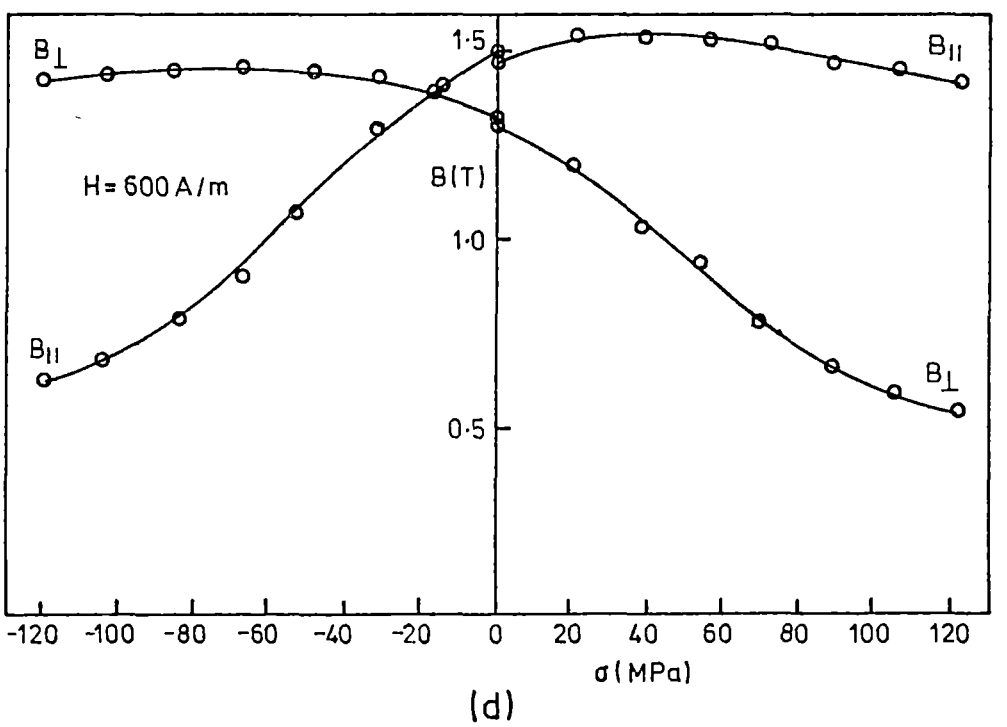

(d)

Figure 8.7 (continued). H=(c) 400A/m, (d) 600A/m.

8.4 B vs. H curves for anhysteretic conditions

There is surprisingly little information available on the anhysteretic or ideal (the latter word will be used here as it is shorter) magnetisation curve. Bozorth [B7,1951, page 547] deals briefly with it as does an interesting book by Ashworth [A5,1938]. It is discussed further in Part III of this thesis.

I repeated the measurements described in section 8.3, using exactly the same equipment and the same mild steel sample S44, but with an extra pair of magnetising coils wound on the poles of the U-core. These carried alternating current and enabled the ideal B vs. H curves to be measured. The procedure to obtain these ideal B vs. H curves for magnetisation parallel and perpendicular to the stress is: firstly demagnetise the steel (with A.C.), then apply the stress, then the D.C. field, then the A.C. field, decrease it to zero, and switch the integrator onto the search coil. The D.C. field is reversed, the A.C. field applied and reduced to zero as before, and the integrator reading noted. The amplitude of the A.C. field is a potential extra variable, but as long as its peak value H_{ac} is made larger than the D.C. field, the value of the flux density is substantially independent of H_{ac}.

Figure 8.7 shows the results in the form of graphs of B vs. σ. Each graph is for a different value of D.C. field H. Although stress is shown as a variable, it was held constant during the magnetising. Figure 8.8 shows the ideal B vs. H curves for various stresses, measured separately from figure 8.7.

Comparison of figures 8.7 and 8.6 show that they are similar in shape and that they show the same symmetry ($+\sigma,B_{\parallel}$ is like $-\sigma,B_{\perp}$; $-\sigma,B_{\parallel}$ is like $+\sigma,B_{\perp}$).

Figure 8.9 is included to show that the difference between the U-core curve and the permeameter one is rather larger for the ideal case than for the initial curve of figure 8.5. However, presumably the assumption - that the difference (in figure 8.9) is a systematic one - still holds and the

curves of figures 8.7 and 8.8 correctly show the trends relative to each other.

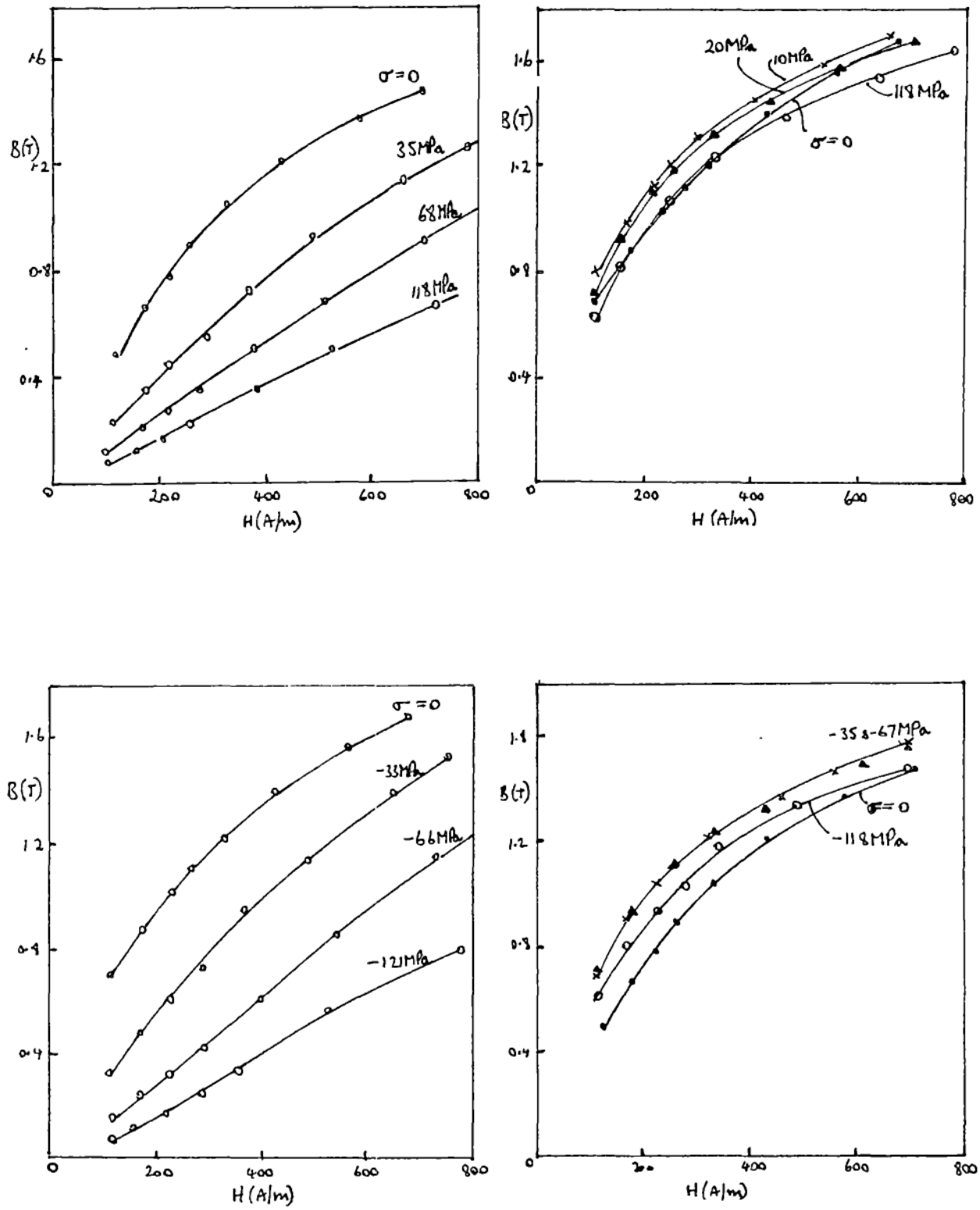

Figure 8.8 Ideal B vs. H curves for mild steel, for different values of stress. (a) tension perpendicular to magnetisation, (b) tension parallel to magnetisation, (c) compression parallel to magnetisation, (d) compression perpendicular to magnetisation.

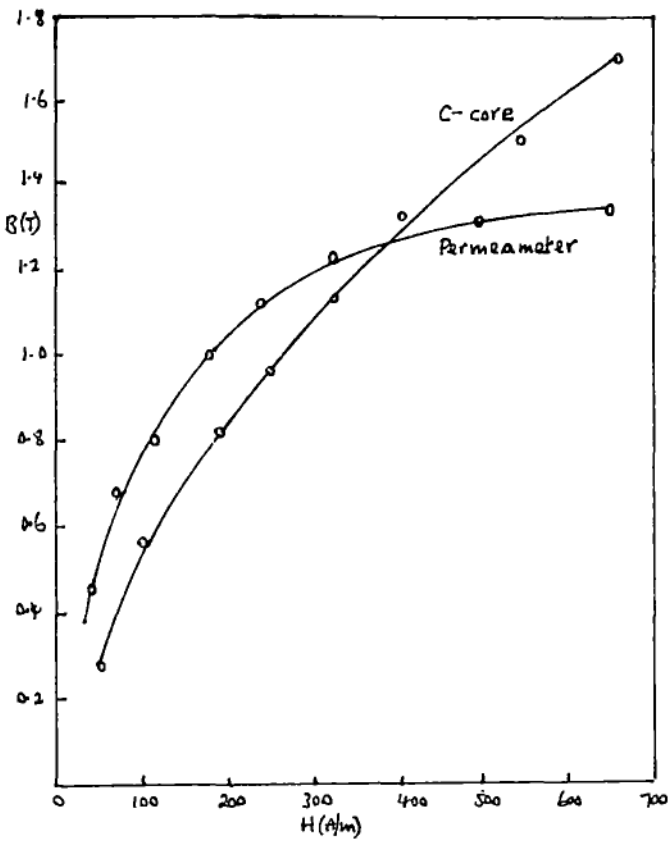

Figure 8.9 Ideal B vs. H curves at zero stress measured with the permeameter and with the U-core.

8.5 Chinese results: a comparison

Figure 1.24 is reproduced here as figure 8.10a. It shows curves of I_x and I_y, corresponding to changes in permeabilities for magnetisation parallel (X) and perpendicular (Y) to the applied stress. It should be compared with figure 8.10b, which is from figure 8.6c turned sideways and the stress axis moved to where the curves cross the B axis. The two diagrams are substantially the same shape but with one difference: $B_{||}$ corresponds to I_y and $B_{\perp}$ to I_x. I have assumed in figure 8.10a that I_y is for the permeability measured in the Y direction but it may not be so. If I_y were to correspond to $B_{||}$ the agreement between the diagrams would be qualitatively complete.

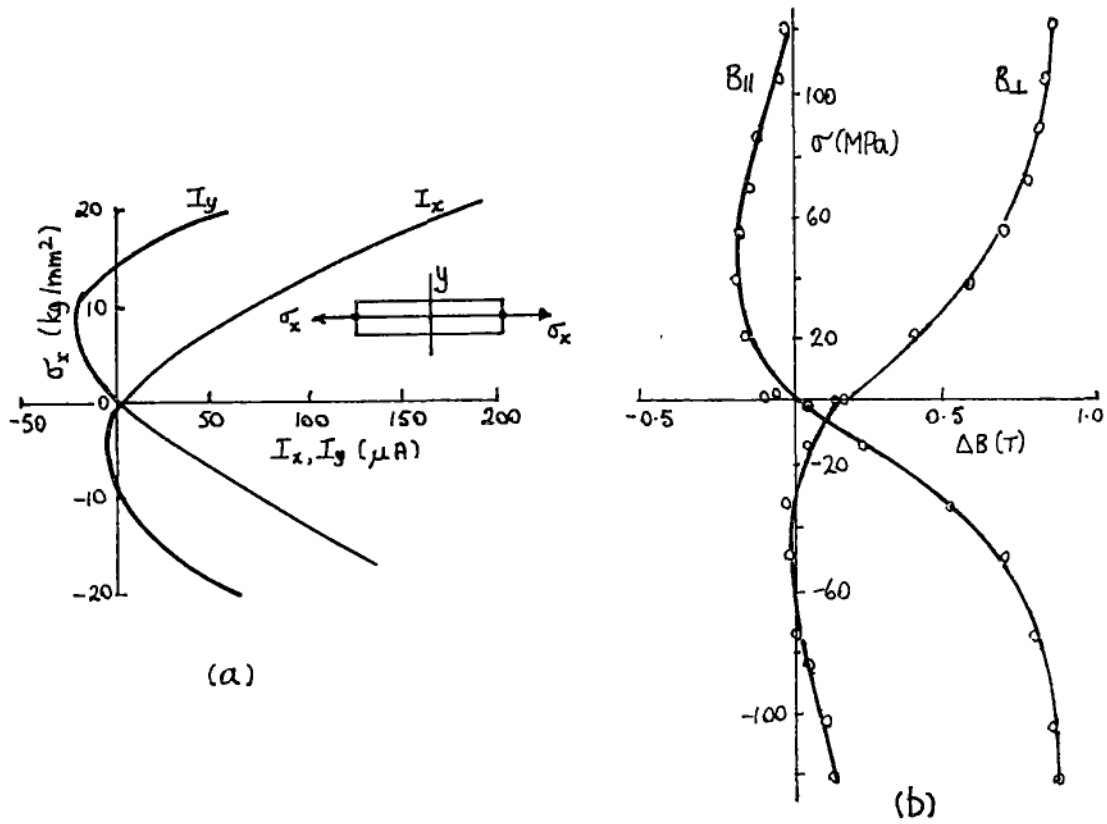

Figure 8.10 (a) Haosen et al [H2]: stress σ_x vs. transducer output I_x (magnetisation parallel to stress), and vs. I_y (magnetisation perpendicular to stress), (b) flux density change B for magnetisation parallel ($B_{\parallel}$) and perpendicular ($B_{\perp}$) to stress (adapted from figure 8.6c).

The fact that the Chinese can calculate absolute values of stress make their method better than the rotation rig. However, I think that there could be large errors in their results due to surface roughness (which would introduce unknown air gaps). It was for just this reason that I abandoned any attempt to make direct measurements of permeability and instead concentrated on the difference in permeability between perpendicular directions. This in turn means that the rotation rig can measure only *differences* of principal stress (as well, of course, as their directions).

CHAPTER 9

ROTATION RIG MEASUREMENTS FOR STRAIN BEYOND THE YIELD POINT

9.1 Introduction

All the tests so far in part II have been on annealed samples of mild steel that were reasonably free of residual stress. However, structural steel components such as I-beams or rolled hollow sections are strained plastically during their forming process. Depending on how hot they are when this is done, and on how rapidly they cool, they will when cold contain varying amounts of residual stress. Steel that has been cold rolled (usually thin sheet) tends to contain more residual stress than hot rolled steel, and is harder mechanically. It is also harder magnetically. There is general agreement [C2] that these increases result from the increased density of dislocations due to the deformation, and, on a microscopic scale - that of the crystal grains or even smaller - the high residual microstresses in the steel.

From the point of view of using the rotation rig, steels that differ magnetically are likely to have different sensitivities to stress. An extreme example is the comparison between mild steel and railway line steel; rail steel is about six times less sensitive than mild steel. However these have different chemical compositions. If the discussion is restricted to steel of the same composition, then the changes in magnetic properties due to plastic deformation must be related, somehow, to the changed structure of the steel and its residual stresses. An externally applied stress adds to the complicated unknown pattern of the residual stress; the effective stress is not known.

The measurements on plastically strained steel that are described in the rest of this chapter should be regarded as preliminary ones that, in fact, raise more questions than they answer.

9.2 Rotation rig characteristics on thick steel

One problem of working in the plastic region of steel is that of getting it to strain uniformly. It tends to yield locally by large amounts rather than uniformly by smaller amounts. Just what does happen depends to some extent on the shape of the sample. When the 12mm thick bar, described in chapter 5, is bent so that its surface just yields but the interior is still strained elastically, then presumably the surface strain is fairly uniform since it is constrained by the elastic interior.

Figure 9.1 shows the R_v vs. strain graph for the small rotation rig on a 12mm x 102mm (or 1/2" x 4") mild steel bar that was first annealed and then bent in the 4 point bending rig of figure 5.3. The steel yielded at about 1200 microstrain. (A tensile test on an 8.5mm diameter test piece machined from the parent bar gave an upper yield stress of 260MPA and a lower one of 240MPa). Strain was calculated from the deflection of the sample and the value so obtained was checked initially against readings of Huggenberger strain gauges. A check was also made that the deformation was anticlastic.

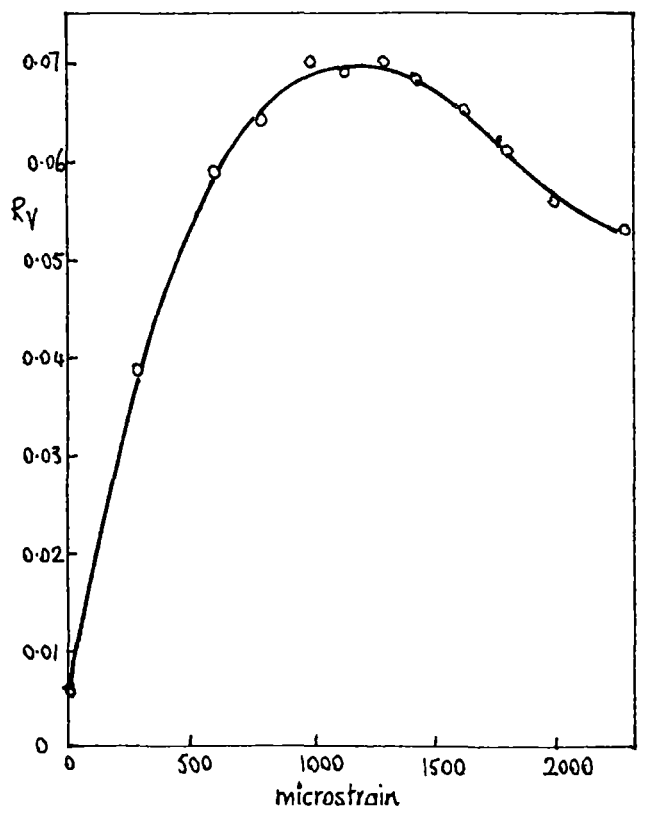

Figure 9.1 R_v vs. surface strain for a 102mmx12mm section mild steel bar bent beyond its yield point.

The graph shows that R_v reaches its maximum at the yield point but then decreases for higher strains. Since the surface stress would, if anything, increase slightly with strain after yield, then the rotation rig gives an ambiguous result. This is a serious drawback to its use.

Figures 9.2 and 9.3 show the effect on R_v of loading and unloading another bar. Curve 1 of figure 9.2a is for initial bending up to the maximum attainable bending moment, i.e. when the bar had yielded throughout its thickness and the bending moment remained constant even though the surface strain increased. Curve 2 is when the load was reduced back to zero, leaving permanent strain. Curves 3 and 4 are a repeat of the process on the same sample. All are for the face in tension.

Curves 5, 6, 7, and 8 in figure 9.2b are for the process repeated twice more. Each time the bending moment was taken to its maximum attainable value.

Curves 1 to 8 in figures 9.3a and b show the corresponding results for the compression face of the bar. In all cases the rotation rig magnetising current was adjusted to give a constant field strength (off the steel) of 800A/m R.M.S. For comparison, the coercivity of the steel was about 400A/m.

For the results in figures 9.2 and 9.3 the residual voltage in coil SCn was backed off by adding to it a portion of the voltage from SCp. A correction was also made that allowed (approximately) for the curvature of the bar at the higher strains, which did not let the faces of the core lie flush against the bar, causing a reduction in reading from SCn.

Discussion

The results show clearly that on return to zero bending moment there was residual stress on each face of the bar, of opposite sign to the applied stress. Thus the upper face was in residual tension and the lower one in residual compression. Whether the residual tension was less than the

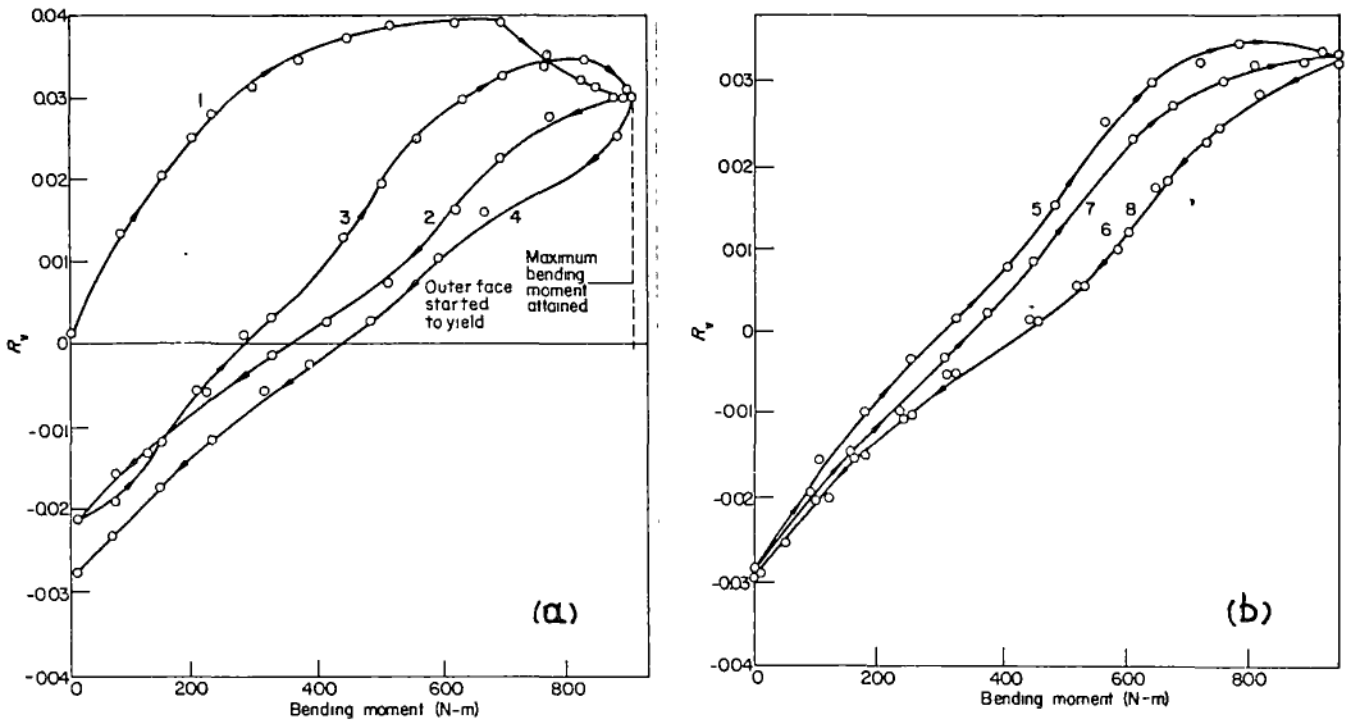

Figure 9.2 R_v vs. bending moment for the 12mm bar. Rotation rig on the tension face. (a) two loading (1,3) and unloading (2,4) cycles from new, (b) two more loading (5,7) and unloading (6,8) cycles.

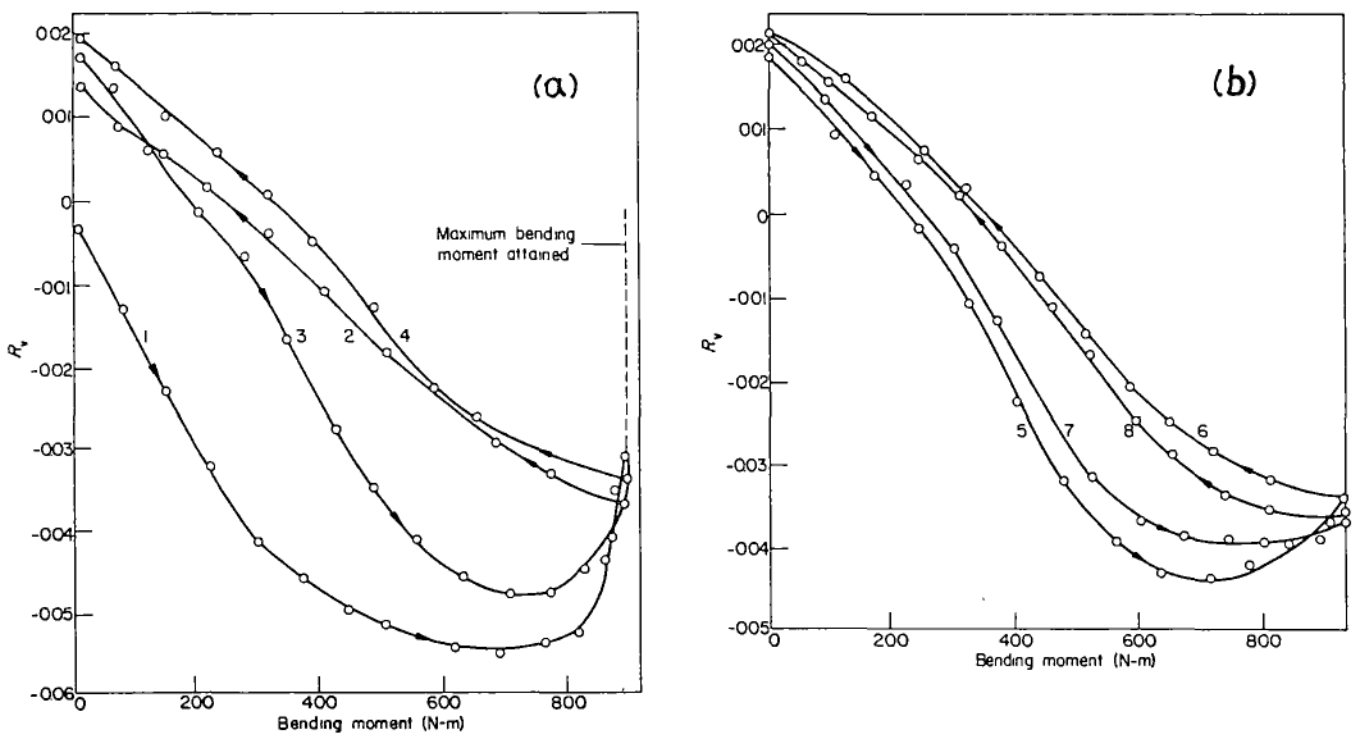

Figure 9.3 As figure 9.2 but for the compression face.

residual compression, as is suggested by the graphs (R_v was 0.02 for the upper face and 0.03 for the lower face) is not known. It was not possible on this sample to reduce the noise in SCp to less than R_v = 0.005. Since the residual R_v values differ by about twice this (0.03 - 0.02), 0.005 added to the tension reading and subracted from the compression reading would make them about equal. From the symmetry of the bending, the residual stresses should be about equal, since the yield stress of steel is approximately equal for compression and tension.

9.3 Plastic tensile strain on thin steel

Rotation rig results

Figure 9.4 shows graphs of R_v vs. stress for uniaxial tension on a 0.4mm thick mild steel sheet. Curve 1 is for the steel after it had been annealed (650°C for 2 hours, then cooled in the oven) and then tensioned within the elastic region. Curve 2 is for the same sample after it had been pre-strained by about 10%. (Straining was continued until the diagonal slip bands had broadened and joined up. There was no significant work-hardening since the applied force stayed at the lower yield value). The negative sign of R_v at zero load indicates that there was apparently residual compression in the direction of plastic pre-strain (or perhaps residual tension at right angles). According to Cullity, any grain re-orientation due to plastic strain would result in a biaxial rather than uniaxial anisotropy, and therefore cannot explain this effect.

The R_v reading stayed the same when the rotation rig was moved across the sample. It could be put close enough to the edges to show that there could not be enough tension at the edges to balance the compression in the middle. Also, since the sample was so thin, the R_v reading was for the stress averaged right through the steel so that, again, surface compression could not be balanced by internal tension.

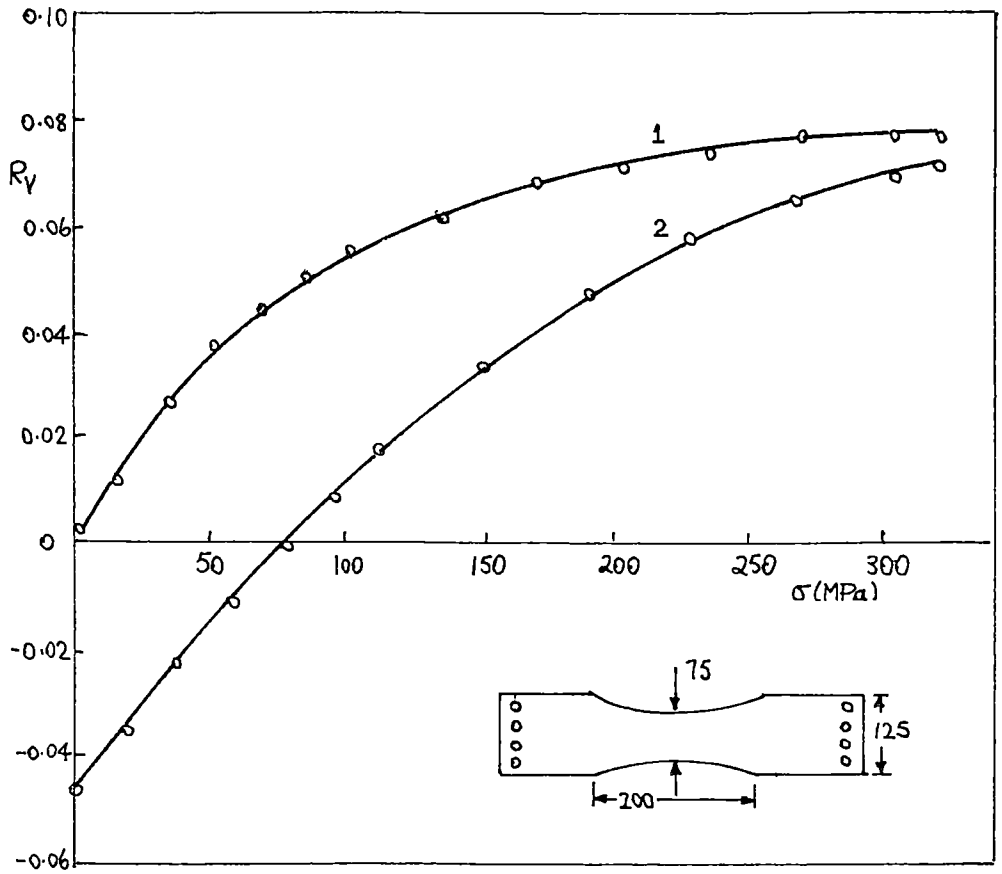

Figure 9.4 R_v vs. stress. Curve 2 is for a plastically prestrained sample of mild steel. Curve 1 is for the sample before plastic strain.

B vs. H data

These were obtained using the C-core rig on a different piece of the parent sheet of mild steel. Figure 9.5 is a sketch of the stress vs. strain diagram for this sample with parallel ($B_{\parallel}$) and perpendicular ($B_{\perp}$) values of flux density marked. The peak applied field was kept constant at 270A/m. B and H values are for the tips of the B vs. H loops. (One problem is that the sample would not strain uniformly in the waisted central part. As a result it was impossible to measure the strain where the C-core rig was located with useful accuracy and the error in the strain is about 20%). However, despite this error, two aspects of figure 9.5 are worth mentioning.

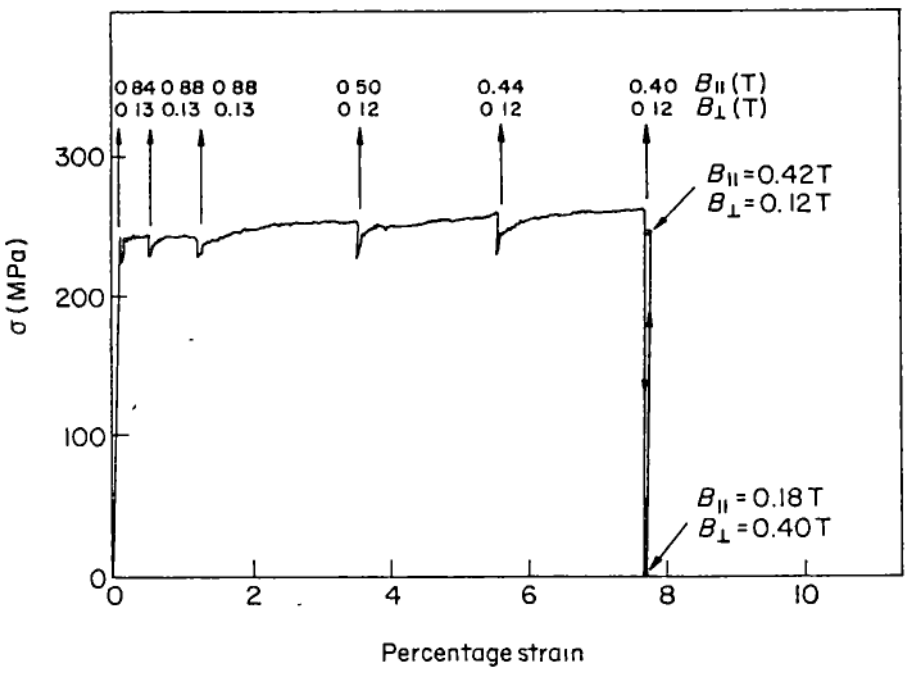

Figure 9.5 Sketch of the stress vs. strain diagram for annealed mild steel in tension up to a strain of 8%. Values of peak flux density of the B vs. H loops measured parallel ($B_{\parallel}$) and perpendicular ($B_{\perp}$) to the stress are shown. H=270A/m peak.

Firstly, both $B_{\parallel}$ and $B_{\perp}$ stay constant at their yield point values of 0.84T and 0.13T respectively, up to a strain of 1.5%. $B_{\parallel}$ then decreases to 0.4T at a strain of 8%. Since the stress (230MPa) does not vary significantly up to the 8% strain, then clearly $B_{\parallel}$ is affected by these large strains as well as by stress.

Secondly, when the force is reduced to zero at the strain of 8%, $B_{\parallel}$ decreases to 0.18T but $B_{\perp}$ increases to 0.4T - virtually a swap of their previous values. Re-application of the same force restores $B_{\parallel}$ to 0.42T and $B_{\perp}$ to 0.12T, and then removal of the force again makes $B_{\parallel}$ = 0.16T and $B_{\perp}$ = 0.4T. This suggests that when the force is removed there is residual tension in the perpendicular direction.

Comments on figure 9.4

The magnetic evidence is that when the steel is strained plastically in uniaxial tension there is residual compression in the same direction when

the load is released. What looks like the same effect is mentioned by Cullity, in his book, and also in a later paper [C4,1975]. He calls it pseudomacrostress. Quoting from the book, page 378:

"Examination of the deformed specimens by X-ray diffraction revealed the presence of residual stress, because the X-ray lines were both shifted and broadened. The line shift indicates a stress which is more or less constant over most of the specimen volume, and the broadening reflects stress variations about the mean in this volume. The X-ray observations are consistent with the assumed stress distribution of [my] figure 9.6 for a specimen previously deformed in tension. The material can then be imagined as consisting of regions in longitudinal compression (C regions) and regions in tension (T regions). The C regions comprise most of the specimen volume and are responsible for the X-ray effects, while the smaller T regions add nothing observable to the X-ray pattern. The C regions have been tentatively identified with the subgrains which form within each plastically deformed grain, and the T regions with the subgrain boundaries"

This statement refers to a nickel sample, but Cullity also says that there is no reason not to believe that plastic tension or compression would produce the same kind of residual stress in other polycrystalline ferromagnetic metals.

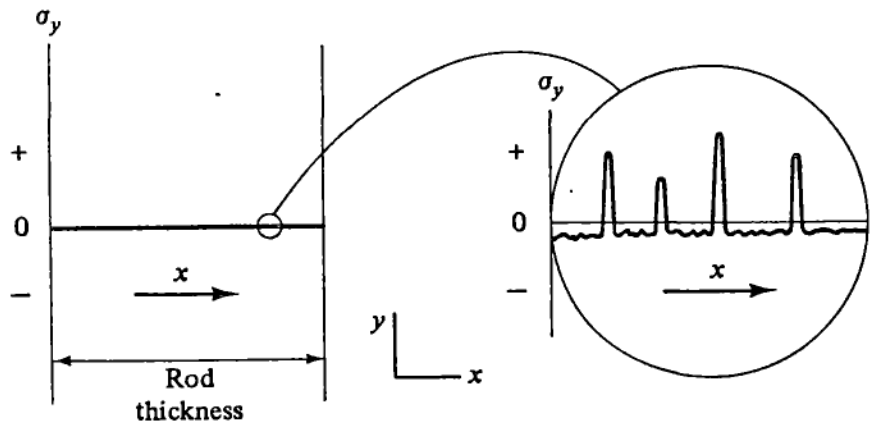

Figure 9.6 Distribution of longitudinal residual stress σ_y across the diameter (x direction) of a rod after plastic elongation in the y direction. (Cullity, ref. C2).

Reference C4 gives magnetic evidence for this effect in the form of the variation of magnetostriction with field strength for different applied stress.

Secondly, this may be related to the Bauschinger effect. Hill [H4,1970] states:

> "When a plastically deformed specimen is unloaded, residual stresses on a microscopic scale remain, due mainly to the different states of stress in the variously orientated crystals before unloading. If a different loading is now applied such residual stresses must influence the plastic yielding. For example, if the previous strain was a uniform extension and the specimen is then reloaded in compression it is observed that yielding (of the specimen as a whole) occurs at a much reduced stress. This is known as the Bauschinger effect, and in so far as it is absent from single crystals of pure metals it is attributable to a particular kind of residual stress due to the grain boundaries".

These two comments suggest that, at least on a microscopic scale, the prestrained sample is in residual compression when unloaded, and this is supported by the flux density data of figure 9.5. Similar results have been reported by the Japanese research into M.S.A. that is described in section 1.8.

When the strained sample is loaded again, the resulting R_v vs. σ graph, curve 2, differs from curve 1 in two important aspects: firstly the maximum R_v value is less for curve 2 than for curve 1, yet the applied stress at yield is the same. Secondly, curve 2 has a much steeper slope at yield than does curve 1, yet tests on elastic straining give R_v vs. σ curves that have nearly zero slope at yield.

This suggests that the steel in curve 2 has been changed magnetically, and so differs from curve 1 for the same reason as would a curve for an un-annealed sample in which the grains would have some texture resulting from the method of manufacture. It shows a serious

weakness in the rotation rig (as it is understood and used at present) as a method of measuring stress differences. Unless plastic strain can somehow be distinguished from elastic strain, results using the rotation rig could be misleading.

9.4 Barkhausen noise, the rotation rig, and plastic strain

Section 11 of chapter 1 describes the detection of plastic tensile strain in mild steel by the measurement of Barkhausen noise (B.N.). I repeated the test of section 2 of chapter 9 on the 12mm bar in order to relate the B.N. to the rotation rig output.

Figure 9.7 shows the dimensions of a small E-core, made of silicon steel laminations, for magnetising the mild steel and detecting the B.N. The single cell flux pattern gives a slightly higher signal to noise ratio than the two cell one, and so was used in preference. Figure 9.8 shows the rather crude signal processing that went with the E-core transducer. The applied field was about 600A/m, varied sinusoidally at 0.3Hz. The filter was set at 1kHz to 10kHz with a fourth order Butterworth characteristic. The B.N. was recorded as the peak R.M.S. voltage that was registered twice a cycle (at 0.3Hz) on the voltmeter.

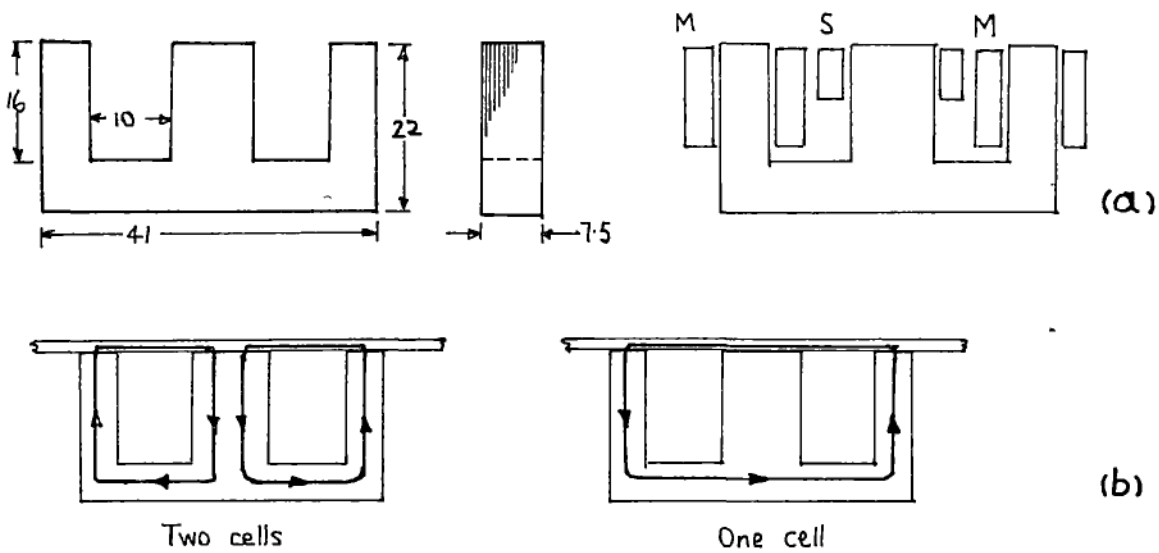

Figure 9.7 Barkhausen noise transducer. (a) dimensions, in mm, of the E-core and coils. M=magnetising coils of 2000turns each, S=search coil of 1500 turns. (b) flux patterns.

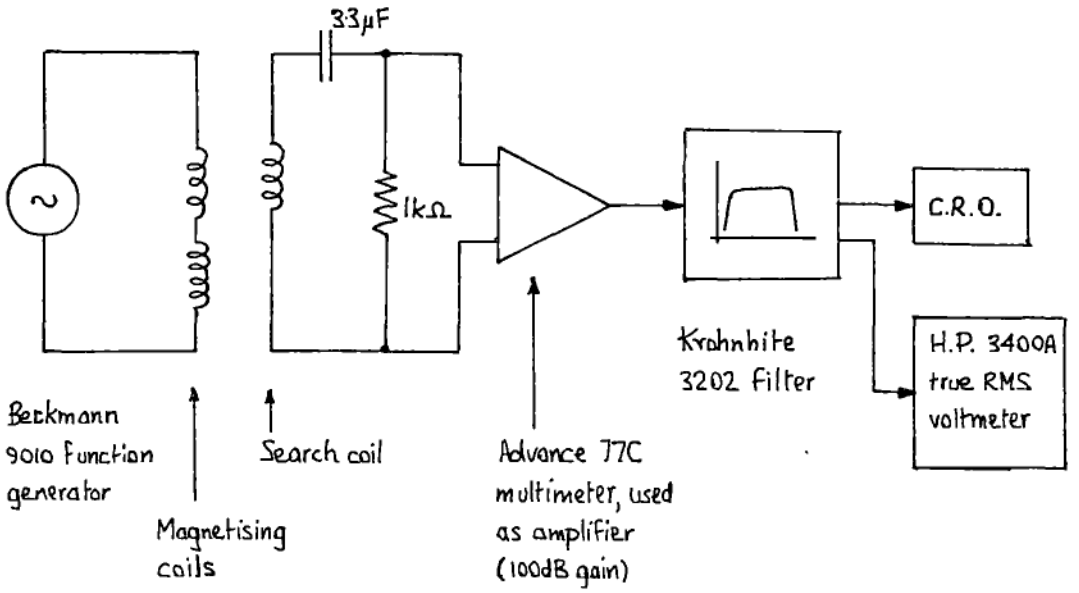

Figure 9.8 Signal processing for Barkhausen noise.

The B.N. was measured for magnetisation along the bar parallel to the stress ($BN_{\parallel}$) and across ($BN_{\perp}$) the bar; the results are shown in figure 9.9. Surface strain was estimated from the deflection of the bar and was not measured directly.

This variation of B.N. with strain has some resemblance to the variation of R_v with strain of figures 9.2 and 9.3. In order to display this more clearly figure 9.10 shows $BN_{\parallel}/BN_{\perp}$ vs. R_v. I suspected that there should be symmetry for tension and compression, and to bring this feature out I plotted $BN_{\parallel}/BN_{\perp}$ when this ratio is greater then 1.0 in the right hand half of the graph. When the ratio is less than 1.0, I took the reciprocal, $BN_{\perp}/BN_{\parallel}$, and plotted it in the left hand half of the graph. In this way ratios of say, $BN_{\parallel}/BN_{\perp} = 2.0$ and $BN_{\parallel}/BN_{\perp} = 0.5$ are equidistant from the vertical axis. Figure 9.10 shows that these ratios of B.N. values are related almost linearly to R_v.

These measurements of R_v and Barkhausen noise are for the same area of the steel bar; the probes were not moved but the stress was varied. When each was moved along the bar, the B.N. did not follow the R_v value so closely.

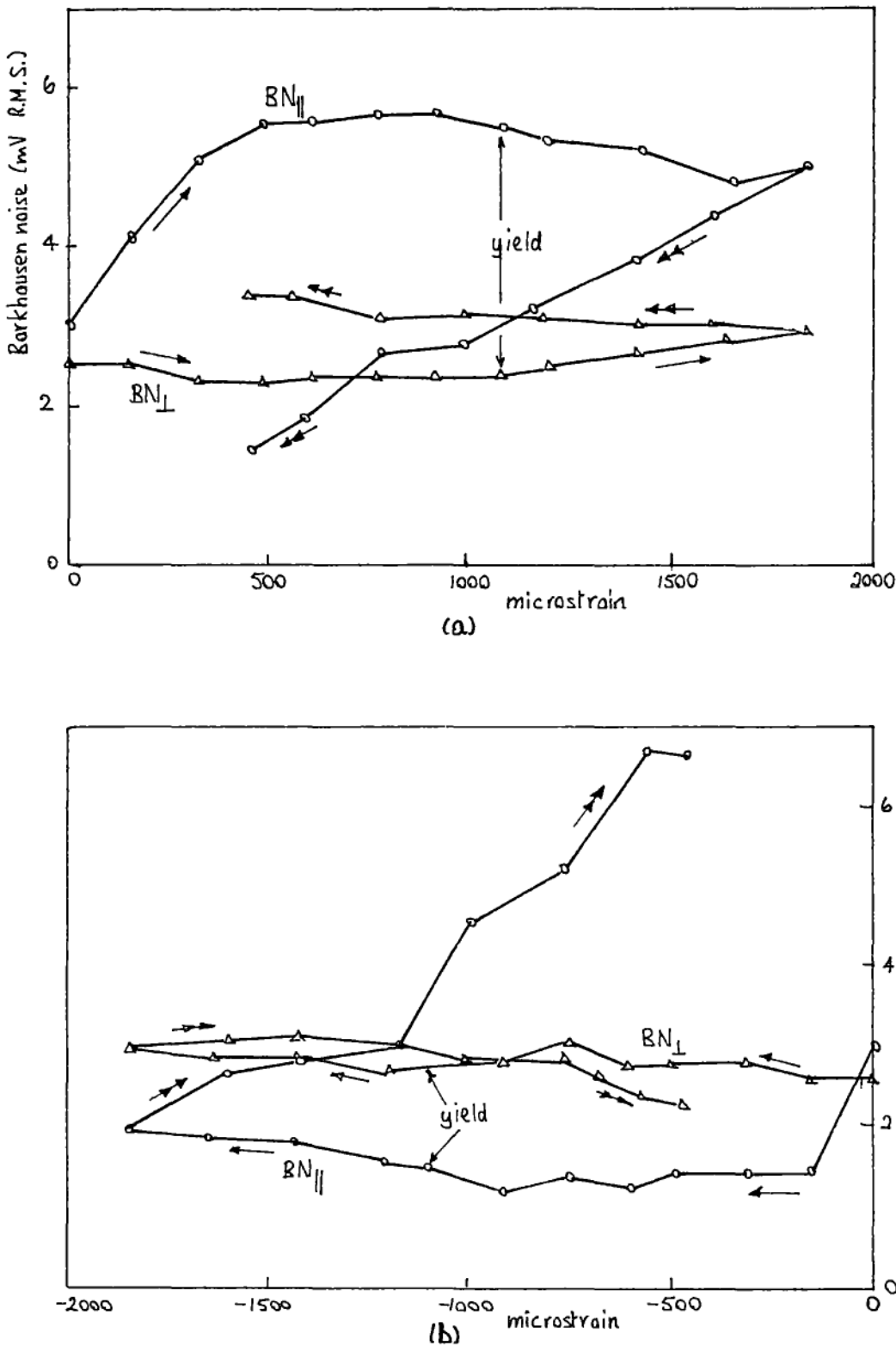

Figure 9.9 Barkhausen noise (B.N.) vs. strain for a bending test on a 12mm thick mild steel bar. The bar was loaded until it was permanently bent and then unloaded. B.N. was measured for magnetisation parallel ($BN_{\parallel}$) and perpendicular ($BN_{\perp}$) to the principal stress. (a) Lower face, in tension on loading, (b) upper face, in compression on loading. → = loading, ↠ = unloading.

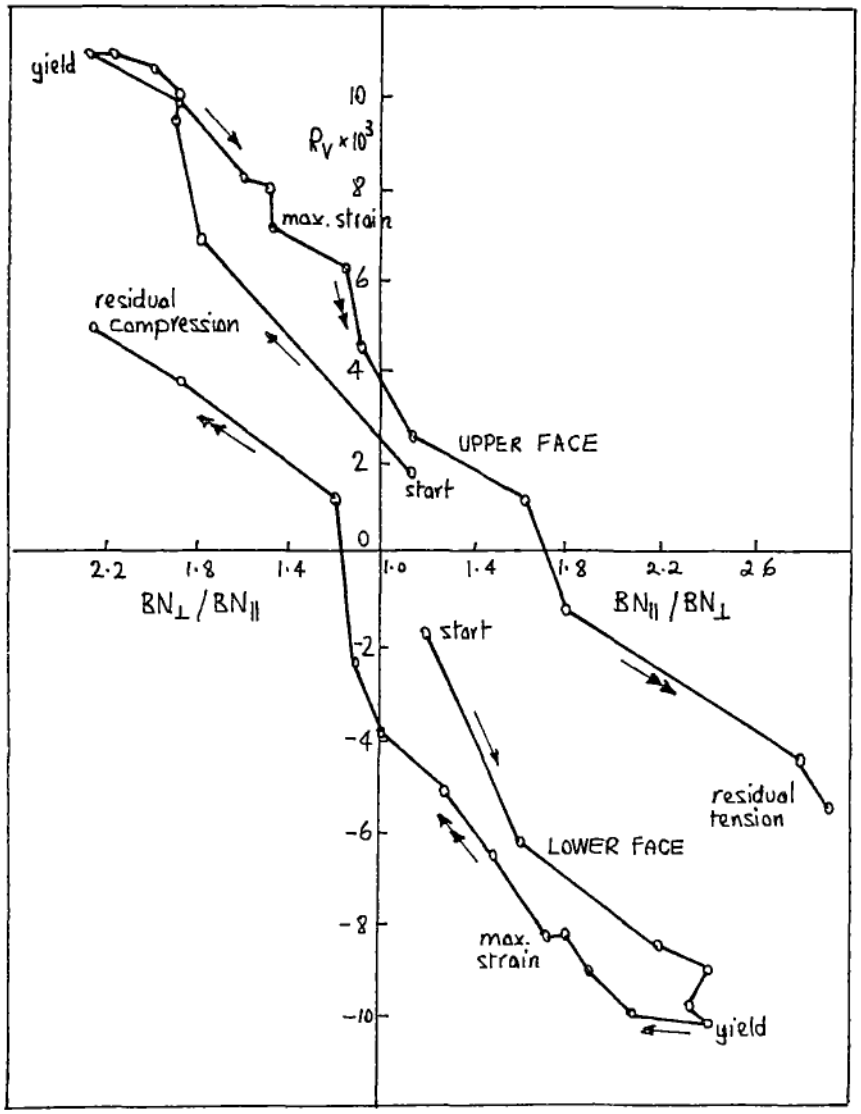

Figure 9.10 R_v vs. ratio of Barkhausen noise for the bar of figure 9.9. Refer to the text for an explanation of $BN_\parallel / BN_\perp$.

Figure 9.11 shows $BN_\parallel$, $BN_\perp$, and R_v for a scan along each side of a 4" x 1/2" annealed mild steel bar that was not loaded. The rotation rig shows the residual stress (or stress difference) to be less than 10MPa. If figure 9.9 is used as a crude kind of calibration for the B.N. then a change in tensile stress from almost zero (the annealed value) to yield causes a change in $BN_\parallel$ from 3mV to 6mV. The same change in compression causes a change in $BN_\parallel$ from 3mV to 1.5mV. $BN_\perp$ is hardly affected by stress of either sign. Hence the $BN_\parallel$ readings on the bar in figure 9.11 suggest

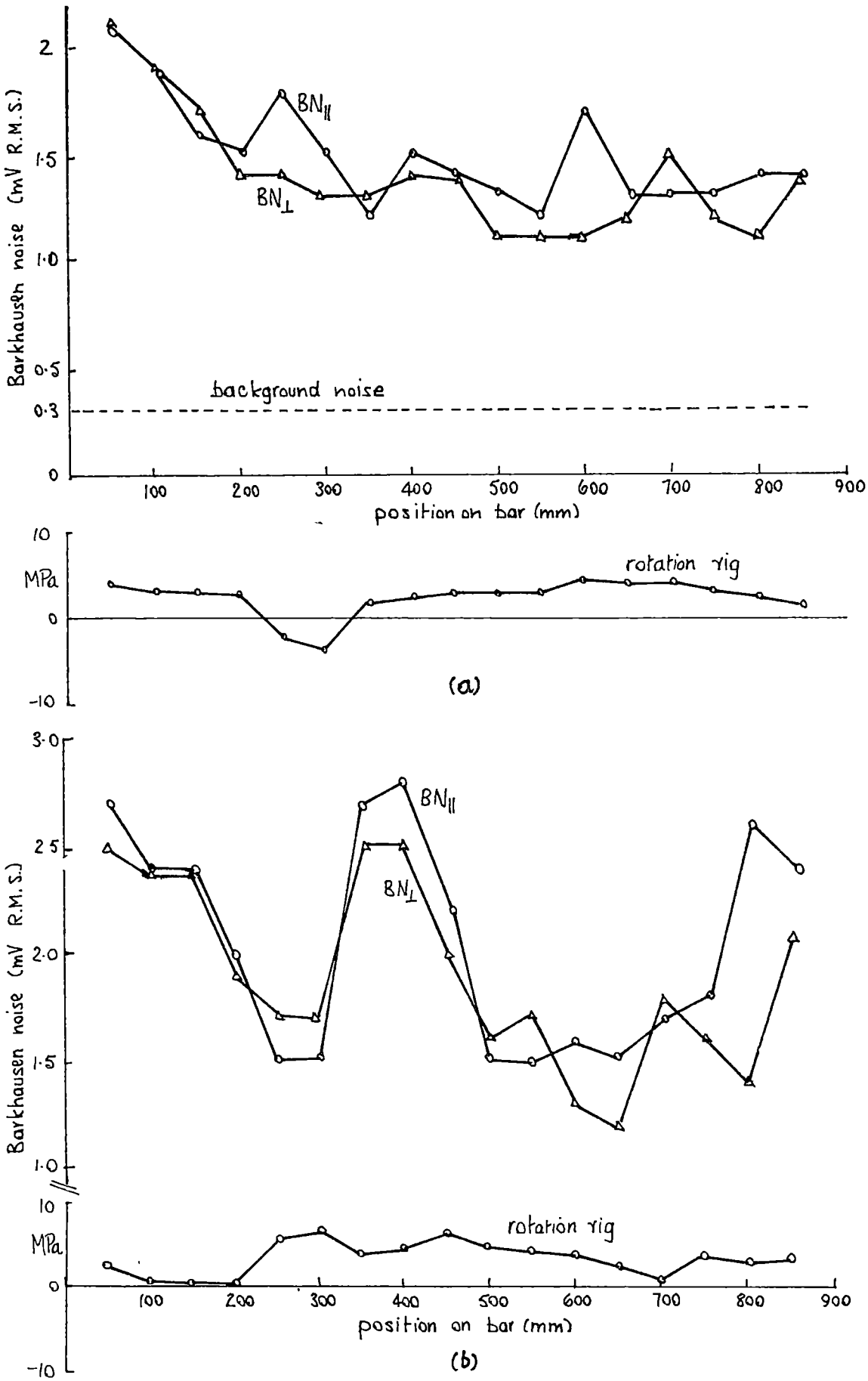

Figure 9.11 Scan along a 4"x1/2" annealed unloaded mild steel bar with a B.N. transducer ($BN_{\parallel}$ and $BN_{\perp}$), and with the rotation rig: (a) and (b) correspond to opposite faces of the bar. (See text for the relation between B.N. voltage and stress).

residual stress of the order of 100MPa; the $BN_{\perp}$ values vary similarly but according to figure 9.9 they should hardly change: clearly at odds with the R_v readings.

My opinion of these (admittedly superficial) Barkhausen noise measurements is that they are too sensitive to slight changes in, presumably, the structure or texture of the metal. They are also adversely affected by spurious electrical noise while the measurements are being made, and in general, they seem to be less use in determining the stress then is the rotation rig.

CHAPTER 10

INTRODUCTION TO PART III AND SUMMARY OF ITS CONTENTS

10.1 Magnetoelastic energy

The two phenomena of crystal anisotropy and magnetostriction are of dominant importance in determining how steel magnetises. Cullity gives a most lucid account of crystal anisotropy in chapter 7 of his book, and of magnetostriction - and the effect of stress - in chapter 8. There is therefore no point in repeating Cullity's material here. However, a simple example (from Cullity) can serve to illustrate, and generalise, the connection between stress and magnetisation. The concept is simple; the complications in practice are due to the (usually) unknown details of crystal structure such as grain shape, microstresses, and dislocations.

Consider a sphere of unit radius of a magnetic material that is isotropic (magnetically). Suppose it contains equal volumes of domains in all directions so that it is demagnetised overall. Let it then be magnetised to saturation M_s. Its change in length is λ_{si}, the saturation magnetostriction of an ideally demagnetised sample. If λ_{si} is positive, there is a contraction perpendicular to the direction of magnetisation of $\lambda_{si}/2$. It follows that its change in length at an angle θ to the magnetisation is

$$\lambda_\theta = 1.5\lambda_{si}(\cos^2\theta - 1/3)$$

This is illustrated in figure 10.1a.

Suppose now that the sphere be magnetised to saturation parallel to an applied (tensile) stress σ, and that then M_s is (somehow) rotated by θ. As it does so there is a contraction along the stress axis because λ_θ is less than λ_{si} (figure 10.1b). This contraction, in the presence of the tension, means that work is done on the material and so its internal (potential) energy will increase. This is called the magnetoelastic energy E_σ. For a small rotation of $d\theta$,

$dE_\sigma = -\sigma d\lambda$, and so

$$E_\sigma = \int_0^{E_\sigma} dE = -\int_{\lambda_{si}}^{\lambda_\theta} \sigma d\lambda$$

$$= -\sigma[\lambda_\theta - \lambda_{si}]$$

$$= -\sigma[1.5\lambda_{si}(\cos^2\theta - 1/3) - \lambda_{si}]$$

$$E_\sigma = 1.5\lambda_{si}\sigma\sin^2\theta$$

When M_s is parallel to σ, $\theta = 0°$ and so E_σ is zero (a minimum). When E_σ is normal to σ, $\theta = 90°$ and $E_\sigma = 1.5\lambda_{si}\sigma$ (its maximum). Since the potential energy will always try to be a minimum then the effect of applied tension with positive magnetostriction is to keep M_s in the direction of the tension. Notice that since E_σ contains the product of λ_{si} and σ, the effect of applied compression and negative magnetostriction is the same as that of tension and positive magnetostriction. Also, in this example the crystal anisotropy is absent; there is no preferred direction of magnetisation when the stress is zero. The equations for steel are more complicated.

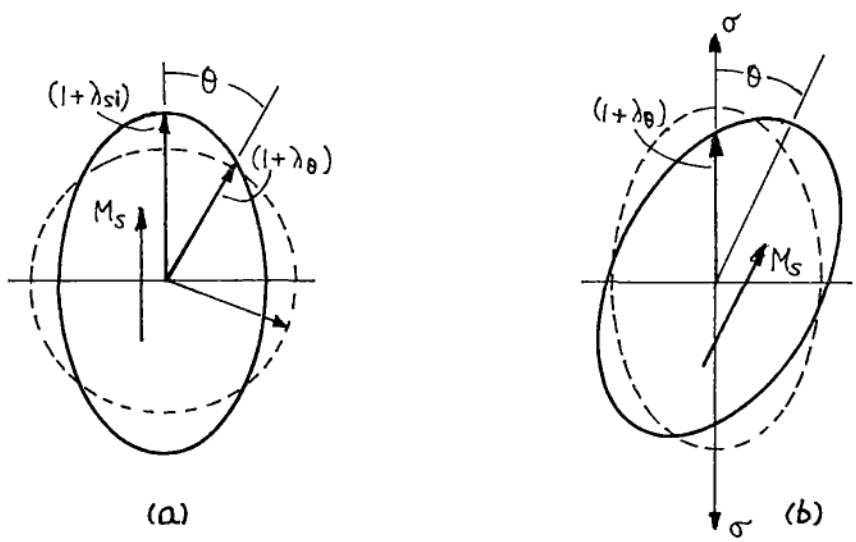

Figure 10.1 Isotropic magnetostriction, illustrating λ_{si} and λ_θ: (a) zero applied stress, (b) applied tension, [after Cullity, C2].

10.2 The three regions of the B vs. H curve

Figure 10.2 shows an initial B vs. H curve for annealed mild steel. The curve may be divided into three regions in which changes in magnetisation or flux density are assumed to occur by different processes. The division between the regions is indistinct, and although in general one process may predominate in its particular region the others are not excluded.

Region 1: low field strengths

This is known as the Rayleigh region. Changes in overall magnetisation occur by means of small, sometimes irreversible, movements of domain walls. The directions of intrinsic magnetisation of all the domains are along the <100> crystal axes, i.e. the "easy" directions of magnetisation. The upper limit of field for this region is usually a few times less than the coercive force.

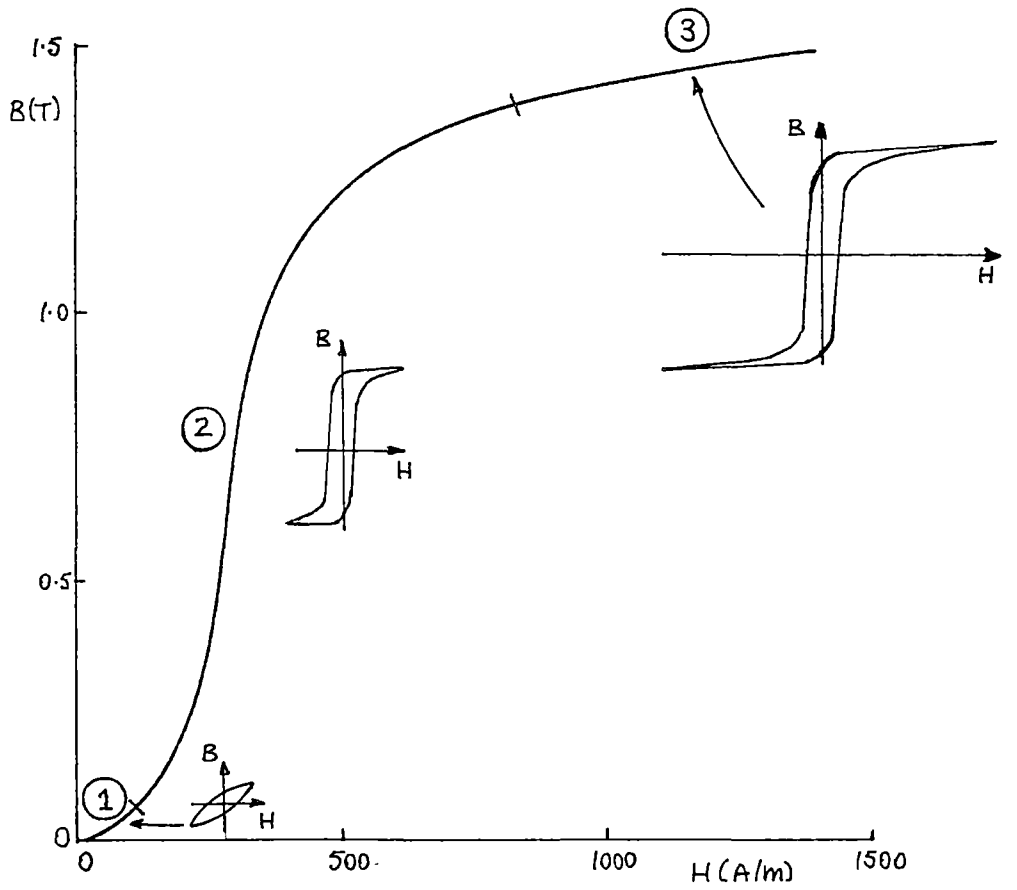

Figure 10.2 Initial magnetisation curve for mild steel with representative shapes of B vs. H loops for each of the three regions.

Region 2: moderate field strengths

Changes in magnetisation occur by means of large irreversible wall movements; domains that are in directions opposing the applied field may vanish. However the intrinsic magnetisation of domains is still predominantly along the crystal axes. At the top end of this region, perhaps around the kneepoint of the magnetisation curve, all domains are magnetised along crystal axes that are nearest to the direction of the applied field. (The kneepoint is defined, in a transformer design context, as the point on the curve where a 10% increase in B requires a 50% increase in H. It is used here merely as a convenient label for the indistinct transition between regions 2 and 3).

Region 3: high field strengths

Increase of overall magnetisation can only occur by rotation of the intrinsic magnetisation of the domains away from the easy axes and toward the direction of the applied field. Only small increases in overall magnetisation can occur as it tends towards the saturation value.

10.3 Rearrangement of domains, due to stress, for steel

What happens (in general) when both a moderate field and stress are applied to a material like steel, with a cubic structure and easy directions of magnetisation along the cube edges, is shown in figure 10.3. The square represents a single crystal. Figure 10.3a shows an ideally demagnetised state with all four possible directions occupying equal areas. Tension might move the domain pattern to (b). The 90° domains have shrunk at the expense of the 180° ones. Application of a field H results in some net magnetisation, as in (c), by means of relatively easy movement of 180° walls that does not increase the magnetoelastic energy.

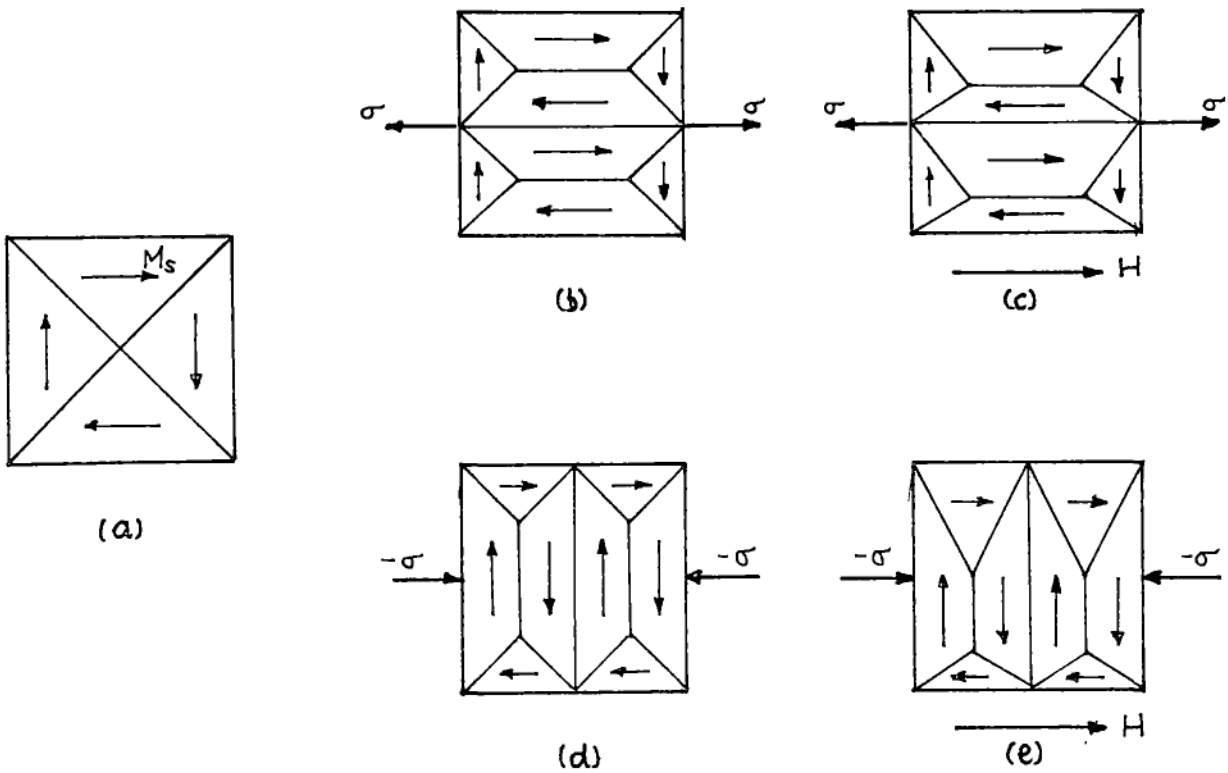

Figure 10.3 The effect of applied stress and field on the domain pattern of steel: two dimensional representation. (a) ideally demagnetised, (b) tension applied, (c) tension and field, (d) compression, (e) compression and field, [C2].

Starting again from (a), compression would favour the growth of 90° domains, as in (d). Application of a field then results in a smaller magnetisation (e) than in (c), since domain movement to increase the magnetisation also increases the magnetoelastic energy.

Summarising figure 10.3: stress alone can cause domain wall motion, but cannot, by virtue of its bi-directionality, cause overall magnetisation. Only an applied field can do this. However, stress can affect the amount of magnetisation resulting from an applied field.

10.4 Contents of Part III

The remaining chapters of part III review various magnetomechanical "models". Chapters 11 and 12 deal with models for low and high fields respectively; the theory for the latter seems substantially correct in that it

is supported by experiment. Chapter 13 deals with moderate fields, for which very little theory exists. Some theory is proposed here by the author. Chapters 14 and 15 present models or ideas that do not fall conveniently into the earlier categories, but that could be relevant and in any case provide food for thought. Chapter 14 is a summary of some work by V.B.Ginsburg. This is an ambitious attempt to predict the behaviour of a particular domain model over a wide range of applied fields and stresses. Chapter 15 covers three more models.

Note that my use of the word "theory" is perhaps a bit misleading, since what is different in each case is not the basic theory itself - that of magnetoelasticity - but the model to which the theory is applied. Different authors make different simplifications depending mainly on which energy components are ignored. The point is that the real situation inside a piece of steel, i.e. the crystal structure with its dislocations, non-magnetic inclusions, and meandering grain boundaries, is unknown and very complicated. Simplifications have to be made in order that the model be amenable to analysis, and the validity of these cannot be quantified.

CHAPTER 11

THE EFFECT OF STRESS AT LOW MAGNETIC FIELDS

An authoritative and comprehensive account of the magnetomechanical effect in the low field (or Rayleigh) region is given in a review paper by Birss [B9,1971]. An important part of it is the theory of W.F.Brown [B10,1949] in which the irreversible magnetic effects of stress are predicted quantitatively by means of Rayleigh's equations for the B vs. H loop, and the equivalence of applied stress and applied magnetic field. Brown's original presentation was for the three dimensional case in which he considered the movement of 15 possible types of domain that separate the 6 easy directions of magnetisation in an iron crystal. Because these concepts are important for an appreciation of some of the later theories, a simplified two dimensional version of Brown's theory is presented here.

11.1 Preliminary concepts

Rayleigh's equations for the B vs. H curve and loop

Rayleigh found by experiment that for many ferromagnetic materials in low magnetic fields the initial B vs. H curve follows the equation

$$B = \mu_1 H + vH^2$$

and that the B vs. H loop is made up of two parabolae

$$B = (\mu_i + vH_m) \pm v(H_m^2 - H^2)/2$$

(These are taken from Cullity's book [C2] with a slight alteration in notation. μ_i, the initial permeability, and v are called the Rayleigh constants). Figure 11.1 shows the lentil-shaped B vs. H loop that is typical of the Rayleigh region. The maximum field should be a few times less than the coercivity; according to Birss [B9] this limit can only be found by experiment.

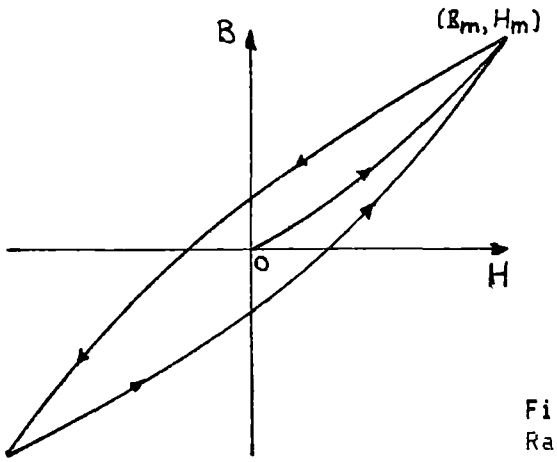

Figure 11.1 B vs. H loop for the Rayleigh region [from Cullity, C2].

Magnetic field as a pressure on domain walls

Consider a rectangular crystal of iron that is divided into four domains, as in figure 11.2a. Each domain is magnetised to saturation along a <100> axis. A is a 180° wall and B, C, D, and E are 90° walls.

Suppose a field H is applied. The walls will move to new positions so as to increase the overall (bulk) magnetisation in the direction of H, as in figure 11.2b. Look only at the motion of the 180° wall, ignoring the others for the moment, and assume it moves dx. Suppose also that H is established

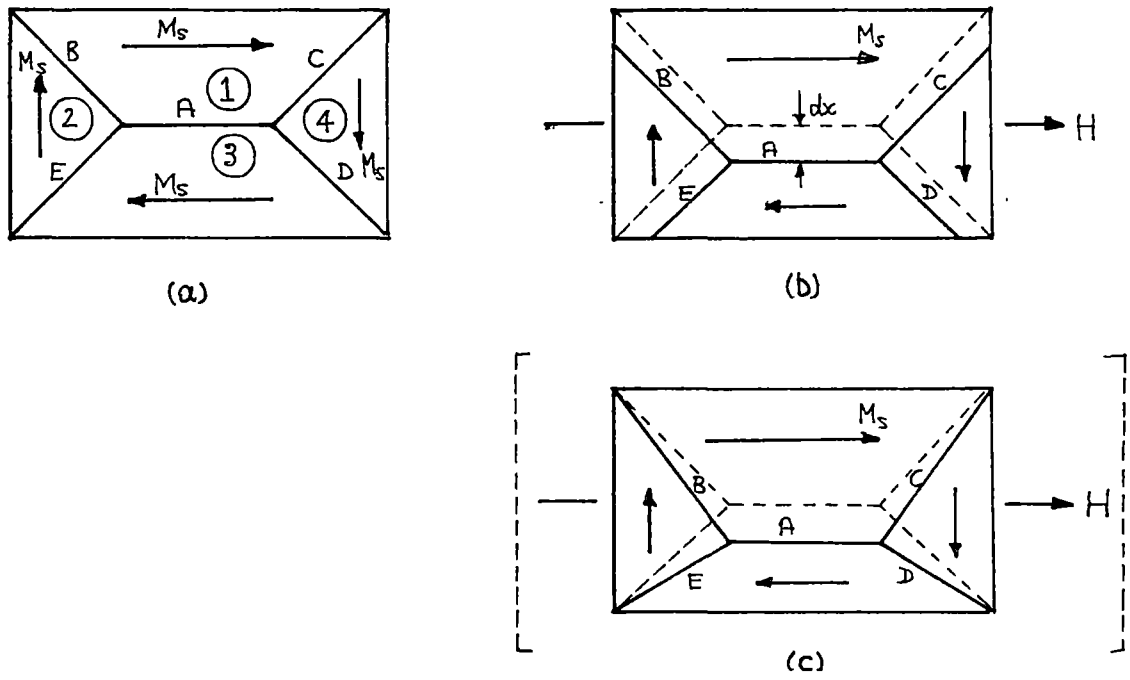

Figure 11.2 Magnetic field as a pressure on domain walls. Domains are labelled 1,2,3,4. Walls are labelled A,B,C,D,E. (a) demagnetised overall, (b) possible wall movements in an applied field H, (c) alternative wall movement to (b) [adapted from C2].

by increasing the current in a coil that surrounds the crystal. The energy supplied via the coil is

$$E = \int H.dB \ J/m^3$$

Since $B = \chi_0 H + M$,

$$E = \chi_0 \int H.dH + \int H.dM$$

(In this example M (= M_s) and H are parallel and so the vector notation can be dropped). The first term is the energy to produce the field H, and the second term is the increase in magnetisation due to motion of the 180° wall. This motion through a distance dx changes the magnetisation per unit area of wall perpendicular to dx by an amount

$$dE = [M_s H - (-M_s H)].dx$$

$$= 2M_s H.dx \ J/m^3$$

Since energy is force times distance and force per unit area is pressure P, then $P = 2M_s H \ N/m^2$.

In this case, the application of H is equivalent to a pressure, on the 180° wall, of $2M_s H$. If a 90° wall is considered to move dx (perpendicular to the wall) it is not hard to show that the change in energy of magnetization is $dE = M_s H.dx$ so that the application of H is equivalent to pressure $P = M_s H$ perpendicular to the wall.

(Figure 11.2b ignores the considerable demagnetising energy that would result from the new vertical boundaries to domain 1. Perhaps figure 11.2c is slightly more realistic, except that now the walls have moved away from the 45° directions. Both diagrams are of course highly idealised).

The overall movement of the walls will be such as to give minimum potential energy in the crystal. The volume of domain 1 will increase at the expense of domain 3, thus contributing a net decrease in energy. The volumes of domains 2 and 4 stay about constant, but in any case their contribution to the potential energy is always zero since M_s is perpendicular to H. Note that the walls C and E have moved in the same direction as the field, but walls B and D have moved in the opposite sense.

Stress as a pressure on domain walls

When an iron crystal is cooled through its Curie temperature it is magnetised spontaneously into domains, and each domain undergoes a small increase in length dl parallel to its magnetisation. The strain (= dl/l) is denoted by λ_{100} and is a characteristic constant for iron of about 20×10^{-6}. Suppose the crystal shown in figure 11.2a is compressed by a stress parallel to wall A and then cooled through its Curie point. Domains 1 and 3 expand against the compression, and so positive energy is supplied to them from whatever source is doing the compressing. The energy of the domain is changed by $E_\sigma = -\lambda_{100}(-\sigma)\cos^2\theta$, where θ is the angle between the directions of stress and magnetisation. Thus $E_\sigma = \lambda_{100}\sigma$ J/m^3, since $\theta = 0^\circ$ or 180°. E_σ is the magnetoelastic component of crystal energy. Now take the case of wall A, a 180° wall, moving dx when σ is present. Domain 1 changes its magnetoelastic energy by $\lambda_{100}\sigma\,dx$ and domain 3 by $-\lambda_{100}\sigma\,dx$ per unit area of wall so there is no overall change in energy. When a 90° wall moves dx, domain 1 changes its energy E_σ by $\lambda_{100}\sigma\,dx$ but domain 2 has no change in E_σ since $\theta = 90^\circ$. Thus only 90° wall motion can cause a change in E_σ. If we equate $\lambda_{100}\sigma dx = M_s H dx$, then $H = H_\sigma = \lambda_{100}\sigma/M_s$. H_σ is the equivalent field of the stress σ. The sign of this equivalent field must be chosen carefully, and this is dealt with in the next section.

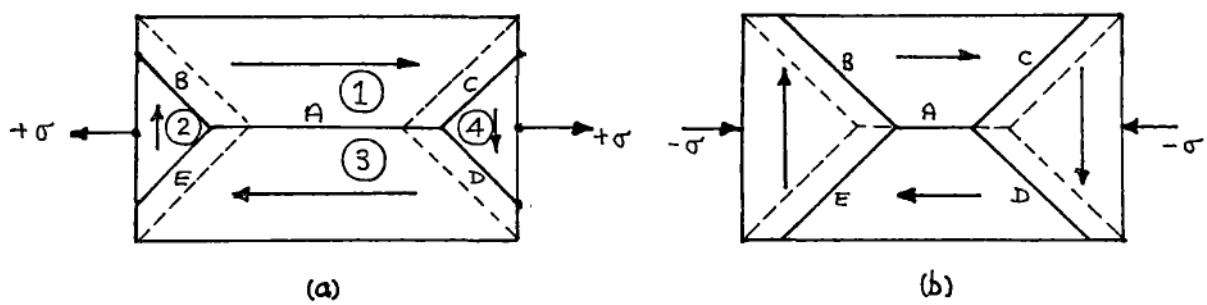

Figure 11.3 Stress as a pressure on domain walls. Domain wall movement for (a) applied tension, (b) compression [adapted from C2].

Wall motion when stress is applied

If the principle of minimum potential energy is used for a sample in zero field with a tensile stress ($+\sigma$) applied, it predicts that the walls will move to the new position shown in figure 11.3a. Walls B and C have moved in the same sense as they did when $\sigma = 0$ and H was applied along domain 1. Walls D and E have moved in the opposite sense. If a compressive stress is applied the walls move as in figure 11.3b. This time walls B and C move in the opposite sense to tension but walls D and E move in the same sense.

There are thus in our simple model two 90° walls (B and C) labelled by Birss as type (i) for which both field and a stress produce energy changes and motion of the same sign, and two 90° walls A and D labelled type (ii), for which the corresponding energy changes and motion are of opposite sign.

11.2 The theory of W.F. Brown

Brown considered the "processes"

(a) demagnetization in zero tension,

(b) application of field H,

(c) application of tension σ,

(d) removal of tension.

He assumed that the sample obeyed Rayleigh's laws and that the tension was equivalent to a fictitious field $\lambda_{100}\sigma/M_s$

The magnetization after (b) is

$$M(b) = \mu_i H + vH^2$$

For walls of type (i) the magnetization after steps (c) and (d) is

$$M(c) = \mu_i(H + \lambda_{100}\sigma/M_s) + v_1(H + \lambda_{100}\sigma/M_s)^2$$

$$M(d) = \mu_i H + v_1(H + \lambda_{100}\sigma/M_s) - 0.5v_1(\lambda_{100}\sigma/M_s)^2$$

v_1 differs from v to allow for movement of 90° walls instead of 180° walls. Birss sets out these, and corresponding values of magnetization for walls of type (ii) and 180° walls (for which the fictitious field H_σ is zero), and

there is no point in merely duplicating his work. Suffice to say that, for walls of type (i), (ii), and 180°, the changes in magnetization are shown in figures 11.4a-c. If one assumes that the areas of type (i) and type (ii) walls are equal, and averages the above effect over all crystal orientations in a randomly orientated polycrystalline sample, then the net effect is as shown in figure 11.4d. There remains an irreversible increase in magnetization on removal of the tension.

What is more significant is that the b, c, and d parts of the curve are an even function of σ: thus for compression the M vs. σ relation is the reflection in the M axis of the curve for tension. This is shown in figure 11.4e.

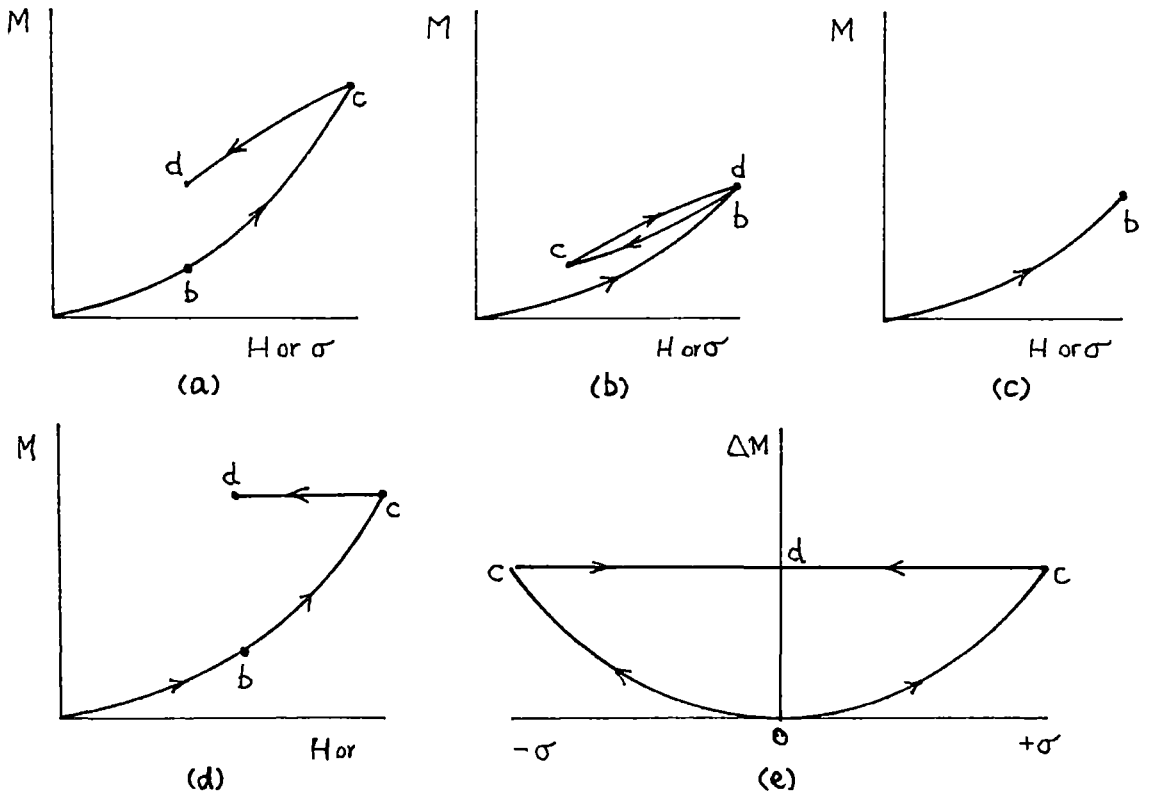

Figure 11.4 Change of magnetisation M due to an applied field and the application and removal of stress: (a) type (i) 90° walls, (b) type (ii) 90° walls, (c) 180° walls, (d) averaged for a polycrystalline sample, (e) theoretical change of magnetisation ΔM for application and then removal of tension or compression at constant field [from Birss, B9].

Experimental work by Faunce (unpublished) showed that Brown's theory is correct for soft magnetic materials for an applied field (step b) of less than $0.1H_c$ and for an equivalent stress field of the same order. By soft materials is meant, for example, iron in the annealed state with up to 0.1% carbon. Annealed iron with 0.1% carbon has $H_c \simeq 200A/m$, so the maximum field must be less than 20A/m, and H_σ about the same, implying a stress $\sigma < 0.1H_cM_s/\lambda_{100} = 2x10^6N/m^2$ or 2MPa. (This is a very small stress; by comparison the yield point for this material is of the order of 200MPa).

At higher fields there is inequality between the effects of tension and compression, as sketched in figure 11.5a for a field of 80A/m. For harder materials the equality between tension and compression does persist (of course H_c is higher; of the order of $10^3A/m$ for iron plus 0.2% carbon in the cold-worked state) but then the change in magnetization with σ is up to five times the predicted value (figure 11.5b: H=160A/m).

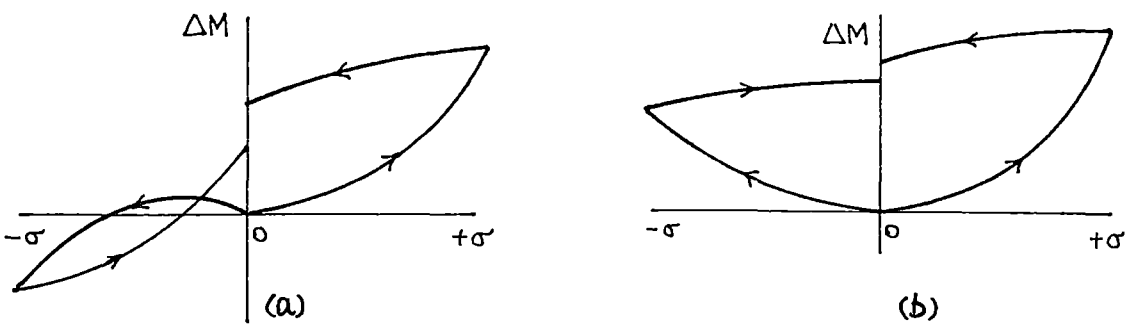

Figure 11.5 Measured change of magnetisation ΔM for application and then removal of stress at constant field: (a) annealed 0.1% carbon steel, (b) work-hardened 0.1% carbon steel [from Faunce, F2].

11.3 Shortcomings of Brown's theory

Birss gives a thorough discussion of these discrepancies. The following sub-sections outline what it is assumed happens inside the iron that makes Brown's theory inadequate. There are two more or less distinct phenomena at work.

(1) Large scale changes in domain pattern - soft magnetic materials

Work on 3% silicon Iron by (to name but one team amongst several) Corner and Mason [C5,1963; C6,1964] showed that over the range of compressive stress of -1 to -3kg/mm² there was a complete rearrangement of domains in a demagnetized specimen. Above σ = 3kg/mm² the domains were all turned at right angles to their original positions, and this new "texture" or preferred orientation will obviously alter the magnetization characteristics.

Brown's theory assumes that the domain walls are springy and can be moved slightly out of their equilibrium (i.e. zero applied stress and field) positions by either field or stress, but it excludes any large scale changes in the domain pattern. This accounts qualitatively for the asymmetry of figure 11.5a.

(2) "L'opposition" - hard magnetic materials

Magnetization changes occur by means of motion of domain walls. If we consider a 180° wall, and ignore the effect of any neighbouring 90° walls, the 180° wall can move a small distance dx without any change in the exchange, anisotropy, or magnetostrictive energy. Since the magnetization is irreversible (assuming that Rayleigh's laws hold) we must assume that the wall energy E_w (J/m² of wall area) depends on position x as suggested in figure 11.6. In zero field the wall sits at x = o, and as H = 0, $2M_sH = 0$. The pressure on a 180° wall has been shown to be $2M_sH$. Pressure can also be obtained from (energy per unit area)/(distance x) = dE_w/dx as $x \rightarrow 0$. Hence $dE_w/dx = 0$.

A small increase in H will cause the wall to move to P, and if H is reduced to zero the wall retraces to 0. IF H is increased further reversible wall motion continues until it reaches Q. The system is then unstable and the wall hops to point R where the energy gradient is the same as at Q. A reduction of H to zero now results in wall motion to S.

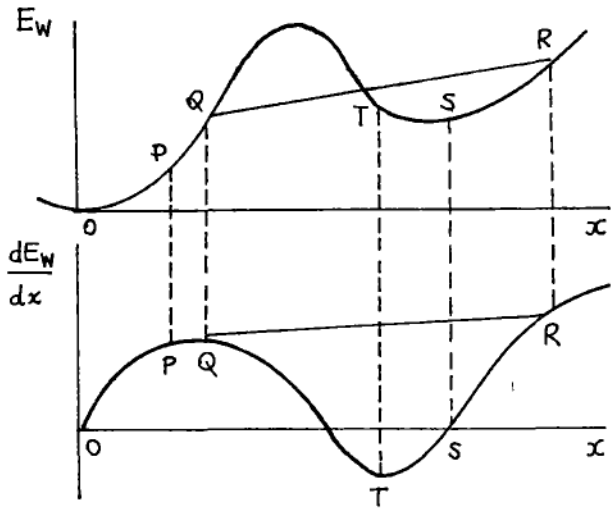

Figure 11.6 Wall energy E_w and pressure dE_w/dx on a domain wall, and their variation with position x [B9].

However, just what causes E_w to vary is not known. The most likely explanation is that differences in composition and inclusions (for example, cementite in alpha-iron) cause strains and hence fluctuations in the magnitude and direction of the magnetisation on a microscopic scale. Also, non-magnetic inclusions may cause "free" magnetic poles. The picture emerges of the domain wall snaking randomly about its average position as it moves. This is, superficially, the idea behind Néel's "disperse field theory"; mathematically it is very complicated.

Since the magnetoelastic energy must play a big part in the random variation of total energy, then applied stress could indirectly alter the variation of wall energy with position, dE_w/dx. There must be a balance between wall pressure ($2M_sH$) and this opposing energy gradient. Néel refers to dE_w/dx as "l'opposition", since a rather wider interpretation of this term than just "wall energy gradient" is required by the disperse field theory.

No doubt these rather vague ideas mean different things to anyone who thinks about them, but the end aim is that somehow the equivalent pressure of the fictitious stress field must be larger than the value given by $\lambda_{100}\sigma/M_s$. The harder the material the greater is the increase in effective value of $\lambda_{100}\sigma/M_s$, up to about five times for cold-worked 0.2% carbon steel.

11.4 Internal stress and initial permeability

The assumed interaction between residual micro-stresses and domain walls leads to the prediction of values of the initial permeability μ_i. Various models of how the stress might vary with the width of domains and with the domain wall pattern have been proposed, dating back to the early 1930s. All these lead to an equation for μ_i of the form $\mu_i = CM_s^2/(\lambda\sigma_r)$, where C is a constant, $\lambda = \lambda_{100}$ (for iron), and σ_r is the RMS amplitude of the residual stress. Since the latter can be related to the elastic modulus E by $\sigma_r = \lambda E$, then $\mu_i = CM_s^2/(\lambda^2 E)$. This expression is based on reversible domain wall movement. An account of this topic is in the book by Hoselitz [H1,1952], with a more up to date review in a thesis by Rusnak [R4,1967]. One of the conclusions is that wall motion is easiest, and hence μ_i highest, when the magnetostriction and stress gradients are low. Another is that the effect of an applied stress is predicted to be zero; for this reason these results are not of direct interest here, but they merit mention because Ginsburg's model (chapter 14) includes the interaction of wall energy and residual stress.

(In this context, Cullity [C2, page 331] gives a warning: "Some writers have assumed regular, periodic, stress variations, such as sinusoidal, and then made fairly elaborate calculations on the basis of such a model. The results of such calculations are no better than the assumed stress distribution, which is quite unreal").

CHAPTER 12

THE EFFECT OF STRESS AT HIGH MAGNETIC FIELDS

12.1 Magnetoelastic energy and domain rotation

The change of overall magnetisation at high magnetic fields occurs by means of rotation of domains away from the easy direction of magnetisation. (In contrast, at low fields, the domains always point in easy directions, and change of magnetisation is by small movements of domain walls). The expression for the magnetoelastic component of crystal energy for a cubic crystal is usually attributed to Becker and Döring [B11,1939]:

$$E_{me} = -1.5\sigma[\lambda_{100}f_1(\alpha_{ik}, \gamma_{ik}) + \lambda_{111}f_2(\alpha_{ik}, \gamma_{ik})] \quad (12.1)$$

in which f_1 and f_2 are homogeneous second order functions, α_{ik} and γ_{ik} (i,k = 1,2,3) are respectively the direction cosines of the magnetisation and stress directions relative to the <100> lattice directions, and λ_{100} and λ_{111} are the saturation magnetostrictions when the crystal is magnetised and the strains are measured in the <100> and <111> directions. (Becker and Döring's book is in german but a review article, in english, by Lee [L3,1955] is useful for the derivation of equation 12.1).

A polycrystalline material that has randomly orientated grains will appear isotropic, and in such a case the magnetoelastic energy expression reduces to the form

$$E_{me} = -1.5\lambda\sigma\cos^2\phi \quad (12.2)$$

where λ is an appropriate magnetostriction constant and ϕ is the angle between stress and magnetisation. (Equation 12.2 differs from that of chapter 10 only by a constant term). This leads to the prediction for polycrystalline nickel that permeability is inversely proportional to stress, which was found to be the case, experimentally, by Kersten in 1931. Details of this are in the book by Hoselitz.

The behaviour of iron or steel is more complicated than nickel, since (for iron) λ_{100} and λ_{111} are of opposite signs. However, good agreement between theory and experiment was obtained by, for example, Barton and Ionides [B3,1965]. Their experimental work on torquemeters is described in chapter 1, section 4; their theoretical predictions are described here in order to illustrate the technique of energy minimisation and also to show the various forms of the energy components.

12.2 Theoretical analysis of the torquemeter of Barton and Ionides

Magnetic energy components

Each crystal of steel is assumed to be a single domain magnetised to saturation. There is no change of wall position so wall energy need not be included. Demagnetising energy is also neglected. Three relevant sources of energy remain: the magnetoelastic field energy E_H, the anisotropy energy E_K, and the magnetoelastic energy E_σ.

$$E_H = -M_s H \cos\phi \ \text{J/m}^3$$

in which M_s is the saturation magnetisation, H is the applied field, and ϕ the angle between them.

$$E_K = K_1(\alpha_1^2\alpha_2^2 + \alpha_2^2\alpha_3^2 + \alpha_3^2\alpha_1^2) + K_2\alpha_1^2\alpha_2^2\alpha_3^2 \ \text{J/m}^3$$

in which K_1 and K_2 are anisotropy constants.

E_σ due to a compressive stress σ (taken as a *positive* number) is

$$E_\sigma = 1.5\sigma[\lambda_{100}(\alpha_1^2\gamma_1^2 + \alpha_2^2\gamma_2^2 + \alpha_3^2\gamma_3^2) + 2\lambda_{111}(\alpha_1\alpha_2\gamma_1\gamma_2 + \alpha_2\alpha_3\gamma_2\gamma_3 + \alpha_3\alpha_1\gamma_3\gamma_1)] \ \text{J/m}^3$$

Figure 12.1a shows the arrangement of torque tube, magnetising coil, and search coil. For pure torsion, equal tensile and compressive stresses are produced on the principal planes, as shown in figure 12.1b. The expression for E_σ then becomes

$$E = 1.5\sigma\{\lambda_{100}[\alpha_1^2(\gamma_1^2 - \epsilon_1^2) + \alpha_2^2(\gamma_2^2 - \epsilon_2^2) + \alpha_3^2(\gamma_3^2 - \epsilon_3^2)] + 2\lambda_{111}[\alpha_1\alpha_2(\gamma_1\gamma_2 - \epsilon_1\epsilon_2) + \alpha_2\alpha_3(\gamma_2\gamma_3 - \epsilon_2\epsilon_3) + \alpha_3\alpha_1(\gamma_3\gamma_1 - \epsilon_3\epsilon_1)]\} \qquad (12.3)$$

in which ϵ_1, ϵ_2, ϵ_3 are the direction cosines of the tensile stress relative to the crystal axes.

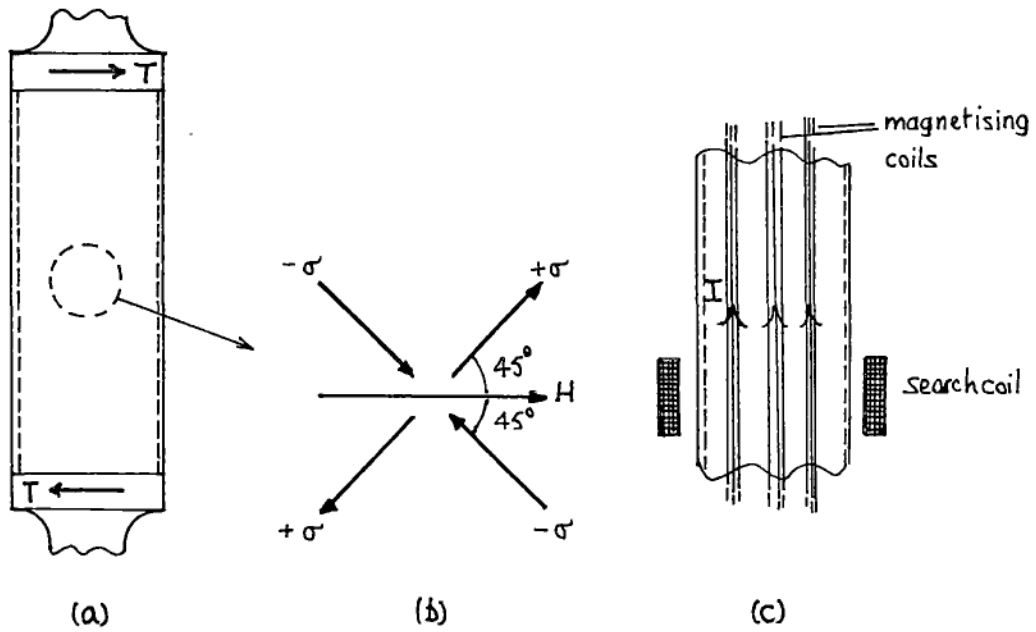

Figure 12.1 The torquemeter of Barton and Ionides [B2,B3]: (a) thin-walled rotating steel tube under torsion T, (b) directions of applied field H and principal stresses $\pm\sigma$, (c) magnetising coils rotating with the tube (supplied with AC current via slip rings), and the stationary search coil.

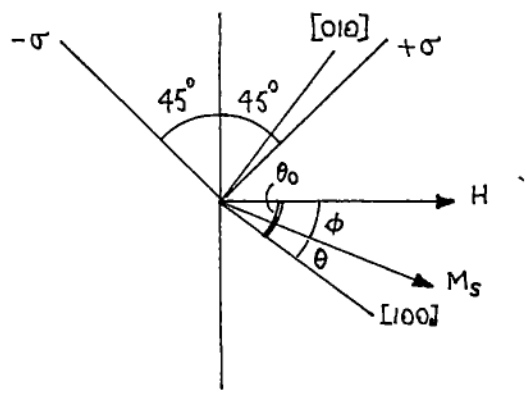

Figure 12.2 Vector quantities and angles used in computing the axial flux density in the torque tube [B3].

Energy expression for iron

Iron has cubic symmetry, the easy directions of magnetisation being the <100> axes. Figure 12.2 shows M_s assumed to be rotated away from the [100] axis by an angle θ. H is at an angle θ_0 to this axis. For this configuration the direction cosines are

$$\alpha_1 = \cos\theta \qquad \alpha_2 = \sin\theta \qquad \alpha_3 = 0$$

$$\gamma_1 = \cos(\theta_o+3\pi/4) \quad \gamma_2 = \sin(\theta_o+3\pi/4) \quad \gamma_3 = 0$$

$$\epsilon_1 = \cos(\theta_o+\pi/4) \quad \epsilon_2 = \sin(\theta_o+\pi/4) \quad \epsilon_3 = 0$$

$$\phi = \theta_o-\theta$$

Hence the total energy density E_T is

$$E_T = E_H + E_K + E_\sigma$$

$$= -M_s H\cos\phi + K_1(1-\cos4\theta)/8$$

$$+1.5\sigma(\lambda_{100}\cos2\theta\,\sin2\theta_o-\lambda_{111}\sin2\theta\,\cos2\theta_o) \qquad (12.4)$$

The magnetic constants needed in the calculations are K_1, K_2, λ_{100}, λ_{111}, and M_s. These vary with the material, its physical state (annealed, cold-worked, etc.), and its temperature. In the absence of data for steel of 0.15% carbon, data for iron was used; the values are given below for a temperature of 80°C (the A.C. magnetisation of 2400A/m R.M.S. heated the steel tube to about this temperature).

$$K_1 = 4.05\times10^{-4}\text{J/m}^3 \qquad K_2 = 2.2\times10^{-4}\text{J/m}^3$$

$$\lambda_{100} = 9.2\times10^{-6} \qquad \lambda_{111} = -15.2\times10^{-6}$$

$$M_s = 2.14\text{T}$$

Computational method: two dimensional case

The direction of M_s depends upon the orientation of the crystal and the externally applied constraints H and σ, and is such that the total magnetic energy of the crystal is a minimum. In theory the determination of this direction is simply a matter of location of this energy minimum; however, the expression for the energy is complicated and yields a number of minima, of which only the lowest is of interest. As this point cannot be located analytically, a numerical solution was used.

The search for the energy minimum should be carried out in three dimensions. This would lead to an enormous quantity of computation which, in view of the approximate nature of the problem, is not justified. The work was greatly reduced, with probably only a small decrease in accuracy,

by limiting crystal orientations to those having the vectors H, σ, and M_s in the same plane.

Specific values of H, σ, and crystal orientation were substituted into equation 12.4 and the direction of M_s for an energy minimum was found. The computation was repeated for a series of crystal orientations, and the behaviour of a randomly orientated material was found by averaging the results. The computations were then repeated at other stress levels until a complete picture of stress-dependent behaviour was established.

The axial flux density

Some results obtained by the search procedure are in figure 12.3, which shows for a single crystal of iron the rotation of M_s away from the easy direction by the action of the applied field and stress. A noteworthy point is the smallness of the rotation θ, the largest angle shown being 2.75°. Once θ is known, the axial magnetisation or flux density B_a can be calculated from $B_a = B_s \sin\theta$ ($B_s = M_s$). The resulting voltage induced in the circumferential search coil for $\theta_0 = 0°$, 45°, and for a random orientation of crystals, is shown in figure 12.4. The experimental result is also shown. The difference (about 10%) between the two lines for random orientation might be attributable to the neglect of the demagnetising component of energy, or to a non-random orientation of the crystals. In any event, the agreement is considered to be good for this type of analysis.

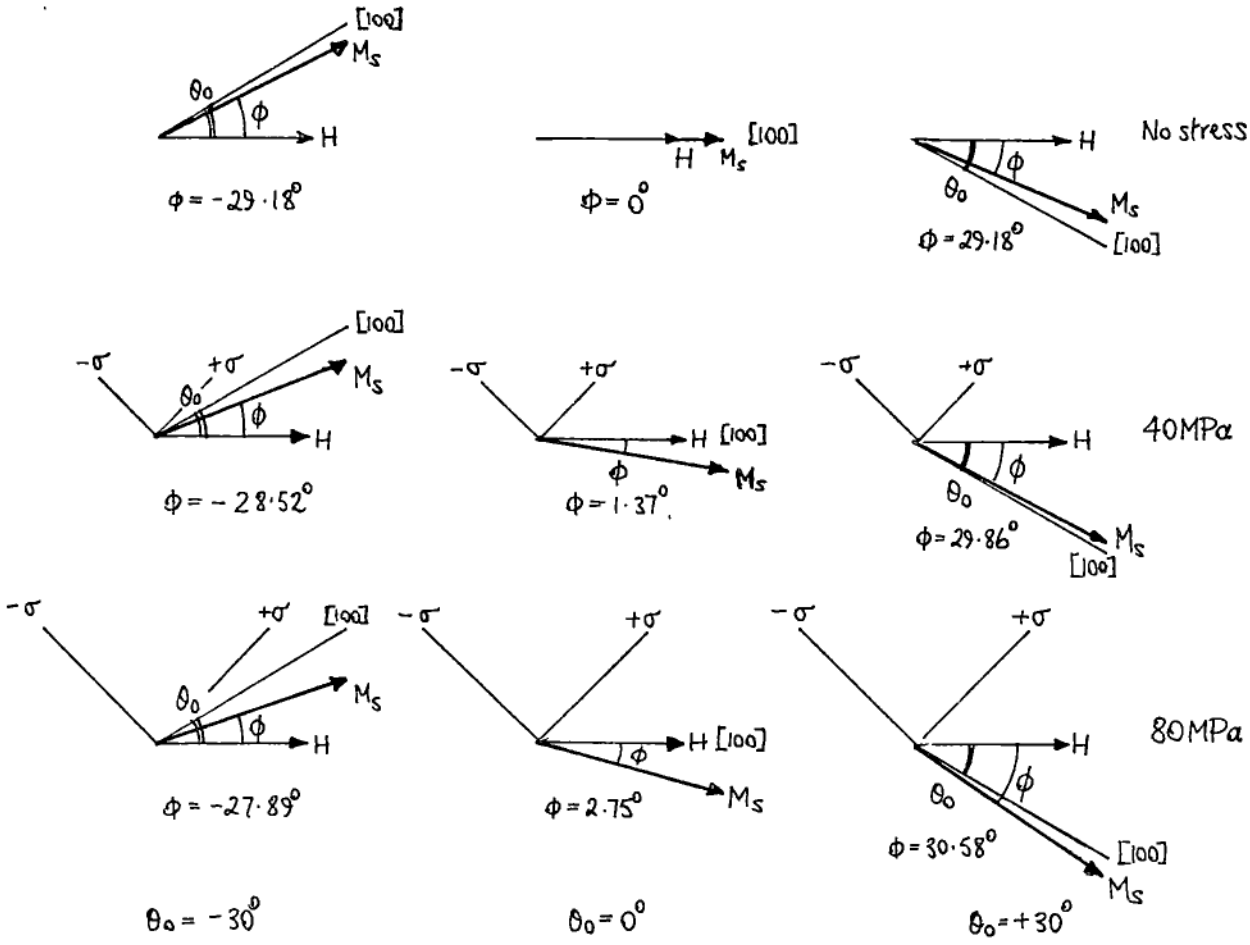

Figure 12.3 Vector diagrams showing the effect of stress on the orientation of M_s in a steel torque tube; RMS field strength 2400A/m, 60Hz, temperature 80°C [B3].

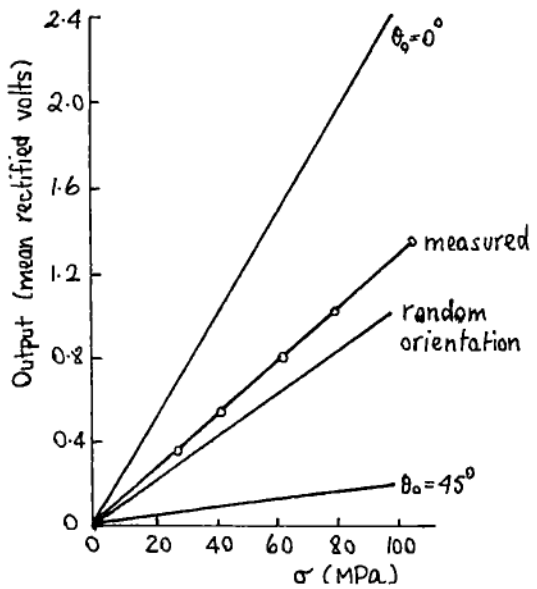

Figure 12.4 Search coil output voltage vs. applied stress for a tube of mean diameter 30mm, wall thickness 1.25mm, RMS magnetising force 2400A/m, 60Hz. The search coil has 300 turns. The computed results are from data for iron; the measured ones are for mild steel [B3].

CHAPTER 13

THE EFFECT OF STRESS ON THE MAGNETISATION OF STEEL AT MODERATE MAGNETIC FIELD STRENGTHS; ANALYSIS BY THE AUTHOR

13.1 Introduction

The rearrangement of domains in polycrystalline steel that results from compression parallel to the (original) direction of the 180° domains can be predicted quantitatively by assuming that the criterion for the rearrangement is that the sum of the magnetoelastic energy E_σ and magnetostatic energy E_H is thereby reduced. This was seen to happen in silicon steel by Corner and Mason [C5,1963; C6,1964] at stresses between -10 and -30MPa.

The analysis given in this chapter is an attempt to justify theoretically the results of measurements of B vs. H characteristics of stressed mild steel (given in chapter 8) by means of a minimisation of E_σ + E_H. The assumption is made that the domain motion is reversible, i.e. there is no hysteresis. Although this is only true in practice for anhysteretic (ideal) magnetising conditions, the measurements of chapter 8 show that the effects of stress are similar for both hysteretic and ideal conditions. It follows that the major discrepancies between theory and measurement do not result from the neglect of hysteresis.

(Although reference RL5 covers the essential part of this analysis for a two dimensional case, slightly more detail is given here for the former, and the three dimensional case is dealt with in the appendix).

13.2 Prediction of the magnetisation vs. stress curve for the two dimensional case

The magnetic state of the steel

The magnetic state of the steel is assumed to be at the transition from region 2 to region 3 of figure 10.2 - the kneepoint of the B vs. H curve. All domains are magnetized in the nearest easy direction of the applied field. In a two dimensional representation, figure 13.1a shows domains pointing in all possible directions for an ideally demagnetized condition (i.e. random orientation of domains). Figure 13.1b shows the range of directions when magnetized to the knee of the magnetisation curve.

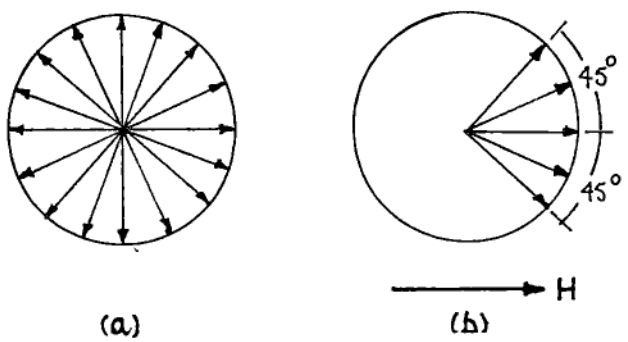

Figure 13.1 Two dimensional representation of domain directions in polycrystalline steel: (a) demagnetised with random orientations, (b) magnetised to the knee of the B vs. H curve.

Magnetic energy components

There are five of these that affect the domain pattern (but not equally at all field strengths): (1) magnetostatic, (2) magnetoelastic, (3) domain wall, (4) crystal anisotropy, (5) demagnetizing energy.

Assuming that the steel is already magnetised as in figure 13.1b, the domain walls have moved to their limits and component (3) can be ignored. Component (4) can be ignored because the field is not enough to rotate the direction away from the easy axes. Component (5), the demagnetising energy, is present, but is assumed constant. This assumption may involve considerable errors but it is very difficult to do anything else. It is discussed in section 13.4. Components (1) and (2) remain to be examined in more detail.

(1) Magnetostatic energy

$$E_H = - M_s \cos\theta \ J/m^3$$

where θ is the angle between the intrinsic magnetisation M_s and the applied field H.

(2) Magnetoelastic energy

$$E_\sigma = -1.5\lambda_{100}\sigma(\alpha_1^2\gamma_1^2 + \alpha_2^2\gamma_2^2 + \alpha_3^2\gamma_3^2)$$

$$-3\lambda_{111}\sigma(\alpha_1\alpha_2\gamma_1\gamma_2 + \alpha_2\alpha_3\gamma_2\gamma_3 + \alpha_3\alpha_1\gamma_3\gamma_1) \ J/m^3$$

where α_1 α_2 α_3 are the direction cosines of M_s relative to the crystal axes, and γ_1 γ_2 γ_3 are the direction cosines of stress σ relative to the crystal axes. λ_{100} and λ_{111} are the magnetostrictions along the <100> and <111> axes.

Range of domain directions for tensile stress perpendicular to the field

Suppose a domain is initially (for zero stress) along the +X crystal axis, at an angle θ to the field H. If a tensile stress (positive σ) is applied perpendicular to H, then, depending on the relative combined values of the two energy components (magnetostatic and magnetoelastic), the domain magnetisation might change to any of the other three directions, as shown in figure 13.2. The ±X and ±Y axes are all easy directions of magnetisation, and are in fact the crystal axes. The energies for the four directions are:-

+X: $-M_s H\cos\theta - 1.5\lambda_{100}\sigma\sin^2\theta$

+Y: $M_s H\sin\theta - 1.5\lambda_{100}\sigma\cos^2\theta$

-X: $M_s H\cos\theta - 1.5\lambda_{100}\sigma\sin^2\theta$

-Y: $-M_s H\sin\theta - 1.5\lambda_{100}\sigma\cos^2\theta$

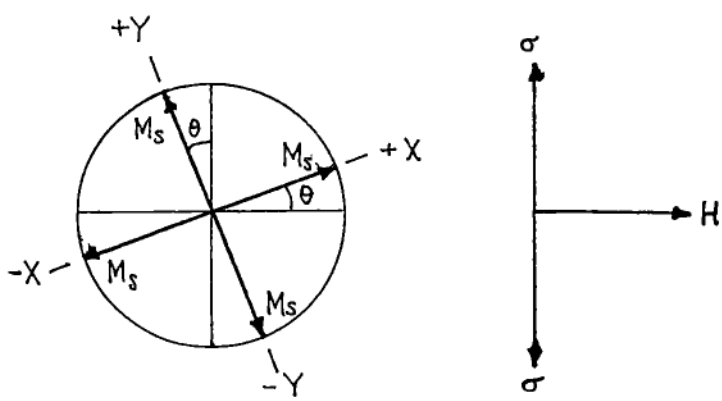

Figure 13.2 Four domain directions for a particular crystal orientation θ relative to the applied field H, with tensile stress σ perpendicular to the field.

The second term is always negative (λ_{100} is positive) and since $0<\theta<45^\circ$, the energies of the -X and +Y directions will always be more positive than the other two directions. Since the assumption is made that the domain direction will be such as to keep the energy to a minimum, then only the +X and -Y directions need to be considered. Similarly, for $-45^\circ<\theta<0^\circ$, only the +X and +Y directions need be considered. Hence for $-45^\circ<\theta<45^\circ$, domains can lie only in the first and fourth quadrants of figure 13.2.

Threshold stress to change domain direction for tensile stress perpendicular to the field

For $0^\circ<\theta<45^\circ$ the domain pointing along the +X axis in the absence of stress may change to point along the -Y axis when the stress is applied, if thereby the energy is lowered. Suppose that a fraction f (figure 13.3) of these domains are along the +X axis, and a fraction (1-f) are along the -Y axis; f takes the value 1 or 0. The total energy is

$$E_T = f(-M_sH\cos\theta - 1.5\lambda_{100}\sigma\sin^2\theta) + (1-f)(-M_sH\sin\theta - 1.5\lambda_{100}\sigma\cos^2\theta)$$

writing $M_sH = k$, $1.5\lambda_{100}\sigma = k'$, and rearranging gives

$$E_T = -f(k'\sin^2\theta - k'\cos^2\theta + k\cos\theta - k\sin\theta) - (k'\cos^2\theta + k\sin\theta)$$

The second term is independent of f and can be ignored. For minimum E_T, the first term, $f[k'\cos2\theta - k(\cos\theta - \sin\theta)]$, (re-written without the negative sign outside the square brackets) must be a minimum. If $k(\cos\theta - \sin\theta) > k'\cos2\theta$ the minimum is for $f = 1$, otherwise it occurs for $f = 0$.

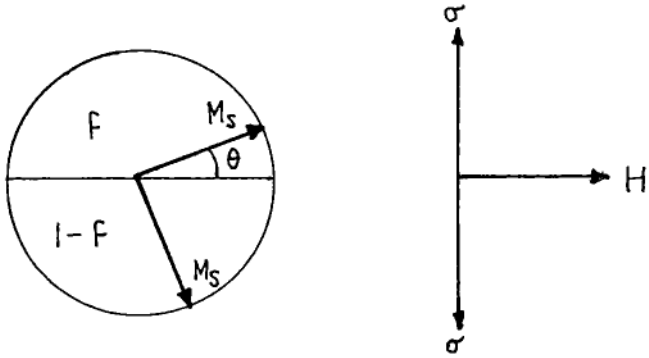

Figure 13.3 The two possible domain directions for consideration of minimum energy; tension perpendicular to field.

Putting in the values M_s = 2.16T, H = 900 A/m (about the kneepoint of the B vs. H curve), λ_{100} = 21x10^{-6}, and letting θ take values between 0° and 45° gives threshold values of stress that are summarised in figure 13.4a. The following table shows the threshold stresses in more detail. Because of the bi-directionality of stress, the results for $-45° < \theta < 0°$ are the same as those for $0° < \theta < 45°$.

θ°	k(cosθ-sinθ)	k'cos2θ	Threshold stress (MPa)
0	1.00k	1.00k	62
7.5	0.86k	0.96k'	55
15	0.71k	0.87k'	50
22.5	0.54k	0.71k'	47
30	0.37k	0.50k'	45
37.5	0.18k	0.26k'	44
41	0.10k	0.14k'	44
43	0.049k	0.069k'	44
45	0	0	44

One point to note is that as θ tends to 45° the two energy components both tend to zero and would be less effective in determining the threshold stress than when θ is nearer 0°.

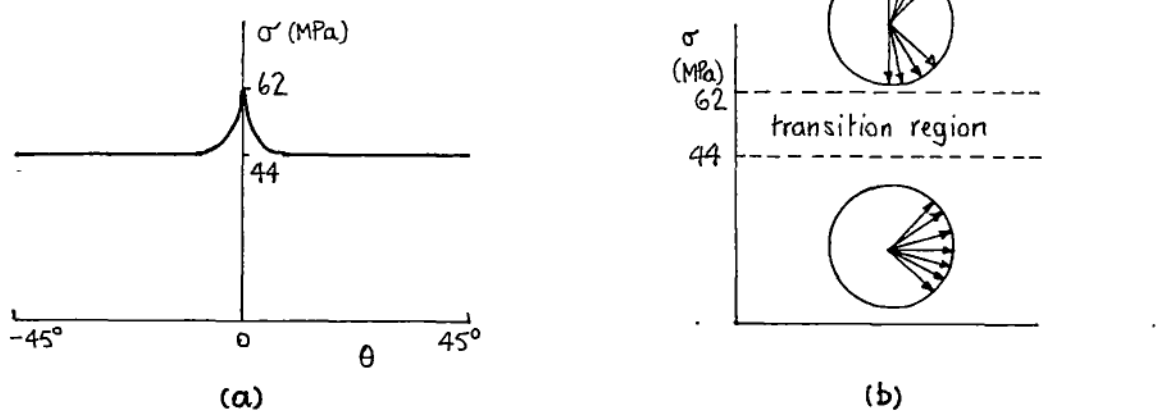

Figure 13.4 Stress limits for the two domain directions: (a) variation of threshold stress σ with θ, (b) range of domain directions for low and high stresses.

Figure 13.4b gives slightly different information: below 44MPa all domains in the steel are within ±45° of the direction of H, but above 62MPa they are all within the two octants -90° to -45° and 45° to 90°. In a transition region between these stresses, only some domains will have switched round.

Magnetisation for tensile stress perpendicular to the field

For σ<44MPa, the overall magnetisation M is the mean value of $M_s\cos\theta$ for domains distributed evenly between ±45°:

$$M = \frac{M_s}{\pi/2}\int_{-\pi/4}^{\pi/4}\cos\theta.d\theta = 0.90M_s$$

and for σ>62MPa,

$$M = \frac{M_s}{\pi/4}\int_{\pi/4}^{\pi/2}\cos\theta.d\theta = 0.53M_s$$

The graph of M/M_s vs. σ is shown in figure 13.5.

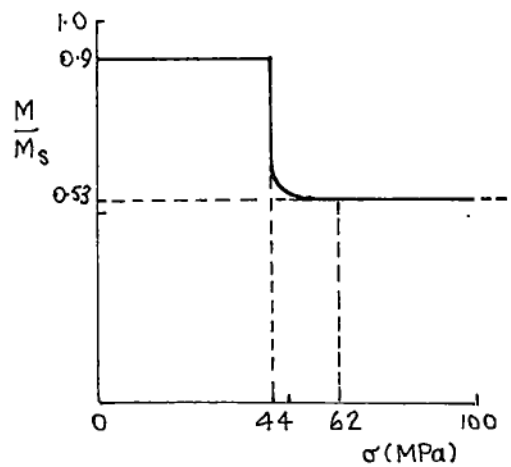

Figure 13.5 Magnetisation vs. stress σ for tension perpendicular to field.

Magnetisation for tensile stress parallel to the field

The steps of the last three subsections are followed. Figure 13.6a shows the two possible domain directions for tensile stress parallel to the field. The energy is

$$E_T = f[-k'\sin^2\theta - k\cos\theta] + (1-f)[-k'\cos^2\theta - k\sin\theta)]$$

$$= -f[k'(\cos^2\theta - \sin^2\theta) + k(\cos\theta - \sin\theta]$$

$$-[k'\sin^2\theta - k\sin\theta]$$

Again ignoring the second term, for minimum energy $f[k'\cos 2\theta + k(\cos\theta - \sin\theta]$ should be a minimum. For $0° < \theta < 45°$, the terms inside the square brackets are always positive, and so $f = 1$ for all values of k' and hence of tensile stress. There is no threshold stress; the domains always remain pointing in the nearest direction to the field and stress. Figure 13.6b shows the range of domain directions and figure 13.6c shows the resulting magnetisation vs. stress graph. Again, there is symmetry between $0° < \theta < 45°$ and $-45° < \theta < 0°$.

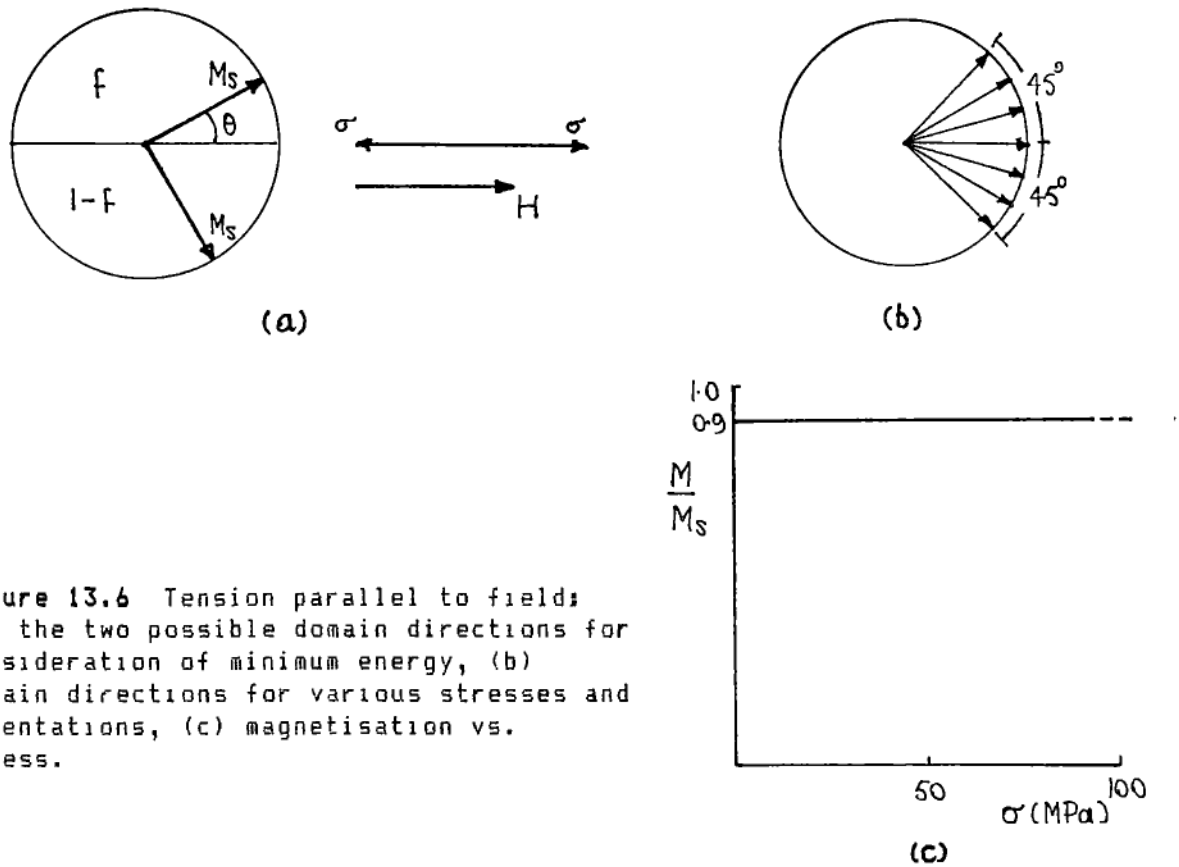

Figure 13.6 Tension parallel to field: (a) the two possible domain directions for consideration of minimum energy, (b) domain directions for various stresses and orientations, (c) magnetisation vs. stress.

Magnetisation for compressive stress

The only difference between these energy equations and those for tension is that now k' is negative. It turns out that:

(1) For compression parallel to the field, the energy equation is the same as tension parallel to the field but with k' negative. This equation can be rewritten

$$E_T = f[|k'|(\cos^2\theta - \sin^2\theta) - k(\cos\theta - \sin\theta)]$$

$$= [|k'|\sin 2\theta + k\sin\theta]$$

For minimum energy, $f[|k'|\cos 2\theta - k(\cos\theta - \sin\theta)]$ should be a minimum, which is the same as the condition for tension perpendicular to the field.

(2) For compression perpendicular to the field,

$$E_T = -f[|k'|\cos 2\theta + k(\cos\theta - \sin\theta)]$$

$$+ [|k'|\cos^2\theta - k\sin\theta]$$

For minimum energy , $-f[|k'|\cos 2\theta + k(\cos\theta - \sin\theta]$ must be a minimum, which is the same as for tensile stress parallel to the field. Figure 13.7 summarises the four cases.

Note that the threshold stress is directly proportional to the applied field. However, the field is restricted to a small range of values within which the steel is (originally, at zero stress) magnetised to its kneepoint.

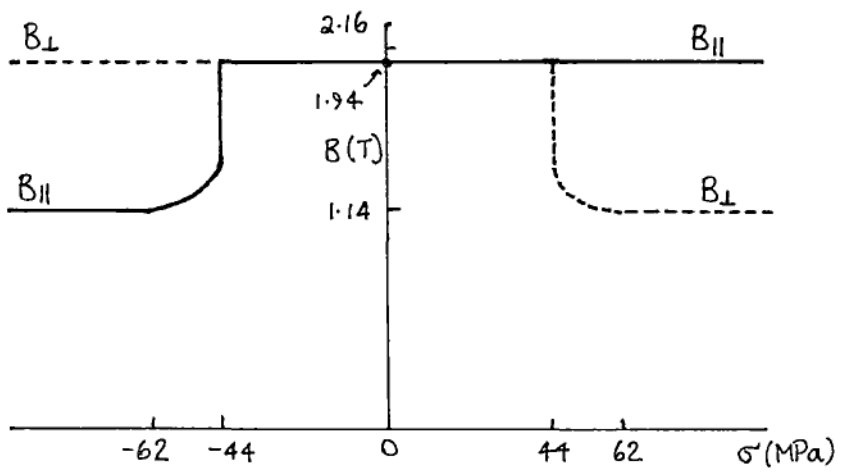

Figure 13.7 Theoretical magnetisation vs. stress curves for the two dimensional model.

13.3 Prediction of magnetisation vs. stress curve for the three dimensional case

This is more complicated than the two-dimensional case, and to save effort an exact analysis has not been attempted. Some simplifying assumptions have been made in the method of calculation that should not affect the result by more than a few per cent. Since (for reasons discussed

later) the error between theory and measurement is several tens of per cent, I think that approximations are justified.

The two cases to be dealt with are for stress parallel or perpendicular to the field. The former is the simpler analytically, as stress and field must be in the same direction; the shaded area of figure 13.8a shows the range of directions of H and σ that must be considered. The latter case is shown in figure 13.8b. Stress lies in any direction in the plane perpendicular to H, and so for every direction of H described by polar angles ϕ and θ, stress is described by angles ψ and η.

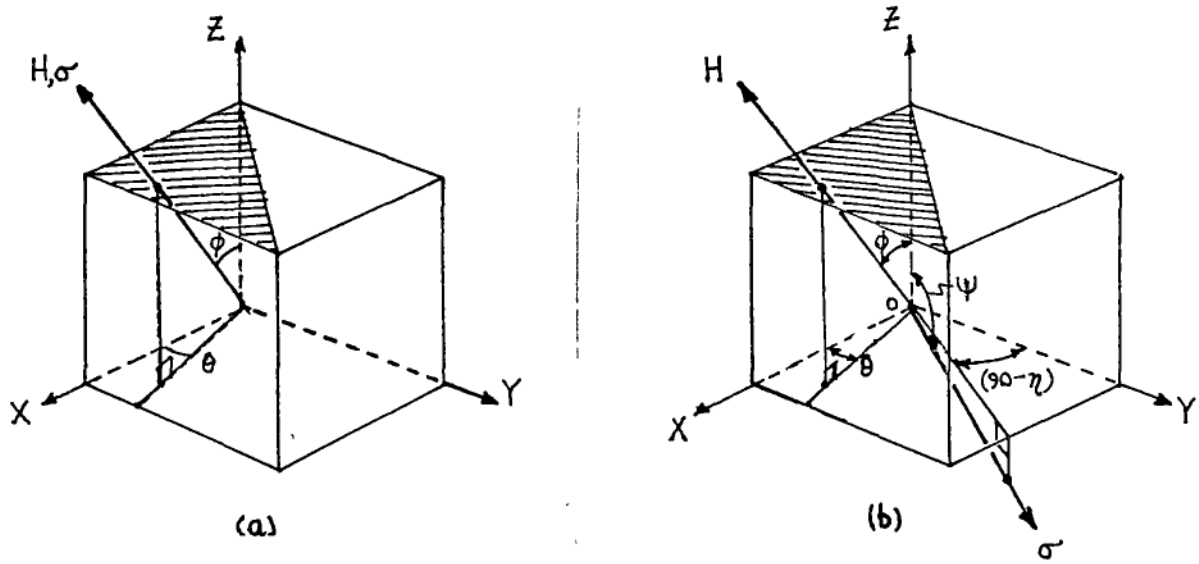

Figure 13.8 Range of directions of stress and field for the three dimensional model: (a) stress parallel to field, (b) stress perpendicular to field.

Appendix 1 deals in detail with the prediction of the M vs. σ graphs, but the results are somewhat inconclusive. The main problem is that the demagnetising energy for magnetisation in any direction other than in the plane of the steel is very large, and so in practice the three dimensional case is forced into the two dimensional case, and the resulting M vs. σ graph might be rather like that of figure 13.7.

13.4 Discussion

Detailed explanations as to why the theoretical result differs from the experimental one are not given. Since what is perhaps the most important secondary characteristic - the initial magnetisation curve - cannot be predicted with an error of less than about 10%, then any attempt to get a reasonably close fit when the effect of stress is included would seem to be pointless. Assumptions such as (initial) uniform distribution of domains, that at 900A/m all domain walls have moved to their limits, that the residual stresses and demagnetising effects of grain boundaries and inclusions are zero, that anisotropy energy can be ignored, are just not true and involve unknown errors.

The only claim that can be made is that the two dimensional theory agrees qualitatively with experiment in these respects:

(1) Tension parallel to the field has very little effect on flux density, whereas tension perpendicular to the field considerably reduces the flux density.

(2) There is a form of symmetry between tension and compression: perpendicular compression is equivalent to parallel tension, and parallel compression is equivalent to perpendicular tension.

A puzzling feature of the experimental results is the continuing decrease of flux density as stress increases (the theory predicts that it should decrease to a constant value of about half the zero-stress value). This is particularly marked at the lower field strengths: at 400A/m (figure 8.6c) 120MPa of tension perpendicular to the field reduces the flux density by a factor of about six.

Figure 13.2 shows four possible directions of a domain for an orientation θ of the crystal axes relative to the applied field. In order for the magnetisation to decrease by a factor of six, the domains in the +X and -Y directions must shrink and those in the -X and +Y directions must grow. The energies for each direction are given in section 13.2, which

shows that the -X and +Y domains have higher magnetostatic energies than the +X and -Y ones (but the same magnetoelastic energies). Thus by this argument the effect of the applied stress cannot reduce the magnetisation by a factor of six. Clearly there are other effects to be taken into account. One possibility, that of reverse domain formation, is discussed in section 2 of chapter 15.

CHAPTER 14

THE ALL-FIELD DOMAIN MODEL OF V.B.GINSBURG

14.1 The domain-pair model and its energy components

Figure 14.1 shows the basic "building block". A polycrystalline ferromagnetic consists of a large number of these blocks orientated randomly. Each block consists of two anti-parallel domains, labelled B_s' and B_s'', magnetized to saturation B_s. The block has these features:-

(1) The thickness of the boundary between the two domains is negligible in comparison with dimension b.

(2) The boundary is plain and parallel to the face of the block.

(3) There are no non-magnetic inclusions.

(4) There is an internal stress σ_r that originated during the formation of the material. It has a very strong effect on the direction of magnetisation compared with the influence of magnetostrictive, crystalline, and shape anisotropies.

(5) σ_r is parallel to the domain-pair boundary when magnetostriction $\lambda_s > 0$ and normal to it for $\lambda_s < 0$.

(6) The absolute value of σ_r varies with position x.

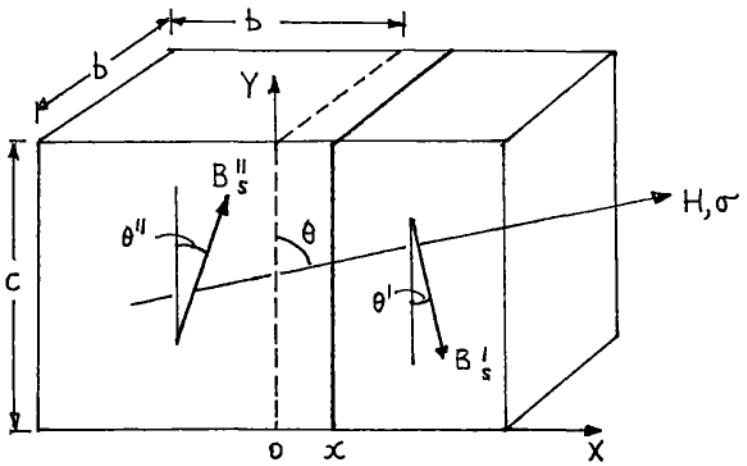

Figure 14.1 The basic building block: a domain pair (after Ginsburg [G4]).

(7) The directions of applied field H and applied stress σ are the same.

(8) No domain-pair affects any others.

The two domains may alter so that their potential energy is always a minimum. Their shape may change by wall motion, and the directions of magnetization may rotate, when a field or a stress (or both) is applied.

The five components of energy are listed below. (The equation numbers with a G refer to the same equations in the original paper. I have also kept to the same notation most of the time, except where an obviously unconventional symbol was used in the original).

(1) Internal stress

$$\left.\begin{aligned} e_r' &= E_r(1-u)\sin^2\theta' \\ e_r'' &= E_r(1+u)\sin^2\theta'' \\ e_r &= e_r' + e_r'' \end{aligned}\right\} \qquad \text{(G1)}$$

where $u = x/b$.

(2) Magnetostatic energy due to the applied field

$$\left.\begin{aligned} e_h' &= B_sH(1-u)\cos(\theta+\theta') \\ e_h'' &= B_sH(1+u)\cos(\theta-\theta'') \\ e_h &= e_h'' + e_h'' \end{aligned}\right\} \qquad \text{(G2)}$$

(3) Magnetoelastic energy due to applied stress

$$\left.\begin{aligned} e_\sigma' &= 1.5\lambda_s\sigma(1-u)\sin^2(\theta+\theta') \\ e_\sigma'' &= 1.5\lambda_s\sigma(1+u)\sin^2(\theta-\theta'') \\ e_\sigma &= e_\sigma' + e_\sigma'' \end{aligned}\right\} \qquad \text{(G3)}$$

(4) Variation of energy due to the fluctuation of internal stress and the displacement of the domain wall.

$$e_u = e_u' + e_u'' = E_u\sin^2\pi u \qquad \text{(G4)}$$

where $E_u \propto \Delta\sigma_r$, the maximum variation of σ_r.

(5) Demagnetising energy

$$e_m = e_m' + e_m'' = E_mu^2\cos^2\bar{\theta} \qquad \text{(G5)}$$

where $\bar{\theta} = (\theta'+\theta'')/2$

14.2 Energy equations

The total potential energy of the domain-pair is

$e_t = e_r + e_h + e_\sigma + e_u + e_m$

When $H = \sigma = 0$, $\theta' = \theta'' = u = 0$. When H and σ are non-zero the directions of B's and B"s and the wall position u change so that e_t is still a minimum. This condition can be put mathematically as

$$\frac{de_t}{d\theta'} = 0, \quad \frac{de_t}{d\theta''} = 0, \quad \frac{de_t}{du} = 0 \qquad \text{(G6)}$$

Substituting from equations G1-G5 into G6 and doing the differentiations gives

$de_t/d\theta' = 0$:

$$\frac{HB_s}{E_r} = \frac{(1-u)\sin 2\theta' + s(1-u)\sin 2(\theta+\theta') - 0.5u^2(E_m/E_r)\sin 2\bar{\theta}}{(1-u)\sin(\theta+\theta')} \qquad \text{(G7)}$$

$de_t/d\theta'' = 0$:

$$\frac{HB_s}{E_r} = \frac{(1+u)\sin 2\theta'' - s(1+u)\sin 2(\theta-\theta'') - 0.5u^2(E_m/E_r)\sin 2\bar{\theta}}{(1+u)\sin(\theta-\theta'')} \qquad \text{(G8)}$$

$de_t/du = 0$:

$$\frac{HB_s}{E_r} = \frac{\pi(E_u/E_r)\sin 2\pi u + 2(E_m/E_r)u\cos^2\bar{\theta} + (\sin^2\theta'' - \sin^2\theta')}{\cos(\theta+\theta') + \cos(\theta-\theta'')}$$

$$- \frac{s[\sin^2(\theta+\theta') - \sin^2(\theta-\theta'')]}{\cos(\theta+\theta') + \cos(\theta-\theta'')} \qquad \text{(G9)}$$

where $s = \sigma/\sigma_r$, the per unit stress.

Equations G7, G8, and G9 can be used to calculate θ', θ'', and u if values of e, H, σ, σ_r, B_s, E_u, E_r, E_m, and E_σ are known.

The resulting flux density B is the sum of the components of B_s' and B_s'' in the direction of H:

$$B = B_s(1+u)\cos(\theta-\theta'') - B_s(1-u)\cos(\theta+\theta'') \qquad \text{(G10)}$$

Equations G7, G8, G9 are complicated non-linear functions of θ', θ'', and u. They could be solved by, for example, the Newton-Raphson method, but

since there are three independent variables (θ, H, σ) plus the energy coefficients E_u, E_r, E_m, (that are not known numerically) the number of solutions would be enormous and not much help. Ginsburg instead looks at the effect of firstly domain rotation only, then domain wall movement only, and finally both together.

14.3 Domain rotation

If the domain walls do not move, u = 0. Equation G9 is neglected and equation G7 and G8 become

$$\frac{HB_s}{E_r} = \frac{\sin 2\theta' + s.\sin 2(\theta+\theta')}{\sin(\theta+\theta')} \qquad \text{(G12)}$$

$$\frac{HB_s}{E_r} = \frac{\sin 2\theta'' - s.\sin 2(\theta-\theta'')}{\sin(\theta-\theta'')} \qquad \text{(G13)}$$

Equation G12 relates the rotation of domain B_s' by an angle θ' to the applied field H and per unit stress s. Equation G13 does the same for domain B''_s, and is independent of G12.

Effect of varying H only (s = 0)

Equations G12 and G13 can be simplified even more by assuming that s = 0. Then

$$\frac{HB_s}{E_r} = \frac{\sin 2\theta'}{\sin(\theta+\theta')} \qquad \text{(G12a)}$$

$$\frac{HB_s}{E_r} = \frac{\sin 2\theta''}{\sin(\theta-\theta'')} \qquad \text{(G13a)}$$

H is the independent variable, but rather than solve for θ' and θ'', given H, it is easier to take various values of θ' and θ'' and calculate the corresponding values of H. The resulting flux density B in the direction of H is given by equation G10.

Figure 14.2 shows the resulting initial magnetization curves and the B vs. H loop for $\theta = 45°$. It is useful to look at what happens in detail, and see how both reversible and irreversible rotations occur.

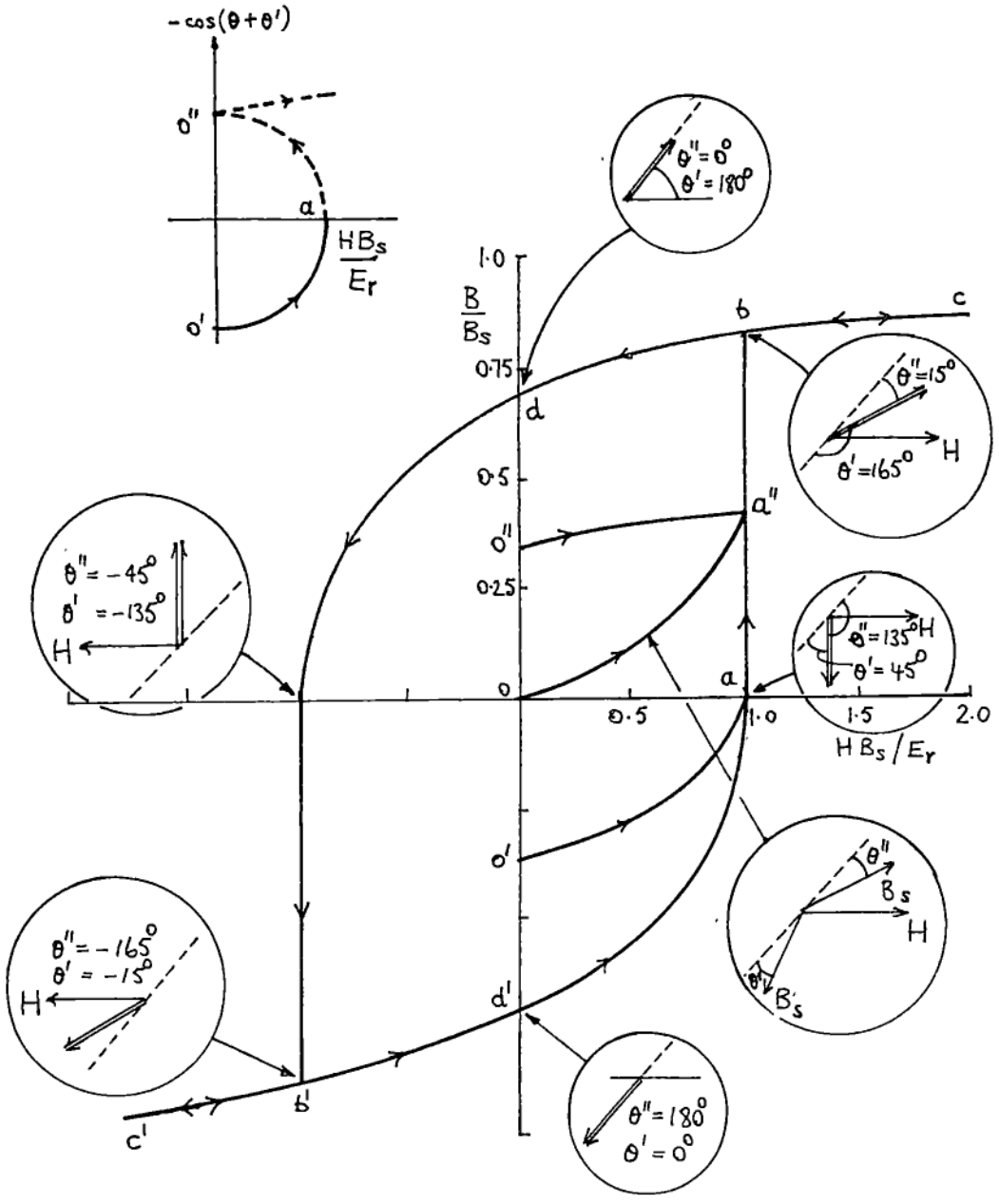

Figure 14.2 Theoretical B vs. H curve and loops for a domain pair with zero stress and the applied field at θ=45° to the domain pair axis.

Start at H = 0 with θ' = θ''= 0. Then B = B_s(cos45° - cos45°) = 0 and the two domains have equal and opposite flux density: points O' and O'' in figure 14.2. The net flux density is B = 0, i.e. the magnetization curve starts at the origin O. As H increases domain B_s' follows the lower curve O'a until point a where θ' = 45° and HB_s/E_r = 1.0. B_s'' follows the upper curve O''a'' to a point a'' where θ'' = 15° and HB_s/E_r = 1.0. If θ' were to go past 45°, HB_s/E_r would start to decrease, as the sketch inset in figure 14.2 shows. Since HB_s/E_r is required to be greater than 1.0, θ' must rotate suddenly and irreversibly (i.e. flip over) from 45° to 165°.

The two domains are now in the same direction, each produces a flux density of $0.866B_s$, and have in effect become one domain. The flux density jumps to point b. Further increase in H slowly increases B as the single domain rotates reversibly towards point c.

From now on the two domains always stay together as one. Reduction of H results in reversible rotation from c to d where $H = 0$, $\theta'' = 0°$, and $\theta' = 180°$.

As H goes negative the flip-over occurs at a' where $HB_s/E_r = 1.0$ and $\theta'' = -45°$, $\theta' = -135°$. The (now) single domain rotates by 120° to a point b' where $\theta'' = -165°$ and $\theta' = -15°$. For values of HB_s/E_r beyond -1.0 reversible rotation occurs to c'. Increase of HB_s/E_r retraces the path from c' to d' and finally back to a'. The B vs. H loop has now been traversed once.

The succeeding figures 14.3a-c are for $s = 0$ and $\theta = 30°$, 60°, and 75°. When $\theta = 0°$ the B vs. H loop is square (only irreversible rotation occurs), whereas $\theta = 90°$ gives a straight line through the origin (only reversible rotation occurs).

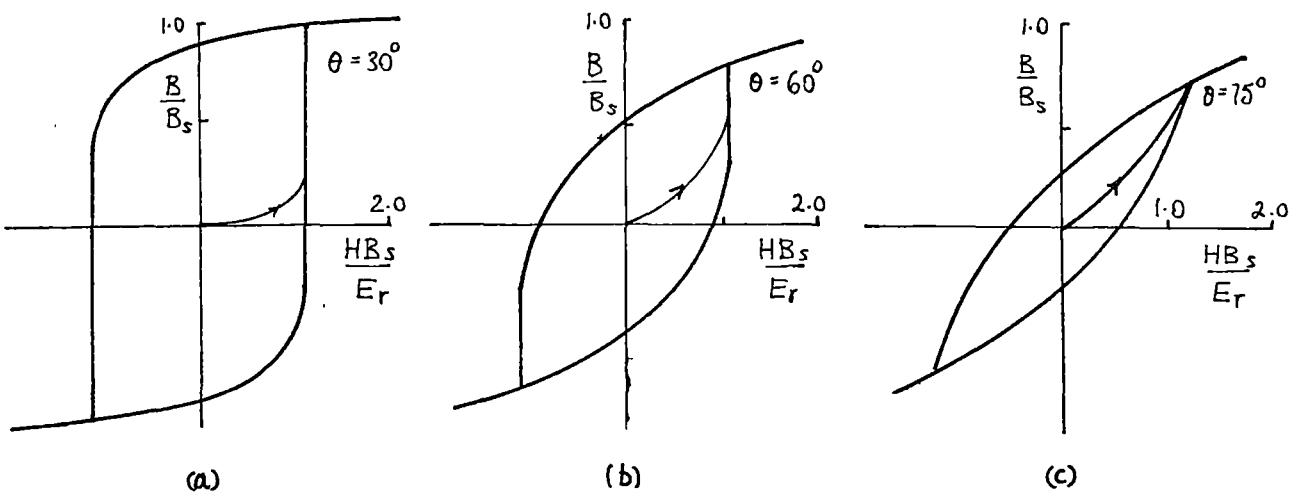

Figure 14.3 B vs. H curve and loop for per unit stress s=0 and θ=(a) 30°, (b) 60°, (c) 75°. Rotation only.

The B vs. H loop of a polycrystalline substance made up of domains at all angles θ would be an average of all these shapes of B vs. H loop. Later on in his paper, Ginsburg states that instead of averaging over all values of θ (by integration) the average of a few discrete values such as 0°, 15°, 30°, 45°, 60°, 75°, 90° give a result that is in error by less than 1%.

The effect of varying s as well as H

The starting equations are G12 and G13. Figures 14.4a and b show the B vs. H loop for θ = 45° and s = ±0.2, ±0.4. Tension increases B (for a given H) and compression decreases it, by equal factors. Figure 14.4c shows the B vs. H loop for θ = 75° and s = ±0.4. Again tension increases B, compression decreases it, by equal factors.

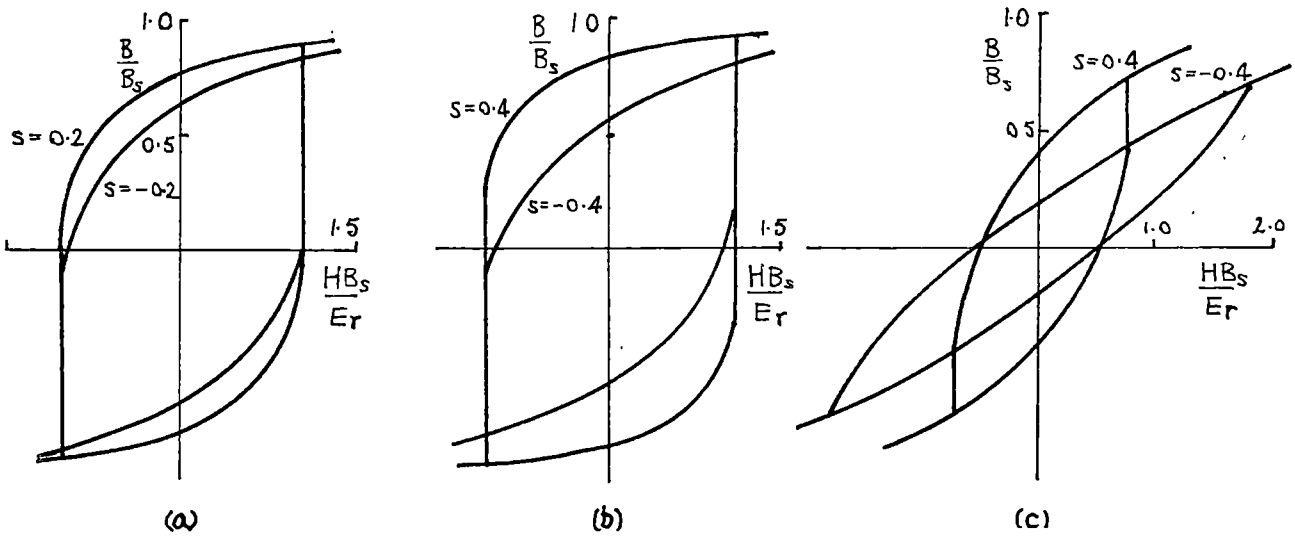

Figure 14.4 B vs. H loops for (a) θ=45° and s=±0.2, (b) θ=45°, s=±0.4, (c) θ=75°, s=±0.4. Rotation only.

The Stoner-Wohlfarth model

When s = 0 (zero applied stress) and the two domains have also combined into a single one, Ginsburg's result is the same as that of Stoner and Wohlfarth [S6,1948]. They dealt with one domain in the shape of a prolate spheroid that has an anisotropy energy

$$e_a = K_1 \sin^2 \theta \quad (K_1 \equiv E_r)$$

and a magnetostatic energy of

$$e_h = -HM_s\cos(\theta-\theta'') \quad (M_s \equiv B_s)$$

Thus $e_t = e_a + e_h$

$$= K_1\sin^2\theta'' - HM_s\cos(\theta-\theta'')$$

The equilibrium position of M_s is given by

$$de_t/d\theta'' = 0 = 2K_1\sin\theta''\cos\theta'' - HM_s\sin(\theta-\theta'')$$

i.e. $$\frac{HM_s}{K_1} = \frac{\sin 2\theta''}{\sin(\theta-\theta'')}$$

which is the same as G13a.

Stoner and Wohlfarth also calculated the B vs. H loop of an assembly of such domains with their axes randomly orientated. One stipulation is that the domains do not interact, i.e. the external field of each does not have an effect on any of the others. Cullity states (p387) that this is a serious limitation and that the interaction of the domains has not in fact been dealt with theoretically.

14.4 Domain wall movement

In this case θ' and θ'' are kept at zero and so only equation G9 is used which simplifies to

$$\frac{HB_s}{E_r} = \frac{(\pi E_u/E_r)\sin 2\pi u + 2E_m u/E_r}{2\cos\theta} \qquad \text{(G18)}$$

Dividing each side by E_u gives

$$\frac{HB_s}{E_u} = \frac{\pi\sin 2\pi u + 2E_m u/E_u}{2\cos\theta} \qquad \text{(G18a)}$$

E_r, the component of energy due to internal stress, does not appear and, as will be shown, the ratio E_m/E_u (demagnetising energy / wall energy) now influences the shape of the B vs. H loop. The value of θ does not alter the shape of the loop but merely the scale of one axis relative to the other.

Figures 14.5a-c show the B vs. H loops predicted from equation G18a for $\theta = 45°$ and for E_m/E_u = 10, 3, and 1. Flux density is proportional to $u\cos\theta$.

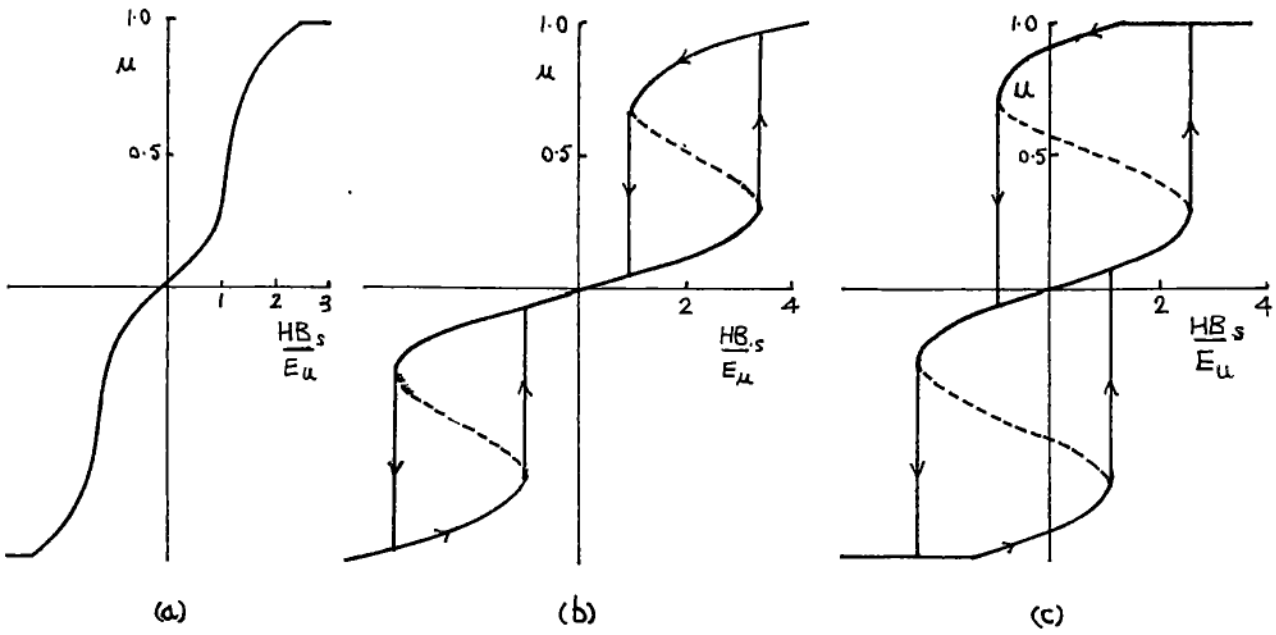

Figure 14.5 B vs. H loops for $\theta = 45°$ and for E_m/E_u = (a) 10, (b) 3, (c) 1. Wall movement only.

When E_m/E_u = 10 only reversible wall movement occurs and so there is no hysteresis. E_m/E_u = 10 implies $E_m >> E_u$, i.e. the demagnetising energy E_m is much greater than the energy E_u associated with the fluctuation of internal stress and wall movement. $E_m/E_u = \pi^2$ is the changeover point where irreversible wall movement starts.

When E_m/E_u = 3 there are two hysteresis loops, separated by a reversible part that goes through the origin. This kind of behaviour is actually shown by some ferromagnetics, e.g. Perminvar, and is known as a constricted B vs. H loop. The dashed line shows the theoretical path of equation G18a. The vertical part represents a wall jump from u = 0.3 to u = 0.7 in this instance.

14.5 Combined rotation and wall movement

Figures 14.6a-c show B vs. H loops corresponding to those of figure 14.5 but averaged over all domain orientations and allowing for domain rotation and wall movement. (These are from the solution of equations G7 - G10). Ginsburg describes these as follows:-

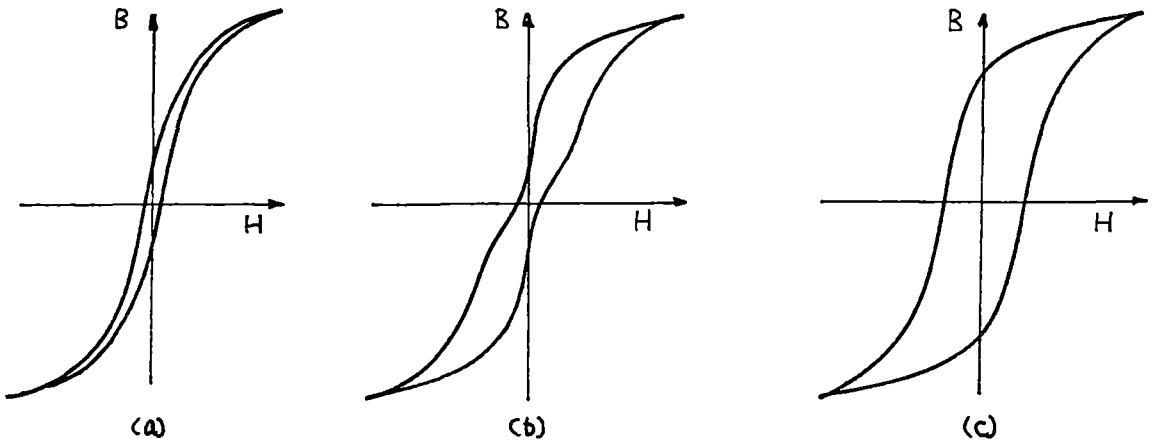

Figure 14.6 B vs. H loops averaged for all domain orientations, allowing for rotation and wall movement. E_m/E_u= (a) 10, (b) 3, (c) 1. Zero stress [64].

Magnetic materials with narrow hysteresis loops

($E_m/E_u > \pi^2$, figure 14.6a).

"In these materials, irreversible boundary displacement does not occur and reversible boundary displacement plays a major role during magnetization and demagnetization. In this case the hysteresis loop depends only on irreversible domain rotation."

Magnetic materials with constricted hysteresis loops

($2.144 < E_m/E_u < \pi^2$, figure 14.6b).

"In these materials irreversible boundary displacements occur during magnetization, demagnetization, and remagnetization. After demagnetization the boundaries return to the initial positions and the hysteresis loop depends only on irreversible domain rotation."

Ordinary soft-magnetic materials

($0 < E_m/E_u < 2.144$, figure 14.6c).

"In these materials irreversible boundary displacements occur during magnetization and remagnetization. Unlike the previous case, after irreversible displacement, some domain zones which are magnetized opposite

to the magnetization field are retained as the magnetic field is decreased to zero. Therefore, the hysteresis loop depends on both irreversible domain rotation and irreversible boundary displacement."

The effects of applied stress on polycrystalline materials are summed up in figure 14.7, which shows loops for the constant conditions $E_m/E_u = 1$ and $E_m/E_r = 0.1$, and for (a) tension (b) zero stress, and (c) compression.

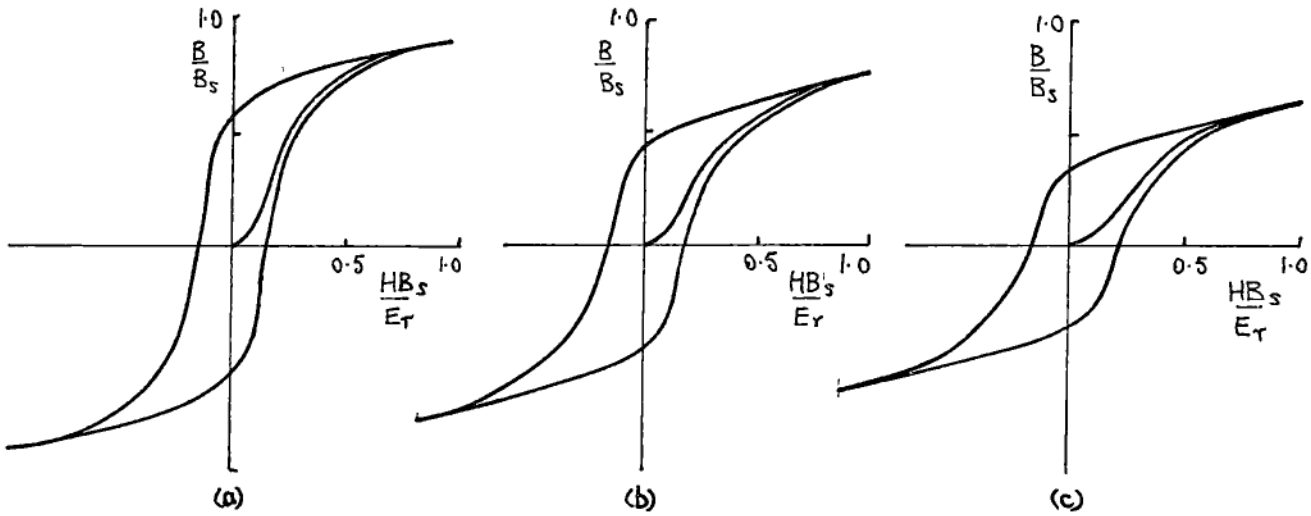

Figure 14.7 B vs. H curves and loop when $E_m/E_u=1$, $E_m/E_r=0.1$ for (a) per unit tension s = +0.5, (b) zero stress, (c) per unit compression s = -0.5 [G4].

14.6 Comments and discussion on Ginsburg's model

Internal stress σ_r

Ginsburg calculates this to be about 50MPa from a value he states for the magnetoelastic sensitivity (possibly obtained from a book he wrote on magnetoelastic transducers, published in Moscow in 1970, in Russian). The form of the internal stress component of energy is

$$e_r' = E_r(1-u)\sin^2\theta' \ J/m^3$$

$$e_r'' = E_r(1-u)\sin^2\theta''$$

where $E_r = 1.5\lambda_s\sigma_r$

These are the same form as the anisotropy energy for a uniaxial crystal [C2]:

$$E_a = K_0 + K_1\sin^2\theta'' + K_2\sin^4\theta'' + \ldots$$

For cobalt, $K_1 = 4.5\times10^5 J/m^3$, $K_2 = 1.5\times10^5 J/m^3$, $\lambda_s = 1.1\times10^{-4}$. Hence, neglecting K_2, $\sigma_r = K_1/1.5\lambda_s = 2.7\times10^9 N/m^2$ or 2700MPa.

An important question is: is E_r the same as the anisotropy energy? If it is not, no other author I know of mentions it. If it is, why doesn't Ginsburg call it the anisotropy energy? Since all his results and predictions involve the ratio of applied stress to internal stress, it is essential to know just what is meant by σ_r.

Wall boundary or internal stress energy

$$e_u = e_u' + e_u'' = E_u\sin^2\pi u \qquad (G4)$$

in which $E_u \propto \Delta\sigma_r$, the maximum variation of the internal stress whose mean value is σ_r. Ginsburg assumes that this stress varies sinusoidally:

$$\sigma_r = \Delta\sigma_r\cos2\pi u$$

Cullity (p328) states that,

(1) if there is no spatial variation of internal stress (so that $\sigma_r = 0$) then

$$\gamma_w = 2K_1 d$$

where γ_w = wall energy, K_1 = the first anisotropy constant, and d = wall thickness.

(2) If $\sigma_r \neq 0$, then

$$\gamma_w = 2d(K_1+K_\sigma)$$

in which K_σ is a stress anisotropy constant.

i.e. $\gamma_w = 2d(K_1 - 1.5\lambda_{100}\sigma_r\cos2\pi u)$

The negative sign is chosen so that at u = 0 and u = 1 the potential energy is a minimum, which is where the walls are stable. Since $\cos2\pi u = 1-2\sin^2\pi u$,

$$\gamma_w(u) = 6d\lambda_{100}\Delta\sigma_r\sin^2\pi u$$
$$= E_u\sin^2\pi u$$

as in equation G4 above.

There are many approximations in this and I am unsure of their reliability or limitations. Ginsburg refers to a soviet book by Vonsovsky and Shur (in Russian) and also to Becker and Döring's classic book of 1939, "Ferromagnetismus" (in German).

Demagnetizing energy e_m

$e_m = e_m' + e_m'' = E_m u^2 \cos^2 \bar{\theta}$ (G5)

This equation is derived from a paper by Rhodes and Rowland [R5,1954]. The following notes are from their paper.

For uniformly magnetized ferromagnetics (this applies strictly only to ellipsoids of revolution) the demagnetizing energy is given by $0.5 N_d B_s^2/\mu_o$ J/m³. N_d is the demagnetising factor and can be calculated accurately for ellipsoids from the magnetic field equations. For the special case of a sphere, which is an ellipsoid with equal length axes, $N_d = 4\pi/3$ and so $e_m = 2\pi B_s^2/3\mu_o$.

Rhodes and Rowland do not use this method of calculation; instead they obtain the equivalent charged surfaces of the rectangular domains and calculate for a single cubic domain $e_m = 2\pi B_s^2/3\mu_o$, which is the same as for a sphere.

For two domains magnetised in opposite direction which is the Ginsburg model with $\theta' = \theta'' = 0$, e_m is given by the curves in figure 14.8a. When $\theta' = \theta'' = 0$ Ginsburg's formula is $e_m = E_m u^2$, i.e. he ignores the component of e_m that does not depend on u and then states that the remaining curve is parabolic. This is not obvious, nor does it follow from any of the series expansions that Rhodes and Rowland give for their rather complicated functions that have to be evaluated to get the graphs of e_m vs. u.

Rhodes and Rowland also state that if the directions of magnetization are not parallel to one side of the block (but are both the same) then the

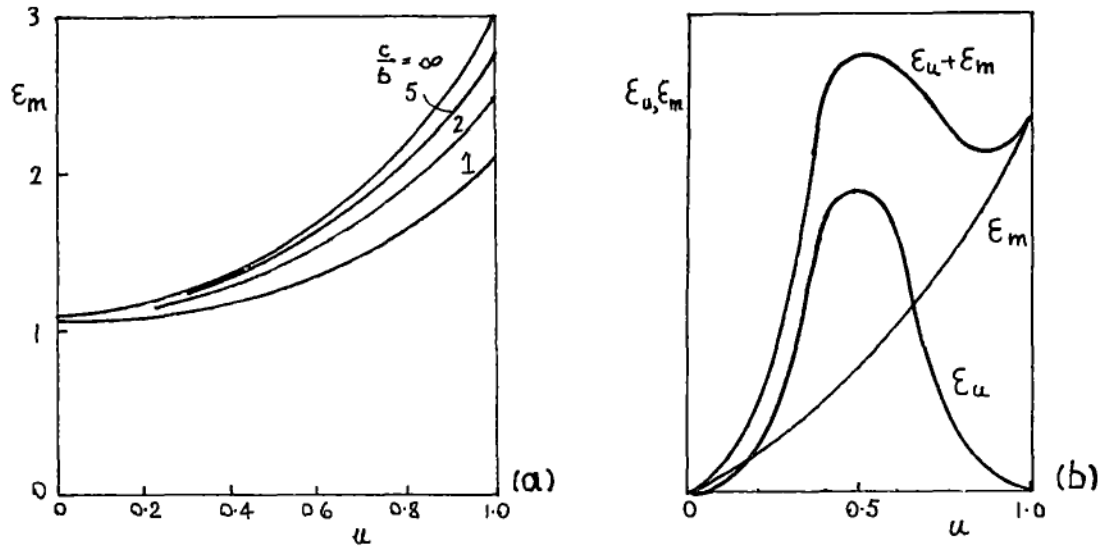

Figure 14.8 (a) Demagnetising energy E_m vs. wall position u. c/a = 1 corresponds to a cube. (after Rhodes and Rowland [R51], (b) Combined variation of E_m and wall (internal stress) energy E_u vs. u [G4].

above graphs are still useable provided allowance is made for the equivalent charge density on each face. If the magnetization has direction cosines α, β, γ, then the equivalent densities will be αM_s, βM_s, γM_s on faces normal to the X, Y, and Z axes. When θ' and θ'' are small so that $\beta,\gamma \ll \alpha$, then $e_m = E_m u^2 \cos^2\theta$. There are several approximations here: the larger are θ' and θ'' the larger is the error in the $\cos^2\theta$ term. Other approximations are more subtle.

Ginsburg combines the e_u and e_m terms as shown in figure 14.8b. No clues are given as to the relative values of E_m or E_u.

Application to iron crystals

All Ginsburg's theory is for a uniaxial crystal (like Cobalt) which has one easy direction of magnetization i.e. uniaxial anisotropy. Iron has three such directions, along the axes of the (cubic) crystal lattice. The domains in iron are thus able to form a closed path for the flux within the grain and so reduce the demagnetising energy E_m to a small value. However Goodenough (see chapter 15) has suggested that E_m still plays a significant part in the nucleation of reverse domains at the grain boundary.

However, notwithstanding these criticisms, I feel that this model and analysis by Ginsburg is a significant contribution to the understanding of domain behaviour. For this reason I have dealt with it in some detail; some similarities will be noticed between his model and the results from other models, to be discussed in chapter 15.

CHAPTER 15

THREE MORE MODELS INVOLVING THE MAGNETOMECHANICAL EFFECT

15.1 J.B.Goodenough: reverse domain creation

In 1954 J.B.Goodenough [G3] wrote a paper that sets out ways in which domains might form in the reverse direction with the applied field H still in the forward direction. His analysis is in places complicated, even with many simplifying assumptions, but his predictions support much experimental work that was previously unexplained. (This particular paper seems to have been largely ignored since, although there are a few references to his paper of a year later on switching phenomena in ferrite cores). I have copied exactly some of the paragraphs from his paper, since it proved difficult to improve on his most succinct style.

Introduction

"Current magnetic-domain theory and experiment has shown that if a magnetic specimen, which is not finely divided, is in a strong, external, slowly alternating magnetic field, then the induced change in magnetic flux through the sample is primarily due to the motion of domain walls. In order to understand the characteristics of any B-H hysteresis loop, it is necessary to know the origins of the individual domain walls and the factors which hinder their motion through the sample when driven by an external magnetic field."

"The principal cause of flux change may be assumed to be the motion of 180° domain walls if the specimen does not have a special geometry or orientation of its axes of easy magnetisation which would energetically favour the creation of many domains at right angles to the applied field. It will be assumed that the specimen has a cubic lattice, is polycrystalline,

and is in the form of a toroid or of a long rod parallel to the applied field."

"If a specimen is saturated, no domain walls exist within it. If the flux in a saturated sample is to be reversed by the motion of 180° domain walls, domains of reverse magnetisation must first be created. The new domains will be bounded by 180° walls, and as any domain grows in the presence of a favorably orientated external field, its boundary walls will move".

"If an external field, which has saturated a magnetic specimen, is reduced and reversed, domains of reverse magnetisation may be created in several regions of the specimen before irreversible wall motion, or irreversible domain growth begins. H_{ni} will be defined as the critical field strength for domain creation in any ith region of the specimen. It will be defined as positive if it is orientated in the direction of the magnetization within the new domain."

"If all $H_{ni} > 0$, the difference in induction between saturation, B_s, and the remanence, B_r, is given by the rotation of the elementary atomic moments from the external-field direction to a crystallographically preferred direction of magnetization.If some $H_{ni} > 0$, however, there is a further reduction of the remanence which is included in the reverse domains. In order to obtain a material of high retentivity, therefore, one requirement is that all $H_{ni} > 0$."

If $H_{ni} < 0$, reverse domains will be created in the first quadrant of the B vs.H loop. Experiments have shown that compressive stress parallel to the applied field, or tension perpendicular to the field, will make $H_{ni} < 0$.

Grain Boundaries

"A crystal lattice is, in general, anisotropic with regard to ease of magnetisation. If a crystal is not under tensile stress, this anisotropy is determined by the crystallographic configuration. The grain boundaries in a polycrystalline specimen separate regions of different crystallographic

orientation of easy-magnetization direction. At low field strengths, the magnetization vectors of the neighboring grains are not rotated from their easy-magnetization directions into complete alignment. Consequently there is generally a discontinuity (across the boundaries) in the magnetization-vector component normal to the boundary. Therefore magnetic poles exist at the grain boundaries, and magnetic energy is associated with these poles. If θ_1 and θ_2 are the angles made by the spontaneous-magnetization vector M_s of the neighbouring grains and the normal to their common boundary, the grain-boundary-surface pole density is $w^* = M_s(\cos\theta_1 - \cos\theta_2)$."

"The magnetic energy associated with these surfaces of magnetic poles would be reduced if domains of reverse magnetization existed to produce a pole distribution of alternating sign. This is illustrated in figure 15.1a. Work must be done, however, in the formation of the domains of reverse magnetization. The grain boundaries or lamellar precipitates will act as nucleating centers for domains of reverse magnetization only if the resulting reduction in energy is larger than the work required to form the domains."

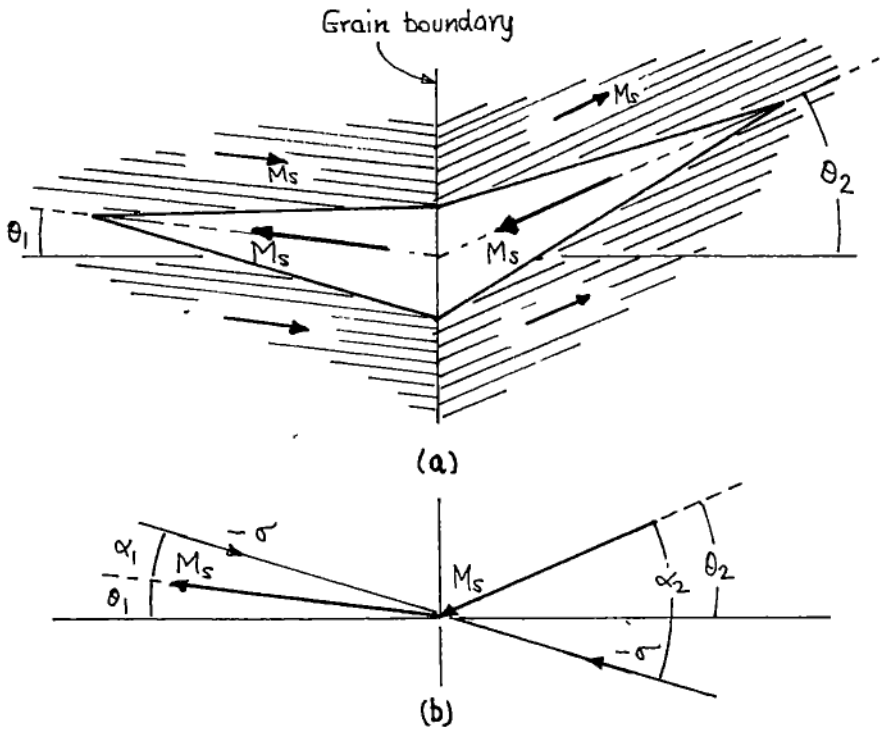

Figure 15.1 (a) Reverse domain creation (after Goodenough, [G3]), (b) application of compression decreases θ_1 and θ_2.

"In order to determine the critical field strength for domain creation at a planar surface of surface magnetic-pole density w^*, further simplifying assumptions are made. Firstly the applied field H is assumed to be so small and the anisotropy constant K so large that the magnetization in any domain is directed along an easy axis of magnetization. A subsequent correction for this assumption does not, in zero approximation, alter the calculated critical field strength. Secondly the surfaces containing magnetic poles are assumed so far apart that the magnetoelastic interactions between them can be neglected. It is further assumed that when reverse-domain creation occurs, it occurs periodically over the planar surface. The domains of reverse magnetization are taken to be prolate ellipsoids of semimajor axis l and semi-minor axis r such that $r/l \ll 1.0$. The angles θ_1 and θ_2 are assumed small so that the two halves of the domain of reverse magnetization can be considered to have a common major axis in the estimation of the demagnetization factor, the volume, and the surface area."

Goodenough then estimates the critical field to be

$$H_n = C_1 - C_2(\cos\theta_1 - \cos\theta_2)^2$$

in which C_1 and C_2 are positive constants. Their relative values are such that on the assumption that θ_1 and θ_2 are both less than, say, 20° a small change in θ_1 and θ_2 could change the sign of H_n. An applied stress could change these angles slightly, as illustrated in figure 15.1b. The magnetoelastic energy is given by

$$E_\sigma = 1.5\lambda_s\sigma\sin^2\alpha$$

in which α is the angle between σ and M_s. When σ is negative, (compression), E_σ is negative and an increase in α would make E_σ go more negative, i.e. a decrease in potential energy. An increase in α_1 or α_2 would reduce θ_1 and increase θ_2, thus increasing $(\cos\theta_1 - \cos\theta_2)^2$, and perhaps making H_n change from positive, giving a squarish B vs. H loop, to negative, giving a lentil-shaped loop. (Of course there are also ranges of angles of θ and α for which $(\cos\theta_1 - \cos\theta_2)^2$ would decrease).

However Goodenough goes on to argue that the very high sensitivity to stress of the shape of the B vs. H loop of 68 Permalloy results from the effect of stress on reverse domain creation. Figure 15.2, taken from Bozorth [B7] shows an example of this. A detailed qualitative explanation is given by Goodenough, which is not repeated here.

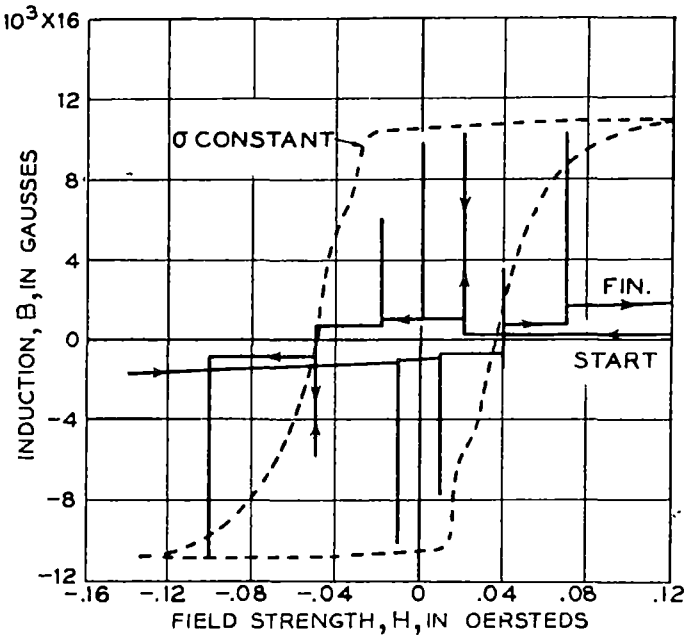

Figure 15.2 Hysteresis loop of 68 Permalloy. Tension is zero except when applied and removed at certain field strengths. The dashed line is for constant tension (after Bozorth, [B7]).

15.2 J.N.Watson: B vs. H loops of stressed magnetic materials with granular interaction

Watson's model [W4,1968; W5,1972] is an attempt to allow for the effect of domains on each other in a polycrystalline ferromagnetic. In so much that it uses only domain rotation it is a high field model, and therefore not strictly applicable to moderate fields; in fact it appears to contradict the symmetry that is described in chapter 8, but it is deemed to be worth including since it is a model that has not been used before and is the only one described in this thesis that allows for domain interaction.

Energy components

The three components of energy that are assumed relevant are the anisotropy E_K, the magnetoelastic E_σ and the magnetostatic E_H. For a cubic crystal:

$$E_K = K_1(\alpha_1^2\alpha_2^2 + \alpha_2^2\alpha_3^2 + \alpha_3^2\alpha_1^2) \quad (1)$$

in which K_1 is the first anisotropy constant, and α_1, α_2, α_3 are the direction cosines of the intrinsic magnetisation M_s relative to the crystal axes.

$$E_\sigma = -1.5\lambda_{100}\sigma(\alpha_1^2\gamma_1^2 + \alpha_2^2\gamma_2^2 + \alpha_3^2\gamma_3^2) - 3\lambda_{111}\sigma(\alpha_1\alpha_2\gamma_1\gamma_2 + \alpha_2\alpha_3\gamma_2\gamma_3 + \alpha_3\alpha_1\gamma_3\gamma_1) \quad (2)$$

in which γ_1, γ_2, γ_3 are the direction cosines of the stress σ.

$$E_H = -M_sH_a\cos\theta \quad (3)$$

in which θ is the angle between M_s and the applied field H_a.

Granular interaction

The analysis of Barton and Ionides (chapter 11) minimises the sum $E_K + E_\sigma + E_H$ for the particular case of torsional stresses $\pm\sigma$ at $\pm45°$ to H_a, and for an arbitrary direction θ_o of H_a relative to the crystal axes. The applied field shifts M_s, by a small angle, away from the nearest <100> direction to H_a, and the stress further alters this angle to give a rotation θ of M_s. The component of M_s parallel to H_a gives the net magnetisation and, of course, stress affects this. The minimisation is repeated for a range of values of θ_o to simulate a random orientation of crystal grains as in polycrystalline steel. Each grain is assumed to take up a direction (of magnetisation) that depends only on σ, θ_o, and H_a; the effect of neighbouring domains is ignored.

Watson reasons that this last effect - which he calls granular interaction - may be very strong; enough to prevent domains acting independently of each other. He points out that the demagnetising energy is lowest when the magnetisations of grains are all parallel to each other.

If this is the case, then all grains switch in unison as the applied field is reversed (giving a squarish B vs. H loop). This he calls positive interaction: "Each grain switches as if it is following the average energy contour of all the magnetisations".

But if the interaction is not quite strong enough to bring about parallel alignment of all grain magnetisations, the situation of figure 15.3a might exist. M_s departs from being parallel to H_a by some angle θ (to be calculated). For random orientation of crystal axes relative to H_a, angle ϕ in the diagram can take all values yet θ stays constant. The average anisotropy energy (stress is assumed zero) can be calculated for arbitrary θ by averaging it over all values of ϕ

$$\langle E_K \rangle = 0.5\pi \int_0^{2\pi} E_K d\phi$$

Similarly, when stress is applied and the magneto-elastic component of energy is included,

$$\langle E_K + E_\sigma \rangle = 0.5\pi \int_0^{2\pi} (E_K + E_\sigma) d\phi = E(\theta) \qquad (4)$$

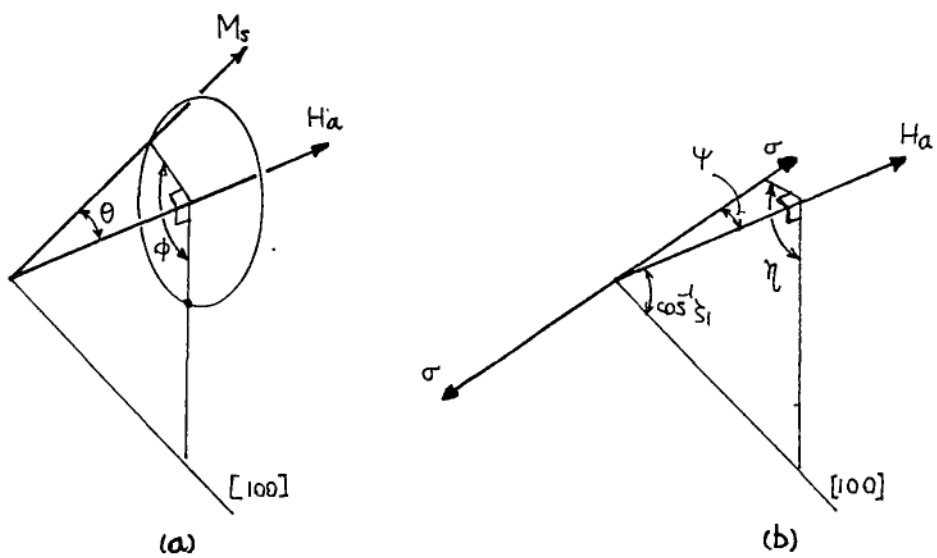

Figure 15.3 (a) Angles between intrinsic magnetisation M_s and applied field H_a. H_a has direction cosines ζ_1, ζ_2, ζ_3 relative to the crystal axes. M_s can take all values of θ for the purpose of averaging the anisotropy and magnetoelastic energies, (b) angles between stress σ, field H_a, and crystal axes (from Watson, [W5]).

This can be evaluated in terms of the angles ψ and η associated with σ and H_a in figure 15.3b to give (after considerable arithmetic)

$$E(\theta) = -0.0625K_1(1-5\zeta)\cos 2\theta - 2.25\sigma\{0.5\lambda_{100}[(1-2\zeta)\cos^2\psi + \zeta\sin^2\psi] - \lambda_{100}/6 + \lambda_{111}[\zeta\cos^2\psi - 0.5\zeta\sin^2\psi]\}\cos 2\theta - 0.1094K_1(1-5\zeta)\cos 4\theta + \text{constant} \quad (5)$$

in which $\zeta = \zeta_1^2\zeta_2^2 + \zeta_2^2\zeta_3^2 + \zeta_3^2\zeta_1^2$, and ζ_1, ζ_2, ζ_3 are the direction cosines of H_a relative to the crystal axes. Omitting the constant, equation 5 can be written in the condensed form

$$E(\theta) = M\cos 2\theta + N\cos 4\theta \quad (6)$$

The shape of B vs. H loops

The total energy is

$$E_T = -M_sH_a\cos\theta + M\cos 2\theta + N\cos 4\theta \quad (7)$$

This is then solved in order to calculate the value of θ that gives minimum energy for particular values of H_a, M and N. The magnetisation is the component of M_s parallel to H_a, namely $M_s\cos\theta$. The resulting M vs. H loops have different shapes depending on the ratio of M/N. Figures 15.4a and b show how Watson classifies these loops as types I, II, III, and IV, and figure 15.4c shows their shapes. The threshold fields H_1 and H_2 are given by

$$H_1 = \frac{-4M + 16N}{M_s} \quad (8)$$

$$H_2 = \frac{4}{3M_s}\left|\sqrt{\frac{(M-3N)^3}{-6N}}\right| \quad (9)$$

This completes the summary of Watson's paper. However there are some interesting deductions to be made from it.

The value of ζ for a randomly orientated assembly of domains

The following result is required for the next subsection. Since only domain rotation is assumed by Watson, the applied field iis presumably high enough for all domains to point along their easy direction nearest to H_a.

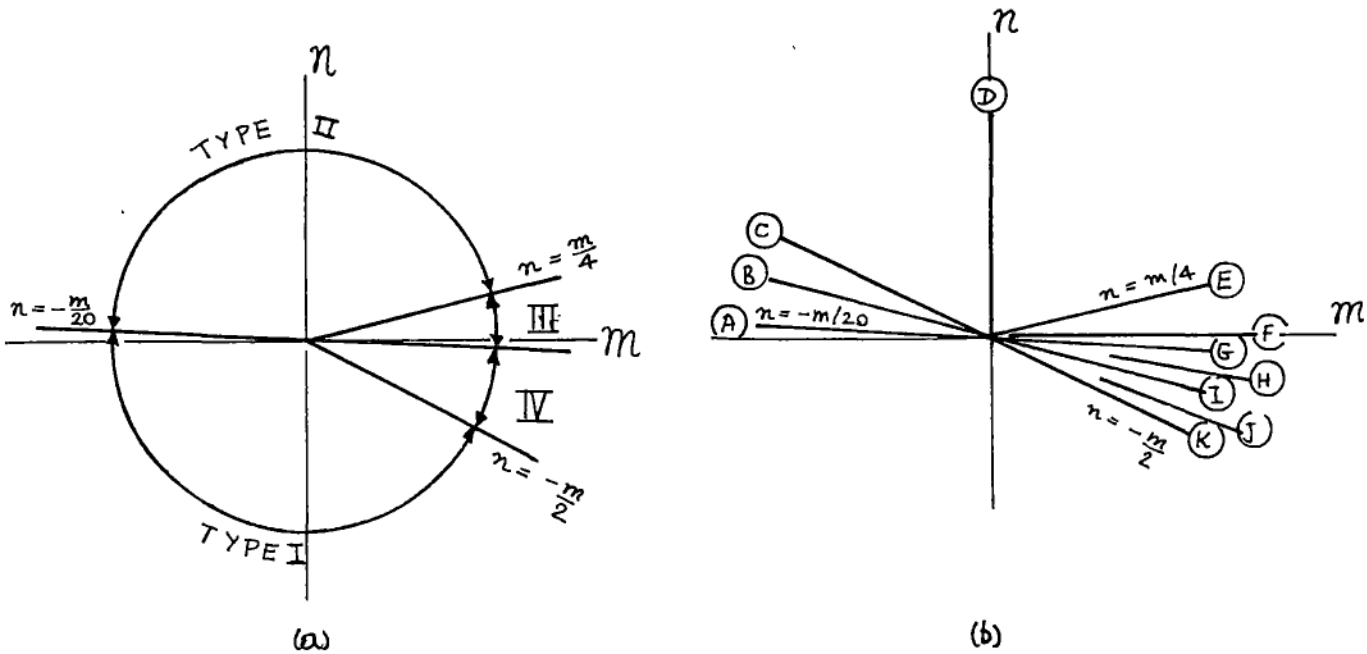

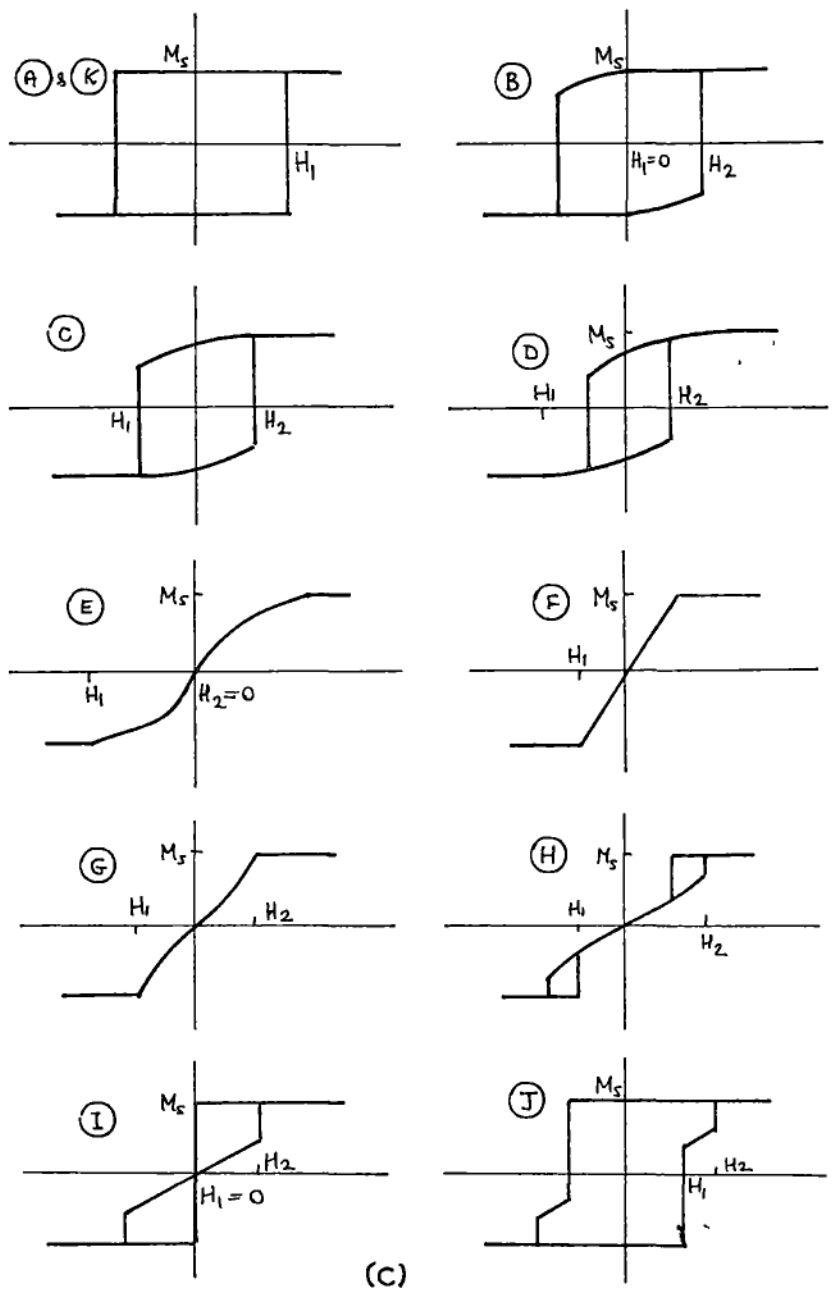

Figure 15.4 (a) Classification of M vs. H loops in the *M,N* plane, (b) selected directions A-K in the *M,N* plane for the M vs. H loops, (c) shapes of M vs. H loops and curves according to the directions A-K [W5].

Figure 15.5a shows H_a at angles α, β, γ to the X, Y, Z axes; $\zeta_1 = \cos\alpha$, $\zeta_2 = \cos\beta$, $\zeta_3 = \cos\gamma$. These are related to the polar angles ϕ' and θ' as shown in figure 15.5b, and from which $\zeta_1 = \sin\theta'\cos\phi'$, $\zeta_2 = \sin\theta'\sin\phi'$, $\zeta_3 = \cos\theta'$.

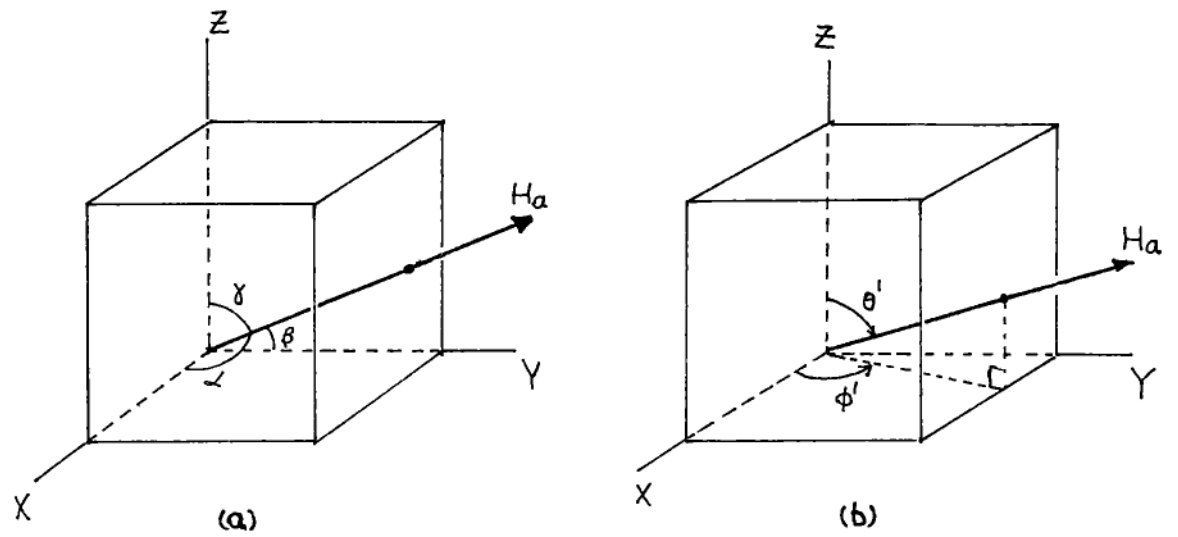

Figure 15.5 (a) Direction cosines α, β, and γ of H_a relative to the crystal axes, (b) polar angles ϕ' and θ' of H_a relative to the crystal axes.

The average value of ζ, if H_a can take all directions within the cube (which is the same mathematically as the axes taking all directions relative to H_a) is

$$\langle\zeta\rangle = \frac{4}{\pi^2}\int_0^{\pi/2}\int_0^{\pi/2}(\zeta_1^2\zeta_2^2 + \zeta_2^2\zeta_3^2 + \zeta_3^2\zeta_1^2)\,d\theta'd\phi'$$

$$= \frac{4}{\pi^2}\int_0^{\pi/2}\int_0^{\pi/2}[(\sin\theta'\cos\phi'\sin\theta'\sin\phi')^2 + (\sin\theta'\sin\phi'\cos\theta')^2 + (\cos\theta'\sin\theta'\cos\phi')^2]\,d\theta'd\phi' \qquad (10)$$

$$= 11/64 \text{ or } 0.172$$

The value of M for a random assembly of domains, for stress parallel or perpendicular to field

In equation 7, for the total energy E_T, only M contains σ. From equation 5, the part of M that contains σ is

$$M_\sigma = -2.25\sigma\{0.5\lambda_{100}[(1-2\zeta)\cos^2\psi + \zeta\sin^2\psi] - \lambda_{100}/6 + \lambda_{111}[\zeta\cos^2\psi - 0.5\zeta\sin^2\psi]\} \qquad (11)$$

Substituting $\langle\zeta\rangle$ into equation 11 will give the average value of M_σ for a random assembly of domains. Figure 15.5b shows that ψ is the angle between σ and H_a and is independent of the orientation of the domains. For stress parallel or perpendicular to the field, $\psi = 0°$ or $90°$ respectively. Putting $\lambda_{100} = -\lambda_{111} = 20\text{x}10^{-6}$ for iron makes M_σ very much smaller than the other coefficient of 2θ, namely $-0.0625K_1(1-5\zeta)$. In fact, if one works backwards and solves for $M_\sigma = 0$, it turns out that $\zeta = 1/6 = 0.167$, which is very close to its average value, and suggests that for an ideal (random) distribution, the total energy should not be affected by stress if the latter is parallel or perpendicular to the field.

This is at odds with the measurements of chapter 8 and is perhaps, in a rather negative sense, evidence that domain rotation by itself cannot account for the large decrease of permeability for $+\sigma,H_\perp$ or $-\sigma,H_\parallel$.

15.3 D.C.Jiles and D.L.Atherton: stress and anhysteretic magnetisation

In 1984 Jiles and Atherton described two advances in our understanding of ferromagnetism and stress.

(1) They formulated a new equation to describe the B vs. H loop. This is based on the equation of the anhysteretic, or ideal, B vs. H curve but modified in a particular way in order to describe an ordinary B vs. H loop.

(2) They reasoned that the application of stress, either tensile or compressive, at constant field strength, would shift the magnetisation from a point on the B vs. H loop toward the anhysteretic B vs. H curve, and backed this up with experimental proof.

(1) A new equation for the B vs. H loop

An ideal B vs. H curve, for 2% manganese steel, is shown in figure 15.6a. The full line is from the Langevin-Weiss equation

$$\frac{M}{M_s} = \coth\left[\frac{\mu_o m(H + \alpha M)}{k_B T}\right] - \frac{k_B T}{\mu_o m(H + \alpha M)} \qquad (1)$$

where M_s = saturation magnetisation (A/m)

m = magnetic moment per unit volume

H = applied field (A/m)

k_B = Boltzman's constant

T = degrees Kelvin

α = an (empirical) field factor

Equation (1) can be written more concisely as

$$M = L\left\{\frac{H + \alpha M}{\mu_o a}\right\} = L\left\{\frac{B_e}{\mu_o a}\right\} \qquad (2)$$

where L is the Langevin function: $L\{\theta\} = \coth\theta - 1/\theta$, B_e is the effective field $= \mu_o(H + \alpha M)$ Tesla, and $a = k_B T/\mu_o m$. M is the molecular field; a concept put forward by Weiss in 1907.

The authors then modify equation (2) to allow for hysteresis, which they view as the result of an impediment to the motion of domain walls; the walls are temporarily "pinned" by dislocations or crystal imperfections. On the assumption that the irreversible work done in moving the domains from their pinning sites is proportional to the change in magnetisation, equation 3 is obtained

$$M = L\left\{\frac{B_e}{\mu_o a}\right\} + \delta k \frac{dM}{dB_e} \qquad (3)$$

in which $\delta = -1$ when dM/dB_e is positive

$\delta = +1$ when dM/dB_e is negative

k = an empirical "constant", that in fact varies slightly with H.

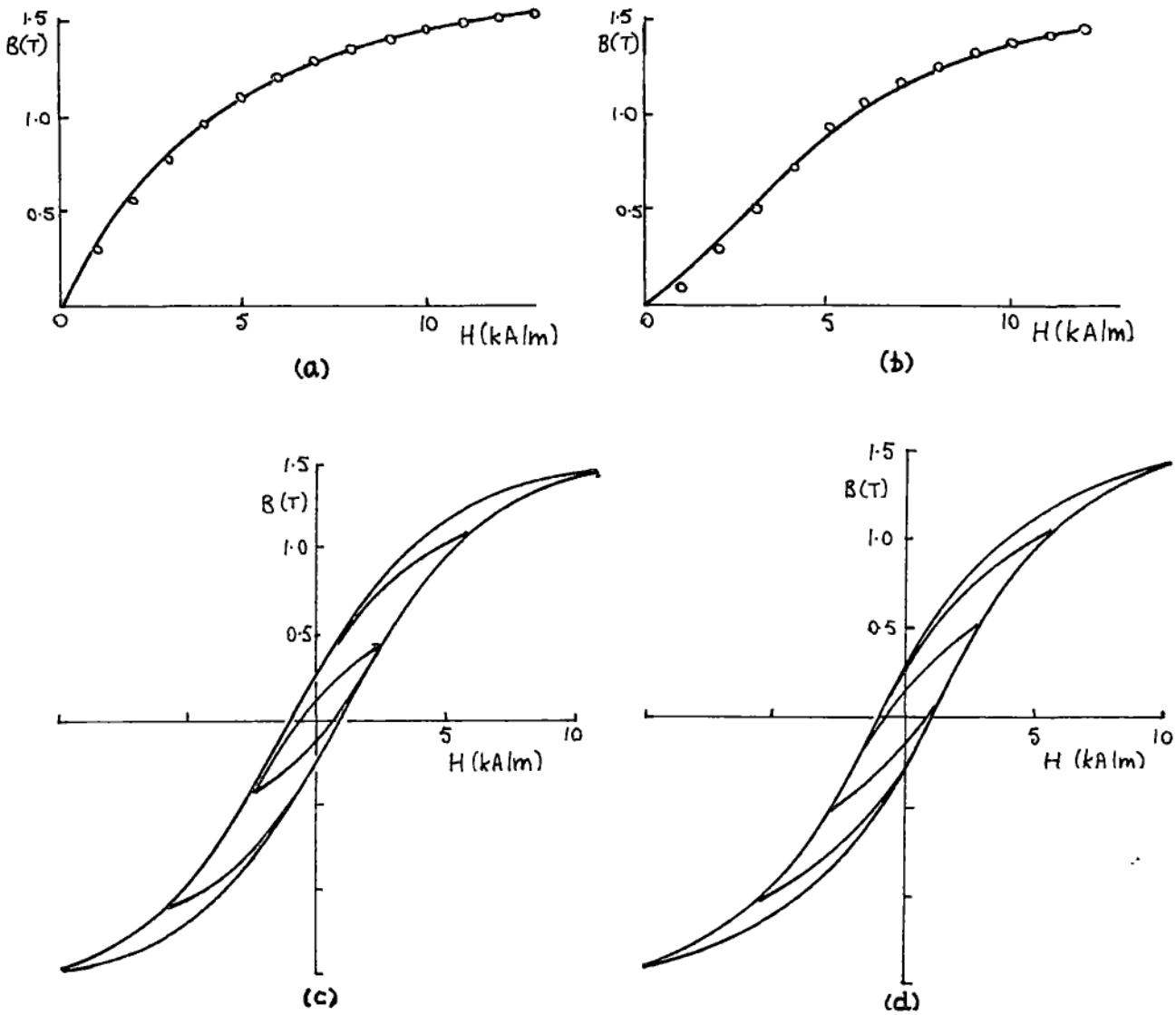

Figure 15.6 Comparison of experimental and theoretical B vs. H characteristics for 2% Manganese steel.
(a) Anhysteretic or ideal; o experimental, —— theoretical with a=3750A/m and α=0.0033 in equation 2, (b) hysteretic or initial; o experimental, —— theoretical with a=3750A/m, α=0.0033, and k=0.0044 in equation 3, (c) experimental B vs. H loops, (d) theoretical B vs. H loops, predicted from equation 3; k depends on H.
Composition of 2% Manganese steel: 0.08%C, 1.98%Mn, 0.08%S, 0.015%P, 0.055%Cu, 0.235%Mo. Yield point 610MPa. (from Jiles and Atherton,[Ji1]).

Figure 15.6b shows measured points on an initial B vs. H curve for the 2% manganese steel, together with a best-fit curve from equation 3 with δ = -1 and k kept constant. Figures 15.c and d show predicted and experimental B vs. H loops, for the same steel, in which k depends on the value of H. In all cases there is excellent agreement between theory and

experiment. Equation 3 can closely describe the B vs. H loops for magnetisation under tension or compression provided the factors α and k are chosen appropriately.

(2) Stress and change of magnetisation from the hysteretic towards the anhysteretic B vs. H curve

Jiles and Atherton point out that since the pinning effect of dislocations (or other inhomogeneities) causes the B vs. H curve to be modified to the hysteresis loop, then anything that reduces the pinning effect would move the hysteresis loop towards the ideal curve. They assume that applied stress has this effect; it weakens the ability of the pinning sites to restrict domain wall movement. They assume that, further, in order to tie in with experimental evidence, the stress alters the ideal B vs. H curve itself.

Figure 15.7 shows the change in flux density caused by a single stress cycle of (a) 100MPa tension and (b) 100MPa compression at different points along the initial B vs. H curve and on the B vs. H loop. Changes in B, whether caused by tension or compression, are always towards the ideal curve - although here they are insufficient to reach it.

Figure 15.7c compares the change in flux density ΔB for a stress cycle of 140MPa tension, starting firstly at different points on the initial B vs. H curve and secondly on the ideal curve. The latter shows negligible change in flux density. Figure 15.7d gives the differences of flux density, for the same values of applied field, between the anhysteretic (B_{an}) and the initial (B_i) B vs. H curves (zero stress). These are larger than the changes of figure 15.7c by an order of magnitude and show that application of stress takes B from the initial toward the ideal value by only about 10% or so of the required value.

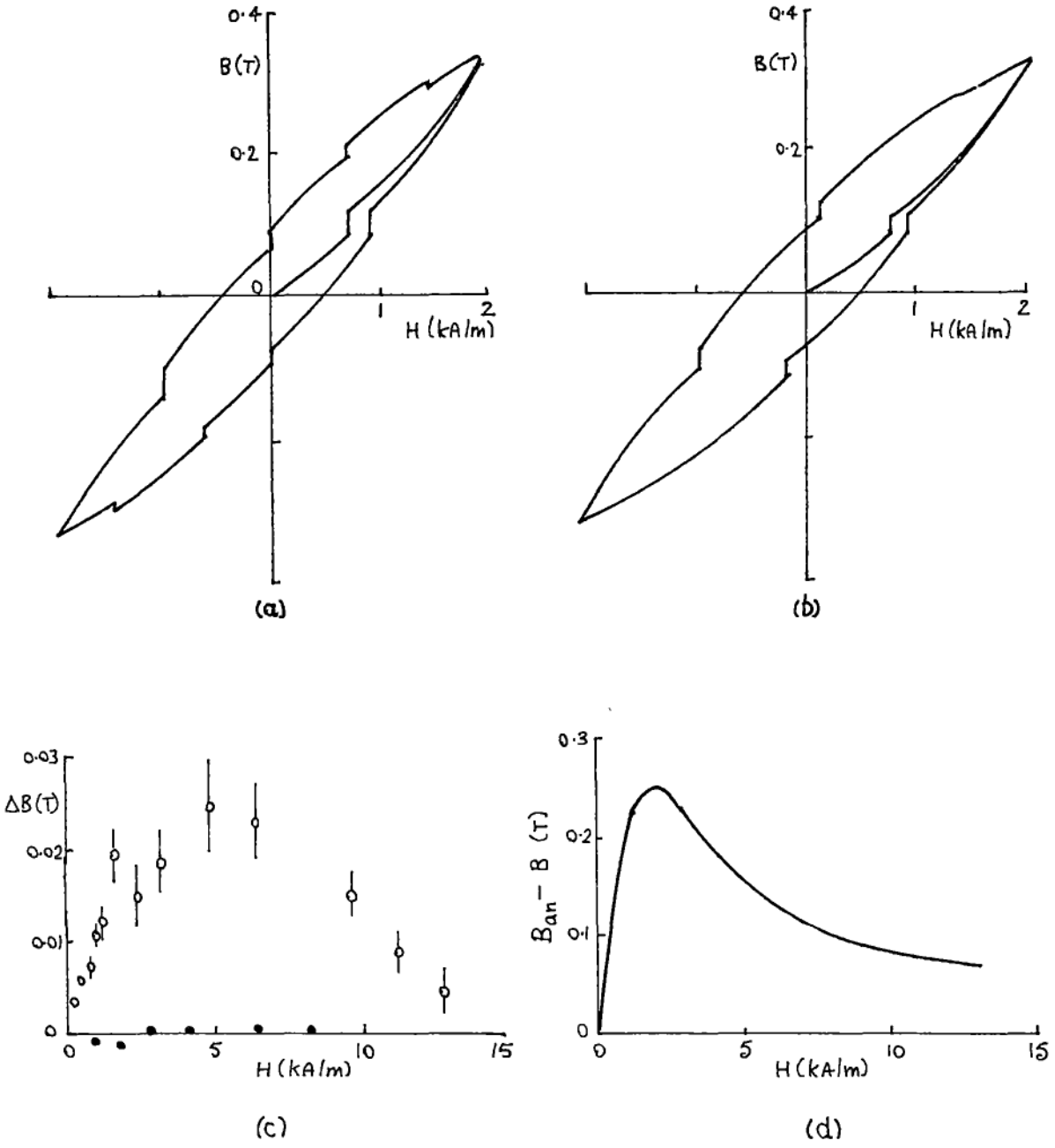

Figure 15.7 (a) The effect (shown by vertical jumps of flux density) of a single stress cycle of 100MPa tension at various points along the initial magnetisation curve and around a hysteresis loop for 1% Manganese steel, (b) as (a) but for a 100MPa compression cycle, (c) changes in flux density B for a stress cycle of 140MPa tension starting on the initial magnetisation curve (circles) and starting on the ideal magnetisation curve (dots), (d) the difference between anhysteretic (B_{an}) and initial (B_i) values of flux density.
(figures a and b are for 2% Mn steel; c and d are for 1% Mn steel of composition 0.25%C, 1.08%Mn, 0.02%S, 0.01%P; yield point 460MPa) [J1].

Qualitative explanation of the asymmetrical effect of tension and compression on changes in flux density

The experimental results given by Jiles and Atherton are for a steel that is fairly hard magnetically. There are only slight differences in the ideal B vs. H curves under constant tension or compression, and hence, as shown in figure 15.7, the changes in B caused by a cycle of stress of either sign are almost the same.

If the stress affects the ideal B vs. H curves rather more, the asymmetry noticed by Craik and Wood [C3] and by Faunce [F2] in 1970 can be predicted. Figure 15.8a shows a set of ideal B vs. H curves for steel at six different stresses, three tensile and three compressive, plus the ideal and initial curves at zero stress. (These are assumed curves, but they vary in the same way as those in figure 1.1). Assume the steel is initially demagnetised and is then magnetised at zero stress to point o' on the initial B vs. H curve. Suppose that when a stress is applied the flux density moves 50% towards the corresponding ideal curve. Thus in figure 15.8b three increments of compression added and then removed give increments of B at points 1, 2, 3, 4, 5, 6 (double arrows). Figure 15.8c shows B plotted against stress, on the left hand side of the ordinate. The curve on the right hand side is for tension. These curves are the same shape as figure 11.5a (reproduced here as 15.8d) which was measured by Craik and Wood on mild steel.

Perhaps the main achievement of Jiles and Atherton in the context of the magnetomechanical effect is to draw attention to the significance of the ideal B vs. H curve. However, what is still missing is a quantitative prediction of how stress alters this ideal B vs. H curve.

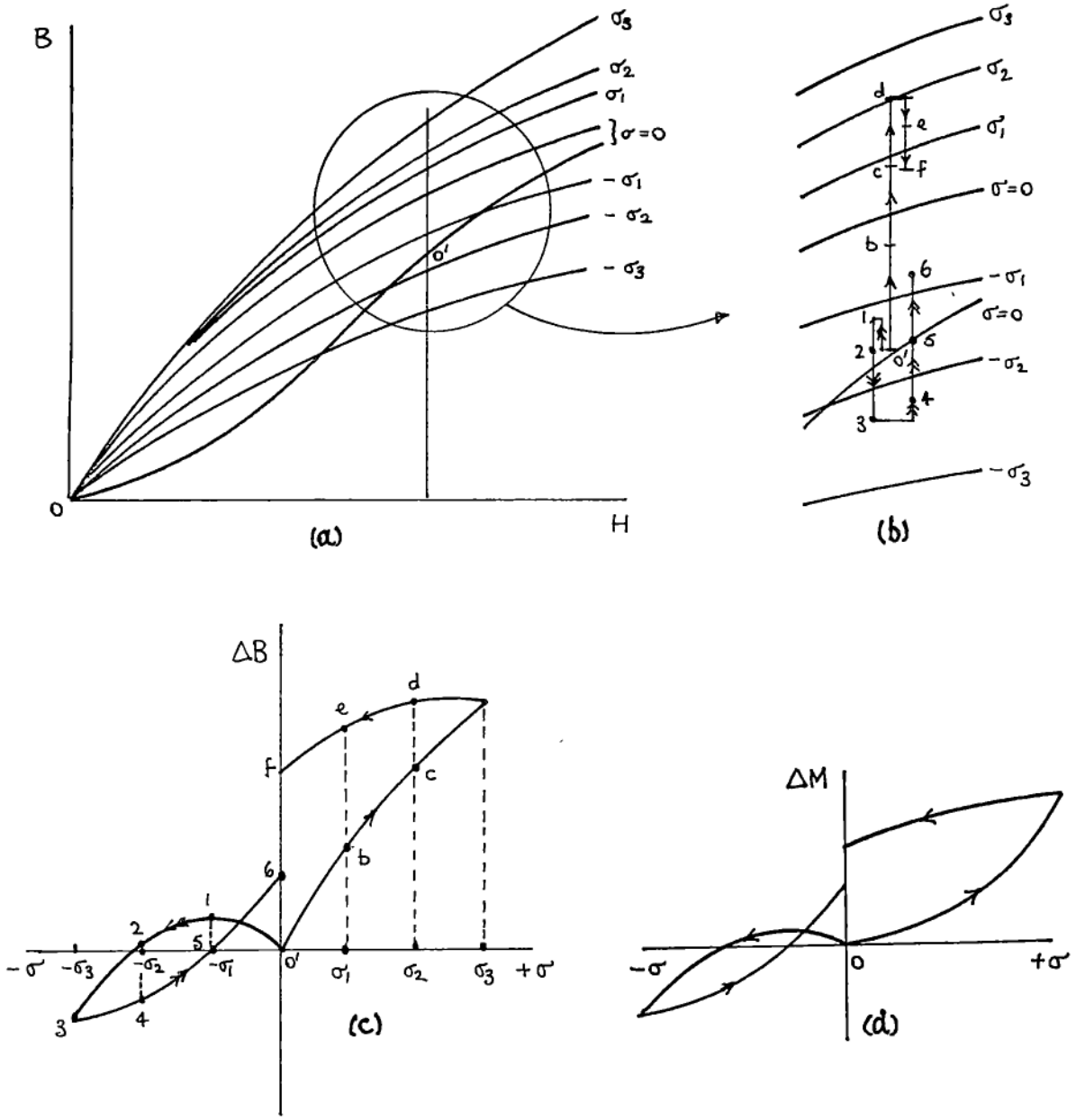

Figure 15.8 An example of the qualitative prediction of the change of flux density with stress at constant field.
(a) Ideal B vs. H curves for different stresses, plus the initial curve at zero stress, (b) increments of B for application and removal of stress, (c) increments ΔB vs. stress σ, corresponding to (b), (d) measured increments ΔM vs. σ, from Craik & Wood.

CHAPTER 16

CONCLUSIONS

There are individual conclusions at the end of several chapters, but here I would like to set down conclusions based on the whole of the thesis. These are conveniently put under three headings:

(1) Non-destructive measurement of stress in general.

(2) The rotation rig in particular.

(3) The theoretical aspect of stress and the B vs. H characteristics of mild steel.

16.1 Non-destructive measurement of stress

A review paper by Ruud (R6,1981) deals with one partially non-destructive and three non-destructive methods for the measurement of residual stress. These are hole drilling, X-ray diffraction, ultrasonics, and Barkhausen noise. Strictly speaking, the first three are related to strain rather than stress, and we do not really know which Barkhausen noise is related to. Also, if a method can measure residual stress at a point it must also be able to measure total stress there (i.e. residual plus applied stress).

The following table, from Ruud's paper, gives a qualitative comparison of these four methods, plus a standard destructive one in which the sample is cut up and its strain, as the stress relaxes, is measured.

The accuracy of the stress determination is not stated - an irritating omission. Presumably the row "reliability" is related to accuracy. Some figures for hole drilling are ±8%, and for X-ray diffraction ±2% or ±10MPa, under good conditions. (These are from a symposium on residual stresses held by the Australian Institute of metals, December 1982).

Method	Hole-drilling	X-ray	Ultra-sonics	Bark'n noise	Stress relief
Non-destructive	partially	yes	yes	yes	no
Reliability	good	good	poor	poor	good
Bulk stress	no	no	yes	no	yes
Spatial resolution	>30mm^3	<1	>5	>10	4
Cost	1	0.1 to 1	<0.1	<0.1	1 to 10
Speed	slow	moderate	fast	fast	slow

(The original table included rows for portability and the ability to tell the direction of the stress; all methods are "yes" for both).

Ruud concludes that:

(1) X-ray diffraction is the only non-destructive technique that is generally reliable and is widely applicable.

(2) Ultrasonics holds much promise, especially for three dimensional stress fields, but is unlikely to be implemented in the near future. The theory is reasonably well understood but there are many practical difficulties. These are due mostly to the very small change in ultrasonic velocity with strain - at most 1 part in 10^3 at yield for mild steel, and is compounded by the much larger changes in velocity that result from crystallographic texture. The latter is in general not well defined nor easily measured.

(3) Barkhausen noise (B.N.) suffers from more unknown quantities than does ultrasonics (in theory as well as in practice) and its application is limited to surface stresses only.

Measurements in chapter 9, in which an unloaded annealed mild steel bar was scanned with a B.N. transducer and with the rotation rig, show that the rotation rig is rather better than B.N. as a guide to stress. The B.N. readings varied by a factor of 2 or 3 and indicated stress up to 100MPa. The rotation rig showed stresses up to 10MPa The latter stress is

the more likely for annealed mild steel.

In fact - not to put too fine a point on it - I feel that the B.N. technique is not worth bothering with until the rotation rig has been more widely tested. This statement is based not only on my B.N. measurements, but also on the rather unsatisfactory B.N. results that have been achieved by several other investigators.

16.2 The Rotation Rig

I stated in the preface that the original aim of the project was to design an instrument that would make use of the stress-dependence of the magnetic properties of steel in order to give an indication of the pattern of stress on a steel surface. This has been achieved; the development of the instrument - the Rotation Rig - and its output voltage vs. stress characteristic are described in chapter 5. The main features of the Rotation Rig RR7 are listed below; figure 16.1 is a photograph of the instrument.

(1) Measures the difference in principal stresses on the surface of steel and also gives their directions.

(2) Accuracy : ±5MPa for stress less than 50MPa on mild steel; the accuracy decreases for higher stresses.

(3) Should work, with different sensitivities, on any ferromagnetic material (but has only been tested on mild steel and rail steel).

(4) Area of surface examined in one reading is about 5mm x 5mm. The clearance required is 12mm all round and the surface should be flat.

(5) Works through paint or rust, but uneven scale should be removed.

(6) Hardly affected by texture.

(7) Apparently not much affected by temperature - but this aspect has not been tested thoroughly.

(8) The electronic controls are simple and cheap to make, as is the probe itself.

Figure 16.1 Rotation Rig R.R.7. (above) The probe and its control box, (below) measuring the residual stress on a piece of steel Voltage SCn is read on the digital voltmeter.

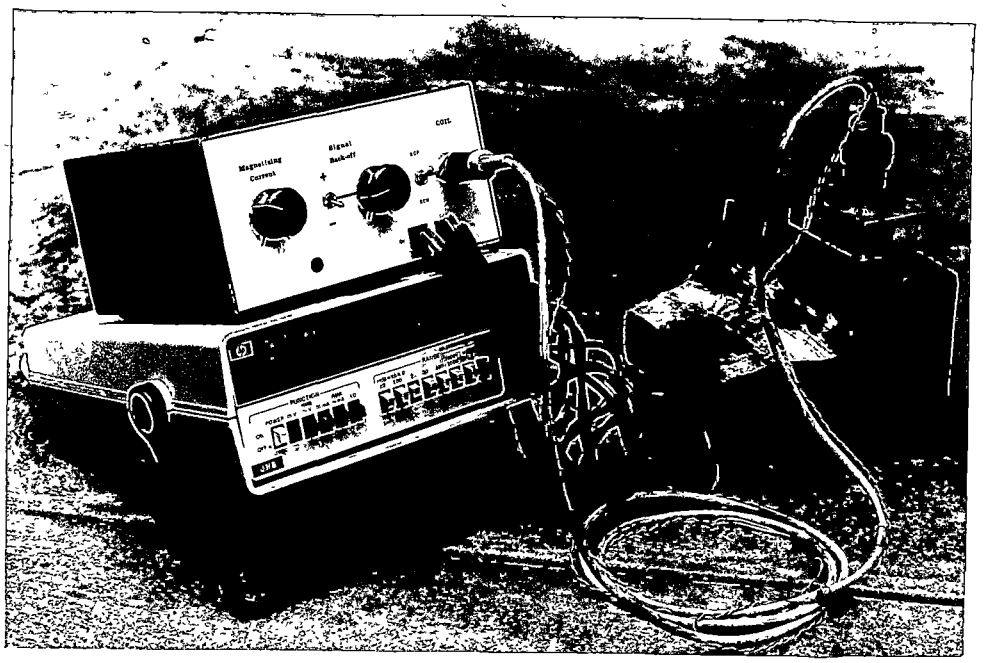

(9) A reading can be taken in 10 seconds.

(10) A serious disadvantage is that its sensitivity decreases for steel that has been plastically strained, and so the R_v value in this case is not uniquely related to stress-difference.

Chapter 7 gives results of measurements of the pattern of stress on a steel disc that was compressed at the ends of a diameter. The close agreement between the measured and theoretical pattern is satisfying for several reasons: readings were obtained quickly; there was negligible processing of data since the output voltage (R_v) of the rotation rig corresponds directly to a stress-difference; other means of measuring stress non-destructively, such as X-rays or ultrasonics are more expensive to implement and complicated to use.

Chapter 1 of the thesis also reviews the use of Barkhausen noise (B.N.) as a possible non-destructive magnetic means of detecting stress and plastic strain. For a scan along an annealed mild steel bar the B.N. measurements (in chapter 9) suggest that the rotation rig is rather better than B.N. as a guide to stress in mild steel. The B.N. readings varied randomly by a factor of 2 or 3 fron point to point on the steel and indicated stresses of up to 100MPa. The rotation rig showed stresses up to 10MPa, varying by only a few tens of percent. The latter stress pattern is the more likely for an annealed bar.

The R_v vs. stress characteristics given here have been obtained experimentally. It would be satisfying to be able to predict these, but there are two major obstacles:

(1) The change of the B vs. H loop itself with stress cannot be predicted (see the next section).

(2) The effect of eddy currents, and the geometry of the rotation rig, makes calculation of the amplitude and direction of the field at the surface of the steel very complicated. (There are programmes to compute three dimensional eddy current patterns but only for isotropic steel). The

measurements and analysis of chapter 3 show that the directions of B and H can differ by several tens of degrees on anisotropic steel under D.C. conditions, but there is evidence from use of the rotation rig that much smaller rotations (of only a degree or so in the change of direction of H at the surface of the steel) occur under A.C. conditions.

From the practical point of view the lack of theory does not matter, since the rotation rig should always be calibrated on a piece of steel with a known stress. Should it be accepted as a useful technique then no doubt its behaviour would be examined in more detail and the theoretical side extended accordingly.

An immediate improvement in consistency and hence of accuracy would be achieved by using a motor to rotate the probe against the steel, and also automatically recording the output signal. Since the SCn signal is only tens of microvolts, some averaging (using digital sampling) would improve the signal to noise ratio. All this could be summed up as improving the signal processing, and would be a relatively straight-forward task.

The list of features earlier in this section is a guide to the potential uses of the rotation rig. It is restricted to magnetic steels and its sensitivity is best on low carbon steels. Uses that come to mind are:

(1) To scan along beams in order to measure the static stress pattern in them.

(2) To measure stress at a point as the loading changes, i.e. dynamic conditions.

(3) Residual stress can quickly be measured in components before fabrication.

(4) It will work under water.

16.3 Stress and the B vs. H characteristics of mild steel

This still cannot be predicted quantitatively at low or moderate field strengths; many very good physicists have tried and not succeeded. In fact, since what is probably the most important secondary magnetic

characteristic - the initial magnetization curve - cannot be predicted with an error of less than several tens of percent, it is not surprising that the additional effect of stress cannot be predicted either.

The recent (1984) work by Jiles and Atherton, on the significance of the anhysteretic B vs. H curve and stress, is an exciting advance in magnetomechanical theory, and tempts one to hope that the mechanism of the interaction of stress and domain patterns could soon be understood rather better. The biaxial stress work described in chapter 8 should help with this. It would be interesting to repeat tests on pure iron and on alloy steel to see if the symmetry (tension parallel to magnetization has the same effect as compression perpendicular to magnetization: permeability is not much affected; tension perpendicular has the same effect as compression parallel to magnetization: permeability is greatly decreased) still holds. The failure of the author's model of 90° wall movement to predict sufficient decrease of permeability (chapter 13) suggests that 180° wall movement and reversal of domains is also necessary to explain the measurements. Goodenough's concept of reverse domain creation appears to offer a means of accounting for such a large decrease in permeability, but the link with stress is rather tenuous, and there is scope for more work on this.

The interaction between domains has been ignored by most investigators (because of mathematical difficulties) and it is for this reason that the work of Watson is described in chapter 15. However, one criticism of it is that no details are given of what happens at grain boundaries; consideration of this returns the train of thought to Goodenough's 1954 paper.

Ewing's book was published in 1892 and was the first book to describe magnetomechanical effects. Perhaps by 1992 we might understand them. It would be a fitting anniversary achievement.

APPENDIX 1

PREDICTION OF MAGNETISATION VS. STRESS CURVE AT MODERATE FIELD STRENGTHS FOR POLYCRYSTALLINE STEEL: THREE DIMENSIONAL CASE

A1.1 Stress parallel to field

Range of directions of applied field and stress

Figure A1.1a represents a cubic crystal with easy directions of magnetisation along the <100> axes. The limiting directions of field H for the magnetisation to stay along OZ are those of a vector from the origin to the edges of the top of the cube. Thus the maximum angles between H and OZ vary from 45° when H is along [011] or [101] to 55° when it is along [111]. Strictly, of course, H can be in any of the four top faces of identical cubes, as shown in figure A1.1b, but it is sufficient to deal with only one quarter of the top surface (the shaded area).

Suppose that a compressive stress ($-\sigma$) is applied parallel to H. If the stress is high enough, the magnetisation should switch to be along the

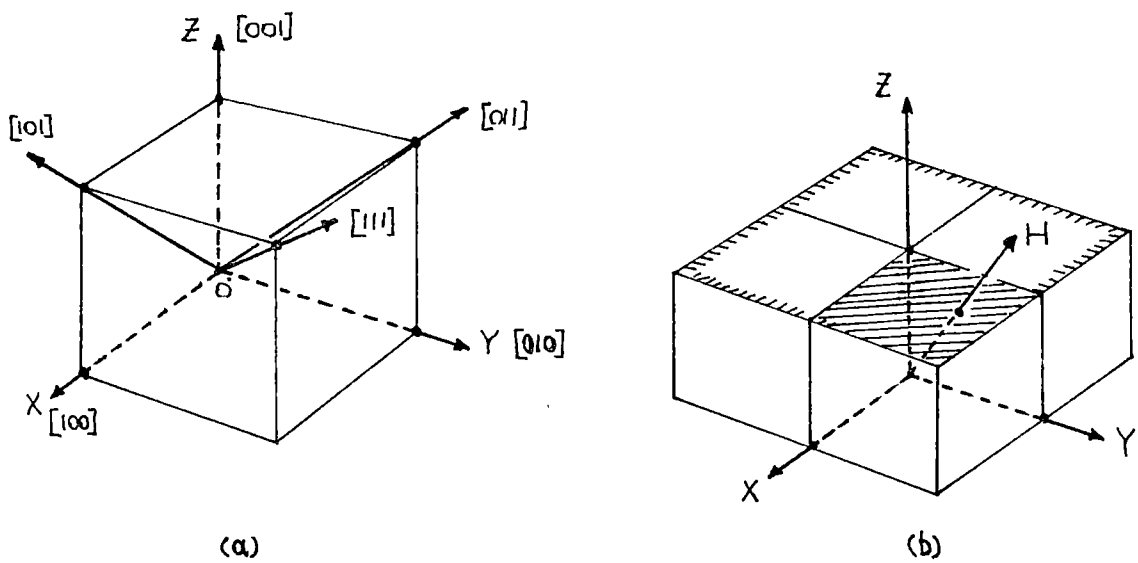

Figure A1.1 Three dimensional case: (a) coordinates and some directions for a cubic crystal, (b) the shaded boundary is for the complete range of directions of field H relative to the axis OZ. The shaded area is the minimum representative range of directions of H for energy considerations.

crystal axis at right angles to the field (as in the two dimensional case for σ <-62MPa). In figure A1.2a the direction of H is described by polar angles ϕ and θ. Let ϕ be fixed and θ vary. When $\theta = 0°$, M_s will lie along OX at high compression. This will be so until $\theta > 45°$, when M_s will switch from OX to lie along OY. (For $\theta < 45°$ angle YOH is less than angle XOH, and so M_s along OY gives a higher magnetoelastic energy than along OX. The magnetostatic energy is independent of θ and so stays constant). Hence in order to evaluate the threshold stress, only directions of M_s along OZ and OX need be considered for the range of angles $0°<\theta<45°$, $0°<\phi<55°$. In the following sections, magnetisation along axes OX, OY, or OZ is denoted by M_X, M_Y, or M_Z.

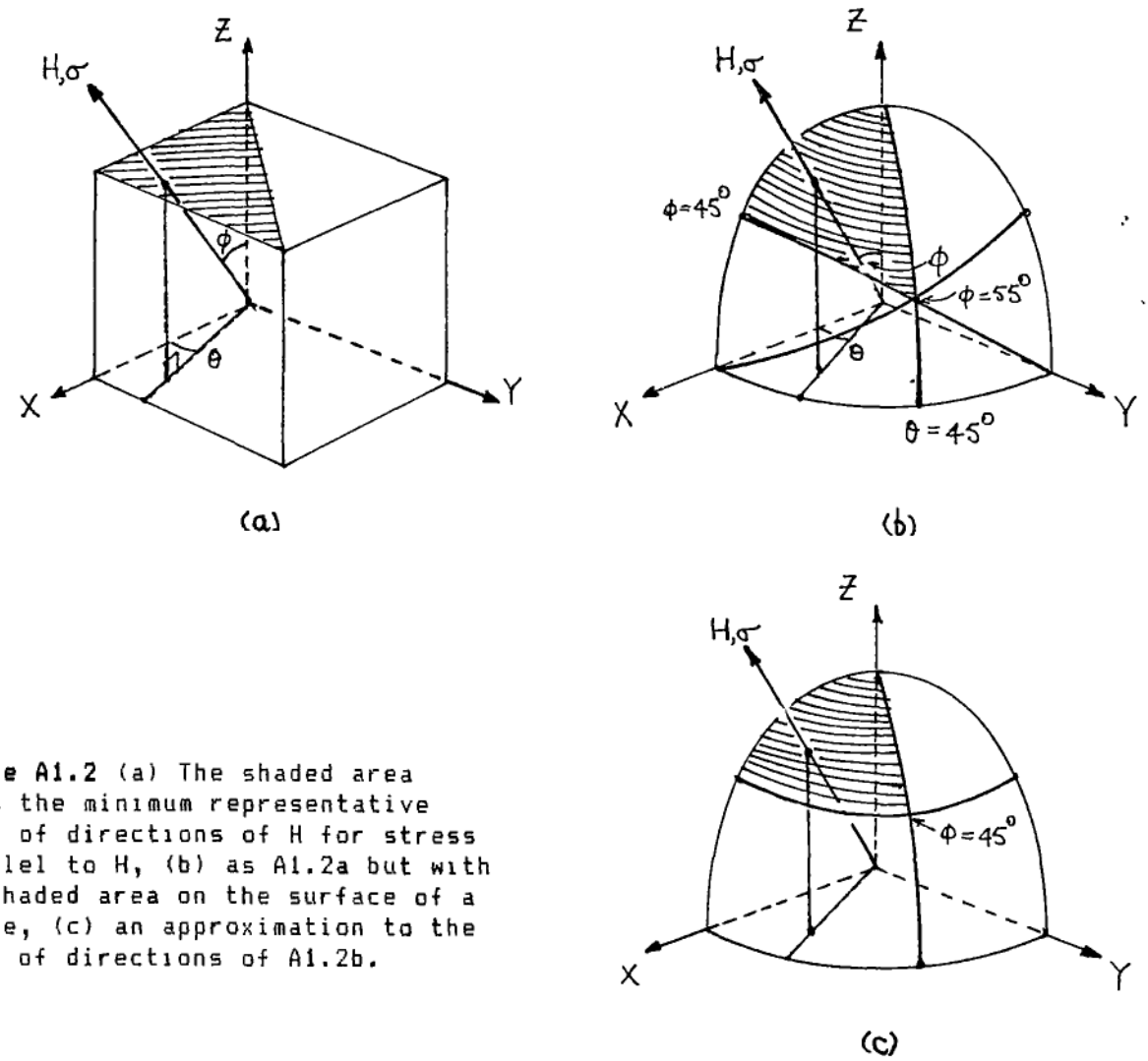

Figure A1.2 (a) The shaded area shows the minimum representative range of directions of H for stress parallel to H, (b) as A1.2a but with the shaded area on the surface of a sphere, (c) an approximation to the range of directions of A1.2b.

Energy components

Magnetostatic energy:

$$E_H = -M_s H(\alpha_1\beta_1 + \alpha_2\beta_2 + \alpha_3\beta_3) \ J/m^3$$

Magnetoelastic energy:

$$E = -1.5\lambda_{100}\sigma(\alpha_1^2\gamma_1^2 + \alpha_2^2\gamma_2^2 + \alpha_3^2\gamma_3^2)$$
$$- 3\lambda_{111}\sigma(\alpha_1\alpha_2\gamma_1\gamma_2 + \alpha_2\alpha_3\gamma_2\gamma_3 + \alpha_3\alpha_1\gamma_3\gamma_1) \ J/m^3$$

in which the α's, γ's, and β's are the direction cosines of M_s, σ, and H respectively relative to the crystal axes OX, OY, and OZ. (Subscripts 1 = X, 2 = Y, 3 = Z).

If M_s lies along OZ (i.e. M_Z), $\alpha_1 = \alpha_2 = 0$ and $\alpha_3 = 1.0$. The only other direction cosines needed are β_3 and γ_3; $\beta_3 = \gamma_3 = \cos\phi$. Hence

$$E_Z = E_H + E_\sigma = -M_s H\cos\phi - 1.5\lambda_{100}\cos^2\phi$$

For M_X, $\alpha_2 = \alpha_3 = 0$ and $\alpha_1 = 1.0$. Only β_1 and γ_1 are needed; $\beta_1 = \gamma_1 = \sin\phi.\cos\theta$, and so

$$E_X = -M_s H\sin\phi.\cos\theta - 1.5\lambda_{100}\sigma\sin^2\phi.\cos^2\theta$$

If a fraction f (f=1 or 0) of the domains remain along OZ and the rest (1-f) turn to be along OX when the stress is applied, the total energy is

$$E_T = fE_Z + (1-f)E_X$$
$$= -f[k\cos\phi + k'\cos^2\phi]$$
$$-(1-f)[k\cos\theta.\sin\phi + k'\cos^2\theta.\sin^2\phi]$$
$$= -f[k(\cos\phi - \cos\theta.\sin\phi) + k'(\cos^2\phi - \cos^2\theta.\sin^2\phi)]$$
$$-[k\cos\theta.\sin\phi + k'\cos^2\theta.\sin^2\phi]$$

in which $k = M_s H$ and $k' = 1.5\lambda_{100}\sigma$.

The second square brackets term can be ignored since it does not depend on f. E_T is a minimum when the first term (inside the square brackets) is a positive maximum, and then f = 1; otherwise if the same term is negative, f = 0.

Magnetisation for tension

For tension, σ is positive. For $0° < \phi < 55°$, $0° < \theta < 45°$, the coefficients of k

and k' inside the first square brackets are always positive, and so f = 1 makes E_T a minimum. Thus the domains point along OZ for all values of tension.

The overall magnetisation M for all orientations of domains is obtained from the component of M_Z parallel to H (which is $M_s\cos\phi$), averaged over the shaded area. This is the same if the summation, or integration, is part of the surface of a sphere as in figure A1.2b. An approximation that gives easier integration is to use the shaded area shown in figure A1.2c, in which $0°<\phi<45°$ and $0°<\theta<45°$. The surface area of this shaded part is

$$\int_0^{\pi/4} \frac{\pi r^2}{4}\sin\phi.d\phi = 0.23r^2$$

and so

$$M = \frac{M_s}{0.23r^2} \int_0^{\pi/4} \frac{\pi r^2}{4}\sin\phi.\cos\phi.d\phi = 0.853M_s$$

(The accurate value is $0.83M_s$: see Chikazumi [C7], p250. Since all this theory relates to an idealised, rather impractical situation, such an approximation, which makes only a few percent difference, is deemed justifiable. Other effects, discussed later, cause errors of several tens of percent).

Magnetisation for compression

A switch from M_Z to M_X is to be expected for compressive stress. The energy terms involving f only are

$$E_T = -f[k(\cos\phi - \cos\theta.\sin\phi) + k'(\cos^2\phi - \cos^2\theta.\sin^2\phi)]$$

where, now, k' is negative. If

$$k(\cos\phi + \cos\theta.\sin\phi) > k'(\cos^2\phi - \cos^2\theta.\sin^2\phi)$$

then minimum energy is for f = 1; otherwise f = 0. The threshold value of stress is obtained from

$$\frac{k}{k'} = \frac{M_sH}{1.5\lambda_{100}\sigma} = \frac{\cos^2\theta.\sin^2\phi - \cos^2\phi}{\cos\phi - \cos\theta.\sin\phi}$$

Solution of this equation with M_s = 2.16T, H = 900A/m, λ_{100} = 20×10^{-6}, and for a range of values of ϕ and θ at 10 degree intervals gives the threshold stresses shown in the following table.

θ =	0°	10°	20°	30°	40°	45°
ϕ = 0°	-61MPa	-61	-61	-61	-61	-61
10°	-53	-53	-54	-54	-55	-56
20°	-48	-48	-49	-50	-51	-52
30°	-45	-45	-46	-47	-49	-51
40°	-44	-44	-45	-47	-49	-51
45°	-44	-44	-45	-47	-49	-51
50°				-47	-50	-52
55°					-51	-54

The table shows that inbetween -44MPa and -62MPa all domains will switch from OZ to OX. The magnetisation at less than -62MPa is calculated by integrating the component of M_X that is parallel to H over the shaded area of figure A1.2c. This component is $M_s\sin\phi.\cos\theta$, and so

$$M = \frac{M_s}{0.23r^2}\int_{\theta=0}^{\pi/4}\left[\int_{\phi=0}^{\pi/4} r^2\sin^2\phi.d\phi\right]\cos\theta.d\theta = 0.435M_s$$

The graph of M vs. σ for tension and compression is shown in figure A1.3. Values of M for the transition region inbetween -44 and -62MPa are dealt with next.

Magnetisation in the transition region

Figure A1.4 shows the threshold stresses marked at nodes at 10 degree intervals on a distorted mesh or map of the shaded area of figure A1.2c. In order to calculate the overall magnetisation at, say, -52MPa, a -52MPa contour has been drawn as a dashed line. All domains with a

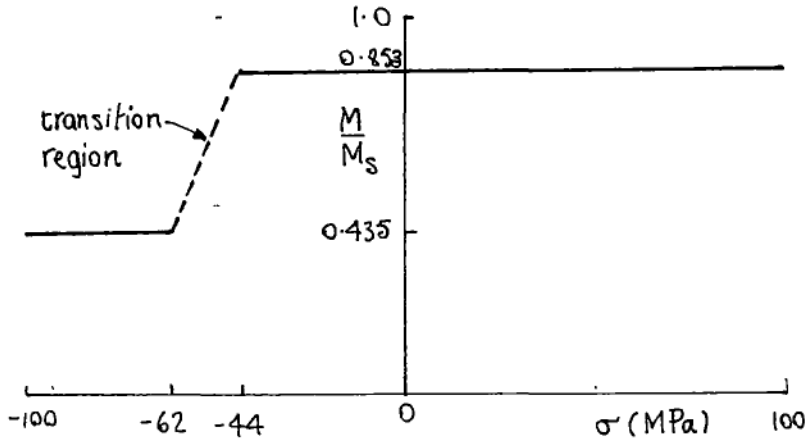

Figure A1.3 M/M_s vs. σ for stress parallel to the field. The transition region is shown by the dashed line.

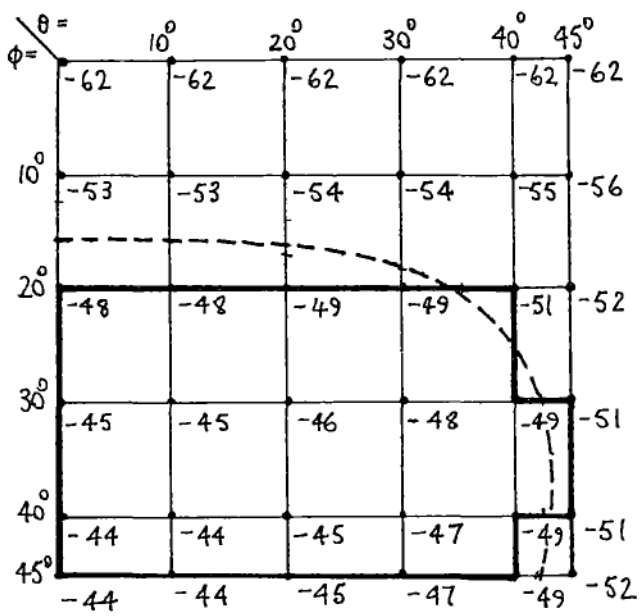

Figure A1.4 Map of threshold stresses for compression parallel to the field. The dashed line is the -52MPa contour. The thick lines are an approximation to this with straight lines.

threshold stress greater than -52MPa (i.e. less compressive) will still point along OZ, while those associated with directions inside the contour point will along OX.

Subsequent calculations are made slightly easier if the -52MPa contour is drawn as a set of straight lines (shown thick in figure A1.4) so as to include only whole squares. Some judgement is needed about which squares should be included, but this is not critical for an estimation.

The component of M_s parallel to H is $M_s \sin\phi.\cos\theta$. Each component must be multiplied by a suitable area so that when all are added up the whole of the shaded area is covered. The total of these magnetisation-area products is then divided by the surface area.

As an example, in figure A1.5, H is shown going through the middle of the curvilinear square bounded by ϕ = 20° and 30°, θ = 10° and 20°. The threshold stress for this area is greater than -52MPa, so the domain that was originally along OZ is now along OX. The magnetisation component is $M_s \sin 25° . \cos 15° = 0.408 M_s$ and must be multiplied by the area of the curvilinear square. The average width between longitude lines is $2\pi r \sin 25° (10/360)$ and the average width between latitude lines is $2\pi r (10/360)$, which gives an area of $0.014 r^2$. The magnetisation-area product is $0.006 M_s r^2$. Products for all other squaresare added together and the total is then divided by the surface area of the shaded part which is $0.23 r^2$. The result is that at -52MPa the magnetisation is about $0.55 M_s$. However, these intermediate points are not shown on the M vs. σ graph at this stage since the assumptions on which their calculation is based must be modified.

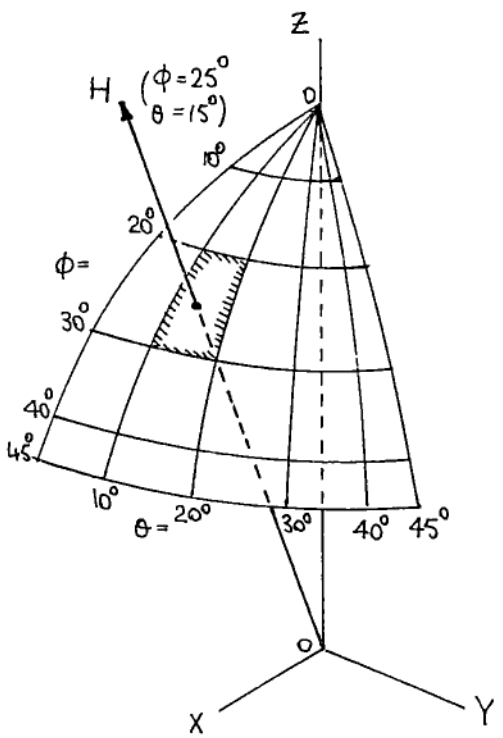

Figure A1.5 Diagram for the sample calculation of (magnetisation component) x (area).

Magnetisation at high compression

An assumption has been made that sufficient compression will switch M_s from OZ to OX (i.e. M_X), for $0° < \theta < 45°$. A switch from OZ to OY was ruled out because the magnetoelastic energy for M_Y is higher than for M_X. However, when the total energy at high compression is examined, the picture alters somewhat.

Firstly, the threshold stresses needed for M_s to switch from OZ to OY are evaluated for $0° < \theta < 45°$. From figure A1.2a, when M_s is along OY, $\alpha_1 = \alpha_3 = 0$ and $\alpha_2 = 1.0$. Only β_2 and γ_2 are needed; $\beta_2 = \gamma_2 = \sin\phi.\sin\theta$. Thus for a fraction f of domains along OZ and (1-f) along OY, the total energy is

$$E_T = -f[k\cos\phi - k'\cos^2\phi]$$
$$+(1-f)[-k\sin\phi.\sin\theta - k'\sin^2\phi.\sin^2\theta]$$
$$= -f[k(\cos\phi - \sin\phi.\sin\theta) + k'(\cos^2\phi - \sin^2\phi.\sin^2\theta)]$$
$$-[k\sin\phi.\sin\theta + k'\sin^2\phi.\sin^2\theta]$$

If the coefficient of f is positive, f = 1 gives minimum energy, otherwise f = 0. The threshold stress is obtained from the solution of

$$k(\cos\phi - \sin\phi.\sin\theta) + k'(\cos^2\phi - \sin^2\phi.\sin^2\theta) = 0$$

Results of this for the shaded area of figure A1.2c are in the following table (for the same values of M_s, H, and λ_{100} as before).

θ =	0°	10°	20°	30°	40°	45°
ϕ = 0°	-62MPa	-62	-62	-62	-62	-62
10°	-63	-61	-59	-58	-56	-55
20°	-66	-62	-58	-55	-53	-52
30°	-71	-65	-60	-55	-52	-51
40°	-81	-70	-63	-57	-52	-51
45°	-86	-74	-65	-58	-53	-51
50°				-60	-54	-52
55°					-56	-54

This shows that for all domain directions the threshold stress needed to switch M_s from OZ to OY is higher than to switch from OZ to OX. Hence all domains will switch to OX first of all - although a comparison with the first table shows that there is not much difference between many pairs of corresponding threshold stresses.

Secondly, the total energies for M_X and M_Y are evaluated. If, at high compressive stress, E_Y is less than E_X then M_s would in principle switch from OX to OY in order to lower its energy. The energies are

$$E_X = -k\sin\phi.\cos\theta - k'\sin^2\phi.\cos^2\theta$$

$$E_Y = -k\sin\phi.\sin\theta - k'\sin^2\phi.\sin^2\theta$$

If we take as an example $\theta = \phi = 30^\circ$, then for $M_s = 2.16T$, $H = 900A/m$, $\lambda_{100} = 21\times10^{-6}$, and σ in MPa:

$$E_X = -1944\sin30^\circ.\cos30^\circ - 31.5\sigma\sin^2 30^\circ.\cos^2 30^\circ$$

$$= -842 - 5.906\sigma$$

$$E_Y = -486 - 1.969\sigma$$

These are shown in figure A1.6. Also shown is

$$E_Z = -k\cos\theta - k'\cos^2\phi$$

$$= -1683 - 22.5\sigma$$

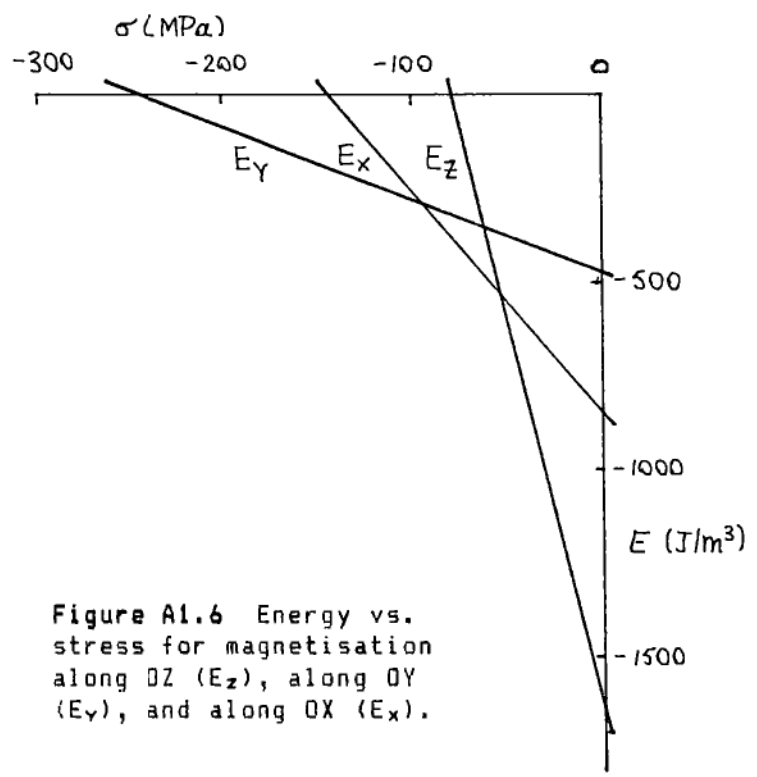

Figure A1.6 Energy vs. stress for magnetisation along OZ (E_Z), along OY (E_Y), and along OX (E_X).

This shows clearly that as the compressive stress is increased from zero, M_s lies firstly along OZ, then switches to OX at -50MPa, and then switches to OY at -90MPa. The following table gives the threshold stresses for the change from OX to OY for the whole range of directions of ϕ and θ. (Stresses for $\phi = 0^o$ tend to infinity and for $\theta = 45^o$ the equation is indeterminate).

θ =	0°	10°	20°	30°	40°	45°
ϕ =0°	$-\infty$	$-\infty$	$-\infty$	$-\infty$	$-\infty$	-
10°	-355MPa	-306	-277	-260	-252	-
20°	-180	-155	-141	-132	-128	-
30°	-123	-106	-96	-90	-88	-
40°	-96	-83	-75	-70	-68	-
45°	-87	-75	-68	-64	-62	-

Details of the calculation of the overall magnetisation at various stresses are not shown here, but by 100MPa roughly half the domains will have switched from OX to OY. In the limit, at very high compression, all domains will switch to OY, giving a magnetisation of

$$M = \frac{M_s}{0.23r^2} \int_{\theta=0}^{\pi/4} \int_{\phi=0}^{\pi/4} r^2 \sin^2\phi . \sin\theta . d\phi . d\theta = 0.18 M_s$$

The graph of M/M_s vs. σ for all values of stress parallel to the field is sketched in figure A1.7. However, the important effect of the demagnetising energy, which is ignored here, makes a switch of M_s to OY most unlikely. As a result, M/M_s would probably decrease only to a value of about 0.5, as in the two dimensional case. The demagnetising energy is dealt with in more detail in the next section.

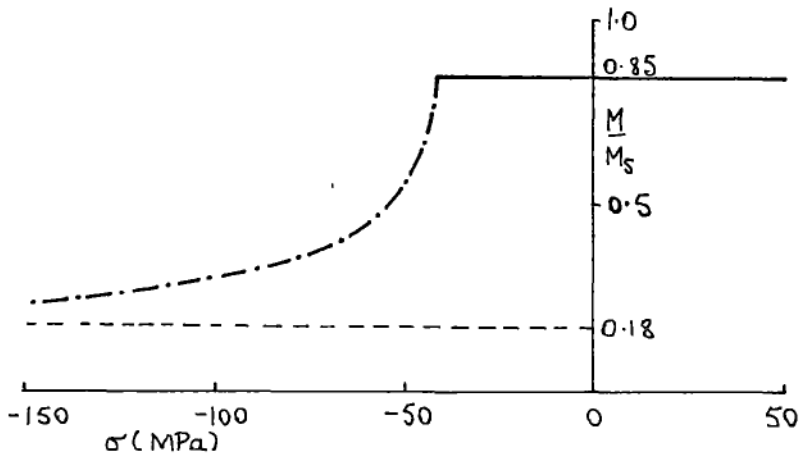

Figure A1.7 M/M_s vs. σ for stress parallel to the field. Domains switch to OY at high compression. The dot-and-dash portion is approximate.

A1.2 Stress perpendicular to the field

Range of directions of stress and field

Figure A1.8 shows the applied field at angles ϕ and θ. The combination of angles to be looked at is now far greater than for stress parallel to the field. If the stress vector is described by angles ψ and η, then for each direction of H described by ϕ and θ ($0°<\phi<45°$, $0°<\theta<45°$), η can take all values between 0° and 360°. ψ is determined by the fact that the angle between stress and field is always 90°, and hence ψ depends on θ, ϕ, and η.

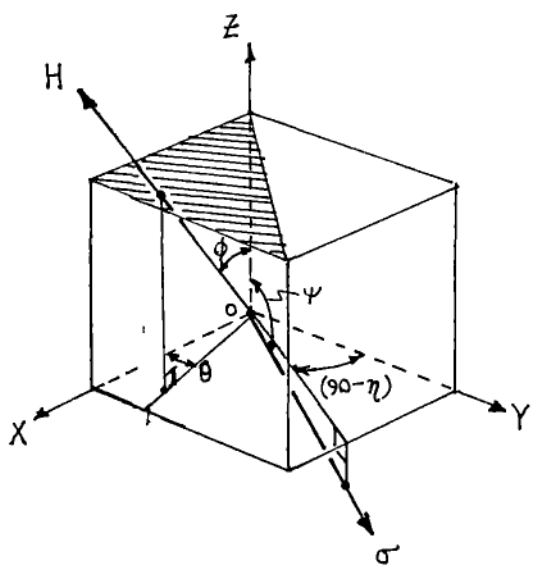

Figure A1.8 Directions of H and σ for stress perpendicular to the field.

The two dimensional analysis for stress perpendicular to field shows that a high enough tension switches M_s from OZ to an axis nearest to the stress. In the three dimensional case, this suggests: (1) a switch of M_s from OZ to OX (denoted by M_X) for $0^\circ<\eta<45^\circ$ and (2) a switch from OZ to OY (denoted by M_Y) for $45^\circ<\eta<90^\circ$. (Symmetry limits the range of η for purposes of analysis to between 0° and 90°). However, there is the possibility that for $0^\circ<\eta<45^\circ$, M_Y may give a lower energy than M_X. So all the combinations of energies must be checked numerically. In the next section, case (X) denotes the calculation of the stress threshold for M_X and case (Y) does the same for M_Y.

Value of ψ

The direction cosines of H and σ relative to the crystal axes X, Y,and Z are β_i and γ_i (i = 1, 2, 3). Since the angle between H and σ is always 90°

$$\cos 90^\circ = 0 = \beta_1\gamma_1 + \beta_2\gamma_2 + \beta_3\gamma_3$$

In terms of ϕ, θ, and η,

$$\beta_1 = \cos\theta.\cos(90^\circ-\phi) = \cos\theta\sin\phi$$

$$\beta_2 = \sin\phi.\sin\theta$$

$$\beta_3 = \cos\phi$$

$$\gamma_1 = \cos\eta.\cos(90^\circ-\psi) = \cos\eta.\sin\psi$$

$$\gamma_2 = \cos(90^\circ-\eta)\cos(90^\circ-\psi) = \sin\eta.\sin\psi$$

$$\gamma_3 = \cos\psi$$

Substituting for the β's and γ's and solving for ψ gives

$$\cot\psi = -\sin\psi(\cos\theta.\cos\eta + \sin\theta.\sin\eta)/\cos\phi$$

Energy components

$$E_H = -M_sH(\alpha_1\beta_1 + \alpha_2\beta_2 + \alpha_3\beta_3)$$

$$E_\sigma = -1.5\lambda_{100}\sigma(\alpha_1^2\gamma_1^2 + \alpha_2^2\gamma_2^2 + \alpha_3^2\gamma_3^2)$$
$$-3\lambda_{111}\sigma(\alpha_1\alpha_2\gamma_1\gamma_2 + \alpha_2\alpha_3\gamma_2\gamma_3 + \alpha_3\alpha_1\gamma_3\gamma_1)$$

where α_1, α_2, α_3 are the direction cosines of M_s relative to the crystal axes.

Case (X)

For M_Z, $\alpha_1 = \alpha_2 = 0$ and $\alpha_3 = 1.0$. Only β_3 and γ_3 are needed. $\beta_3 = \cos\phi$ and $\gamma_3 = \cos\psi$

$$E_Z = -M_s H\cos\phi - 1.5\lambda_{100}\,\sigma\cos^2\psi$$

$$= -k\cos\phi - k'\cos^2\psi$$

For M_X, $\alpha_1 = 1.0$, $\alpha_2 = \alpha_3 = 0$. Only β_1 and γ_1 are needed.

$\beta_1 = \cos\theta.\sin\phi$ and $\gamma_1 = \cos\eta.\sin\psi$.

$$E_X = -k\cos\theta.\sin\phi - k'\cos^2\eta.\sin^2\psi$$

For a fraction f (f = 0 or 1) of domains along OZ and (1-f) along OX, the total energy is

$$E_T = -f[k\cos\phi + k'\cos^2\psi]$$

$$- (1-f)[k\cos\theta.\sin\phi + k'\cos^2\eta.\sin^2\psi]$$

$$= -f[k(\cos\phi - \cos\theta.\sin\phi) + k'(\cos^2\psi - \cos^2\eta.\sin^2\psi)]$$

$$-[k\sin\phi\cos\theta + k'\cos^2\eta.\sin^2\psi] \qquad (A1)$$

The threshold values of stress (σ_{th}) are obtained from the solution of

$$k(\cos\phi - \cos\theta.\sin\phi) + k'(\cos^2\psi - \cos^2\eta.\sin^2\psi) = 0 \qquad (A2)$$

Case (Y)

For M_Z, E_Z is the same as for case (X):

$$E_Z = -k\cos\phi - k'\cos^2\psi$$

For M_Y, $\alpha_1 = \alpha_3 = 0$ and $\alpha_2 = 1.0$. Only β_2 and γ_2 are needed:

$$\beta_2 = \cos(90^o-\theta).\cos(90^o-\phi) = \sin\theta.\sin\phi, \text{ and}$$

$$\gamma_2 = \cos(90^o-\eta).\cos(90^o-\psi) = \sin\eta.\sin\psi$$

Hence

$$E_Y = -k\sin\theta.\sin\phi - k'\sin^2\eta.\sin^2\psi$$

For a fraction f of domains along OZ and (1-f) along OY,

$$E_T = -f[k\cos\phi + k'\cos^2\psi)]$$

$$- (1-f)[k\sin\phi.\sin\theta + k'\sin^2\eta.\sin^2\psi]$$

$$= -f[k(\cos\phi - \sin\theta.\sin\phi) + k'(\cos^2\psi - \sin^2\eta.\sin^2\psi)]$$

$$-[k\sin\theta.\sin\phi + k'\sin^2\eta.\sin^2\psi] \qquad (A3)$$

The threshold values of stress are obtained from the solution of

$$k(\cos\phi - \sin\theta.\sin\phi) + k'(\cos^2\psi - \sin^2\eta.\sin^2\psi) = 0 \qquad (A4)$$

Threshold stresses

The following tables show σ_{th} for energy cases (X) and (Y) for values of η from 1° to 89° in steps of 11°, and for ϕ and θ from 1° to 45° in steps of 11°. (Values of η of 0° and 90° are not used in order to avoid indeterminate or infinite results).

The behaviour of σ_{th} is rather more complicated than for stress parallel to the field. Here, although most values of σ_{th} are tensile, as expected, there are also some compressive values, which are not expected. The main problem is to display the results so as to bring out trends and features without their being obscured by the large amount of data. If we examine the effect of differing directions (η) of stress, and ignore the detailed effects of the ranges of values of ϕ and θ, these trends are apparent:

(1) for η = 1°, σ_{th} is tensile for M_X and (high) compressive for M_Y. (Section A1.1 shows that if all domains are along OZ, OX, or OY the overall magnetisation is 0.85Ms, 0.435Ms, or 0.18Ms respectively). Thus tension gives M/M_s = 0.435 and high compression gives M/M_s = 0.18 (figure A1.9a),

(2) for η = 89°, σ_{th} is tensile for M_Y and (high) compressive for M_X. Thus tension gives M/M_s = 0.18, and high compression gives M/M_s = 0.435 (figure A1.9b),

(3) for η = 45° there is not much difference between σ_{th} for M_X and M_Y; slightly less tension is needed to switch to M_X compared to M_Y,

(4) for η between 1° and 34°, 100MPa switches nearly all domains from OZ to OX; and for η between 56° and 89°, 100MPa switches nearly all domains from OZ to OY.

In general, both tension and compression can act to reduce the magnetisation. This feature is the most important difference between the parallel and the perpendicular stress cases, and is at odds with my experimental results which show that only perpendicular tension decreases magnetisation significantly and that perpendicular compression has little effect.

ϕ \ θ	1°	12°	23°	34°	45°
	Eta = 1 degree				
1°	61	61	61	61	61
12°	52	52	52	53	54
23°	47	47	47	48	48
34°	44	45	44	44	43
45°	-59	52	46	43	40
	Eta = 12 degrees				
	63	63	63	64	64
	54	55	55	56	57
	49	50	52	53	54
	46	50	54	55	55
	-2	-44	-999	143	86
	Eta = 23 degrees				
	72	72	72	72	72
	61	62	63	65	66
	55	58	61	64	66
	51	61	72	79	82
	-1	-16	-45	-126	-999
	Eta = 34 degrees				
	88	88	88	89	89
	75	77	79	81	83
	66	72	79	86	91
	60	82	112	141	155
	-1	-10	-25	-48	-91
	Eta = 45 degrees				
	121	121	121	122	122
	102	105	109	114	118
	88	100	116	132	147
	78	128	248	526	864
	-1	-8	-18	-32	-51
	Eta = 56 degrees				
	194	194	194	195	195
	162	169	178	189	199
	137	165	210	269	335
	117	278	-999	-400	-306
	-1	-7	-15	-25	-39
	Eta = 67 degrees				
	397	397	398	399	400
	330	352	384	424	468
	274	377	636	999	-999
	231	999	-290	-178	-156
	-1	-7	-14	-23	-34
	Eta = 78 degrees				
	999	999	999	999	999
	999	999	999	999	999
	967	999	-999	-805	-536
	843	-584	-209	-145	-128
	-1	-9	-16	-24	-33
	Eta = 89 degrees				
	999	999	999	999	999
	999	-999	-999	-999	-999
	999	-999	-999	-661	-468
	-999	-784	-278	-174	-141
	-9	-20	-24	-30	-37

(a)

ϕ \ θ	1°	12°	23°	34°	45°
	Eta = 1 degree				
1°	-999	999	999	999	999
12°	-999	-999	-999	-999	-999
23°	-370	-351	-354	-386	-468
34°	-162	-144	-134	-132	-141
45°	-86	-70	-58	-47	-38
	Eta = 12 degrees				
	999	999	999	999	999
	-999	-999	-999	999	999
	-507	-446	-426	-448	-536
	-184	-155	-137	-127	-128
	-91	-72	-57	-44	-33
	Eta = 23 degrees				
	405	404	402	401	400
	549	552	538	509	468
	-999	-999	-999	-999	-999
	-295	-221	-181	-160	-156
	-113	-84	-63	-47	-34
	Eta = 34 degrees				
	197	197	196	196	195
	221	219	215	208	199
	342	379	400	386	335
	-999	-780	-431	-326	-306
	-187	-117	-80	-56	-39
	Eta = 45 degrees				
	123	123	123	122	122
	129	127	125	122	118
	152	156	159	156	147
	236	323	481	744	864
	-999	-289	-137	-81	-51
	Eta = 56 degrees				
	90	89	89	89	89
	91	89	87	85	83
	95	95	95	94	91
	108	129	135	150	155
	159	309	-999	-208	-91
	Eta = 67 degrees				
	77	73	72	72	72
	72	70	69	67	66
	71	70	69	68	66
	70	72	76	80	82
	73	89	122	228	-999
	Eta = 78 degrees				
	64	64	64	64	64
	63	61	60	58	57
	60	58	56	55	54
	55	54	54	55	55
	50	51	56	66	86
	Eta = 89 degrees				
	62	61	61	61	61
	60	58	56	55	54
	56	53	50	49	48
	51	46	44	43	43
	43	38	37	38	40

(b)

Values of threshold stresses (in MPa) for the magnetisation to switch from (a) M_z to M_x, (b) M_z to M_y.
(999 indicates a threshold stress greater than 999MPa, and -999 indicates one less than -999MPa).

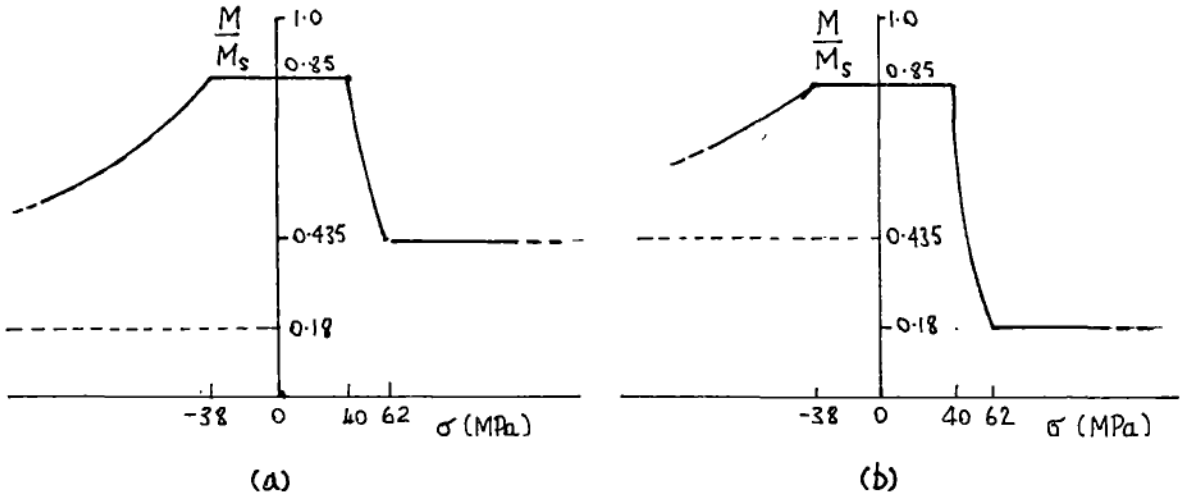

Figure A1.9 M/Ms vs. σ, for polycrystalline steel, for change of magnetisation from (a) OZ to OX, i.e. M_x, (b) OZ to OY, i.e. M_y.

Demagnetising energy

Figure A1.10 shows the position of the U-core with which B vs. H curves were measured for field perpendicular to stress. The sample is a thin sheet of steel and so it will only magnetise in directions in the plane of the sheet, since the demagnetising factor perpendicular to this plane is very large indeed. (The energy density needed to magnetise the steel perpendicular to the sheet is similar to that needed to give the same flux density in air, namely $M_s^2/\mu_o \sim 3\times10^6$ J/m³. By comparison, the magnetostatic and magnetoelastic energy densities are of the order of 1000J/m³).

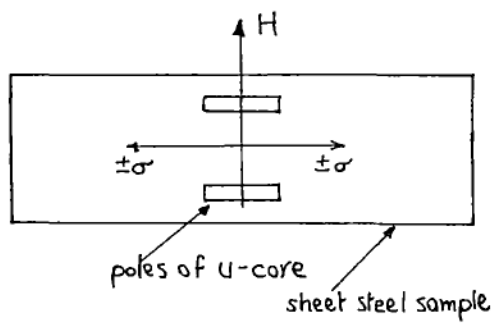

Figure A1.10 The position of the U-core on a thin sheet of steel. Stress will not switch the magnetisation into a direction perpendicular to the plane of the sheet.

If, for example,in figure A1.10, H and σ are in the (010) plane, perpendicular to OY, then M_s will not switch along OY. Thus in figure A1.9a, M_Y is not allowed. By the same argument, if H and σ are in the (100) plane, then in figure A1.9b M_X is not allowed. In both cases this means

that the effect of perpendicular compression in changing the magnetisation is small, but perpendicular tension still has its same effect: that of reducing magnetisation.

In general, the very high demagnetising energy for a component of magnetisation out of the surface of the steel greatly restricts the number of combinations of stress and field directions for stress perpendicular to the field, and makes the two dimensional case not quite as unrealistic as it might otherwise be. One can conclude that for the particular shape of test sample used for the measurements this three dimensional analysis adds very little to the predictions of the two dimensional case. Also, once the demagnetising energy is included then logically the anisotropy energy must also be included (since its energy density is of the order of $10^5 J/m^3$). This makes the situation extremely complicated and its analysis a major undertaking.

PUBLISHED PAPERS

Five papers have been published by the author in connection with this work; they are listed below.

RL1 "Prediction and measurement of rotation of magnetization in an anisotropic polycrystalline ferromagnetic material", Trans. IEEE Magnetics, Vol.17, Jan. 1981, pp1159-1168.

RL2 "Measurement of the mechanical stress in mild steel by means of rotation of magnetic field strength", NDT International, Vol.14, No.5, Oct. 1981, pp255-262.

RL3 "Measurement of the mechanical stress in mild steel by means of rotation of magnetic field strength - part2: biaxial stress", NDT International, Vol.15, No.2, April 1982, pp91-97.

RL4 "Measurement of the mechanical stress in mild steel by means of rotation of magnetic field strength - part3: practical applications", NDT International, Vol.16, No.2, April 1983, pp59-65.

RL5 "The effects of stress on the magnetisation of mild steel at moderate field strengths", Trans. IEEE Magnetics, Vol.21, July 1985, pp1314-1320.

REFERENCES

A1 P.P.ASTASHENKO, N.N ZATSEPIN: "A method and instrument for measuring the mechanical properties of ferromagnetic parts", Defektoskopiya, No.3, March 1979, pp26-29 (English translation pages 198-200).

A2 D.L.ATHERTON, L.W.COATHUP, D.C.JILES, C.WELBOURNE, A. TEITSMA: "Stress-induced magnetization changes of steel pipes - laboratory tests", IEEE Trans. Magnetics, Vol.19, No.4, July 1983, pp1564-1568.

A3 D.L. ATHERTON: "Stress-shadow magnetic technique for far-side anomalies in steel pipes", NDT Intl., Vol.16, No.3, June 1983, pp145-149.

A4 D.L.ATHERTON, C.WELBOURNE, D.C.JILES, L.REYNOLDS, J.SCOTT-THOMAS: "Stress-induced magnetization changes of steel pipes - laboratory tests, part 2", IEEE Trans. Magnetics, Vol.20, Nov.1984, pp2129-2136.

A5 A.M. ARMOUR, A.J.KING, J.W.WHALLEY: "Some developments and simplifications in permeameters', Proc.IEE, Vol.99, part IV, 1952, pp74-82.

A6 D.R.ASHWORTH: "Ferromagnetism. The development of a general equation to magnetism", Taylor and Francis, London, 1938.

A7 S.ABUKU, C.TAKIZAWA: "Magnetic measurement of residual stress induced in carbon steel by uniaxial plastic deformation", Proc. 17th. Japan Cong. Water Res., 1974, pp50-52.

B1 R.A.BETH, W.W.MEEKS: "Magnetic measurement of torque in a rotating shaft", Rev. of Sci. Inst., Vol.25, No.6, June 1954, pp 603-607.

B2 T.H.BARTON, R.J.IONIDES: "A precision torquemeter based on magnetic stress anisotropy", Trans. IEEE Power Apparatus and Systems, Vol.85, No.2, Feb.1966, pp152-159.

B3 T.H.BARTON, R.J.IONIDES: "Quantitative theory of magnetic anisotropy torque transducers", Trans. IEEE Inst. and Meas. Vol.14, No.4, Dec.1965, pp247-254.

B4 J.R BARTON, F.N.KUSENBERGER, R.E.BEISSNER, G.A MATZKANIN: "Advanced quantitative nondestructive evaluation methods - theory and experiment", Sagamore Army Materials Research Conference Vol.23, 1979, pp435-476.

B5 J.BEAR, D.ZAVSLAVSKY, S.IRMAY: "Physical principles of water percolation and seepage", Paris, France, Unesco, 1968.

B6 "Handbook of operational amplifiers", Burr-Brown Research Corp., USA, publication LI227, 1969.

B7 R.M.BOZORTH: "Ferromagnetism", Van Nostrand, New York, 1951.

B8 A.BASAK, A.J.MOSES, "Influence of stress on rotational loss in silicon iron", Proc.IEE, Vol.125, 1978, pp165-168.

B9 R.R.BIRSS: "Magnetomechanical effects in the Rayleigh region", Trans. IEEE Magnetics, Vol.7, March 1971, pp113-133.

B10 W.F.BROWN: "Irreversible magnetic effects of stress", Phys. Rev., Vol.75, 1949, pp147-154.

B11 R.A.BECKER, W.DÖRING: "Ferromagnetismus", Springer, Berlin, 1939 (in German).

C1 P.E.CAVANAGH: "A method for predicting the failure of metals", ASTM Bulletin Vol.143, Dec.1946, pp30-35.

C2 B.D.CULLITY: "Introduction to magnetic materials", Addison-Wesley Pub. Co., 1972.

C3 D.J.CRAIK, M.J.WOOD: "Magnetisation changes induced by stress in a constant applied field", J. Phys. D: Appl. Phys., Vol.3, 1970, pp1009-1016.

C4 B.D.CULLITY: "Magnetic methods", Proc. Workshop on non-destructive examination of residual stress, NITAC-76-2, San Antonio, Texas, Aug.1975, pp227-236.

C5 W.J.CORNER, J.J.MASON: "The effect of stress on the domain structure of Goss-structured silicon iron", Brit. Jour. Appl. Phys., Vol.15, 1964, pp709-718.

C6 W.J.CORNER, J.J.MASON: "The effect of stress on the domain structure of cube-structured silicon iron", Proc. Phys. Soc., Vol.81, 1963, pp925-933.

C7 S.CHIKAZUMI: "Physics of magnetism", R.E.Krieger Pub. Co., 1978.

C8 P.E.CAVANAGH, T.W.WLODEK: "Magnetic stress analysis", ASTM Symp. on magnetic testing, 1948, pp123-139.

D1 O.DAHLE: "The Ring Torductor - a torque gauge without sliprings, for industrial measurement and control", ASEA Jour., Vol.33, No.3, 1960, pp23-32.

D2 G.F.DIONNE: "Effect of external stress on remanence ratios and anisotropy fields of magnetic materials", IEEE Trans. Magnetics Vol.5, No.3, Sept.1969, pp596-599.

E1 J.A.EWING: "Magnetic induction in iron and other metals", The Electrician Printing and Publishing Company, London, 1892.

F1 M.M.FROCHT: "Photoelasticity", Vol.2, John Wiley, New York, 1948.

F2 C.A.FAUNCE: "Magnetomechanical effects in ferromagnetic materials", PhD thesis, University of Salford, U.K., 1970.

G1 C.G.GARDNER, G.A.MATZKANIN, D.L.DAVIDSON: "The influence of mechanical stress on magnetisation processes and Barkhausen jumps in ferromagnetic materials", Intl. Jour. NDT, Vol.3, 1971, pp131-169.

G2 J.N.GOODIER: "Compression of rectangular blocks, and the bending of beams, by non-linear distributions of bending forces", Trans. A.S.M.E. Vol.54, 1932, pp173-183.

G3 J.B.GOODENOUGH: "A theory of domain creation and coercive force in polycrystalline ferromagnetics", Phys. Rev., Vol.95, Aug.1954, pp917-932

G4 V.B.GINSBURG: "The calculation of magnetisation curves and hysteresis loops for a simplified model of a ferromagnetic body", Trans. IEEE Magnetics, Vol.12, No.2, March 1976, pp119-126.

G5 V.B.GINSBURG: "The magnetoelastic properties of a simplified model of a ferromagnetic body in a low magnetic field", Trans. IEEE Magnetics, Vol.13, No.5, Sept.1977, pp1657-1663.

H1 K.HOSELITZ: "Ferromagnetic properties of metals and alloys", Clarendon Press, Oxford, 1952.

H2 Z.HAOSEN, C.LIGONG, S.ZHONGXIAN: "Study of the technique of stress determination by measuring magnetism", Intl. conf. of quality and reliability in welding, Sept.1984, Hangzhau, China.

H3 V.HAUK, E.SCHNEIDER, P.STUITJE, W.THEINER: "Comparison of different methods to determine residual stresses nondestructively", New procedures in nondestructive testing, Ed. P.Holler, Springer-Verlag, Berlin, 1983, pp575-585.

H4 R.HILL: "The mathematical theory of plasticity", Clarendon Press, Oxford, 1950.

J1 D.C.JILES, D.L.ATHERTON: "Theory of the magnetisation process in ferromagnets and its application to the magnetomechanical effect", J. Phys. D, Vol.17, No.6, June 1984, pp1265-1281.

K1 A.V.KAPTSOV, V.V.IVANOV: "Electromagnetic transducer for mechanical stress with a microcalculator", Defektoskopiya, No.4, April 1983, pp21-25 (English translation pp243-245).

K2 G.V.KINGS: "Recent advances in Barkhausen noise measurement",J. of magnetism and magnetic materials, Vol.26, 1982, pp258-260.

K3 L.P.KARJALAINEN, M.MOILANAN: "Detection of plastic deformation during the fatigue of mild steel by the measurement of Barkhausen noise", NDT Intl., April 1979, pp51-55.

K4 G.S.KINO, D.M.BARNETT, N.GRAYELI, G.HERRMANN, J.B.HUNTER, D.B.ILIC, G.C.JOHNSON, R.B.KING, M.P.SCOTT, J.C.SHYNE, C.R.STEEL: "Acoustic measurement of stress fields and microstructure", J. Nondestructive Evaluation, No.1, March 1980, pp67-77.

L1 D.A.LEWIS: "Magnetic and electrical methods of non-destructive testing", George Allen and Unwin, London, 1951.

L2 M.LAMBECK: "Indication of stress by transverse and longitudinal internal induction", J. of magnetism and magnetic materials, Vol.4, 1977, pp231-234.

L3 E.W.LEE: "Magnetisation and magnetomechanical effects", Rep. on Prog. in Phys., Vol.18, 1955, pp184-229.

M1 W.J.McGONNAGLE: "Non-destructive testing", McGraw Hill, 1961.

M2 J.H.MICHELL: "Elementary distributions of plane stress", Proc. London Math. Soc., Vol.32, 1900, p44.

M3 M.N.MIKHEEV, E.S.GORKUNOV: "Relationship of magnetic properties to the structural condition of a substance - the physical basis of magnetic structure analysis (review)", Defektoskopiya, Aug.1982, pp5-22 (english trans. pp579-592).

R1 N.M.RODIGIN, V.P.SYROCHKIN: "Feasibility of electromagnetic inspection for the strength and hardness of structural steel under elastic tension", Defectoscopy, Vol.9, No.4, July-Aug. 1973, pp453-460.

R2 N.M.RODIGIN, V.P.SYROCHKIN: "Possibility of electromagnetically testing the strength and hardness of 40Kh steel using elastic compression", Defectoscopy, Vol.9, No.5, 1973, pp514-518.

R3 P.RUUSKANEN, P.KETTUNEN: "Two ferromagnetic methods for the evaluation of the fatigue limit in polycrystalline iron", NDT Intl., June 1980, pp105--108.

R4 R.RUSNAC: "The effect of plastic deformation on the magnetic aftereffect in iron", PhD dissertation, University of Notre Dame, Indiana, U.S.A., 1967.

R5 P.RHODES, G.ROWLAND: "Demagnetising energies of uniformly magnetised rectangular blocks", Proc. Leeds Phil. & Lit. Soc., Vol.6, June 1954, pp191-210.

R6 C.O.RUUD: "A review of selected non-destructive methods for residual stress measurement", NDT Intl., Vol.14, No.1, Feb.1982, pp15-23.

S1 T.SPOONER: "Properties and testing of magnetic materials", McGraw Hill, New York, 1927.

S2 G.SYKE, I.MURRAY: "Some magnetic methods of non-destructive examination: Part 2 - Measurement of shape of rolled strip", Iron and Steel Inst. Pub.103, 1967, pp126-134.

S3 S.SAYNAJAKANGAS: "A new surface transducer for generating and detecting magnetic field transients in ferromagnetics", Trans. IEEE Magnetics, Vol.10, 1954, pp44-50.

S4 C.M.SMITH, G. SHERMAN: "A study of the magnetic properties of stressed iron and steel", Phys. Rev., Vol.4, 1914, pp267-273.

S5 P.W.SELWOOD: "Magnetochemistry", Interscience Publishers Inc., New York, 1956.

S6 E.C.STONER, E.P.WOHLFARTH: "A mechanism of magnetic hysteresis in heterogeneous alloys", Phil. Trans. Royal Soc., A-240, 1948, pp599-664.

T1 W.A.THEINER, I.ALTPETER: "Determination of residual stresses using micromagnetic parameters", New procedures in non-destructive testing, Ed.:P.Heller, Springer Verlag, Berlin, 1983, pp561-573.

T2 S.P.TIMOSHENKO, J.N.GOODIER: "Theory of elasticity", McGraw Hill, 1970.

W1 T.W.WLODEK: "The possibility of exploiting magnetic phenomena in the testing of steel", The Canadian inst. of mining and metallurgy, Trans., Vol.47, 1944, pp5-15.

W2 F.J.WILKINS, A.E.DRAKE: "Instrument for measuring local power losses in uncut electrical sheet steel", Proc. IEE, Vol.112, No.4, April 1965, pp786-793.

W3 F.J.WILKINS, A.E.DRAKE: "Automatic measurement of local power losses in grain orientated silicon iron", Proc. IEE, May 1970, pp1048-1051.

W4 J.M.WATSON: "The M-H loops of stressed single domain ferrite particles by averaging energies under interaction", MSc thesis, Lehigh University, Bethlehem, Pennsylvania, U.S.A., 1968.

W5 J.M.WATSON: "The static M-H loops of stressed magnetic materials with intergranular interaction", IEEE Trans. Magnetics, Vol.8, No.2 June 1972, pp201-204.

W6 J.R.WAIT: "Review of electromagnetic methods in nondestructive testing of wire ropes", Proc. IEEE, Vol.67, No.6, June 1979, pp892-903.

Y1 H.YAMADA, Y.YAMADA, H.WAKIWAKA: "Indirect measurement of the hardened depth using a magnetic anisotropy sensor", The NDT Jour. of Japan, Vol.1, No.1, 1981(?), pp11-16.

Z1 YU D.ZHELEZNOV, N.C.BETS, A.G.ZHURANSKII, A.J.KONDRATOV: "Determining the stress in ferromagnetic plates", Steel in the U.S.S.R. (translation by the iron & steel inst., U.K.) March 1972, pp221-222.

Z2 YU D.ZHELEZNOV, L.B.KAZADZHAN, G.G.GRIGORYAN, A.G.ZHURAVSKII, V.F.KREPAKOVA: "Specific losses in transformer steel controlled by a non-destructive method", Steel in the U.S.S.R., Nov.1974, pp928-930.

Z3 A.G.ZHURAVSKII, L.B.KAZADZHAN, S.P.SLAUTA: "An instrument for measuring the mechanical stresses in transformer steel", Defektoskopiya, No.5, May 1983, pp34-38 (English trans. pp340-344).